



UNIVERSITÀ DI ROMA TRE
FACOLTÀ DI SCIENZE MATEMATICHE, FISICHE E NATURALI
Dipartimento di Matematica e Fisica

XXIX Ciclo

ASPECTS OF NEW PHYSICS BEYOND THE
STANDARD MODEL IN THE LEPTONIC SECTOR

Tesi di Dottorato

Relatore:
Dott. Davide Meloni

Candidato:
Andrea Giuseppe Di Iura

Coordinatore:
Prof. Roberto Raimondi

To my parents

*Tolstoy had doubted the value
of his own enormous labours.
Tolstoy, a genius, had been unsure whether
what he did was of any use to anyone.
Not so the physicists.
They had no doubts.*

VASILY GROSSMAN, LIFE AND FATE, 1959

Contents

1	Introduction	1
1.1	Three neutrino mixing formalism	2
1.1.1	Two neutrino approximation	4
1.1.2	Oscillation in matter	4
1.2	Neutrino experimental status	5
1.2.1	The Majorana nature of the neutrino	8
1.3	Thesis outline	9
2	Lepton Mixing from $A_5 \otimes CP$	11
2.1	Lepton mixing from discrete symmetry	11
2.1.1	TBM and BM from discrete symmetries	13
2.2	Group A_5	14
2.2.1	Subgroups of A_5	16
2.2.2	Golden Ratio Predictions	16
2.3	CP invariance	18
2.3.1	Neutrino sector invariant under $Z_2 \otimes CP$	19
2.3.2	Accidental CP symmetry	22
2.3.3	CP transformation of A_5	22
2.4	Classification	24
2.4.1	Sector $Q \in Z_5$	25
2.4.2	Sector $Q \in Z_3$	31
2.4.3	Sector $Q \in V$	33
2.5	Numerical discussion	36
3	Models of Neutrino Masses	42
3.1	Case II	42
3.1.1	Flavons of Case II	44
3.1.2	Two step symmetry breaking	45
3.2	Constraints on neutrino masses	45
3.2.1	Equivalence between different mechanisms	45
3.3	Analytic results	48
3.3.1	Mechanism I	48
3.3.2	Mechanism II a-1	53
3.3.3	Mechanism II a-2	58
3.3.4	Mechanism II c-2	66
3.4	Numerical results	74
3.4.1	Mechanism I	76
3.4.2	Mechanism II a-1	78
3.4.3	Mechanism II a-2	78
3.4.4	Mechanism II c-2	80
3.5	Predictions for m_β and $m_{\beta\beta}$	82
3.5.1	Mechanism I	82
3.5.2	Mechanism II a-1	83
3.5.3	Mechanism II a-2	83

3.5.4	Mechanism II c-2	84
3.6	Model for Mechanism II c-2: $f_r = f_i = 0$	85
3.6.1	LO superpotential	86
3.6.2	NLO corrections	87
3.6.3	Neutrino mass spectrum	88
3.6.4	Charged lepton masses	90
3.6.5	PMNS matrix summary	91
4	New Physics at Neutrino Facilities	93
4.1	Effective Theory	93
4.1.1	Large Extra Dimensions	94
4.1.2	Non Standard Interactions	96
4.2	Statistical Analysis	99
4.2.1	T2K Experiment	99
4.2.2	Daya Bay Experiment	101
4.2.3	Definition of $\Delta\chi^2$	103
4.2.4	Priors	104
4.3	Results	104
4.3.1	Standard oscillation parameters	105
4.3.2	LED fit	108
4.3.3	NSI fit	109
4.4	Discussion	111
5	Conclusions	113
A	SM oscillation probabilities	115
B	Non abelian discrete groups	116
B.1	Group theory	116
B.2	Representations and characters	117
B.3	The group S_4	119
C	Kronecker products of A_5	120
D	CP invariants	124
E	Neutrino mass sum rules	126
F	Effective operators	128
F.1	Superpotential $\delta\mathcal{W}$	128
F.2	Operators for charged lepton masses	130
G	LED mass eigenstates and matrix elements	132
G.1	Oscillation in vacuum	135
G.2	Sum rule for probability	136
H	NSI oscillation probabilities	138
	Bibliography	140

1

Introduction

In this Ph.D. Thesis I want to investigate the physics of lepton mixing, the nature of massive neutrinos, the problem of flavour and how extensions of physics beyond the Standard Model of particle physics (SM) could modify the oscillation phenomenology in long baseline and reactor experiments.

Neutrino physics has still a large interest on the scientific community, which is clear from the amount of papers that appear every year since the neutrino was postulated in 1930 by Pauli [1], see for instance Fig. 1.1 where the number of papers dealing with neutrino physics are shown as a function of the year. A large increasing in the number of available papers appears after the experimental evidence obtained in 1956 by Cowan and Reines research team at the Savannah River Site [2]. Using a modified version of `pyinspire.py` script ¹ we analyse the `inSpire` database; we can easily observe that the trend is positive.

There has been an impressive progress in the field of neutrino physics in the last sixty years. In this period valuable experimental evidences for three families of massive neutrinos and flavour neutrino oscillations were obtained in various experimental channels, and the parameters which characterize the mixing are known with a relatively high precision. As a consequence, the existence of non-zero neutrino masses and neutrino mixing was established.

However we do not know yet what is the origin of neutrino masses, mixing and some of the fundamental aspects of neutrino mixing. In fact, we do not have information about:

- whether the massive neutrinos are Dirac or Majorana particles
- what kind of spectrum the neutrino masses obeys
- what is the absolute scale of neutrino masses
- what is the octant for the atmospheric mixing angle θ_{23}
- what are the values of the CP violating phases in the leptonic sector.

Determining the nature of massive neutrinos is one of the most pressing and ambitious problems in the field of neutrino physics. Recognizing if neutrinos are Dirac fermions,

¹The code is available online at <https://github.com/agdiura/PyInspireStat>.

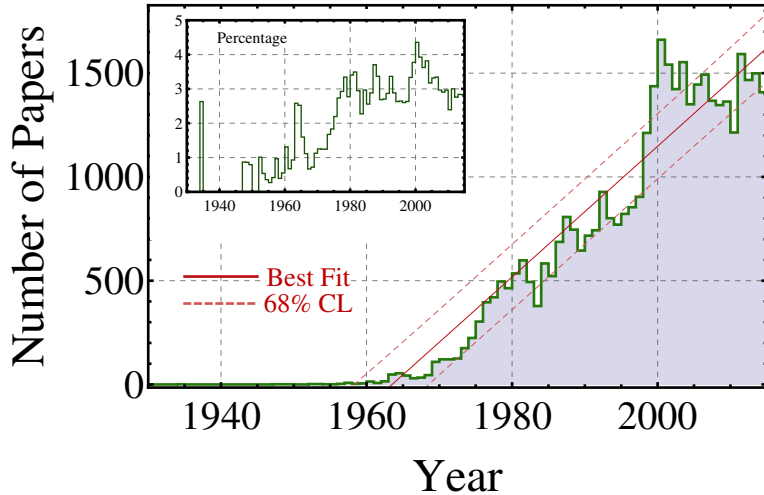


Figure 1.1: Number of papers on inSPIRE that contain in the title the word *neutrino* as a function of the Year in the interval [1930, 2015]. In the inset we show the percentage of papers with respect to the full database. The fit is performed with a power law function from the data after 1956, the year of the experimental discovery. We get: Number of papers $\propto \text{Year}^{1.28}$ with $\chi^2/\text{dof} = 58.78/56 = 1.05$. The prediction for Year 2016 at 95% CL is [1320, 1986].

possessing distinct antiparticles, or Majorana fermions, *i.e.* spin $1/2$ particles that are identical with their antiparticles [3], is of fundamental importance for correctly understand the origin of neutrino masses and mixing and, thus, the underlying symmetries of the Lagrangian of particle interactions.

Determining the type of spectrum the neutrino masses and the absolute mass scale is also of crucial importance for making progress in our understand of the origin of neutrino masses and mixing. From a theoretical point of view the knowledge of the θ_{23} octant, as well as the CP phase, might be useful to construct a theory of flavour. Getting information about the status of CP symmetry in the leptonic sector might allow us to make progress in the understand of the origin of the observed matter-antimatter asymmetry of the Universe.

1.1 Three neutrino mixing formalism

The existence of massive neutrinos implies that the left-handed (LH) neutrino flavour fields $\nu_\alpha(x)$, that enter into the expression for the charged lepton current of weak interaction Lagrangian, are linear combinations of three, or even more, massive neutrinos $\nu_j(x)$

$$\nu_\alpha(x) = \sum_j U_{\alpha j} \nu_j(x) \quad \alpha = \{e, \mu, \tau\} \quad j = 1, 2, 3 \dots \quad (1.1)$$

The misalignment between the neutrino mass and flavour eigenstates can be parametrized through an unitary matrix, the Pontecorvo-Maki-Nakagawa-Sakata matrix (PMNS) [4–7]. It contains six real parameters. Three are mixing angles: θ_{12} , the so-called solar angle, θ_{13} the reactor angle and θ_{23} the atmospheric one. U_{PMNS} also contains three phases. We use the following convention for the PMNS matrix

$$U_{\text{PMNS}} \equiv U = \tilde{U} \text{diag}\{1, e^{i\alpha/2}, e^{i(\beta/2+\delta)}\} \quad (1.2)$$

and \tilde{U} is the CKM-like parametrization of the mixing matrix, defined as

$$\tilde{U} = \begin{pmatrix} 1 & 0 & 0 \\ 0 & c_{23} & s_{23} \\ 0 & -s_{23} & c_{23} \end{pmatrix} \begin{pmatrix} c_{13} & 0 & s_{13}e^{-i\delta} \\ 0 & 1 & 0 \\ -s_{13}e^{i\delta} & 0 & c_{13} \end{pmatrix} \begin{pmatrix} c_{12} & s_{12} & 0 \\ -s_{12} & c_{12} & 0 \\ 0 & 0 & 1 \end{pmatrix} \quad (1.3)$$

where $c_{ij} \equiv \cos \theta_{ij}$ and $s_{ij} \equiv \sin \theta_{ij}$. All the angles are in the first quadrant $\theta_{ij} \in [0, \pi/2]$. Here δ is the Dirac CP phase, α and β are the Majorana phases. On the basis of the existing neutrino oscillation data it is impossible to determine whether the massive neutrinos are Dirac or Majorana particles.

Neutrino oscillations are a manifestation of leptonic mixing and they are a quantum mechanical phenomenon in which a neutrino born with flavour α changes to a different flavour β while propagating in vacuum or in matter; for a pedagogical introduction and further details see Ref. [8]. Neutrinos are produced and detected via weak interactions and the state created in the decay $W^+ \rightarrow \ell_\alpha^+ + \nu_\alpha$ is given by (1.1). Observation of neutrino oscillations in various neutrino experiments, see Sec. 1.2 for a general overview, has shown that there is a mismatch between the flavour and mass eigenstates of neutrinos. From (1.1) we get that the probability of finding a neutrino created in a given flavour α to be in the same state, or any other state β , oscillates with time. The time evolution, in quantum mechanics, of a neutrino produced in a given flavour at $\mathbf{x} = \mathbf{0}$ and $t = 0$ is given by

$$|\nu_\alpha(t)\rangle = \sum_j U_{\alpha j}^* |\nu_j(t)\rangle = \sum_j U_{\alpha j}^* e^{-iE_j t} |\nu_j(0)\rangle \quad (1.4)$$

where we use the Dirac notation for quantum eigenstates. The neutrino oscillation probability, that is the probability of transformation from one flavour eigenstate $|\nu_\alpha\rangle$ to another flavour eigenstate $|\nu_\beta\rangle$, can be obtained as

$$\mathcal{P}(\nu_\alpha \rightarrow \nu_\beta) = |\langle \nu_\beta | \nu_\alpha \rangle|^2 = \left| \sum_j \sum_k U_{\alpha j} e^{-iE_j t} U_{\beta k}^* e^{iE_k t} \langle \nu_k | \nu_j \rangle \right|^2. \quad (1.5)$$

The neutrinos are ultrarelativistic, so that $p_j \simeq p_k \simeq p \simeq E_\nu$, therefore

$$E_j = \sqrt{p_j^2 + m_j^2} \simeq p + \frac{m_j^2}{2E_\nu} \quad (1.6)$$

where E_j and m_j are the energy and mass of the neutrino mass eigenstate ν_j . In this case

$$E_k - E_j \simeq \frac{\Delta m_{kj}^2}{2E_\nu} \quad (1.7)$$

where we have defined

$$\Delta m_{kj}^2 \equiv m_k^2 - m_j^2 \quad (1.8)$$

which is the mass-squared difference. Notice that in neutrino oscillation experiments, the propagation time t is not measured. What is known is the distance L between the source and the detector. Since ultrarelativistic neutrinos propagate almost at the speed of light, it is possible to approximate $t = L$. Using (1.6) and the orthogonality relation $\langle \nu_k | \nu_j \rangle = \delta_{jk}$, after some algebra we get for the transition probability

$$\mathcal{P}(\nu_\alpha \rightarrow \nu_\beta) = \delta_{\alpha\beta} - 4 \sum_{k>j} \text{Re} \{ U_{\alpha k}^* U_{\beta k} U_{\alpha j} U_{\beta j}^* \} \sin^2 \left(\frac{\Delta m_{kj}^2 L}{4E_\nu} \right) +$$

$$+ 2 \sum_{k>j} \text{Im} \{ U_{\alpha k}^* U_{\beta k} U_{\alpha j} U_{\beta j}^* \} \sin \left(\frac{\Delta m_{kj}^2 L}{2E_\nu} \right). \quad (1.9)$$

The oscillation probabilities of the channels with $\alpha \neq \beta$ are usually called *transition probabilities* or *appearance channel*, whereas the oscillation probabilities of the channels with $\alpha = \beta$ are usually called *survival probabilities* or *disappearance channel*. In the case of disappearance we have

$$\mathcal{P}(\nu_\alpha \rightarrow \nu_\alpha) = 1 - 4 \sum_{k>j} |U_{\alpha k}|^2 |U_{\alpha j}|^2 \sin^2 \left(\frac{\Delta m_{kj}^2 L}{4E_\nu} \right). \quad (1.10)$$

Thus we expect to have sensitivity to the parameters of PMNS when the argument of the \sin^2 function is $\mathcal{O}(1)$. Usually Δm_{kj}^2 is measured in eV^2 , the baseline L in km and the neutrino energy E_ν in GeV, hence the argument of \sin^2 can be written as $1.267 \times \Delta m_{kj}^2 L / E_\nu$. In the following we discuss the phenomenology in the two-neutrino approximation while in Appendix A we summarize the SM probabilities that are relevant in our analysis.

1.1.1 Two neutrino approximation

For the case of two generations of neutrinos, the above analysis becomes quite simplified without any loss of physical understand. The mixing matrix depends only on one parameter θ (known as mixing angle) and is given by

$$U = \begin{pmatrix} \cos \theta & \sin \theta \\ -\sin \theta & \cos \theta \end{pmatrix} \quad (1.11)$$

and there is a single mass-squared difference Δm^2 . The oscillation probability in Eq. (1.9) becomes

$$\mathcal{P}(\nu_\alpha \rightarrow \nu_\beta) = \sin^2 2\theta \sin^2 \left(\frac{\Delta m^2 L}{4E_\nu} \right). \quad (1.12)$$

Within this simplified model it is possible to analyse some features of the neutrino phenomenology. In fact it was common during the nineties to study the oscillation in a simplified framework with only two active neutrinos. The solar neutrino problem (see later) can be studied in term of two effective parameters, the solar angle $\theta_\odot \equiv \theta_{12}$ and the solar mass-squared difference Δm_\odot^2 , while the deficit in the neutrino flux from cosmic rays has been studied using the atmospheric angle $\theta_A \equiv \theta_{23}$ and the atmospheric mass-squared difference Δm_A^2 .

1.1.2 Oscillation in matter

The propagation of neutrinos becomes significantly modified in the presence of matter due to their interactions with the elements composed of electrons, protons, and neutrons. The coherent forward elastic scattering amplitudes are not the same for all neutrino flavours ν_α . The electron neutrinos have additional contribution due to their charged current (CC) interactions with matter which are mediated by weak bosons. On the basis of this fact, Mikheyev and Smirnov [9], following the work of Wolfenstein [10], showed that an interesting phenomenon occurs when neutrinos travel in dense matter.

In the two-flavour case, discussed in Sec. 1.1.1, if neutrinos ν_e and ν_μ travel through the Sun, the propagation of ν_1 and ν_2 will be modified due to the different interactions of ν_e and ν_μ with electrons. The mixing angle in the presence of matter is given by

$$\sin^2 2\theta_m = \frac{\sin^2 2\theta}{(\cos 2\theta - L/L_m)^2 + \sin^2 2\theta} \quad (1.13)$$

where L_m , a length characteristic of motion in matter of density n_e , is given by

$$L_m = \frac{\sqrt{2}\pi}{G_F n_e} \quad (1.14)$$

and G_F is the Fermi constant. Eq. (1.13) has a resonance when n_e is such that $L/L_m = \cos 2\theta$ so that $\sin^2 2\theta_m = 1$, resulting in maximal mixing and the survival probability, to a very good approximation, can be written as

$$\mathcal{P}(\nu_\alpha \rightarrow \nu_\alpha) = \frac{1}{2} [1 + \cos 2\theta \cos 2\theta_m]. \quad (1.15)$$

This is just a simple example of neutrino propagation in matter, for further details see Ref. [8].

1.2 Neutrino experimental status

The first hint that neutrinos have mass came from the Homestake experiment [11] during the sixties. In this experiment, it was found that only about one-third of the number of neutrinos predicted by standard solar model (SSM) were reaching the detector on the earth. The idea of neutrino oscillations gained support from the Japanese experiments Kamiokande [12] and Super-Kamiokande [13, 14], during the nineties, in which similar deficit was observed in the atmospheric neutrino flux.

Results from several solar neutrino experiments: Homestake [15], SAGE [16], GALLEX [17] as well as Super-Kamiokande [18] that collected data for more than four decades have shown that the large mixing angle (LMA) solution could be explained the solar neutrino problem. The latest addition to this huge repertoire of experimental data are the results from the SNO [19–21] and Borexino experiments [22–24] which are consistent with the LMA solution. This conclusion from the solar neutrino experiments has been investigated independently by the KamLAND reactor antineutrino experiment [25–27] and a combined analysis of the solar and KamLAND experimental data gives $\Delta m_{\odot}^2 = 7.6 \times 10^{-5} \text{ eV}^2$ and $\sin^2 2\theta_{12} = 0.32$, see for instance the global analysis performed in 2005 by the Authors of Ref. [28].

Similar deficit in the ratio of the flux of muon to electron flavour atmospheric neutrinos produced in cosmic rays has been observed. The other mass splitting Δm_{A}^2 and the atmospheric angle θ_{23} are well determined by the zenith angle dependent atmospheric ν_μ data from Kamiokande [29], Super-Kamiokande [13, 14, 18, 30] and the long baseline experiments (LBL) K2K [31, 32] and MINOS [33] in both appearance and disappearance channels. The combined data from the atmospheric and long baseline experiments give us $|\Delta m_{\text{A}}^2| = 2.4 \times 10^{-3} \text{ eV}^2$ and $\sin^2 2\theta_{23} = 1$. More recently disappearance and appearance results from LBL experiments in the form of the energy distribution of ν_μ and $\bar{\nu}_\mu$ in T2K [34, 35], and ν_μ events in NO ν A at the beginning of 2016 [36, 37] confirm the neutrino oscillation hypothesis with high accuracy. Similar results were obtained by the OPERA collaboration for the channel $\nu_\mu \rightarrow \nu_\tau$ [38].

With the observation of a non-zero reactor angle θ_{13} in 2012 by Double Chooz in France [39], Daya Bay in China [40] and RENO in Korea [41], we now have complete knowledge of all the three mixing angles θ_{12} , θ_{13} and θ_{23} . However, we do not have any information on the Dirac-type CP violating phase δ and it is fully unconstrained as yet, although a small hint for maximal CP violation from combined analyses give $\delta \sim 3\pi/2$. Due to matter effects we expect that NO ν A, as well as the proposed experiments such as T2HK [42], LBNE [43] and ESS ν SB [170], could confirm this preliminary result. We also expect an improvement on the measurement of the solar parameters by the planned JUNO experiment [44].

We report in Tab. 1.1 the best fit points with the 1σ errors and the 3σ confidence region for Normal Ordering (NO) and Inverted Ordering (IO), that we will discuss in details later. All the data are extracted from the latest global analysis performed in Ref. [45] using the August 2016 data. Similar results were obtained in Refs. [46,47].²

Parameter	Normal Ordering		Inverted Ordering	
	Best Fit	3σ Range	Best Fit	3σ Range
$\sin^2 \theta_{12}/10^{-1}$	$3.08^{+0.13}_{-0.12}$	$2.73 \div 3.48$	$3.08^{+0.13}_{-0.12}$	$2.73 \div 3.48$
$\sin^2 \theta_{13}/10^{-2}$	$2.163^{+0.074}_{-0.074}$	$1.938 \div 2.388$	$2.175^{+0.075}_{-0.074}$	$1.950 \div 2.396$
$\sin^2 \theta_{23}/10^{-1}$	$4.40^{+0.23}_{-0.19}$	$3.88 \div 6.30$	$5.84^{+0.18}_{-0.22}$	$3.98 \div 6.32$
δ	$5.04^{+0.66}_{-0.89}$	$0 \div 2\pi$	$4.69^{+0.68}_{-0.79}$	$0 \div 2\pi$
$\Delta m_{21}^2/10^{-5} [\text{eV}^2]$	$7.49^{+0.19}_{-0.17}$	$7.02 \div 8.08$	$7.49^{+0.19}_{-0.17}$	$7.02 \div 8.09$
$\Delta m_{3\ell}^2/10^{-3} [\text{eV}^2]$	$+2.526^{+0.039}_{-0.037}$	$+2.413 \div +2.645$	$-2.518^{+0.038}_{-0.037}$	$-2.643 \div -2.406$

Table 1.1: Latest results for the global fit of Ref. [45] (available at the website <http://www.nu-fit.org>). Note that in the last line $\ell = 1$ for NO and $\ell = 2$ for IO. The analysis prefers a global minimum for NO with respect to the local minimum of IO, $\Delta\chi^2 = \chi_{\text{IO}}^2 - \chi_{\text{NO}}^2 = 0.56$.

It is worth noticing that the global fit analyses we are referring to in Tab. 1.1, [45], which are performed within the framework of the three neutrino mixing, suggest that $\sin^2 \theta_{23} < 1/2$ assuming NO while $\sin^2 \theta_{23} > 1/2$ in the case of IO. These results have important consequences from a theoretical perspective, in view of the need of finding a simple principle which could explain the patterns of the masses and of the mixing in the neutrino sector.

Furthermore, the admitted intervals of the absolute values of the elements of the PMNS mixing matrix are at the 3σ level

$$\|U_{\text{PMNS}}\| = \begin{pmatrix} 0.798 \div 0.843 & 0.517 \div 0.584 & 0.139 \div 0.155 \\ 0.234 \div 0.518 & 0.449 \div 0.696 & 0.617 \div 0.787 \\ 0.251 \div 0.528 & 0.463 \div 0.706 & 0.600 \div 0.774 \end{pmatrix}. \quad (1.16)$$

This result does not assume any particular neutrino mass ordering. Notice that the situation is quite different compared to the quark sector, where the quark mixing matrix, the Cabibbo-Kobayashi-Maskawa matrix (CKM), has a hierarchical structure and it is almost diagonal. For a schematic representation see Fig. 1.2, where we plot the absolute values of the V_{CKM} and U_{PMNS} matrix elements.

The experimental data we have summarized in Tab. 1.1 are compatible with different neutrino mass patterns, see for instance Fig. 1.3:

- *Normal Ordering* (NO): $m_1 < m_2 < m_3$, which means $\Delta m_{\odot}^2 \equiv \Delta m_{21}^2 > 0$ and $\Delta m_{\text{A}}^2 \equiv \Delta m_{31}^2 > 0$
- *Inverted Ordering* (IO): $m_3 < m_1 < m_2$, which means $\Delta m_{\odot}^2 \equiv \Delta m_{21}^2 > 0$ and $\Delta m_{\text{A}}^2 \equiv \Delta m_{32}^2 < 0$

where Δm_{\odot}^2 is the solar mass-squared difference and Δm_{A}^2 is the atmospheric one. Depending on the value of the lightest neutrino mass $\min_j \{m_j\}$, the mass spectrum could be:

²A recent analysis with bayesian approach is performed in Ref. [48], where similar results were obtained. The main difference is in θ_{23} , where the maximum of the likelihood occurs for $\theta_{23} > \pi/4$ for both orderings, however we have $\sin^2 \theta_{23}/10^{-1} \in [4.33, 4.96] \oplus [5.30, 5.94]$ @ 1σ CL, and the statistical significance is insufficient to exclude the other octant.

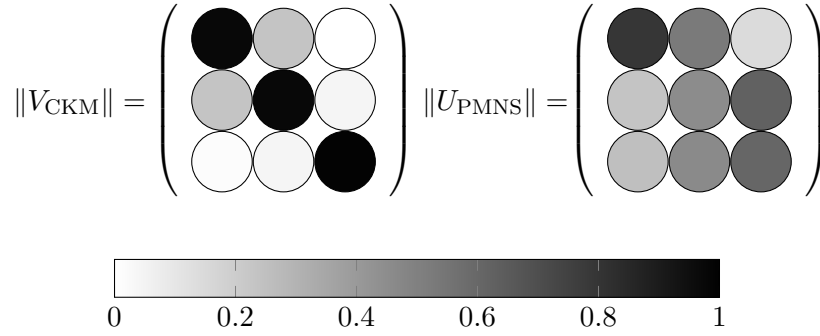


Figure 1.2: Pictorial representation of V_{CKM} and U_{PMNS} matrices, the color is proportional to the absolute value of the matrix element.

- *Normal Hierarchical* (NH): $m_1 \ll m_2 < m_3$, therefore $m_2 \simeq \sqrt{\Delta m_{\odot}^2} \simeq 8.7 \times 10^{-3}$ eV and $m_3 \simeq \sqrt{\Delta m_{\text{A}}^2} \simeq 4.9 \times 10^{-2}$ eV
- *Inverted Hierarchical* (IH): $m_3 \ll m_1 < m_2$, therefore $m_{1,2} \simeq \sqrt{\Delta m_{\text{A}}^2} \simeq 4.9 \times 10^{-2}$ eV
- *Quasi Degenerate* (QD): $m_1 \lesssim m_2 \lesssim m_3 \simeq m_0$ or $m_3 \lesssim m_2 \lesssim m_1 \simeq m_0$, therefore $m_j \gg \sqrt{|\Delta m_{\text{A}}^2|}$ and $m_0 = \mathcal{O}(10^{-1})$ eV.

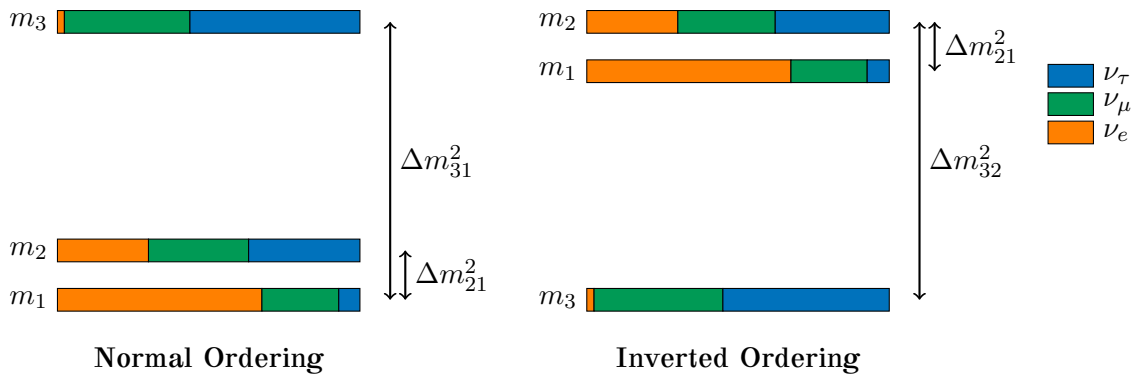


Figure 1.3: Possible mass spectra allowed from neutrino oscillation data. With different colors we indicate the probability of finding one of the flavour eigenstates if the neutrino is in a certain mass eigenstate.

The ratio r_ℓ is defined as

$$r_\ell \equiv \frac{\Delta m_{21}^2}{\Delta m_{3\ell}^2} = \begin{cases} +2.965^{+0.120}_{-0.111} \times 10^{-2} & \text{for NO} \\ -2.975^{+0.111}_{-0.121} \times 10^{-2} & \text{for IO} \end{cases} \quad (1.17)$$

where we have used the best fit values quoted in Tab. 1.1. At the level of 3σ the absolute value of r_ℓ , defined in (1.17), is constrained in the interval

$$2.65 \times 10^{-2} \leq |r_1| \leq 3.35 \times 10^{-2} \quad (1.18)$$

for NO, while for IO

$$2.67 \times 10^{-2} \leq |r_2| \leq 3.36 \times 10^{-2}. \quad (1.19)$$

All possible types of mass spectrum are compatible with the experimental constraints on the absolute scale of neutrino masses coming from β -decay experiments and cosmological/astrophysical data.

The best probe for the β -decay is the nuclear reaction ${}^3\text{H} \rightarrow {}^3\text{He} + e + \bar{\nu}_e$ with a Q -value $Q = M_{{}^3\text{He}} - M_{{}^3\text{H}} = 18.6$ keV. It is possible to measure the electron spectrum near the endpoint and extract the value of m_β , the effective mass that enters in the decay

$$m_\beta \equiv \sqrt{\sum_j m_j^2 |U_{1j}|^2} = \sqrt{\cos^2 \theta_{13} (m_1^2 \cos^2 \theta_{12} + m_2^2 \sin^2 \theta_{12}) + m_3^2 \sin^2 \theta_{13}}. \quad (1.20)$$

The most stringent upper limit on m_β was obtained by the Mainz and Troitzk experiments [49]

$$m_\beta \leq 2.3 \text{ eV @ 95\% CL} \quad (1.21)$$

while the Karlsruhe Tritium Neutrino experiment (KATRIN), which is expected to start the data taking in the next years, will provide informations on the absolute scale of neutrino masses with a sensitivity to $m_\beta \sim 0.2$ eV [50] (see also [51] for a more recent description of the experiment).

Information about the masses of light neutrinos can be obtained also from cosmological observations. In particular the total mass of light active neutrinos, $\sum_j m_j$, can be constrained from measurements of the matter power spectrum, which is a measure of the variance of the distribution of density fluctuations in the Universe. An upper bound for the sum of the masses can be obtained from the part of the power spectrum at small scales, see Ref. [52]. This bound is model dependent and may change under different assumptions. The PLANCK Collaboration presented the results based on the analysis of the cosmic microwave background (CMB) temperature and lensing-potential power spectra. In Ref. [53] the collaboration provided constraints assuming three species of degenerate massive neutrinos and a Λ CDM model using the PLANCK temperature power spectrum with a WMAP polarization low-multipole ($\ell \leq 23$) and Acatama Cosmology Telescope (ACT) high-multipole ($\ell \geq 2500$) data. We refer to this CMB data combination as PLANCK. In this case the upper limit on the sum of the neutrino mass reads

$$\sum_j m_j \leq 0.59 \text{ eV @ 95\% CL}. \quad (1.22)$$

Combining the latter with the Barion Acoustic Oscillation data (BAO), the limit is significantly lowered at

$$\sum_j m_j \leq 0.23 \text{ eV @ 95\% CL}. \quad (1.23)$$

The above upper limits can be converted into limits on the absolute scale of neutrino masses that read respectively $m_{\min} \lesssim 0.19$ eV in the more conservative case of (1.22) and $m_{\min} \lesssim 0.07$ eV in case of (1.23).

In the future we expect that the ESA mission EUCLID will measure the sum of the neutrino masses with a 1σ precision better than 0.03 eV, [54]. EUCLID's measurement of the galaxy power spectrum, combined with PLANCK priors, should yield an error on the sum of the neutrino masses of 0.04 eV [55].

1.2.1 The Majorana nature of the neutrino

The Majorana nature of massive neutrinos manifests itself in the existence of processes where the total lepton charge L changes by two units, for instance $K^+ \rightarrow \pi^- + \mu^+ + \mu^+$ or

$\mu^- + (A, Z) \rightarrow \mu^+ + (A, Z - 2)$. Several studies have shown that the most promising experiments having the potential of establishing the Majorana nature of massive neutrinos are, at present time, experiments searching for neutrinoless double beta decay ($0\nu\beta\beta$ -decay): $(A, Z) \rightarrow (A, Z + 2) + e^- + e^-$. This process can be generated only by the $(V - A)$ charged current weak interaction via the exchange of massive Majorana neutrinos, for a review see for instance Refs. [56–59]. The $0\nu\beta\beta$ -decay amplitude has the form

$$\mathcal{A}(0\nu\beta\beta) = m_{\beta\beta}\mathcal{M}(A, Z) \quad (1.24)$$

where $\mathcal{M}(A, Z)$ is the nuclear matrix element of the decay $(A, Z) \rightarrow (A, Z + 2) + e^- + e^-$ that does not depend on the neutrino mass and mixing parameters, and

$$m_{\beta\beta} \equiv \left| \sum_j m_j U_{1j}^2 \right| = \left| \cos^2 \theta_{13} \left(m_1 \cos^2 \theta_{12} + m_2 \sin^2 \theta_{12} e^{i\alpha} \right) + m_3 \sin^2 \theta_{13} e^{i\beta} \right|. \quad (1.25)$$

is the $0\nu\beta\beta$ -decay effective Majorana mass. The probability of the process is proportional to the square of $m_{\beta\beta}$ through

$$\frac{1}{T_{1/2}^{0\nu}(A)} = |m_{\beta\beta}|^2 |\mathcal{M}(A, Z)|^2 G^{0\nu}(Q, Z) \quad (1.26)$$

where $G^{0\nu}(Q, Z)$ is a known phase factor. The main uncertainty on $m_{\beta\beta}$ comes from the nuclear matrix element.

The neutrinoless double beta decay rate depends on the neutrino mass spectrum, that can be hierarchical, with partial hierarchy or quasi-degenerate. Using the latest data on the neutrino oscillation parameters it is possible to show that in the case of NO one has $m_{\beta\beta} \lesssim 0.005$ eV, while if the spectrum is with IO, 0.01 eV $\lesssim m_{\beta\beta} \lesssim 0.05$ eV. A large value of the effective mass, $m_{\beta\beta} \sim 0.5$ eV, is possible if the neutrino mass spectrum is quasi-degenerate. In QD case $m_{\beta\beta}$ can be close to the existing upper limits. The $0\nu\beta\beta$ experimental search can thus have an enormous impact in constraining the mass hierarchy, the absolute scale of neutrino masses and together with other sources of information could provide a unique insight on the value of the CP violating phases appearing in the leptonic mixing matrix.

The experimental searches for neutrinoless double beta decay have a long history, see for instance Ref. [60] for a review on this topic. The best lower limit on the half-life of ^{76}Ge is $T_{1/2}^{0\nu}(^{76}\text{Ge}) > 2.1 \times 10^{25}$ years @ 90% CL, it was found in the GERDA ^{76}Ge experiment [61]. If we combine the limits obtained in the Heidelberg-Moscow [62], IGEX [63] and GERDA experiments we get $T_{1/2}^{0\nu}(^{76}\text{Ge}) > 3.0 \times 10^{25}$ years @ 90% CL [61].

Other experiments search for $0\nu\beta\beta$ -decay: NEMO3 with ^{100}Mo found $m_{\beta\beta} < (0.61 \div 1.26)$ eV [64] and CUORICINO with ^{130}Te obtained $m_{\beta\beta} < (0.16 \div 0.68)$ eV, both at 90%CL when the nuclear uncertainties are taken into account. The best lower limits on the neutrinoless double beta decay half-life of ^{136}Xe were reported by the EXO and KamLAND-Zen collaborations: $T_{1/2}^{0\nu}(^{136}\text{Xe}) > 1.6 \times 10^{25}$ years @ 90% CL [65] and $T_{1/2}^{0\nu}(^{136}\text{Xe}) > 1.07 \times 10^{26}$ years @ 90% CL [66].

Most importantly, a large number of new generation experiments aim at sensitivity to $m_{\beta\beta} < (0.01 \div 0.05)$ eV, see Refs. [56–59], among them CUORE and SNO+ (^{130}Te), GERDA and MAJORANA (^{76}Ge), SuperNEMO, KamLAND-Zen and EXO (^{136}Xe), AMoRE and MOON (^{100}Mo), COBRA (^{116}Cd), CANDLES (^{48}Ca). The experiments listed above are aiming to probe the QD and IO ranges of $m_{\beta\beta}$.

1.3 Thesis outline

In this Thesis I aim to investigate two realizations of physics beyond the SM. In the first part we will discuss a possible way to predict the mixing patterns that we observe in Na-

ture, in particular the smallness of θ_{13} . In the second part we want to discuss how models of New Physics (NP) could modify the oscillation phenomenon.

The Thesis is organized as follow:

- In **Chapter 2** we will discuss the prediction based on the so-called *Generalized CP symmetry* combined with non-abelian discrete symmetry. We assume $A_5 \otimes CP$ as a symmetry in the full leptonic sector. Under such an assumption it is possible to predict the mixing angles and to obtain sum rules among the oscillation parameters as a function of one real degree of freedom, thus predictive patterns are testable at current and future neutrino facilities.
- **Chapter 3** is a one step further with respect to Chapter 2. In fact we will introduce several explicit realizations of the model based on $A_5 \otimes CP$ that give us the possibility to explore the mass spectrum and obtain prediction for observables as the Majorana effective mass for the $0\nu\beta\beta$ -decay. In particular we will show many realizations where testable relations among mixing angles and the mass spectrum exist.
- In **Chapter 4** we will discuss two extension of the Standard Model, namely the *Large Extra Dimensions* and *Non-Standard Neutrino Interactions*, that modify the oscillation probabilities with respect to the SM. We investigate the effects of NP at the Daya Bay and T2K experiments. We will show how NP could modify our knowledge on the SM oscillation parameters and we will put bounds on the NP parameters.
- In **Chapter 5** we will summarize the results obtained and draw our conclusions.

2

Lepton Mixing from $A_5 \otimes CP$

A possible tool to predict the mixing pattern that we observe in Nature in the leptonic sector is the one based on flavour symmetry, see Refs. [67–69], as well as [70], for reviews on this topic. As it has been discussed in several details in the literature a framework where the mismatch between neutrino and charged lepton mass matrices is associated with the non-trivial breaking of a flavour symmetry is quite interesting and predictive. In particular, in our approach, we use non-abelian discrete symmetry combined with CP as discussed in Refs. [71, 72]. This approach has already been studied for several symmetries: A_4 [71, 73], S_4 [74, 75], T' [76], $\Sigma(36 \times 3)$ [77], $\Delta(48)$ [78], $\Delta(96)$ [79] as well as $\Delta(3n^2)$, [80], and $\Delta(6n^2)$, [80–82], $D_{9n,3n}^{(1)}$ [83], with general $n \in \mathbb{N}$. For a recent review see Ref. [84].

In our study, fully presented in Ref. [85], we assume the non-abelian discrete group A_5 and CP as a symmetry in the full leptonic sector, and we found that four mixing patterns accommodate well the observed values of the mixing angles, which means that the angles are in the 3σ allowed range. Similar results were obtained in Refs. [86, 87].

The Chapter is organized as follows: in Sec. 2.1 we discuss the assumptions of lepton mixing obtained from non-abelian discrete symmetries and we show the simplest examples: the tri-bimaximal and bimaximal mixing patterns. In Sec. 2.2 we discuss the properties of the group A_5 as well as the predictions for the mixing angles in the case of no CP symmetry in the leptonic sector. In Sec. 2.3 we recapitulate the approach with CP symmetry and non-abelian discrete symmetry and in Sec. 2.4 we discuss the analytical patterns assuming $A_5 \otimes CP$ that are in agreement with the experimental data. In the last Sec. 2.5, we discuss the numerical results and the expected improvement at future neutrino facilities.

2.1 Lepton mixing from discrete symmetry

We can obtain the leptonic mixing matrix U_{PMNS} from symmetry consideration using the fact that the full flavour symmetry group in the lepton sector \mathcal{G}_f has a different symmetry subgroups for the neutrino sector, \mathcal{G}_ν , and the charged leptonic sector, \mathcal{G}_ℓ , see Fig. 2.1 for a pictorial representation. This procedure was used assuming several non-abelian discrete groups (further details about non-abelian discrete symmetries are discussed in Appendix B). For Majorana neutrinos the use of non-abelian and discrete symmetry subgroups of $SU(3)$ and $U(3)$ have shown that symmetries giving rise to mixing angles that are in agreement with experimental observations [88]. For instance, the groups A_4 , S_4 and T'

are commonly utilized to generate tri-bimaximal (TBM) mixing [89–91]; the group S_4 can also be used to generate bimaximal (BM) mixing [92–94]; A_5 can be utilized to generate golden ratio (GR) mixing [95–98], we will discuss in details this scenario in Sec. 2.2.2; and the groups D_{10} and D_{12} can lead to another type of GR [99, 100] and hexagonal (HG) mixing [101, 102].

We assume

$$\mathcal{G}_\ell \subset \mathcal{G}_f \quad \mathcal{G}_\nu \subset \mathcal{G}_f \quad \mathcal{G}_\ell \cap \mathcal{G}_\nu = \emptyset. \quad (2.1)$$

Assuming that the neutrinos are Majorana particles we can write the action of the elements of the subgroups of \mathcal{G}_f on the mass matrix as ¹

$$Q^\dagger M_\ell^\dagger M_\ell Q = M_\ell^\dagger M_\ell \quad Q \in \mathcal{G}_\ell \quad (2.2a)$$

$$Z^T M_\nu Z = M_\nu \quad Z \in \mathcal{G}_\nu \quad (2.2b)$$

where in the second equation we used the fact that the neutrinos are Majorana particles. For Dirac neutrinos

$$Z^\dagger M_\nu^\dagger M_\nu Z = M_\nu^\dagger M_\nu \quad Z \in \mathcal{G}_\nu. \quad (2.3)$$

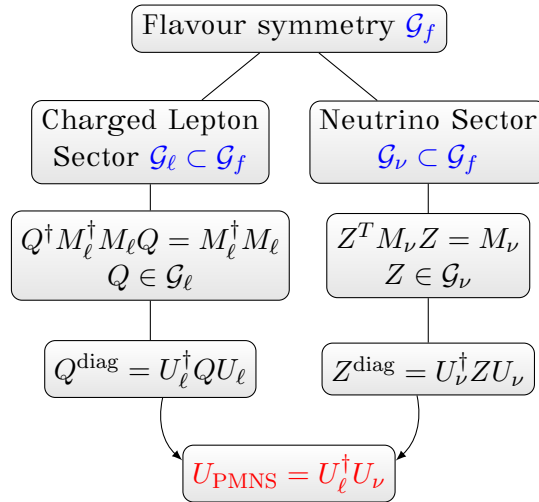


Figure 2.1: Representative scheme of the approach used in this Section, see text for further details. For a similar procedure see Ref. [103].

The maximal invariance group of the neutrino mass matrix which leave the neutrino masses unconstrained is the Klein group $V = Z_2 \otimes Z_2$ [104–107]. The charged leptonic subgroup \mathcal{G}_ℓ is assumed in general as a direct product of cyclic groups $Z_{m_1} \otimes Z_{m_2} \otimes \dots \otimes Z_{m_p}$. We discard residual non-abelian symmetry because their character would result in a complete, or partial degeneracy, of the mass spectrum, and thus it is incompatible with the current data on charged lepton masses. For the same reason we assume that $Z \in \mathcal{G}_\nu$ decomposes into three inequivalent representations under \mathcal{G}_ℓ .

If we diagonalize the mass matrices, using (2.2), we can also rotate the group elements Q and Z through unitary matrices as

$$Q^{\text{diag}} = U_\ell^\dagger Q U_\ell \quad (2.4a)$$

$$Z^{\text{diag}} = U_\nu^\dagger Z U_\nu \quad (2.4b)$$

¹The charged lepton mass matrix M_ℓ is given in the right-left basis.

because both \mathcal{G}_ℓ and \mathcal{G}_ν are abelian. The lepton mixing originates then from the mismatch of the embedding of \mathcal{G}_ℓ and \mathcal{G}_ν into \mathcal{G}_f . The matrices U_ℓ and U_ν are determined uniquely up to diagonal unitary matrices $K_{\ell,\nu}$ and permutation matrices $P_{\ell,\nu}$, respectively

$$U_\ell \longrightarrow U_\ell P_\ell K_\ell \quad (2.5a)$$

$$U_\nu \longrightarrow U_\nu P_\nu K_\nu. \quad (2.5b)$$

Thus the lepton mixing matrix U_{PMNS} is, up to Majorana phases and permutations of rows and columns

$$U_{\text{PMNS}} = U_\ell^\dagger U_\nu. \quad (2.6)$$

The mixing matrix U_{PMNS} is thus determined through \mathcal{G}_ℓ and \mathcal{G}_ν and their relative embedding into \mathcal{G}_f . However, it is determined only up to exchanges of rows and columns, because we do not predict lepton masses in this approach. Hence, the mixing angles are fixed up to a small number of degeneracies, associated with these possible exchanges. Also the Dirac CP phase δ is determined up to a factor π , if the exchange of rows and columns is taken into account. At the same time, Majorana phases cannot be predicted, because they are related to the eigenvalues of the matrix M_ν which remain unconstrained in this framework. Our conventions to extract the mixing angles and the CP phases are discussed in Appendix D.

2.1.1 TBM and BM from discrete symmetries

The two most famous mixing patterns based on a non-abelian discrete symmetry are BM and TBM. These can be obtained from $\mathcal{G}_f = S_4$, which is the symmetric group of degree four, additional details are discussed in Appendix B.3. In the following we do not want to discuss all the features of S_4 , however some basic facts are needed to construct the mixing patterns. The generators S and T satisfy the algebra

$$S^2 = T^4 = (ST)^3 = \mathbb{1}. \quad (2.7)$$

A possible choice for the three dimensional generators is

$$S = \frac{1}{2} \begin{pmatrix} 0 & \sqrt{2} & \sqrt{2} \\ \sqrt{2} & -1 & 1 \\ \sqrt{2} & 1 & -1 \end{pmatrix} \quad T = \begin{pmatrix} 1 & 0 & 0 \\ 0 & e^{i\pi/2} & 0 \\ 0 & 0 & e^{i3\pi/2} \end{pmatrix}. \quad (2.8)$$

The group S_4 contains another three dimensional representation, the generators are related to those in (2.8) with $\{S, T\} \rightarrow \{-S, -T\}$, see (2.7). The abelian subgroups of S_4 are: four Klein groups V , four Z_3 groups and three different Z_4 . These are summarized in Tab. 2.1.

Z_4		Z_3		V	
Algebra	Generators	Algebra	Generators	Algebra	Generators
Q_1	T	C_1	ST	K_1	$\{T^2, ST^2S\}$
Q_2	T^2S	C_2	TS	K_2	$\{S, T^2ST^2\}$
Q_3	STS	C_3	T^2ST	K_3	$\{T^2, ST^2ST\}$
		C_4	TST^2	K_4	$\{ST^2S, T^3ST\}$

Table 2.1: Possible independent algebras of S_4 subgroups. This is the same classification adopted in Ref. [108].

- $\mathcal{G}_\ell = Z_3$ and $\mathcal{G}_\nu = V$

Using these subgroups we could obtain only TBM. We assume $C_3 \in Z_3$ and $K_1 \in V$ as representative algebra. The absolute value of the PMNS matrix is

$$\|U_{\text{PMNS}}\| = U_{\text{TBM}} = \frac{1}{\sqrt{6}} \begin{pmatrix} 2 & \sqrt{2} & 0 \\ 1 & \sqrt{2} & \sqrt{3} \\ 1 & \sqrt{2} & \sqrt{3} \end{pmatrix} \quad (2.9)$$

and thus the mixing parameters are $\sin^2 \theta_{23} = 1/2$, $\sin^2 \theta_{12} = 1/3$ and a vanishing reactor angle θ_{13} . Thus also the Jarlskog invariant J_{CP} [109], defined in Eq. (D.2), is zero. To obtain a realistic mixing pattern with $\theta_{13} \sim 9^\circ$ from the TBM pattern we need to include large corrections from higher dimensional operators. The TBM solar angle (as well as the GR one) is shown in Fig. 2.3 with the allowed experimental value obtained in global analysis of the neutrino oscillation parameters of Refs. [45, 47, 110].

- $\mathcal{G}_\ell = Z_4$ and $\mathcal{G}_\nu = V$

In this case only a unique mixing pattern is possible, the BM one. The absolute value of the matrix elements of PMNS matrix is

$$\|U_{\text{PMNS}}\| = U_{\text{BM}} = \frac{1}{2} \begin{pmatrix} \sqrt{2} & \sqrt{2} & 0 \\ 1 & 1 & \sqrt{3} \\ 1 & 1 & \sqrt{3} \end{pmatrix} \quad (2.10)$$

therefore both θ_{12} and θ_{23} are maximal. Large corrections are needed also to accommodate well the solar angle, thus NLO corrections should have the same order of magnitude of the Cabibbo angle, as discussed in Ref. [111].

- $\mathcal{G}_\ell = V$ and $\mathcal{G}_\nu = V$

This case, discussed in Ref. [112], produces a BM mixing pattern and thus $\|U_{\text{PMNS}}\|$ is the same as (2.10). A representative choice for the subalgebras for \mathcal{G}_ℓ is K_1 and for \mathcal{G}_ν is K_2 .

2.2 Group A_5

The group A_5 is a non-abelian discrete group of even permutations on five elements [67]. It is the symmetry group of the icosahedron, which its net graph is shown in Fig. 2.2. The A_5 elements correspond to all the proper rotations of the icosahedron. Such rotations are classified into five types, that is, the 0 rotation (identity), π rotations about the midpoint of each edge, rotations by $2\pi/3$ about axes through the center of each face, and rotations by $2\pi/5$ and $4\pi/5$ about an axis through each vertex.

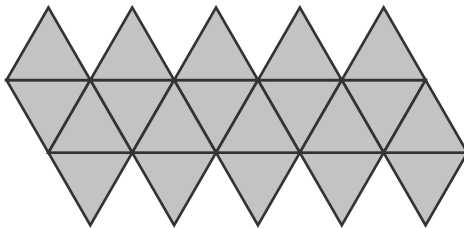


Figure 2.2: Net graphs of icosahedron. The elements of A_5 can be interpreted as rotations in this space. See the main text for further details.

The group A_5 has 60 elements that can be grouped into five conjugacy class with 1, 12, 12, 15

and 20 elements. The characters of A_5 are collected in Tab. 2.2 where φ is the Golden Ratio, defined as

$$\varphi \equiv \frac{1 + \sqrt{5}}{2} \simeq 1.618 \quad (2.11)$$

which is the solution of the equation $\varphi^2 - \varphi - 1 = 0$.²

A_5	C_1	$12C_2^{[5]}$	$12C_3^{[5]}$	$15C_4^{[2]}$	$20C_5^{[3]}$
$\chi^{[1]}$	1	1	1	1	1
$\chi^{[3]}$	3	φ	$1 - \varphi$	-1	0
$\chi^{[3']}$	3	$1 - \varphi$	φ	-1	0
$\chi^{[4]}$	4	-1	-1	0	1
$\chi^{[5]}$	5	0	0	-1	-1

Table 2.2: Characters of the A_5 group.

The group A_5 has two generators S and T which satisfy the following algebra

$$S^2 = T^5 = (ST)^3 = 1. \quad (2.12)$$

The rules $S^2 = (ST)^3 = 1$ are the same as Modular Group Γ_5 [108]. In the context of particle physics the A_5 group is used to describe the symmetry of leptonic sector. The predictions based on A_5 are often called *Golden Ratio* [95–98].

The irreducible representations of A_5 are one singlet $\mathbf{1}$, two triplets $\mathbf{3}$ and $\mathbf{3}'$, one quadruplet $\mathbf{4}$ and one quintuplet $\mathbf{5}$. In the three dimensional representation $\mathbf{3}$ we use the same convention of Ref. [108] for the matrices S and T , where T is a diagonal matrix:

$$S = \frac{1}{\sqrt{5}} \begin{pmatrix} 1 & \sqrt{2} & \sqrt{2} \\ \sqrt{2} & -\varphi & 1/\varphi \\ \sqrt{2} & 1/\varphi & -\varphi \end{pmatrix} \quad T = \begin{pmatrix} 1 & 0 & 0 \\ 0 & e^{2\pi i/5} & 0 \\ 0 & 0 & e^{8\pi i/5} \end{pmatrix} \quad (2.13)$$

The generators in $\mathbf{3}'$ are easily obtained from S and T defined in (2.13) by using the combination $T^2ST^3ST^2$ and T^2 as generators. This shows immediately that the set of all matrices describing the representations $\mathbf{3}$ and $\mathbf{3}'$ is the same and thus all conclusions obtained for mixing patterns derived for the representation $\mathbf{3}$ hold also for $\mathbf{3}'$ and thus, without loss of generality, we assume in the following analysis that Left Handed (LH) leptons transform as $\mathbf{3}$ of A_5 . For the sake of completeness we report the explicit form of the generator in the $\mathbf{3}'$ representation

$$S = -\frac{1}{\sqrt{5}} \begin{pmatrix} 1 & \sqrt{2} & \sqrt{2} \\ \sqrt{2} & 1/\varphi & -\varphi \\ \sqrt{2} & -\varphi & 1/\varphi \end{pmatrix} \quad T = \begin{pmatrix} 1 & 0 & 0 \\ 0 & e^{4\pi i/5} & 0 \\ 0 & 0 & e^{-4\pi i/5} \end{pmatrix}. \quad (2.14)$$

The other representations admit a basis where T is diagonal, as discussed in Ref. [98]. For the representation $\mathbf{4}$ we have

$$S = -\frac{1}{5} \begin{pmatrix} -\sqrt{5} & \varphi - 3 & \varphi + 2 & -\sqrt{5} \\ \varphi - 3 & \sqrt{5} & \sqrt{5} & \varphi + 2 \\ \varphi + 2 & \sqrt{5} & \sqrt{5} & \varphi - 3 \\ -\sqrt{5} & \varphi + 2 & \varphi - 3 & -\sqrt{5} \end{pmatrix} \quad T = \begin{pmatrix} e^{2\pi i/5} & 0 & 0 & 0 \\ 0 & e^{4\pi i/5} & 0 & 0 \\ 0 & 0 & e^{6\pi i/5} & 0 \\ 0 & 0 & 0 & e^{8\pi i/5} \end{pmatrix} \quad (2.15)$$

²Note that the Golden Ratio has many interesting properties. In particular we use the property $\varphi^{n+2} = \varphi^{n+1} + \varphi^n$ with $n \in \mathbb{Z}$ and $n \geq -1$, that implies $\varphi^{-1} = \varphi - 1 \simeq 0.618$.

and for $\mathbf{5}$

$$S = \frac{1}{5} \begin{pmatrix} -1 & \sqrt{6} & -\sqrt{6} & -\sqrt{6} & -\sqrt{6} \\ \sqrt{6} & 2-\varphi & 2\varphi & 2(1-\varphi) & -(1+\varphi) \\ -\sqrt{6} & 2\varphi & 1+\varphi & 2-\varphi & 2(\varphi-1) \\ -\sqrt{6} & 2(1-\varphi) & 2-\varphi & 1+\varphi & -2\varphi \\ -\sqrt{6} & -(1+\varphi) & 2(\varphi-1) & -2\varphi & 2-\varphi \end{pmatrix} T = \begin{pmatrix} 1 & 0 & 0 & 0 & 0 \\ 0 & e^{2\pi i/5} & 0 & 0 & 0 \\ 0 & 0 & e^{4\pi i/5} & 0 & 0 \\ 0 & 0 & 0 & e^{6\pi i/5} & 0 \\ 0 & 0 & 0 & 0 & e^{8\pi i/5} \end{pmatrix}. \quad (2.16)$$

The Kronecker products of A_5 are

$$\mathbf{3} \otimes \mathbf{3} = \mathbf{1}_s \oplus \mathbf{3}_a \oplus \mathbf{5}_s \quad (2.17a)$$

$$\mathbf{3}' \otimes \mathbf{3}' = \mathbf{1}_s \oplus \mathbf{3}'_a \oplus \mathbf{5}_s \quad (2.17b)$$

$$\mathbf{3} \otimes \mathbf{3}' = \mathbf{4} \oplus \mathbf{5} \quad (2.17c)$$

$$\mathbf{3} \otimes \mathbf{4} = \mathbf{3}' \oplus \mathbf{4} \oplus \mathbf{5} \quad (2.17d)$$

$$\mathbf{3}' \otimes \mathbf{4} = \mathbf{3} \oplus \mathbf{4} \oplus \mathbf{5} \quad (2.17e)$$

$$\mathbf{3} \otimes \mathbf{5} = \mathbf{3} \oplus \mathbf{3}' \oplus \mathbf{4} \oplus \mathbf{5} \quad (2.17f)$$

$$\mathbf{3}' \otimes \mathbf{5} = \mathbf{3} \oplus \mathbf{3}' \oplus \mathbf{4} \oplus \mathbf{5} \quad (2.17g)$$

$$\mathbf{4} \otimes \mathbf{4} = \mathbf{1}_s \oplus \mathbf{3}_a \oplus \mathbf{3}'_a \oplus \mathbf{4}_s \oplus \mathbf{5}_s \quad (2.17h)$$

$$\mathbf{4} \otimes \mathbf{5} = \mathbf{3} \oplus \mathbf{3}' \oplus \mathbf{4} \oplus \mathbf{5}_1 \oplus \mathbf{5}_2 \quad (2.17i)$$

$$\mathbf{5} \otimes \mathbf{5} = \mathbf{1}_s \oplus \mathbf{3}_a \oplus \mathbf{3}'_a \oplus \mathbf{4}_a \oplus \mathbf{4}_s \oplus \mathbf{5}_{1,s} \oplus \mathbf{5}_{2,s} \quad (2.17j)$$

where the explicit formulae are reported in the Appendix C. Notice that the Clebsch-Gordan coefficient are defined using a coherent transformation under CP , therefore they are different with respect to the definition of Ref. [98] (another basis is discussed in Ref. [113]). This feature is discussed in more details in Chapter 3 where several realizations of $A_5 \otimes CP$ are given.

2.2.1 Subgroups of A_5

The subgroups of A_5 that are relevant in our analysis are Z_2, Z_3, Z_5 and V , where V is the Klein group, defined as $V = Z_2 \otimes Z_2$.³ The elements of each subgroups can be generated using the representations of the generators of A_5 . We used a brutal force approach, in which we have generated all matrices M in the form

$$M = \prod_{k=1}^6 S^{s_k} T^{t_k} \quad s_k = 0, 1; \quad t_k = 0, 1, \dots, 4 \quad (2.18)$$

where we used the fact that the generators satisfy the algebra defined in (2.12), thus not all choices for s_k and t_k are possible. Hence we isolate only the matrices that satisfy the subgroups algebras and are independent to each others.⁴ We check our results using Ref. [108] and the website WikiGroup. All results are summarized in Tab. 2.3.

2.2.2 Golden Ratio Predictions

Using the results of Section 2.1 and the classification of A_5 subgroups in Tab. 2.3 we can find the PMNS mixing matrix in a simple way. Models based on A_5 are already discussed in literature [97, 98, 108, 112–115].

Our conventions for the PMNS matrix and the way to extract mixing angles and CP invariants are discussed in Appendix D.

³It is possible to have the subgroup Z_4 but its elements are equivalents to those of Z_2 .

⁴Notice that if M is such that $M^q = \mathbb{1}$ also M^p and $1^{1/q}M$ satisfy the same Z_q subalgebras for all values of p .

Z_5		Z_2		Z_3		V	
Algebra	Generators	Algebra	Generators	Algebra	Generators	Algebra	Generators
R_1	T	S_1	S	C_1	ST	K_1	$\{S, T^2ST^3ST^2\}$
R_2	ST^2	S_2	TST^4	C_2	TS	K_2	$\{T^4ST, ST^3ST^2S\}$
R_3	T^2S	S_3	T^2ST^3	C_3	TST^3	K_3	$\{TST^4, ST^2ST^3S\}$
R_4	TST	S_4	T^3ST^2	C_4	T^2ST^2	K_4	$\{T^2ST^2, ST^2ST\}$
R_5	TST^2	S_5	T^4ST	C_5	T^3ST	K_5	$\{T^3ST^2, TST^2S\}$
R_6	T^2ST	S_6	ST^2ST	C_6	ST^3ST		
		S_7	ST^3ST^4	C_7	ST^2ST^3		
		S_8	TST^3ST^3	C_8	ST^3ST^2		
		S_9	$T^2ST^3ST^2$	C_9	ST^2ST^4		
		S_{10}	T^3ST^3ST	C_{10}	ST^2ST^2S		
		S_{11}	ST^2ST^3S				
		S_{12}	ST^2ST^3ST				
		S_{13}	$ST^2ST^3ST^2$				
		S_{14}	$ST^2ST^3ST^3$				
		S_{15}	$ST^2ST^3ST^4$				

Table 2.3: Possible independent algebras of A_5 subgroups. This is exactly the same classification adopted in Ref. [108].

- $\mathcal{G}_\ell = Z_5$ and $\mathcal{G}_\nu = V$

In each realization of $\mathcal{G}_\ell = Z_5$ and $\mathcal{G}_\nu = V$ we find the same absolute values of the PMNS matrix. A representation of the Z_5 residual symmetry can be chosen diagonal, thus $U_{\text{PMNS}} = U_\nu$. We get

$$\|U_{\text{PMNS}}\| = \begin{pmatrix} \cos \phi & \sin \phi & 0 \\ \sin \phi / \sqrt{2} & \cos \phi / \sqrt{2} & 1 / \sqrt{2} \\ \sin \phi / \sqrt{2} & \cos \phi / \sqrt{2} & 1 / \sqrt{2} \end{pmatrix} \simeq \begin{pmatrix} 0.851 & 0.526 & 0 \\ 0.372 & 0.602 & 0.707 \\ 0.372 & 0.602 & 0.707 \end{pmatrix} \quad (2.19)$$

where we have defined $\tan \phi \equiv \varphi^{-1} = \varphi - 1 \simeq 0.618$. We find a vanishing reactor angle θ_{13} and a maximal atmospheric angle θ_{23} with $\sin^2 \theta_{12} \simeq 0.276$, as discussed in details in Refs. [97, 98, 113]. The Jarlskog invariant $J_{\text{CP}} = 0$, thus the Dirac phase is trivial, zero or π . Notice that moderate correction to the mixing angles θ_{12} and θ_{13} obtained at Leading Order (LO) are necessary in order to achieve a good agreement with the experimental measurements. In Fig. 2.3 we compare the prediction for $\sin^2 \theta_{12}$, as well as the TBM quoted in (2.9), in the allowed region for the solar angle obtained from the global analysis on neutrino oscillation.

- $\mathcal{G}_\ell = Z_3$ and $\mathcal{G}_\nu = V$

If we choose $\mathcal{G}_\ell = Z_3$ and $\mathcal{G}_\nu = V$ we get a unique pattern for the PMNS matrix. In fact only for (C_1, K_1) we get as the total group A_5 and not a subgroup. These subgroups give us the absolute value for the PMNS matrix, discussed in Ref. [112]

$$\|U_{\text{PMNS}}\| = \frac{1}{\sqrt{6}} \begin{pmatrix} \sqrt{2}\varphi & \sqrt{2}/\varphi & 0 \\ 1/\varphi & \varphi & \sqrt{3} \\ 1/\varphi & \varphi & \sqrt{3} \end{pmatrix} \simeq \begin{pmatrix} 0.934 & 0.357 & 0 \\ 0.252 & 0.661 & 0.707 \\ 0.252 & 0.661 & 0.707 \end{pmatrix}. \quad (2.20)$$

In this case for the solar mixing angle we get $\sin^2 \theta_{12} = (2 - \varphi)/3 \simeq 0.127$ which is excluded at more than 3σ CL. This means that we need large corrections in order to match the experimental best fit values. Since $\theta_{13} = 0$ we also get $J_{\text{CP}} = 0$ and δ trivial.

- $\mathcal{G}_\ell = V$ and $\mathcal{G}_\nu = V$

The last possibility is $\mathcal{G}_\ell = V$ and $\mathcal{G}_\nu = V$. In this case the unique mixing pattern is given for (K_i, K_j) and $i \neq j$, in fact for $i = j$ the PMNS is trivial, *i.e.* $U_{\text{PMNS}} = \mathbb{1}$. This pattern is discussed in Ref. [108]. The absolute value of the PMNS matrix is

$$\|U_{\text{PMNS}}\| = \frac{1}{2} \begin{pmatrix} \varphi & 1 & 1/\varphi \\ 1/\varphi & \varphi & 1 \\ 1 & 1/\varphi & \varphi \end{pmatrix} \simeq \begin{pmatrix} 0.809 & 0.500 & 0.309 \\ 0.309 & 0.809 & 0.500 \\ 0.500 & 0.309 & 0.809 \end{pmatrix}. \quad (2.21)$$

We can extract the mixing angle from U_{PMNS} , in this case $\sin^2 \theta_{12} = \sin^2 \theta_{23} = (3 - \varphi)/5 \simeq 0.276$ that are excluded at more than 2σ CL and $\sin^2 \theta_{13} = (2 - \varphi)/4 \simeq 0.095$. However it is possible to have another pattern for the PMNS matrix if we exchange the second and the third row. In this case we get $\sin^2 \theta_{23} = (2 + \varphi)/5 \simeq 1 - 0.276 = 0.724$ and thus we expect large corrections to the LO predictions to make the model viable.

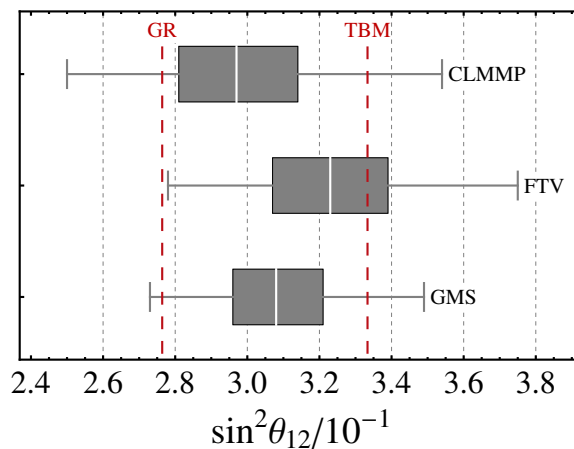


Figure 2.3: Predictions for $\sin^2 \theta_{12}$ for GR and TBM mixing patterns (red dashed lines) where the box charts represent the value of the global fits (we show the results for NO since the allowed region is the same for both orderings) performed in Ref. [46] (labeled as CLMMP), Ref. [47] (labeled as FTV) and Ref. [45] (labeled as GMS). The white lines are the best fit values, the grey boxes the 1σ confidence regions and the grey lines the 3σ allowed regions.

2.3 CP invariance

If we assume CP invariance in the neutrino sector, as discussed in Ref. [71, 72, 116] and [117], we can introduce a continuous parameter θ that could modify the pure A_5 prediction discussed above in Sec. 2.2.2.

We start our discussion considering a generic symmetry group \mathcal{G}_f , as done in Section 2.1. We assume that the residual symmetry in the charged sector \mathcal{G}_ℓ is, in general, a direct product of cyclic symmetry $Z_{m_1} \otimes Z_{m_2} \otimes \dots \otimes Z_{m_p}$, as in Sec. 2.1. The CP symmetry acts on the neutrino sector, but we can discuss in general the action on the field space, see Refs. [118–120]. Under a CP symmetry a generic field Φ transforms as

$$\Phi(x) \longrightarrow \Phi'(x) = X\Phi^*(x_{CP}) \quad (2.22)$$

where X is the representations of the CP operator in field space and x_{CP} is the space-time coordinate transformed under the usual CP transformation $x \rightarrow x_{CP} = (x^0, -\mathbf{x})$. The invariance of the field under \mathcal{G}_f is expressed as

$$\Phi(x) \longrightarrow \Phi'(x) = A\Phi(x) \quad (2.23)$$

where A is an element of the non-abelian discrete symmetry that we are considering. The X can be chosen as a constant unitary symmetric matrix

$$XX^\dagger = XX^* = \mathbb{1}. \quad (2.24)$$

In this way the square of the CP transformation is the identity, $X^2 = \mathbb{1}$. The action of X on the mass matrices, before the symmetry breaking, is

$$X^* M_\ell^\dagger M_\ell X = (M_\ell^\dagger M_\ell)^* \quad (2.25a)$$

$$X M_\nu X = M_\nu^* \quad (2.25b)$$

if neutrinos are Majorana particles. If neutrino are Dirac particles (2.25b) has to be changed into

$$X^* M_\nu^\dagger M_\nu X = (M_\nu^\dagger M_\nu)^* \quad (2.26)$$

The fact that the theory is invariant under some group of flavour symmetry \mathcal{G}_f requires that for the generators of the group A the representations X in the field space must satisfy the following relation

$$(X^{-1}AX)^* = A' \quad A, A' \in \text{Alg}\{\mathcal{G}_f\} \quad (2.27)$$

where in general $A \neq A'$. In A_5 we find that that $A = A'$, so the transformation defined in (2.27) is an isomorphism, see Sec. 2.3.3 for further details. Notice that if X is a solution of (2.24) and (2.27) also $e^{i\rho}X$, with $\rho \in \mathbb{R}$ an arbitrary phase, is a solution. At the same time, it is always possible to find the trivial solution of the problem $X = \mathbb{1}$.

If we perform a change of basis with an unitary matrix Ω in the field space

$$\Phi \longrightarrow \tilde{\Phi} = \Omega^\dagger \Phi \quad (2.28)$$

the unitary matrix X and the generator A transform as

$$X \longrightarrow \tilde{X} = \Omega^\dagger X \Omega^* \quad (2.29a)$$

$$A \longrightarrow \tilde{A} = \Omega^\dagger A \Omega \quad (2.29b)$$

as a consequence of (2.22) and (2.23). The constraints (2.24) and (2.27), applied on X , are covariant under the Ω transformation, *i.e.* also \tilde{X} fulfills the same conditions. A change of basis can be useful in order to reach a basis in which the action of some elements of \mathcal{G}_f or the CP transformation is simple. For example we can use the fact that any unitary symmetric matrix X can be written as the product

$$X = \Omega \Omega^T \quad (2.30)$$

of a unitary matrix Ω in order to go to a basis in which the action of CP is canonical, *i.e.* $\tilde{X} = \mathbb{1}$.

2.3.1 Neutrino sector invariant under $Z_2 \otimes CP$

In the following we consider the case in which the residual symmetry \mathcal{G}_ν is $Z_2 \otimes CP$. This allows us to determine all physical phases and mixing angles in terms of one real parameter θ . A small mixing reactor angle θ_{13} , as well with the solar and atmospheric angles in the observed range, can then be found by an appropriate choice of the parameter θ and further relations among the PMNS parameters are predicted. Such correlations can be testable at future neutrino facilities [121–124]. Once the flavour group \mathcal{G}_f has been chosen, several independent definitions of CP are in general allowed (as discussed above), leading to physically distinct results.

We explain the general setup and show the form of the lepton mixing matrix. We assume that \mathcal{G}_f contains as subgroup Z_2 and we denote as Z the representation of the operator in the field space, therefore $Z^2 = \mathbb{1}$. In order to define the group $Z_2 \otimes CP$ we need to impose the constraint

$$XZ^* - ZX = 0. \quad (2.31)$$

This condition is invariant under the covariance transformations defined in (2.29). Thus, it is always possible to go in the basis where Z is diagonal and X canonical, as defined in Eq. (2.30). In this basis we have

$$Z_c = \Omega^\dagger Z \Omega \quad Z_c = \text{diag}\left\{(-1)^{z_1}, (-1)^{z_2}, (-1)^{z_3}\right\} \quad (2.32)$$

with $z_i = 0, 1$ and two z_i being equal. These conditions have an important consequence for the form of the light Majorana neutrino mass matrix. In fact it has to satisfy the following conditions

$$Z^T M_\nu Z = M_\nu \quad (2.33a)$$

$$X M_\nu X = M_\nu^*. \quad (2.33b)$$

Applying the basis transformation induced by the unitary matrix Ω , defined in (2.30), we see that the combination $\Omega^T M_\nu \Omega$ is constrained to be block-diagonal and real. Thus this matrix can be diagonalized using a rotation in the ij -plane of degenerate eigenvalues of Z by a rotation matrix $R_{ij}(\theta)$. We define three possible matrices

$$R_{12}(\theta) = \begin{pmatrix} \cos \theta & \sin \theta & 0 \\ -\sin \theta & \cos \theta & 0 \\ 0 & 0 & 1 \end{pmatrix} \quad (2.34a)$$

$$R_{13}(\theta) = \begin{pmatrix} \cos \theta & 0 & \sin \theta \\ 0 & 1 & 0 \\ -\sin \theta & 0 & \cos \theta \end{pmatrix} \quad (2.34b)$$

$$R_{23}(\theta) = \begin{pmatrix} 1 & 0 & 0 \\ 0 & \cos \theta & \sin \theta \\ 0 & -\sin \theta & \cos \theta \end{pmatrix} \quad (2.34c)$$

where $\theta \in [0, \pi)$. The plane ij is determined by the subspace of $\Omega^\dagger Z \Omega$ which has degenerate eigenvalues, see Eq. (2.32).

We need also a diagonal matrix K_ν with elements equal to ± 1 or $\pm i$ in order to obtain positive neutrino masses. Without loss of generality we can write the matrix as

$$K_\nu = \text{diag}\left\{1, i^{k_1}, i^{k_2}\right\} \quad (2.35)$$

where $k_{1,2} = 0, 1, 2, 3$. In this way the matrix M_ν can be diagonalized with unitary matrix defined as

$$U_\nu \equiv \Omega R_{ij}(\theta) K_\nu. \quad (2.36)$$

The mass spectrum is not fixed and thus permutations of the columns of U_ν are admitted.

The residual symmetry in the charged leptonic sector is \mathcal{G}_ℓ . The situation is equal of no CP symmetry, as discussed in Sec. 2.1. For Q being a realization of the generator of \mathcal{G}_ℓ in the representation $\mathbf{3} \in \mathcal{G}_f$ we know that the combination $M_\ell^\dagger M_\ell$ fulfills the relation

$$Q^\dagger M_\ell^\dagger M_\ell Q = M_\ell^\dagger M_\ell. \quad (2.37)$$

For non-degenerate eigenvalues of Q the unitary matrix U_ℓ which diagonalizes Q can be found, up to permutations of its columns and overall phases of each column, by the condition

$$U_\ell^\dagger Q U_\ell = Q^{\text{diag}}. \quad (2.38)$$

Given (2.37) the matrix U_ℓ also diagonalizes the product $M_\ell^\dagger M_\ell$, thus

$$(U_\ell^\dagger M_\ell^\dagger M_\ell U_\ell)_{ij} = \pi^{ijk} m_k^2 \quad (2.39)$$

where π^{ijk} is the permutation of three elements and $k = e, \mu, \tau$. The fact that the lepton masses are not fixed in this approach is reflected by the possible permutations of columns of U_ℓ .

The PMNS matrix is given by the misalignment between the residual symmetries in the charged and neutrino sector

$$U_{\text{PMNS}} \equiv U_\ell^\dagger U_\nu = U_\ell \Omega R_{ij}(\theta) K_\nu \quad (2.40)$$

up to unphysical phases and permutation of rows and columns. Therefore in our analysis we always consider $6 \times 6 = 36$ possible permutation of rows and columns for a given combination (Q, Z, X) . A scheme of the methodology used in the case of CP symmetry is shown in Fig. 2.4.

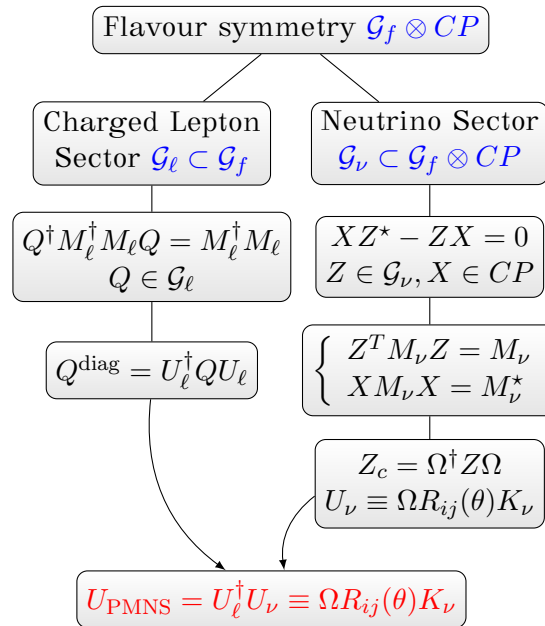


Figure 2.4: Representative scheme of the approach used in this Section, see text for further details.

We expect that one of the PMNS columns is fixed, *i.e.* it does not contain θ , because the rotation $R_{ij}(\theta)$ acts in a subspace of the flavour space. We also notice that the formulae (2.24) and (2.31) are covariant under the basis transformation defined by the unitary matrix $\tilde{\Omega}$, thus the matrices

$$\tilde{Z} = \tilde{\Omega}^\dagger Z \tilde{\Omega} \quad \tilde{X} = \tilde{\Omega}^\dagger X \tilde{\Omega}^* \quad (2.41)$$

satisfy the condition defined in (2.24) and (2.31). If we also change the generator of \mathcal{G}_ℓ in the same way

$$\tilde{Q} = \tilde{\Omega}^\dagger Q \tilde{\Omega} \quad (2.42)$$

we see that U_{PMNS} , defined in (2.40), does not change, since its result does not depend on the transformation $\tilde{\Omega}$. Thus both the triplets⁵ (Q, Z, X) and $(\tilde{Q}, \tilde{Z}, \tilde{X})$ related by $\tilde{\Omega}$ lead to the same results for lepton mixing. We use this property to reduce the number of independent patterns to study.

2.3.2 Accidental CP symmetry

Notice that there exists the possibility that an accidental CP symmetry is present, different from the CP transformation X that we impose in our theory. An accidental CP symmetry⁶ corresponds to a CP transformation Y (if it exists) which satisfies the conditions

$$Y^* M_\ell^\dagger M_\ell Y = (M_\ell^\dagger M_\ell)^* \quad (2.43a)$$

$$Y M_\nu Y = M_\nu^*. \quad (2.43b)$$

In this case all the CP phases α, β and δ of the PMNS matrix have to be trivial, 0 or π . If Y and M_ν fulfill the condition

$$Y^* M_\nu^\dagger M_\nu Y = (M_\nu^\dagger M_\nu)^* \quad (2.44)$$

only the Majorana phases are trivial, while the Dirac phase δ has to be 0 or π . Eq. (2.43a) implies [71]

$$QY - YQ^T = 0. \quad (2.45)$$

This conditions ensures that Y is diagonal in the same basis as Q , that is Y is diagonal in the charged lepton mass basis. Notice that if Y fulfills (2.45) also the quantity Y' satisfies the same condition, where Y' is defined as

$$Y' = Y \prod_{i \leq p} [Q_i^*]^{n_i} \quad 0 \leq n_i \leq m_i \quad (2.46)$$

where m_i is the dimension of one of the cyclic subgroup Z_{m_i} of \mathcal{G}_ℓ and $Q_i \in Z_{m_i}$, (2.43b) implies

$$YZ^* - ZY = 0 \quad (2.47a)$$

$$XY^* - YX^* = 0. \quad (2.47b)$$

Notice that the matrix Y is always diagonal and positive in the neutrino mass basis, thus

$$\tilde{Y} = U_\nu^\dagger Y U_\nu^* = \text{diag}\{y_1, y_2, y_3\} \quad (2.48)$$

where $y_j \in \mathbb{R}^+$. If only the equality in (2.44) holds it is sufficient that only (2.47a) is satisfied with the additional condition that \tilde{Y} is diagonal (2.48).

An accidental CP symmetry that is always present in the neutrino sector for a given transformation Z and X is the one represented by the additional CP transformation $Y = ZX$ that satisfies the condition defined in (2.24), (2.31) and (2.47).

2.3.3 CP transformation of A_5

We report the simplest representation of $X_{\mathbf{r}}$ in the case of group A_5 for a given representation \mathbf{r}

$$X_{\mathbf{1}} = 1 \quad (2.49a)$$

⁵In the following we refer to (Q, Z, X) as a *triplet* or *touple*.

⁶The accidental CP symmetry is similar to the baryonic number $U(1)_B$ in the Standard Model.

$$X_{\mathbf{3}} = P_{23} \quad (2.49b)$$

$$X_{\mathbf{3}'} = P_{23} \quad (2.49c)$$

$$X_{\mathbf{4}} = \begin{pmatrix} 0 & 0 & 0 & 1 \\ 0 & 0 & 1 & 0 \\ 0 & 1 & 0 & 0 \\ 1 & 0 & 0 & 0 \end{pmatrix} \quad (2.49d)$$

$$X_{\mathbf{5}} = \begin{pmatrix} 1 & 0 & 0 & 0 & 0 \\ 0 & 0 & 0 & 0 & -1 \\ 0 & 0 & 0 & 1 & 0 \\ 0 & 0 & 1 & 0 & 0 \\ 0 & -1 & 0 & 0 & 0 \end{pmatrix}. \quad (2.49e)$$

The matrix P_{23} is defined as

$$P_{23} = \begin{pmatrix} 1 & 0 & 0 \\ 0 & 0 & 1 \\ 0 & 1 & 0 \end{pmatrix}. \quad (2.50)$$

The matrix P_{23} represents the so called $\mu - \tau$ reflection symmetry [89, 90, 125, 126]. We may notice that the form of $X_{\mathbf{r}}$ is the same as the invariant contained in the product $\mathbf{r} \otimes \mathbf{r}$ in the flavour space. Using the explicit form of S and T in the representation \mathbf{r} we can check that

$$(X_{\mathbf{r}}^{-1} S_{\mathbf{r}} X_{\mathbf{r}})^* = S_{\mathbf{r}} \quad (2.51a)$$

$$(X_{\mathbf{r}}^{-1} T_{\mathbf{r}} X_{\mathbf{r}})^* = T_{\mathbf{r}} \quad (2.51b)$$

for all the irreducible representations of A_5 , therefore the CP transformations act as an inner automorphism on A_5 .

The form of CP transformations we consider is

$$X = ZX_0 \quad (2.52)$$

where Z is the matrix representative of a Z_2 generating element, $Z^2 = \mathbb{1}$. In general are possible sixteen different CP transformations. All of them are consistent with (2.24) and are the sixteen class-inverting involutive automorphisms of A_5 . We thus discuss all CP transformations that fulfill requirement in (2.24) and are consistently imposed in according to Ref. [116]. These properties, class-inverting and involutive, are given if the twisted Frobenius-Shur indicator $\epsilon_{\iota}(\mathbf{r})$ is +1 in all irreducible representations $\mathbf{r} \in A_5$. From the definition of the twisted Frobenius-Shur indicator in the case of A_5 we have

$$\epsilon_{\iota}(\mathbf{r}) \equiv \frac{1}{\dim\{A_5\}} \sum_{g \in A_5} \chi^{[\mathbf{r}]}(g^{\iota} g) \quad (2.53)$$

where $\chi^{[\mathbf{r}]}(g)$ is the character of the element g in representation \mathbf{r} , see Tab. 2.2, and g^{ι} the image of g under the action of the automorphism ι . We verify that $\epsilon_{\iota}(\mathbf{r}) = +1$ using the fact that if the statement is true then [127–129]

$$\sum_{\mathbf{r} \in A_5} \chi^{[\mathbf{r}]}(e) = \dim\{g \in A_5 \text{ such that } g^{\iota} = g^{-1}\} \quad (2.54)$$

where $\chi^{[\mathbf{r}]}(e)$ is the character of the neutral element in representation \mathbf{r} , thus we sum over the dimensions of all irreducible representations.

2.4 Classification

In this section we report the independent patterns for U_{PMNS} that we can obtain from the possible choice of the triplets (Q, Z, X) assuming $A_5 \otimes CP$ as a full symmetry in the leptonic sector. In particular we want to classify the relevant cases for the phenomenology using a gaussian χ^2 test based on the PMNS parameters extracted from Ref. [45]. This χ^2 is the sum of each mixing angle contribution χ_{ij}^2 . We use the following definition

$$\chi^2(\theta) \equiv \sum_{i \neq j} \chi_{ij}^2(\theta) = \sum_{i \neq j} \left[\frac{\sin^2 \theta_{ij}(\theta) - \sin^2 \theta_{ij}^{\text{exp}}}{\sigma_{ij}} \right]^2 \quad (2.55)$$

The way to extract mixing angles and CP phases from U_{PMNS} is discussed in Appendix D. We consider as interesting categories the triplets which satisfy the condition $\chi_{ij}^2 \leq 9$, *i.e.* the mixing angle θ_{ij} is in the 3σ confidence region, therefore the global minimum is such that $\chi_{\text{min}}^2 \leq 27$. We assume this number because we consider independent gaussian errors for each angle. We do not include the value of δ because the significance is lower than 3σ .

We report our numerical results in several tables, for the relevant categories of tuples (Q, Z, X) . The oscillation parameters are evaluated at the best fit values of θ , that we call θ_{bf} . Two results are reported, the left column is for NO, while the right one is for IO.

To obtain the PMNS matrix we use the following algorithm:

1. The matrix Z is involutory, so it is diagonalizable by a unitary matrix Ω_0 such that $\Omega_0^\dagger Z \Omega_0 = Z_c$.
2. The matrix $\Omega = \Omega_0 P$, where $P = \text{diag}\{e^{i\alpha}, e^{i\beta}, e^{i\gamma}\}$, can be found, up to permutations of columns, using the condition

$$\Omega^\dagger X \Omega^* = \mathbb{1} \quad (2.56)$$

which is equivalent to $\Omega \Omega^T = X$, but easier to compute because the equations for the phases α, β and γ are decoupled.

3. If no solutions can be found for Ω we need to rotate the degenerate subspace defined by the eigenvalues of Z_c with a unitary matrix $V_{ij}(\psi)$. We can find ψ using the non diagonal element of (2.56), imposing $(\Omega^\dagger X \Omega^*)_{13} = 0$.
4. We find the PMNS matrix as $U_{\text{PMNS}} = U_\ell^\dagger \Omega R_{ij}(\theta) K_\nu$, where U_ℓ is the matrix that diagonalizes Q . We extract the mixing parameters through the procedure defined in Appendix D. Then we perform the χ^2 test, defined in (2.55), using all possible permutations of rows and columns of U_{PMNS} to obtain θ_{bf} .

To extract the values of CP phases we use the invariant parameters J_{CP} , I_1 and I_2 , following the same conventions of Ref. [80]. The details are reported in Appendix D.

The independent categories that we study in details are summarize in Tab. 2.4 with the values of χ_{min}^2 for normal (left column) and inverted (right column) ordering. In particular using the similarity transformations, as discussed in (2.41) and (2.42), we find six independent categories for $Q \in Z_5$, described in Sec. 2.4.1, eight categories for $Q \in Z_3$, described in Sec. 2.4.2 and only four categories for $Q \in V = Z_2 \otimes Z_2$, described in Sec. 2.4.3.⁷

⁷We acknowledge Pietro Pugliese for the help to write a fast algorithm to check the independent tuples.

Notice that for each $Z \in Z_2$ we can choose four different values of X that satisfy the conditions (2.24), (2.27) and (2.31). It is easy to find that if Z is in the j -th Klein group, *i.e.* $Z = K_j^a$, the possible non trivial matrices X are in the form

$$X_j^{a,b} = K_j^b X_0 \quad (2.57)$$

where $a, b = 1, 2, 3$ and $j = 1, \dots, 5$.

Q	Z	X	χ_{\min}^2		Q	Z	X	χ_{\min}^2	
$Q \in Z_5$					$Q \in Z_3$				
R_1	S_1	X_0	14.08	17.83	C_4	S_1	X_0	$> 10^2$	$> 10^2$
R_1	S_2	X_0	$> 10^2$	$> 10^2$	C_4	S_2	X_0	$> 10^2$	$> 10^2$
R_1	S_3	X_0	4.04	7.74	C_4	S_3	X_0	$> 10^2$	$> 10^2$
R_1	S_3	$S_1 X_0$	5.64	3.46	C_4	S_4	X_0	8.84	12.57
R_1	S_2	$S_1 X_0$	$> 10^2$	$> 10^2$	C_4	S_1	$S_3 X_0$	$> 10^2$	$> 10^2$
R_1	S_1	$S_2 X_0$	42.18	49.96	C_4	S_2	$S_3 X_0$	$> 10^2$	$> 10^2$
					C_4	S_3	$S_1 X_0$	$> 10^2$	$> 10^2$
					C_4	S_4	$S_5 X_0$	$> 10^2$	$> 10^2$
$Q \in V = Z_2 \otimes Z_2$									
K_2	S_1	X_0	4.48	6.43	K_1	S_1	X_0	$> 10^2$	$> 10^2$
K_1	S_2	X_0	$> 10^2$	$> 10^2$	K_2	S_1	$S_3 X_0$	$> 10^2$	$> 10^2$

Table 2.4: Independent categories for the PMNS matrix with the value of χ_{\min}^2 for normal and inverted ordering. We highlight the realistic patterns with a green colour. The yellow patterns require Next-to-Leading Order (NLO) corrections to have all the mixing angles in the 3σ confidence region. The pink pattern for $Q \in Z_5$ does not fit well the mixing angles but it is interesting because it is related to TBM and BM while the pink one for $Q \in V$ has all non trivial CP invariants. We recall that the algebras are summarized in Tab. 2.3.

In the following we do not consider all possible analytical expressions for each tuple (Q, Z, X) . We consider only seven explicit realization: five for $Q \in Z_5$ (one does not fit well all the mixing angles, but it is related to TBM and BM described in Sec. 2.1.1), one for $Q \in Z_3$ and two for $Q \in V$ even if only one tuple can achieve all the mixing angles in the 3σ confidence region. In fact we want to show an explicit realization with non trivial Majorana phases.

2.4.1 Sector $Q \in Z_5$

There exist $6 \times 15 \times 2 = 180$ triplets (Q, Z, X) assuming $Q \in Z_5$.⁸ However, without loss of generality we can analyse the simplest case $Q = T$: there are similarity transformations for Z defined in a given Klein subgroup K_j , $Z = K_j^a$, with $a = 1, 2, 3$ that connect the different triplets (T, Z, X) as

$$T^{-m} K_j^a T^m = K_i^a \quad (2.58a)$$

$$T^{-m} X_j^{a,b} T^m = X_i^{a,b} \quad (2.58b)$$

$$T^{-m} Q T^m = Q \quad (2.58c)$$

⁸In this counting we use the fact that the triplets (Q, Z, X_0) and (Q, Z, ZX_0) give us the same U_{PMNS} .

where $m = 1, \dots, 4$ and $i \neq j$ and $X_i^{a,b}$ is defined in (2.57).

The general transformations for $X = X_0$ and $Q \neq T$, assume the form

$$C^\dagger K_i^a C = K_j^{a'} \quad (2.59a)$$

$$C^\dagger P_{23} C^\star = P_{23} \quad (2.59b)$$

$$C^\dagger R_p C = R_q \quad (2.59c)$$

where $i, j = 1, \dots, 5$, $a, a' = 1, 2, 3$, and $p, q = 1 \dots 6$. The C matrices are elements of $Z_3 \subset A_5$, hence $C^3 = \mathbb{1}$, see Tab. 2.3. The transformations for $X \neq X_0$ are obtained in the same way. In fact if C fulfills (2.59) with $X = X_0$ then, for a non trivial X of the form (2.57) we have

$$C^\dagger X_j^{a,b} C^\star = C^\dagger K_j^b P_{23} C^\star = C^\dagger K_j^b \mathbb{1} P_{23} C^\star = C^\dagger K_j^b C C^\dagger P_{23} C^\star = K_i^{b'} P_{23} = X_i^{a',b'} \quad (2.60)$$

where $X_i^{a',b'}$ are good representations of the CP operator for a given $K_j^{a'}$.

Therefore we can study only the cases with $Q = T$, which is the simplest choice. In fact we have $U_\ell = \mathbb{1}$, up to permutations of columns, thus the PMNS matrix is given only by the neutrino sector. The results of our numerical analysis are reported in Tab. 2.5 for $X = X_0$ and in Tab. 2.6 for $X \neq X_0$. The analytical treatment of each category with an acceptable value of χ^2 , except when explicitly stated, is reported in the following.

(Q, Z, X)	(R_1, S_1, X_0)		(R_1, S_3, X_0)		(R_1, S_2, X_0)	
θ_{bf}	(0.28, 2.86)		(0.18, 2.97)		(0.58, 2.56)	
χ_{min}^2	14.08	17.83	4.04	7.74	$> 10^2$	$> 10^2$
$\sin^2 \theta_{12}/10^{-1}$	2.60	2.60	2.83	2.83	3.04	3.04
$\sin^2 \theta_{13}/10^{-2}$	2.16	2.17	2.18	2.19	0.00	0.00
$\sin^2 \theta_{23}/10^{-1}$	5.00	5.00	5.00	5.00	5.00	5.00
J_{CP}	± 0.032	± 0.032	± 0.033	± 0.033	0	0
I_1	0	0	0	0	0	0
I_2	0	0	0	0	0	0

Table 2.5: Possible values for the PMNS parameters for a given Z with $Q = T$ and $X = X_0$.

(Q, Z, X)	$(R_1, S_1, S_2 X_0)$		$(R_1, S_3, S_1 X_0)$		$(R_1, S_2, S_1 X_0)$	
θ_{bf}	0.28		0.17	2.97	(0.25, 3.40)	
χ_{min}^2	42.18	49.96	5.64	3.46	$> 10^2$	$> 10^2$
$\sin^2 \theta_{12}/10^{-1}$	2.61	2.61	2.83	2.83	3.04	3.04
$\sin^2 \theta_{13}/10^{-2}$	2.10	2.04	2.17	2.19	0.00	0.00
$\sin^2 \theta_{23}/10^{-1}$	7.30	7.27	4.08	5.92	5.00	5.00
J_{CP}	0	0	0	0	0	0
I_1	0	0	0	0	± 0.10	± 0.10
I_2	0	0	0	0	0	0

Table 2.6: Same as Tab. 2.5 with $X \neq X_0$.

• **Case** (R_1, S_1, X_0)

For the first group in Tab. 2.5 the matrix Ω_0 , up to permutations of columns, is

$$\Omega_0 = \begin{pmatrix} \cos \phi & \sin \phi & 0 \\ \sin \phi/\sqrt{2} & -\cos \phi/\sqrt{2} & 1/\sqrt{2} \\ \sin \phi/\sqrt{2} & -\cos \phi/\sqrt{2} & -1/\sqrt{2} \end{pmatrix} \quad (2.61)$$

where $\tan \phi \equiv \varphi^{-1} = \varphi - 1 \simeq 0.618$. The matrix Ω that satisfies the condition (2.56) is

$$\Omega = \Omega_0 \text{diag}\{-1, 1, i\}. \quad (2.62)$$

The PMNS is given by

$$U_{\text{PMNS}} = \Omega R_{23}(\theta) K_\nu. \quad (2.63)$$

The column of the PMNS matrix which is constant is the first one

$$\|U_{\alpha 1}\| = \begin{pmatrix} \cos \phi \\ \sin \phi/\sqrt{2} \\ \sin \phi/\sqrt{2} \end{pmatrix} \simeq \begin{pmatrix} 0.851 \\ 0.372 \\ 0.372 \end{pmatrix}. \quad (2.64)$$

In this case, we find the following analytic expressions for the mixing angles

$$\sin^2 \theta_{12} = \frac{\tan^2 \phi \cos^2 \theta}{1 + \tan^2 \phi \cos^2 \theta} = \frac{(2 - \varphi) \cos^2 \theta}{1 + (2 - \varphi) \cos^2 \theta} \quad (2.65a)$$

$$\sin^2 \theta_{13} = \sin^2 \phi \sin^2 \theta = \frac{\sin^2 \theta}{2 + \varphi} \quad (2.65b)$$

$$\sin^2 \theta_{23} = \frac{1}{2}. \quad (2.65c)$$

Notice that we have an upper bound for the reactor angle by the inequality $\sin^2 \theta_{13} \leq (2 - \varphi)/(3 - \varphi) \simeq 0.28$ and the same bound is valid for the solar angle θ_{12} . We can write the following relation between $\sin^2 \theta_{12}$ and $\sin^2 \theta_{13}$

$$\sin^2 \theta_{12} = \frac{\varphi - 2 - (\varphi - 3) \sin^2 \theta_{13}}{(\varphi - 3) \cos^2 \theta_{13}} = \frac{\varphi - 2}{\varphi - 3} + \frac{\sin^2 \theta_{13}}{\varphi - 3} + \mathcal{O}(\sin^4 \theta_{13}) \simeq 0.276 - 0.724 \sin^2 \theta_{13}. \quad (2.66)$$

This relation explains the tension between the two mixing angles in the χ^2 analysis, in fact when θ_{13} is close to the best fit value, $\sin^2 \theta_{13} = 2.18 \times 10^{-2}$, the solar mixing angle is disfavored at more than 3σ confidence level, $\sin^2 \theta_{12} = 2.60 \times 10^{-1}$ using the approximate relation. Therefore this category needs large NLO corrections to fits the experimental data.

For the CP invariants we have

$$J_{\text{CP}} = \frac{1}{4} \cos \phi \sin^2 \phi \sin 2\theta = \frac{2 - \varphi}{4(3 - \varphi)^{3/2}} \sin 2\theta \quad (2.67a)$$

$$I_1 = I_2 = 0 \quad (2.67b)$$

thus the CP phases are

$$|\sin \delta| = 1 \quad \sin \alpha = \sin \beta = 0. \quad (2.68)$$

• **Case** (R_1, S_3, X_0)

For the second group in Tab. 2.5 the matrix Ω_0 is the same as the case (T, S_1, X_0) defined in (2.61). The matrix Ω is

$$\Omega = \Omega_0 \text{diag}\{-1, 1, -i\} \quad (2.69)$$

and the PMNS is given by

$$U_{\text{PMNS}} = \Omega R_{13}(\theta) K_\nu. \quad (2.70)$$

The constant column of the PMNS matrix is the second one

$$\|U_{\alpha 2}\| = \begin{pmatrix} \sin \phi \\ \cos \phi / \sqrt{2} \\ \cos \phi / \sqrt{2} \end{pmatrix} \simeq \begin{pmatrix} 0.526 \\ 0.602 \\ 0.602 \end{pmatrix}. \quad (2.71)$$

The expressions for the mixing angles are

$$\sin^2 \theta_{12} = \frac{\tan^2 \phi}{\tan^2 \phi + \cos^2 \theta} = \frac{(2 - \varphi)}{(2 - \varphi) + \cos^2 \theta} \quad (2.72a)$$

$$\sin^2 \theta_{13} = \cos^2 \phi \sin^2 \theta = \frac{\sin^2 \theta}{3 - \varphi} \quad (2.72b)$$

$$\sin^2 \theta_{23} = \frac{1}{2}. \quad (2.72c)$$

In this category we have an upper limit for the reactor angle by the inequality $\sin^2 \theta_{13} \leq (3 - \varphi)^{-1} \simeq 0.72$ while for the solar mixing angle we get the lower bound $\sin^2 \theta_{12} \geq (2 - \varphi)/(3 - \varphi) \simeq 0.28$. There exists a relation between $\sin^2 \theta_{12}$ and $\sin^2 \theta_{13}$, that can be written as

$$\sin^2 \theta_{12} = \frac{1}{(2 + \varphi) \cos^2 \theta_{13}} = \frac{1}{2 + \varphi} \left[1 + \sin^2 \theta_{13} + \mathcal{O}(\sin^4 \theta_{13}) \right] \simeq 0.276(1 + \sin^2 \theta_{13}). \quad (2.73)$$

When θ_{13} is close to the best fit point, $\sin^2 \theta_{13} = 2.18 \times 10^{-2}$, we obtain $\sin^2 \theta_{12} = 2.82 \times 10^{-1}$ using the approximated relation, which is compatible at 2σ confidence level.

For the CP invariants we obtain

$$J_{\text{CP}} = \frac{1}{4} \sin \phi \cos^2 \phi \sin 2\theta = \frac{\varphi - 1}{4(3 - \varphi)^{3/2}} \sin 2\theta \quad (2.74a)$$

$$I_1 = I_2 = 0 \quad (2.74b)$$

thus we get

$$|\sin \delta| = 1 \quad \sin \alpha = \sin \beta = 0. \quad (2.75)$$

Notice that both for the categories (T, S_1, X_0) and (T, S_3, X_0) the main difference in the χ^2 at $\theta = \theta_{\text{bf}}$ for NO and IO is given by θ_{23} . In fact we have $\Delta\chi_{23}^2 \simeq 3.70$ at $\theta_{23} = \pi/4$.

• **Case** (R_1, S_2, X_0)

This case does not fit well the mixing angles that we observe in Nature, however it is quite interesting because for particular values of θ we get the well known TBM or BM patterns discussed in Sec. 2.1.1. We find that the matrix Ω is

$$\Omega = \begin{pmatrix} 1 & 0 & 0 \\ 0 & i/\sqrt{2} & -1/\sqrt{2} \\ 0 & -i/\sqrt{2} & -1/\sqrt{2} \end{pmatrix} \quad (2.76)$$

and the PMNS is

$$U_{\text{PMNS}} = \Omega R_{12}(\theta) K_\nu. \quad (2.77)$$

The constant column is the third one

$$\|U_{\alpha 3}\| = \begin{pmatrix} 0 \\ 1/\sqrt{2} \\ 1/\sqrt{2} \end{pmatrix} \simeq \begin{pmatrix} 0 \\ 0.707 \\ 0.707 \end{pmatrix}. \quad (2.78)$$

In this case the expressions for the mixing angles are

$$\sin^2 \theta_{12} = \sin^2 \theta \quad (2.79a)$$

$$\sin^2 \theta_{13} = 0 \quad (2.79b)$$

$$\sin^2 \theta_{23} = \frac{1}{2}. \quad (2.79c)$$

The CP invariants are trivial

$$J_{\text{CP}} = I_1 = I_2 = 0. \quad (2.80)$$

Notice that for $\theta \rightarrow \sin^{-1}(1/\sqrt{3})$ we obtain the TBM mixing matrix, while for $\theta \rightarrow \pi/4$ we obtain the BM mixing matrix. The CP invariants are trivial, thus there exists an accidental CP symmetry, discussed in Sec. 2.3.2. In this case the matrix Y that fulfills the conditions is

$$Y = S_2 P_{23} = -\mathbb{1}. \quad (2.81)$$

• **Case** $(R_1, S_1, S_2 X_0)$

For the first group in Tab. 2.6 the matrix Ω_0 is the same as (2.61) while the matrix Ω that fulfills the condition (2.56) is

$$\Omega = i\Omega_0 \quad (2.82)$$

and

$$U_{\text{PMNS}} = \Omega R_{23}(\theta) K_\nu. \quad (2.83)$$

The constant column of the PMNS matrix is the first one. The absolute value is the same as (2.64). The mixing angles assume the following analytic expressions

$$\sin^2 \theta_{12} = \frac{\tan^2 \phi \cos^2 \theta}{1 + \tan^2 \phi \cos^2 \theta} = \frac{(2 - \varphi) \cos^2 \theta}{1 + (2 - \varphi) \cos^2 \theta} \quad (2.84a)$$

$$\sin^2 \theta_{13} = \sin^2 \phi \sin^2 \theta = \frac{1}{2 + \varphi} \sin^2 \theta \quad (2.84b)$$

$$\sin^2 \theta_{23} = \frac{1}{2} + \frac{\cos \phi \cos \theta \sin \theta}{\cos^2 \theta + \cos^2 \phi \sin^2 \theta} = \frac{1}{2} - \frac{\sqrt{3 - \varphi} \sin 2\theta}{\varphi - 4 + (\varphi - 2) \cos 2\theta} \quad (2.84c)$$

where we observe that θ_{12} and θ_{13} follow the same relations as category (R_1, S_1, X_0) . The mixing angle θ_{23} is unconstrained in this case. It is interesting to write an expression between the reactor angle θ_{13} and the atmospheric angle θ_{23} through the approximate relation

$$\sin^2 \theta_{23} = \frac{1}{2} \pm \varphi \sin \theta_{13} + \mathcal{O}(\sin^3 \theta_{13}) \simeq 0.500 \pm 1.618 \sin \theta_{13}. \quad (2.85)$$

The connection with the solar angle is the same as (2.66). The global effect is to have $\chi_{\min}^2 \sim 50$ even if the reactor angle θ_{13} is close to the experimental value. In fact when $\sin^2 \theta_{13} = 2.18 \times 10^{-2}$ we get $\sin^2 \theta_{23} = 7.39 \times 10^{-1}$ or $\sin^2 \theta_{23} = 2.61 \times 10^{-1}$ using the approximate relation. Clearly the larger value of θ_{23} gives a better value for χ_{\min}^2 for both orderings. In fact there is a tension between all the mixing angles. In this category the CP invariants are trivial

$$J_{CP} = I_1 = I_2 = 0. \quad (2.86)$$

The accidental CP symmetry is related to the existence of the matrix Y , defined in Sec. 2.3.2

$$Y = S_1 X = S_1 S_3 P_{23} = -\mathbb{1}. \quad (2.87)$$

• **Case** $(R_1, S_3, S_1 X_0)$

For the second group in Tab. 2.6 we have the same matrix Ω_0 defined in (2.61), but in this case the matrix Ω that fulfills the condition (2.56) is

$$\Omega = \Omega_0 \text{diag}\{-1, -i, 1\}. \quad (2.88)$$

We get the following PMNS

$$U_{\text{PMNS}} = \Omega R_{13}(\theta) K_\nu. \quad (2.89)$$

The constant column in the PMNS matrix is the second one. The absolute value is the same as (2.71). However, due to different form of the X matrix the analytic expressions for the mixing angles are different with respect to the case in Tab. 2.5. We have

$$\sin^2 \theta_{12} = \frac{\tan^2 \phi}{\tan^2 \phi + \cos^2 \theta} = \frac{(2 - \varphi)}{(2 - \varphi) + \cos^2 \theta} \quad (2.90a)$$

$$\sin^2 \theta_{13} = \cos^2 \phi \sin^2 \theta = \frac{\sin^2 \theta}{3 - \varphi} \quad (2.90b)$$

$$\sin^2 \theta_{23} = \frac{1}{2} \frac{(\cos \theta + \sin \theta \sin \phi)^2}{\cos^2 \theta + \sin^2 \theta \sin^2 \phi} = \frac{1}{2} \left[1 + \frac{\sqrt{7 - 4\varphi} \sin 2\theta}{\sin^2 \theta + \varphi - 3} \right]. \quad (2.90c)$$

In this category the parameter which is different with respect to the case S_3 evaluated for $X = X_0$ is θ_{23} . Notice that this parameter is unconstrained. We can find the following approximate relation between $\sin^2 \theta_{23}$ and $\sin^2 \theta_{13}$

$$\sin^2 \theta_{23} = \frac{1}{2} \pm (\varphi - 1) \sin \theta_{13} + \mathcal{O}(\sin^3 \theta_{13}) \simeq 0.500 \pm 0.618 \sin \theta_{13} \quad (2.91)$$

In this case for the best fit value of the reactor angle $\sin^2 \theta_{13} = 2.18 \times 10^{-2}$ we obtain two different values for $\sin^2 \theta_{23}$ which are 4.09×10^{-1} and 5.91×10^{-1} . The second value is closer to one of the best fit points for θ_{23} , then the χ_{\min}^2 for IO is better than the value for NO.

The CP invariants are all trivial

$$J_{CP} = I_1 = I_2 = 0. \quad (2.92)$$

As for the previous cases with trivial invariants this fact is related to the existence of an accidental CP symmetry realized by the matrix

$$Y = S_3 X = S_3 S_1 P_{23} = -\mathbb{1}. \quad (2.93)$$

2.4.2 Sector $Q \in Z_3$

In this Section we want to classify the possible patterns for the PMNS matrix in the case of $Q \in Z_3$. In general $10 \times 15 \times 2 = 300$ combinations are possible for the triplets (Q, Z, X) . However, as done for $Q \in Z_5$, due to the similarity transformations defined in (2.41) and (2.42), we can reduce the number to eight patterns to analyse, that are summarized in Tab. 2.4.

To obtain the similarity transformations it is easy to start from $Q = C_4 = T^2ST^2$ and $X \neq X_0$. In this case the matrices $A = T^mST^m$ are good representations of the transformations for Z in the j -th Klein subgroup of A_5 , $Z = K_j^a$, where $a, b = 1, 2, 3$. The transformations can be written as

$$(T^{-m}ST^{-m})K_j^a(T^mST^m) = K_i^b \quad (2.94a)$$

$$(T^{-m}ST^{-m})X_j^{a,b}(T^mST^m) = X_i^{a,b} \quad (2.94b)$$

$$(T^{-m}ST^{-m})Q(T^mST^m) = Q \quad (2.94c)$$

where $m = 1, 2$, $i, j = 1, \dots, 5$ and X is defined in (2.57).

For the general case $Q \in Z_3$ there exists similarity transformations that connects the different triplets, as discussed in Sec. 2.4.1 for $Q \in Z_5$, but these are quite cumbersome. Therefore, without loss of generality, we can study the simplest case $Q = T^2ST^2$ because the matrix U_ℓ is easy to evaluate and it does not contain complex numbers

$$U_\ell^{(C_4)} = \begin{pmatrix} -\sqrt{\frac{1}{3} + \frac{2}{3\sqrt{5}}} & -\sqrt{\frac{1}{15}(5 - \sqrt{5})} & \frac{2}{\sqrt{3(5 + \sqrt{5})}} \\ \frac{2}{\sqrt{3(5 + \sqrt{5})}} & -\frac{1}{2} - \frac{1}{30}\sqrt{75 + 30\sqrt{5}} & \frac{1}{30}(-15 + \sqrt{75 + 30\sqrt{5}}) \\ \frac{2}{\sqrt{3(5 + \sqrt{5})}} & \frac{1}{2} - \frac{1}{30}\sqrt{75 + 30\sqrt{5}} & \frac{1}{30}(15 + \sqrt{75 + 30\sqrt{5}}) \end{pmatrix}. \quad (2.95)$$

Notice that the neutrino sector is exactly the same as $Q \in Z_5$, thus we do not need more informations about the matrices Ω_0 . The results are reported in Tab. 2.7 for $X = X_0$ and in Tab. 2.8 for $X \neq X_0$. In the following we discuss in details only the case (T^2ST^2, S_4, X_0) because the other categories have a huge χ_{\min}^2 .

(Q, Z, X)	(C_4, S_3, X_0)	(C_4, S_1, X_0)	(C_4, S_2, X_0)	(C_4, S_4, X_0)
θ_{bf}	(0.41, 2.73)	(0.39, 2.74)	(0.41, 2.92)	(0.60, 0.97)
χ_{\min}^2	$> 10^2$	$> 10^2$	$> 10^2$	8.84
$\sin^2 \theta_{12}/10^{-1}$	1.09	1.09	1.30	3.41
$\sin^2 \theta_{13}/10^{-2}$	2.06	2.07	2.20	2.17
$\sin^2 \theta_{23}/10^{-1}$	5.00	5.00	5.00	5.00
J_{CP}	± 0.022	± 0.022	± 0.024	± 0.034
I_1	0	0	0	0
I_2	0	0	0	0

Table 2.7: Possible values for the PMNS parameters for a given Z with $Q = T^2ST^2$ and $X = X_0$.

(Q, Z, X)	$(C_4, S_3, S_1 X_0)$		$(C_4, S_1, S_3 X_0)$		$(C_4, S_2, S_3 X_0)$		$(C_4, S_5, S_4 X_0)$	
θ_{bf}	(1.20, 1.94)		(0.53, 2.60)		(0.05, 3.09)		(0.79, 2.36)	
χ_{min}^2	$> 10^2$	$> 10^2$	$> 10^2$	$> 10^2$	$> 10^2$	$> 10^2$	$> 10^2$	$> 10^2$
$\sin^2 \theta_{12}/10^{-1}$	1.13	1.12	4.46	4.46	3.04	3.04	3.49	3.50
$\sin^2 \theta_{13}/10^{-2}$	1.67	1.74	2.16	2.16	0.00	0.00	4.47	4.47
$\sin^2 \theta_{23}/10^{-1}$	8.20	8.27	6.56	6.56	5.00	5.00	6.51	6.51
J_{CP}	0	0	0	0	0	0	$\pm 10^{-9}$	$\pm 10^{-9}$
I_1	0	0	0	0	± 0.21	± 0.21	± 0.21	± 0.21
I_2	0	0	0	0	0	0	$\pm 10^{-9}$	$\pm 10^{-9}$

Table 2.8: Same as Tab. 2.7 with $X \neq X_0$.

• Case (C_4, S_4, X_0)

The matrix Ω in this case is similar to (2.61), but with different exponential factors in the matrix elements

$$\Omega = \begin{pmatrix} \cos \phi & -\sin \phi & 0 \\ \sin \phi/\sqrt{2} e^{-i2\pi/5} & \cos \phi/\sqrt{2} e^{-i2\pi/5} & 1/\sqrt{2} e^{-i9\pi/10} \\ \sin \phi/\sqrt{2} e^{i2\pi/5} & \cos \phi/\sqrt{2} e^{i2\pi/5} & 1/\sqrt{2} e^{i9\pi/10} \end{pmatrix} \quad (2.96)$$

where we recall that $\tan \phi = 1/\varphi$. We obtain the PMNS matrix as

$$U_{\text{PMNS}} = \Omega R_{23}(\theta) K_\nu. \quad (2.97)$$

The constant column of the PMNS matrix is the second one

$$\|U_{\alpha 2}\| = \frac{1}{\sqrt{3}} \begin{pmatrix} 1 \\ 1 \\ 1 \end{pmatrix} \simeq \begin{pmatrix} 0.577 \\ 0.577 \\ 0.577 \end{pmatrix}. \quad (2.98)$$

Thus, one of the columns of the resulting PMNS mixing matrix has to be trimaximal, up to phases. To reach compatibility with the experimental data on lepton mixing angles this column must be identified with the second one of U_{PMNS} . In this case the analytic expressions for the mixing angles are

$$\sin^2 \theta_{12} = \frac{1}{2 + \sin 2\theta} \quad (2.99a)$$

$$\sin^2 \theta_{13} = \frac{1 - \sin 2\theta}{3} \quad (2.99b)$$

$$\sin^2 \theta_{23} = \frac{1}{2}. \quad (2.99c)$$

Notice that in this case the solar angle θ_{12} satisfies the lower bound $\sin^2 \theta_{12} \geq 1/3$, instead the reactor angle θ_{13} fulfills the upper bound $\sin^2 \theta_{13} \leq 2/3$. It is easy to obtain the following relation between the solar and the reactor mixing angles

$$\sin^2 \theta_{12} = \frac{1}{3 \cos^2 \theta_{13}} = \frac{1}{3} \left[1 + \sin^2 \theta_{13} + \mathcal{O}(\sin^4 \theta_{13}) \right] \simeq 0.333(1 + \sin^2 \theta_{13}) \quad (2.100)$$

which is a well-know relation that occurs in case of a TBM column [130–133]. When the reactor mixing angle is evaluated at the best fit point $\sin^2 \theta_{13} = 2.18 \times 10^{-2}$ the solar angle is $\sin^2 \theta_{12} = 3.41 \times 10^{-1}$ which is disfavoured at 2σ CL.

The difference between NO and IO in χ_{min}^2 is given by θ_{23} . We have $\Delta\chi_{23}^2 \simeq 3.70$ at

$\theta_{23} = \pi/4$, as previously noticed for the categories (T, S_1, X_0) and (T, S_3, X_0) . The CP invariants are

$$J_{CP} = \frac{\cos 2\theta}{6\sqrt{3}} \quad I_1 = I_2 = 0. \quad (2.101)$$

We can extract the non trivial Dirac CP phase

$$|\sin \delta| = 1 \quad (2.102)$$

which implies that the CP Dirac phase is maximal.

2.4.3 Sector $Q \in V$

In this section we want to analyse the case $Q \in V = Z_2 \otimes Z_2$. We adopt the notation Q for the couple of matrices $\{Q_1, Q_2\}$. $5 \times 10 \times 2 = 100$ combinations of triplets (Q, Z, X) are possible. As for $Q \in Z_3$ or Z_5 there exists similarity transformations that connects the different triplets, see Eq. (2.41) and (2.42). Only four categories, that are summarize in Tab. 2.4, are independent. These transformations are quite cumbersome and we discard their form.

We consider the simplest case $Q = K_2 = \{T^4ST, ST^3ST^2S\}$ which is easy to compute, as discussed for $Q \in Z_3$ in the category (C_4, S_4, X_0) .

Notice that in this case the matrix U_ℓ has to diagonalize the elements of the Klein subgroup K_2 , which means $Q_1 = T^4ST$ and $Q_2 = ST^3ST^2S$ and the product $Q_1Q_2 = T^2ST^3STS$. This is always possible because the matrices of V commute $[Q_1, Q_2] = 0$.

We report the results of our numerical analysis in Tab. 2.9 for $X = X_0$ and in Tab. 2.10 for $X \neq X_0$.

Notice that if Z is in the same Klein group as Q we have $U_{PMNS} = R_{ij}(\theta)K_\nu$. The third column of the PMNS matrix is constant and it is $\|U_{\alpha 3}\| = (0, 0, 1)^T$. Then this case is ruled out by the χ^2 analysis because it is impossible to have the mixing angles compatible with the experimental data.

(Q, Z, X)	(K_2, S_1, X_0)		(K_1, S_1, X_0)		(K_1, S_2, X_0)			
	P_1	P_2						
θ_{bf}	1.27		1.27		(0.58, 2.56)		(1.14, 2.00)	
χ_{\min}^2	6.19	6.43	4.48	11.84	$> 10^2$	$> 10^2$	$> 10^2$	$> 10^2$
$\sin^2 \theta_{12}/10^{-1}$	3.31	3.31	3.31	3.31	3.04	3.04	3.04	3.04
$\sin^2 \theta_{13}/10^{-2}$	2.20	2.18	2.19	2.24	0.00	0.00	0.00	0.00
$\sin^2 \theta_{23}/10^{-1}$	5.24	5.25	4.76	4.78	0.00	0.00	0.00	0.00
J_{CP}	0	0	0	0	0	0	0	0
I_1	0	0	0	0	0	0	0	0
I_2	0	0	0	0	0	0	0	0

Table 2.9: Possible values for the PMNS parameters for a given Z and $X = X_0$. Notice that the categories (K_1, S_1, X_0) and (K_1, S_2, X_0) are different because it does not exist a similarity transformation that connects the two triplets. However the values of the mixing angles and phases are the same.

- **Case (K_2, S_1, X_0)**

For the first category in Tab. 2.9 we have defined two possible rows permutation of the PMNS matrix (the second and the third row) that can give us a plausible χ_{\min}^2 . P_1 is the

(Q, Z, X)	$(K_2, S_1, S_3 X_0)$			
	P_1		P_2	
θ_{bf}	(1.31, 1.82)		(1.31, 1.82)	
χ_{min}^2	$> 10^2$	$> 10^2$	$> 10^2$	$> 10^2$
$\sin^2 \theta_{12}/10^{-1}$	3.04	3.04	3.04	3.04
$\sin^2 \theta_{13}/10^{-2}$	9.55	9.55	9.55	9.55
$\sin^2 \theta_{23}/10^{-1}$	2.76	2.76	7.24	7.24
J_{CP}	± 0.030	± 0.030	± 0.030	± 0.030
I_1	∓ 0.079	∓ 0.079	∓ 0.079	∓ 0.079
I_2	∓ 0.019	∓ 0.019	∓ 0.019	∓ 0.019

Table 2.10: Same as Tab. 2.9 with $X \neq X_0$.

permutation with $\theta_{23} > \pi/4$ and P_2 is the permutation with θ_{23} in the other octant. The U_{PMNS} is obtained by the matrix Ω defined in Eq. (2.62), and U_ℓ is defined as Ω in Eq. (2.96). The PMNS matrix is

$$U_{\text{PMNS}} = U_\ell^\dagger \Omega R_{23}(\theta) K_\nu. \quad (2.103)$$

In this case the constant column of the PMNS matrix is the first one. These are

$$\|U_{\alpha 1}^{P_1}\| = \frac{1}{2} \begin{pmatrix} \varphi \\ 1 \\ 1/\varphi \end{pmatrix} \simeq \begin{pmatrix} 0.809 \\ 0.500 \\ 0.309 \end{pmatrix} \quad \|U_{\alpha 1}^{P_2}\| = \frac{1}{2} \begin{pmatrix} \varphi \\ 1/\varphi \\ 1 \end{pmatrix} \simeq \begin{pmatrix} 0.809 \\ 0.309 \\ 0.500 \end{pmatrix} \quad (2.104)$$

respectively for P_1 and P_2 . In this category the mixing angles assume the following expressions

$$\sin^2 \theta_{12} = 1 - \frac{6 - 2\varphi}{17\varphi - 31 + (7\varphi - 11)(\cos 2\theta - 2 \sin 2\theta)} \quad (2.105a)$$

$$\sin^2 \theta_{13} = \frac{1}{8} \left[3 - \varphi + (\varphi - 1)(\cos 2\theta - 2 \sin 2\theta) \right] \quad (2.105b)$$

$$\sin^2 \theta_{23} = \begin{cases} \frac{-2(\varphi - 1) \sin 2\theta - (\varphi - 1) \cos 2\theta + \varphi - 3}{(6 - 4\varphi) \sin 2\theta + (2\varphi - 3) \cos 2\theta + 4\varphi - 9} & \text{for } P_1 \\ \frac{(3\varphi - 4) \cos 2\theta - (\varphi - 2)(2 \sin 2\theta - 3)}{(6 - 4\varphi) \sin 2\theta + (2\varphi - 3) \cos 2\theta + 4\varphi - 9} & \text{for } P_2 \end{cases} \quad (2.105c)$$

where the values for θ_{23} depends on the possible permutations of rows in the matrix U_{PMNS} . Clearly $\sin^2 \theta_{23}^{P_1} + \sin^2 \theta_{23}^{P_2} = 1$ because only the second and the third rows are exchanged. The solar and reactor mixing angles follow the upper bound $\sin^2 \theta_{1j} \leq (3 - \varphi)/4 \simeq 0.35$ and $j = 2, 3$, while the atmospheric angle θ_{23} is unconstrained. It is easy to evaluate the following relation between the two angles θ_{12} and θ_{13}

$$\begin{aligned} \sin^2 \theta_{12} &= 1 - \frac{3\varphi - 4}{4(7\varphi - 11) \cos^2 \theta_{13}} = \\ &= \frac{1}{4(7\varphi - 11)} \left[5(5\varphi - 8) + (4\varphi - 3) \sin^2 \theta_{13} + \mathcal{O}(\sin^4 \theta_{13}) \right] \simeq 0.345 - 0.655 \sin^2 \theta_{13} \end{aligned} \quad (2.106)$$

therefore when the reactor angle is close to the best fit point $\sin^2 \theta_{13} = 2.18 \times 10^{-2}$ we obtain $\sin^2 \theta_{12} = 3.31 \times 10^{-1}$ which is in the 3σ confidence region. A similar relation for

θ_{23} is intricate, but can be approximated for P_1 and P_2 as ⁹

$$\begin{aligned}\sin^2 \theta_{23}^{P_1} &= \frac{2+\varphi}{5} - \frac{2}{5}\sqrt{3+4\varphi}\sin\theta_{13} - \frac{4\varphi+3}{5(2\varphi-1)}\sin^2\theta_{13} + \mathcal{O}(\sin^3\theta_{13}) \simeq \\ &\simeq 0.724 - 1.231\sin\theta_{13} - 0.847\sin^2\theta_{13}\end{aligned}\quad (2.107a)$$

$$\begin{aligned}\sin^2 \theta_{23}^{P_2} &= \frac{3-\varphi}{5} + \frac{2}{5}\sqrt{3+4\varphi}\sin\theta_{13} + \frac{4\varphi+3}{5(2\varphi-1)}\sin^2\theta_{13} + \mathcal{O}(\sin^3\theta_{13}) \simeq \\ &\simeq 0.276 + 1.231\sin\theta_{13} + 0.847\sin^2\theta_{13}\end{aligned}\quad (2.107b)$$

thus when θ_{13} is close to the best fit point we get $\sin^2 \theta_{23} = 5.23 (4.77) \times 10^{-1}$ for P_1 (P_2). This explain the difference in the χ^2 analysis in NO and IO for the two permutations. The CP invariants are trivial

$$J_{CP} = I_1 = I_2 = 0. \quad (2.108)$$

In this case a matrix Y for the accidental CP symmetry (discussed in Sec. 2.3.2) is

$$Y = -\text{diag}\{1, e^{-i4\pi/5}, e^{i4\pi/5}\}. \quad (2.109)$$

• **Case** ($K_2, S_1, S_3 X_0$)

This category fails to fit the mixing angles; however, it might be interesting because the CP invariants are non trivial. The PMNS matrix is easy to obtain, in fact the matrix U_ℓ is the same as (2.96) and the matrix Ω is related to Ω_0 defined in Eq. (2.61) by the relation

$$\Omega = P_{13}\Omega_0\text{diag}\{i, 1, -1\} \quad (2.110)$$

where P_{13} is the permutation of first and third columns. The U_{PMNS} is straightforward to evaluate

$$U_{\text{PMNS}} = U_\ell^\dagger \Omega R_{23}(\theta) K_\nu. \quad (2.111)$$

The constant column, fixed by group theory, is the third one

$$\|U_{\alpha 3}^{P_1}\| = \frac{1}{2} \begin{pmatrix} 1/\varphi \\ 1 \\ \varphi \end{pmatrix} \simeq \begin{pmatrix} 0.309 \\ 0.500 \\ 0.809 \end{pmatrix} \quad \|U_{\alpha 3}^{P_2}\| = \frac{1}{2} \begin{pmatrix} 1/\varphi \\ \varphi \\ 1 \end{pmatrix} \simeq \begin{pmatrix} 0.309 \\ 0.809 \\ 0.500 \end{pmatrix} \quad (2.112)$$

where we indicate the two possible permutations of second and third rows. Clearly only the solar mixing angle θ_{12} can be fitted in this category and no non-trivial sum rules can be obtained from the three mixing angles. For this triplet the mixing angles assume the following expressions

$$\sin^2 \theta_{12} = \frac{1 + \varphi \cos^2 \theta}{2 + \varphi} \quad (2.113a)$$

$$\sin^2 \theta_{13} = \frac{2 - \varphi}{4} \quad (2.113b)$$

$$\sin^2 \theta_{23} = \begin{cases} \frac{1}{2 + \varphi} & \text{for } P_1 \\ \frac{1 + \varphi}{2 + \varphi} & \text{for } P_2 \end{cases} \quad (2.113c)$$

Notice that $\sin^2 \theta_{23}^{P_1} + \sin^2 \theta_{23}^{P_2} = 1$. The solar angle is constrained to be $(2 + \varphi)^{-1} \leq \sin^2 \theta_{12} \leq (1 + \varphi)(2 + \varphi)^{-1}$. As discussed above this category is interesting because all CP invariants

⁹Notice that the condition $\sin^2 \theta_{23}^{P_1} + \sin^2 \theta_{23}^{P_2} = 1$ is valid order by order in the perturbation series of $\sin\theta_{13}$.

are non trivial. By definition the Majorana invariants are constant under exchange of second and third rows (see definition in Appendix D), while the Dirac invariant changes sign. We get

$$J_{\text{CP}} = -\frac{\sin 2\theta}{16} \quad (2.114)$$

and the other invariants are

$$I_1 = (-1)^{k_1+1} \frac{(1+\varphi)\sin 2\theta}{16} \quad I_2 = (-1)^{k_2} \frac{(1-\varphi)\sin 2\theta}{16}. \quad (2.115)$$

Using these relations we can extract the value of the CP phases

$$\sin \delta = -\frac{\sqrt{10}\sin 2\theta}{\sqrt{9-\cos 4\theta}} \quad (2.116a)$$

$$\sin \alpha = (-1)^{k_1} \frac{8\sin 2\theta}{\cos 4\theta - 9} \quad (2.116b)$$

$$\sin \beta = (-1)^{k_2+1} \frac{2\sin 2\theta}{\sqrt{5} + \cos 2\theta}. \quad (2.116c)$$

Using the best fit value $\theta_{\text{bf}} = \pm 1.31971$ we get

$$\sin \delta = \mp 0.523206 \quad \sin \alpha = \mp (-1)^{k_1} 0.454979 \quad \sin \beta = \mp (-1)^{k_2} 0.309279. \quad (2.117)$$

2.5 Numerical discussion

All possible patterns for the PMNS matrix that we have analysed above can be represented in the parameter space of mixing angles, as shown in Fig. 2.5, 2.6 and 2.7. In particular we present in the planes $(\sin^2 \theta_{ij}, \sin^2 \theta_{jk})$ the regions of $\Delta\chi^2$ at two degrees of freedom for 1σ (green), 2σ (yellow) and 3σ (blue) confidence level, assuming NO or IO. Notice that two hypotheses for the $\text{NO}\nu\text{A}$ flux were used, namely a *likelihood-based selector* (LID) and *Library Event Matching* (LEM) [37, 134, 135]. As discussed in Ref. [37] LID compares the longitudinal and transverse energy deposition in the particle shower, while LEM compares an input event from either data or simulation to a large and independent library of simulated events. The regions and the best fit points are extracted from the May 2016 results of Ref. [45].¹⁰

The analysis prefers a global minimum for IO, with $\Delta\chi^2 \equiv \chi_{\text{NO}}^2 - \chi_{\text{IO}}^2 = -0.78$ assuming LEM; therefore the confidence regions for NO are larger with respect to those of IO. In the case of the LID method $\Delta\chi^2 = 1.03$, thus IO is preferred. Since the statistical significance of this result is still weak we ignore in our χ^2 analysis the mass ordering effect. At the same time, since the indication of a preferred value of the Dirac phase δ is rather weak, *i.e.* below the 3σ significance, we do not include any information on δ in the χ^2 function. In the planes we report with a black solid line the parametric plot of mixing angles as a function of the internal angle θ . In particular we represent with red dots the values obtained at θ_{bf} , which are summarized in Tabs. 2.11 (assuming LEM) and 2.12 (assuming LID). The interesting categories are classified as follows

$$\begin{array}{ll} \text{Case I} & (R_1, S_3, S_1 X_0) \\ \text{Case III} & (C_4, S_4, X_0) \end{array} \quad \begin{array}{ll} \text{Case II} & (R_1, S_3, X_0) \\ \text{Case IV} & (K_2, S_1, X_0) \end{array} \quad (2.118)$$

where for the Case IV we assume two possible permutations, $(P_1$ and $P_2)$ as discussed above. The arrows in the plots indicate for each category the direction of the increasing value of θ in the interval $0 \leq \theta \leq \theta_{\text{bf}}$ and the arrows always belong to the closest label I-IV.

¹⁰The dataset of one and two dimensional projections are available at the website <http://www.nu-fit.org>.

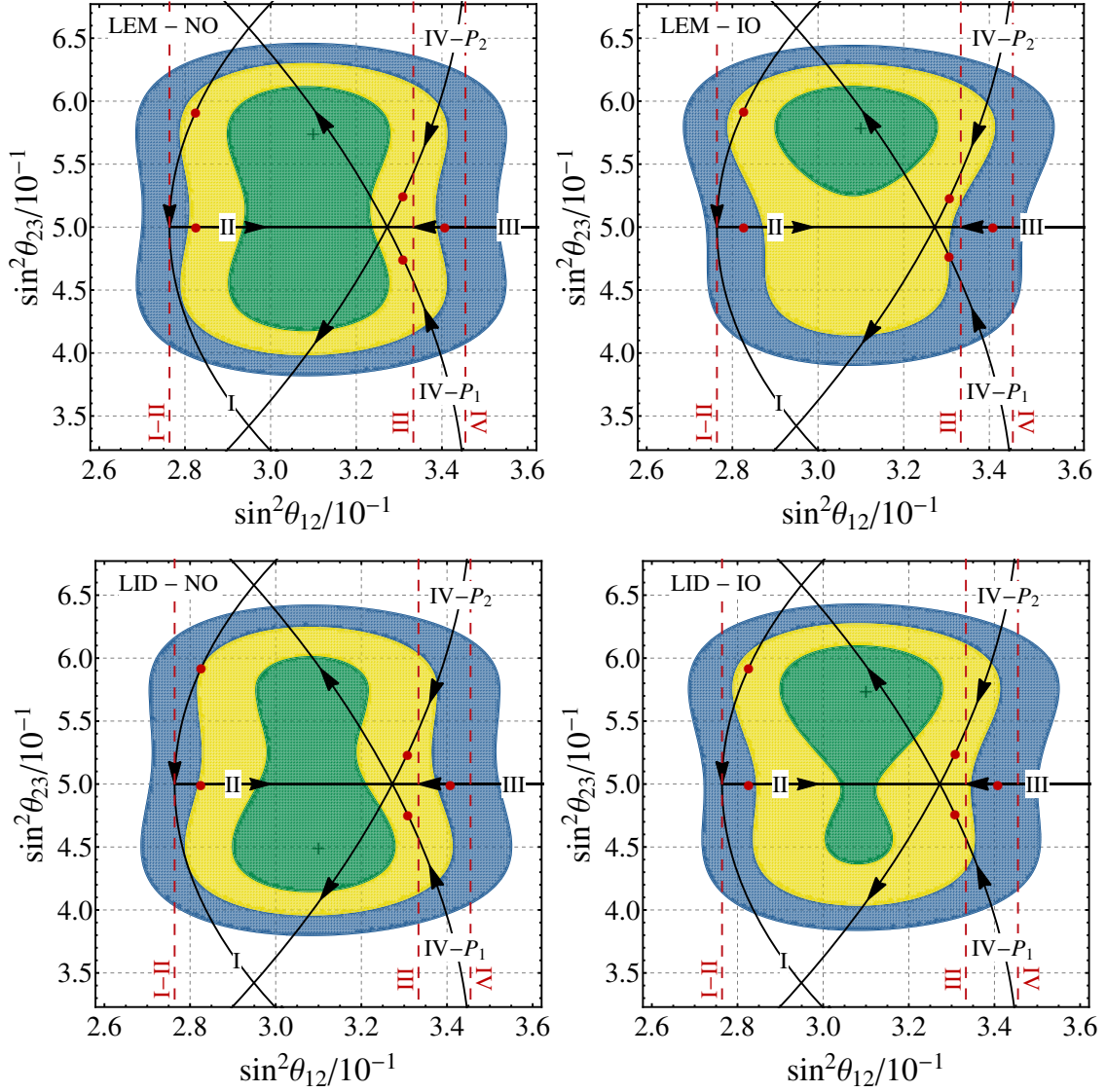


Figure 2.5: Parametric plot of the mixing angles in the planes $(\sin^2 \theta_{12}, \sin^2 \theta_{23})$. The plots are for NO (left panels) and IO (right panels) as a function of the internal angle θ . In upper panels we assume LEM model for $\text{NO}\nu A$ neutrino flux, while in lower panels LID. The red dots are the best fit points obtained using our χ^2 analysis. The categories are classified in Eq. (2.118). For the symbols and the lines see text for further details. Note that the curves II and III partly overlap.

The red dashed lines in Fig. 2.5 over the planes $(\sin^2 \theta_{12}, \sin^2 \theta_{23})$, represent the non trivial lower or upper values for $\sin^2 \theta_{12}$. For Case I and II we have $\sin^2 \theta_{12} \geq (2 - \varphi)/(3 - \varphi) \simeq 0.28$ and in Case III $\sin^2 \theta_{12} \geq 1/3 \simeq 0.33$. For the Case IV we have $\sin^2 \theta_{12} \leq (3 - \varphi)/4 \simeq 0.35$ for both permutations.

The curve of Case I in Fig. 2.6 $(\sin^2 \theta_{13}, \sin^2 \theta_{12})$ appears to be disconnected due to the chosen scales of the axes, thus, for clarity we mark on the curve of Case I some particular values of the internal angle θ with different black symbols: \star for $\theta = \pi/19$, \blacksquare for $\theta = \pi/17$, \bullet for $\theta = 16\pi/17$ and \blacktriangle for $\theta = 18\pi/19$. We also show the results in the plane $(\sin^2 \theta_{13}, \sin^2 \theta_{23})$ in Fig. 2.7.

Since from the data reported in Ref. [45] there is not a strong evidence for a parabolic behaviour around the minimum for the atmospheric angle θ_{23} we used a different definition of χ^2 in order to test the goodness of our previous results. We construct the χ^2 using the

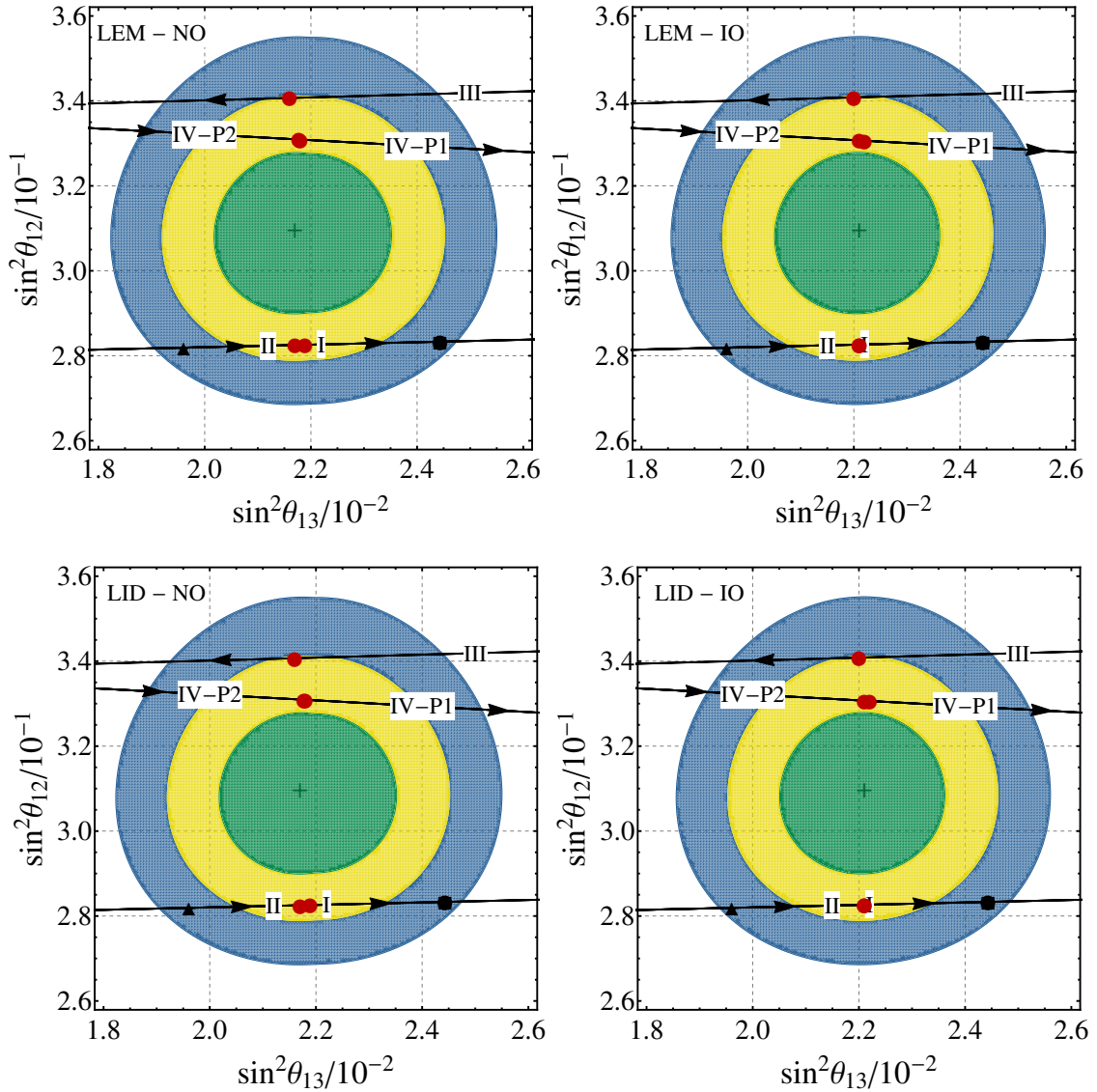


Figure 2.6: Same as Fig. 2.5 but in the planes $(\sin^2 \theta_{13}, \sin^2 \theta_{12})$ using the LEM (upper) or LID model (lower). Notice that the curves II and III overlap in the plane.

public data available at the website <http://www.nu-fit.org>, see Ref. [45]. We use the one dimensional projections χ_q^2 of q -th mixing parameter to construct the test function. The parameters q are $\{\sin^2 \theta_{12}, \sin^2 \theta_{13}, \sin^2 \theta_{23}\}$. The χ^2 is defined as

$$\chi^2 \equiv \sum_q \chi_q^2 \quad (2.119)$$

where the sum is over all the observables assuming a given ordering for the mass spectrum and a given model for the $\text{NO}\nu\text{A}$ flux (LIM or LEM). This hypothesis introduces a small error because we do not consider the correlations among the mixing parameters, however this effect is small and its inclusion is beyond the scope of our work. Since the available data are a discrete collection of points we use a first order polynomial function to interpolate the dataset. In this way we are able to evaluate the χ_q^2 for each point in the parameter space.

The results of our analysis are shown in Tab. 2.11 for Case I through Case IV assuming the LEM model for the neutrino flux, while in Tab. 2.12 we report the case of LID model. The data are consistent with the analysis performed with the simple χ^2 defined in (2.55).

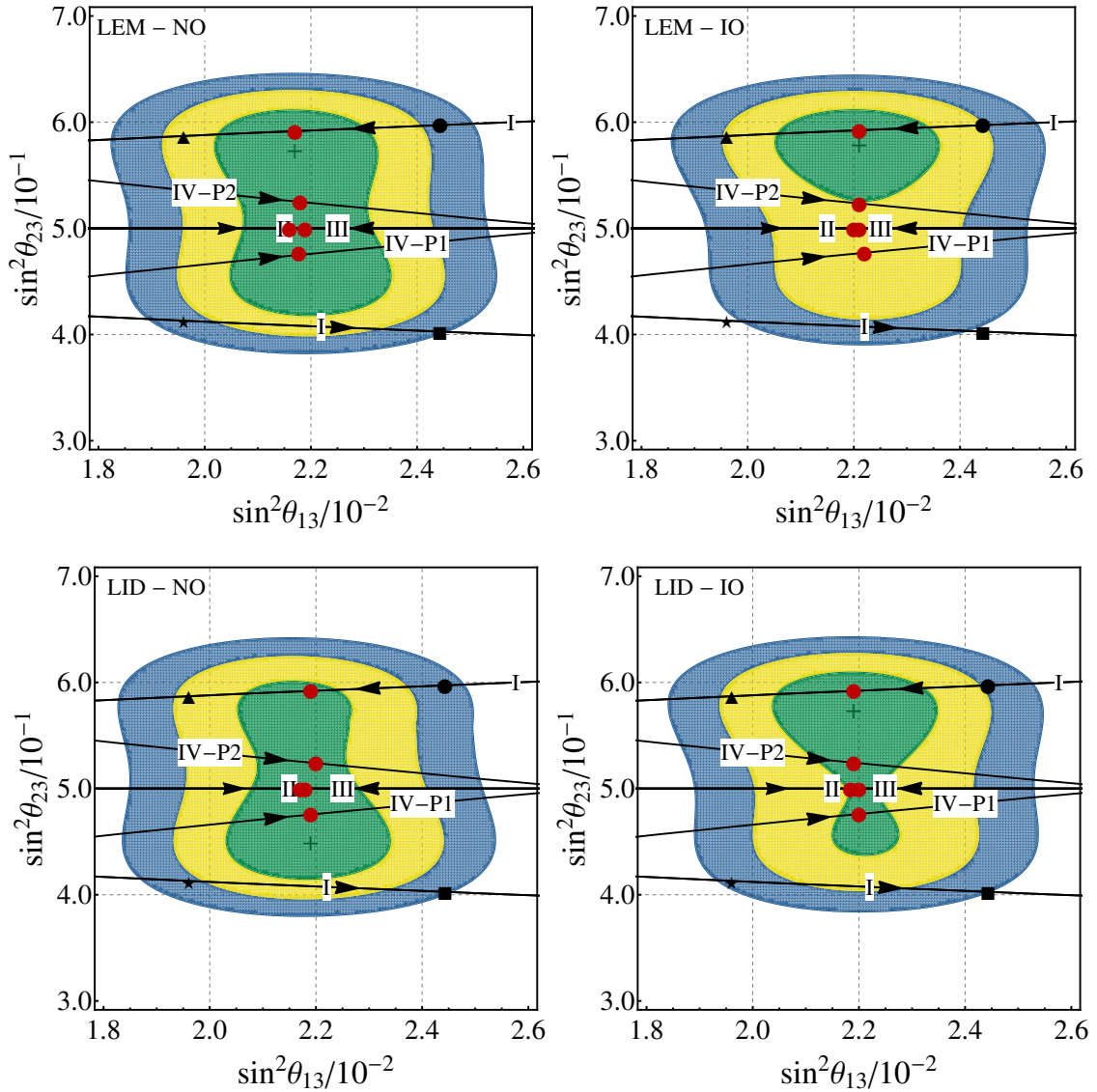


Figure 2.7: Same as Fig. 2.5 but in the planes $(\sin^2 \theta_{13}, \sin^2 \theta_{23})$ using the LEM model (upper) or LID (lower). The curves for Case I and II as well as for the permutations in Case IV, respectively, lie on top of each other in the plane.

The main difference is in Case I where the local minimum becomes the global minimum and vice versa, however the statistical significance is irrelevant. In Fig. 2.8 our results for the χ^2 defined in (2.119) as a function of the internal angle θ are shown.

Notice that the differences between LEM and LID models for the mixing angles are small. Instead the values for χ^2_{\min} , using (2.119), are different because the χ^2 provided by the nu-fit collaboration strongly depends on the neutrino flux method. However, for each Case NO or IO have the same behaviour for LEM and LID methods. For instance in Tab. 2.11 (LEM method) Case I, assuming NO, has a larger χ^2_{\min} with respect to IO, and the same happens in Tab. 2.12 (LID method). This structure is preserved for all Cases.

Our findings for the different Cases are summarized in Tab. 2.11 and Tab. 2.12. As one can see, these results agree well with our analytical estimates made in Sec. 2.4.1 for $Q \in Z_5$, Sec. 2.4.2 for $Q \in Z_3$ and Sec. 2.4.3 for $Q \in V$. In particular, we observe from Tab. 2.11, Tab. 2.12 and Fig. 2.8 that the sum of the best fitting values of θ and the second minimum for NO and IO in Case I approximately equals π , since the formulae for $\sin^2 \theta_{12}$ and $\sin^2 \theta_{13}$ are invariant under the transformation $\theta \rightarrow \pi - \theta$, while $\sin^2 \theta_{23}$ turns into

Case (LEM)	χ_{\min}^2	θ_{bf}	$\sin^2 \theta_{12}$	$\sin^2 \theta_{13}$	$\sin^2 \theta_{23}$	$\sin \delta$
$\mathcal{G}_\ell = Z_5$ - Case I ($T^2, T^2 ST^3 ST^2, SX_0$)	5.13	2.968	0.283	0.0217	0.592	0
	(8.65)	(0.173)	(0.283)	(0.0215)	(0.409)	0
	5.03	2.967	0.283	0.0221	0.593	0
	(12.08)	(0.176)	(0.283)	(0.0219)	(0.408)	0
$\mathcal{G}_\ell = Z_5$ - Case II ($T^2, ST^2 ST, X_0$)	5.60	0.175-2.967	0.283	0.0221	0.5	∓ 1
	7.82	0.175-2.967	0.283	0.0221	0.5	∓ 1
$\mathcal{G}_\ell = Z_3$ - Case III ($T^2 ST^2, ST^2 ST^3 S, X_0$)	6.89	0.604-0.967	0.341	0.0216	0.5	± 1
	9.18	0.603-0.967	0.341	0.0220	0.5	± 1
$\mathcal{G}_\ell = Z_2 \otimes Z_2$ - Case IV-P1 ($\{S, T^2 ST^3 ST^2\}, ST^2 ST, X_0$)	3.40	0.253	0.331	0.0218	0.475	0
	6.26	0.256	0.331	0.0222	0.477	0
$\mathcal{G}_\ell = Z_2 \otimes Z_2$ - Case IV-P2 ($\{S, T^2 ST^3 ST^2\}, ST^2 ST, X_0$)	3.96	0.255	0.331	0.0218	0.525	0
	5.38	0.256	0.331	0.0221	0.523	0

Table 2.11: Values of χ_{\min}^2 obtained using the likelihood function assuming the LEM method for the NO ν A flux, best fit for θ and PMNS parameters for patterns that have $\chi_{\min}^2 \leq 27$. Upper rows are for NO while lower ones are for IO. In the Case I in parenthesis we quote the local minimum. Notice that the Dirac phases are maximal when also the atmospheric angles are maximal, otherwise δ is trivial. The Majorana phases are always trivial if we want to accommodate the mixing angles.

Case (LID)	χ_{\min}^2	θ_{bf}	$\sin^2 \theta_{12}$	$\sin^2 \theta_{13}$	$\sin^2 \theta_{23}$	$\sin \delta$
$\mathcal{G}_\ell = Z_5$ - Case I ($T^2, T^2 ST^3 ST^2, SX_0$)	6.35	2.968	0.283	0.0219	0.592	0
	(8.13)	(0.174)	(0.283)	(0.0217)	(0.408)	0
	5.17	2.967	0.283	0.0219	0.592	0
	(10.11)	(0.175)	(0.283)	(0.0218)	(0.408)	0
$\mathcal{G}_\ell = Z_5$ - Case II ($T^2, ST^2 ST, X_0$)	6.01	0.175-2.967	0.283	0.0219	0.5	∓ 1
	6.91	0.175-2.967	0.283	0.0220	0.5	∓ 1
$\mathcal{G}_\ell = Z_3$ - Case III ($T^2 ST^2, ST^2 ST^3 S, X_0$)	7.34	0.604-0.967	0.341	0.0218	0.5	± 1
	8.25	0.604-0.967	0.341	0.0218	0.5	± 1
$\mathcal{G}_\ell = Z_2 \otimes Z_2$ - Case IV-P1 ($\{S, T^2 ST^3 ST^2\}, ST^2 ST, X_0$)	3.56	0.255	0.331	0.0219	0.476	0
	5.10	0.255	0.331	0.0220	0.476	0
$\mathcal{G}_\ell = Z_2 \otimes Z_2$ - Case IV-P2 ($\{S, T^2 ST^3 ST^2\}, ST^2 ST, X_0$)	4.65	0.255	0.331	0.0220	0.524	0
	4.75	0.256	0.331	0.0219	0.524	0

Table 2.12: Same as Tab. 2.11, assuming the LID method for the NO ν A experiment.

$\cos^2 \theta_{23}$ (see (2.105c)). Similarly, the sum of the two best fitting points (the same for NO and IO) almost equals π in Case II (see Sec. 2.4.1). Also related to the symmetry properties of the formulae for the solar and the reactor mixing angles is the observation in Case III those two best fitting points (for NO and IO) sum up to $\pi/2$ (see Sec. 2.4.2). Case IV does not reveal such a symmetry in the parameter θ and thus we discuss in this case the results corresponding to two different permutations that are related by the exchange of the second and third rows of U_{PMNS} . This allows us to accommodate $\sin^2 \theta_{23} < 1/2$ as well as $\sin^2 \theta_{23} > 1/2$.

We observe maximal CP violation when θ_{23} is also maximal, otherwise δ is trivial. This

is a feature of models with non-abelian discrete symmetry and CP under certain assumptions which are fulfilled by the group A_5 , see for instance Ref. [136] where a detailed analysis was performed.

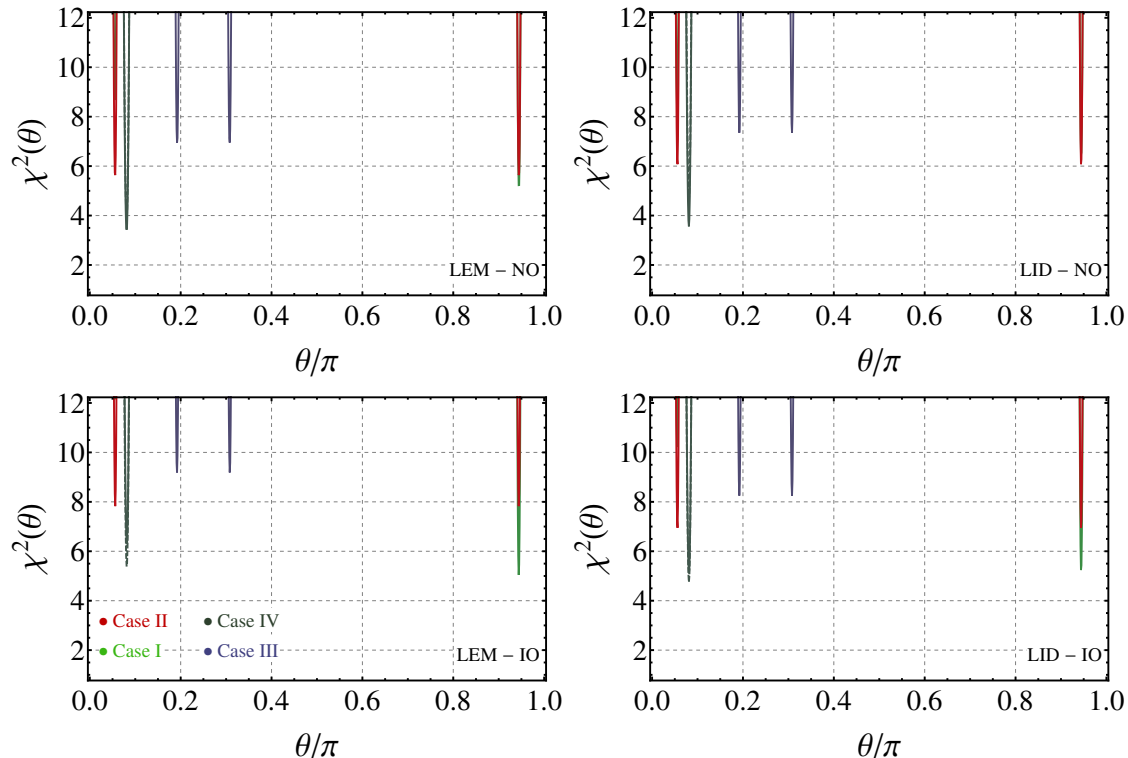


Figure 2.8: Results for the χ^2 constructed from the May 2016 data of Ref. [45] as a function of the internal angle θ for the Cases I-IV. In the Case IV the solid line is for P_1 while the dashed line is for P_2 . In the upper panels we show our results for NO and in the lowers for IO. The left panels are obtained with the LEM assumption of $\text{NO}\nu A$ flux, while the right ones with LID.

We notice that in Tab. 2.11 and Tab. 2.12 the solar mixing angle θ_{12} differs by up to 20% between Case I/Case II with $\sin^2 \theta_{12} \simeq 0.283$ and Case III/Case IV where larger values of $\sin^2 \theta_{12}$ are obtained. In the next years planned experiments will be able to distinguish among different mixing values. The experiment JUNO [44] will be able to reduce the error on the best fit value of $\sin^2 \theta_{12}$ at 1% level, thus allowing for a discrimination among Case I/Case II and Case III/Case IV. According to the RENO-50 collaboration its planned experiment can achieve a similar reduction of the error, see Ref. [137]. For θ_{23} no distinction is possible between Case II and III, since the angle is maximal in both cases. Anyway, the predictions for Case I and Case IV considerably differ: the atmospheric mixing angle is larger in Case I than in Case IV. This difference is large enough to be possibly distinguished in the experiment $\text{NO}\nu A$ [138]. This experiment can also help in measuring the Dirac phase δ , using the data in the appearance $\nu_\mu \rightarrow \nu_e$ and disappearance $\nu_\mu \rightarrow \nu_\mu$ channels, so that a discrimination between Case II/Case III where δ is maximal and Case I/Case IV with $\delta = 0$ or π might be possible. In contrast, the predictions for θ_{13} are almost the same in all cases and, hence, it is unlikely that they can be distinguished at future neutrino facilities.

3

Models of Neutrino Masses

In the analysis performed in Chapter 2 we obtain predictions for the mixing angles based on group theory. However, if we want to get other information about neutrino phenomenology, such as the absolute mass scale, we need to construct an explicit model. This approach was well established and several explicit models with non-abelian discrete symmetry combined with CP were studied in the literature: S_4 [74, 75, 139–141], A_4 [73, 142, 143], T' [76], $\Delta(27)$ [142, 144], $\Delta(48)$ [78, 145], $\Delta(96)$ [79, 146] as well as A_5 [86].

These kind of models need new additional degrees of freedom, the scalar flavon [147]. Flavons transform as irreducible representations of the flavour symmetry. When they acquire a non-zero vacuum expectation value (vev) we obtain the flavour structure of the model. This approach was largely used for models based on non-abelian discrete symmetry within a non-supersymmetric or supersymmetric framework, for a review see Refs. [67–69, 84].

In this Chapter we want to discuss several realizations for the neutrino mass spectrum based on A_5 and CP . In particular we concentrate our investigation on Case II of our previous classification. The basic facts about the neutrino mass matrix and the flavon vevs are summarized in Sec. 3.1. A detailed classification of the different realizations based on particular vacuum alignments is discussed in Sec. 3.3, while in Sec. 3.4 we illustrate our numerical results. In Sec. 3.5 we will discuss the results for the low energy observables: the effective masses m_β , for the β -decay, and $m_{\beta\beta}$, for the $0\nu\beta\beta$ -decay. As a last point, in Sec. 3.6, we will show an explicit model based on the classification performed in Sec. 3.3.

3.1 Case II

We showed in Chapter 2 that four types of neutrino mixing based on $A_5 \otimes CP$ accommodate well the observed oscillation parameters, *i.e.* all the mixing angles are in the allowed 3σ confidence regions. For the residual symmetry in the neutrino sector we assume $Z_2 \otimes CP$. Case I and II in our previous classification are constructed under the assumption of $G_\ell = Z_5$. Case III is based on $G_\ell = Z_3$, while case IV has the Klein group $Z_2 \otimes Z_2$ as a residual symmetry in the charged lepton sector.

In our analysis we consider Case II. Following the discussion of Sec. 2.3 a representative tuple (Q, Z, X) for this category is $(T, T^2 ST^3 T^2, X_0)$. We recapitulate the results discussed in Sec. 2.4.1 for this case. In our approach the PMNS matrix is written as

$$U_{\text{PMNS}} = \Omega_{\text{II}} R_{13}(\theta) K_\nu \quad (3.1)$$

where the matrix Ω_{II} is given by

$$\Omega_{\text{II}} = \begin{pmatrix} -c_\phi & -s_\phi & 0 \\ -s_\phi/\sqrt{2} & c_\phi/\sqrt{2} & -i/\sqrt{2} \\ -s_\phi/\sqrt{2} & c_\phi/\sqrt{2} & i/\sqrt{2} \end{pmatrix} \quad (3.2)$$

and we have defined $s_\phi \equiv 1/\sqrt{2+\varphi} \simeq 0.526$, $c_\phi \equiv \sqrt{1-s_\phi^2} = \sqrt{(1+\varphi)/(2+\varphi)} \simeq 0.851$, and $\varphi \equiv (1+\sqrt{5})/2 \simeq 1.618$ is the Golden Ratio. The matrix $R_{13}(\theta)$ is a rotation matrix in the 1–3 plane of an angle θ and K_ν is a diagonal matrix with entries ± 1 and $\pm i$ needed to have a positive mass spectrum. The neutrino mass matrix M_ν fulfills the conditions of invariance under the residual symmetry in the neutrino sector $\mathcal{G}_\nu = Z_2 \otimes CP$ defined in (2.33): $Z^T M_\nu Z = M_\nu$ and $X M_\nu X = M_\nu^*$ where $Z \in Z_2$ and X is a representation of the CP symmetry on the field space.

We then have the following texture for the neutrino mass matrix

$$M_\nu = m_0 \begin{pmatrix} s+x+z & \frac{3}{2\sqrt{2}}(z+i\varphi y) & \frac{3}{2\sqrt{2}}(z-i\varphi y) \\ \frac{3}{2\sqrt{2}}(z+i\varphi y) & \frac{3}{2}(x+iy) & s - \frac{x+z}{2} \\ \frac{3}{2\sqrt{2}}(z-i\varphi y) & s - \frac{x+z}{2} & \frac{3}{2}(x-iy) \end{pmatrix} \quad (3.3)$$

where all the parameters s, x, y and z are dimensionless and real and m_0 is the absolute neutrino mass scale. The neutrino mass matrix (3.3) can be diagonalized by U_{PMNS} in (3.1) with the additional condition

$$\tan 2\theta = \frac{2\sqrt{7+11\varphi}y}{2x(\varphi+1)+z(2\varphi+1)}. \quad (3.4)$$

The value of θ is independent on the overall sign in neutrino mass matrix M_ν , as expected. Notice that in the limit $y \rightarrow 0$ the neutrino mass matrix is invariant under the $\mu - \tau$ reflection symmetry [89, 90, 125, 126], *i.e.* under the action of the permutation matrix in the 2–3 plane, P_{23} , defined in (2.50).

The atmospheric angle is fixed to be maximal by symmetry, while the reactor angle is related to the internal angle θ through the relation

$$\sin^2 \theta_{13} = \frac{2+\varphi}{5} \sin^2 \theta. \quad (3.5)$$

The solar mixing angle θ_{12} is related to θ_{13} by the sum rule

$$\sin^2 \theta_{12} = \frac{3-\varphi}{5 \cos^2 \theta_{13}} \simeq \frac{0.276}{\cos^2 \theta_{13}}. \quad (3.6)$$

The Jarlskog invariant is

$$J_{\text{CP}} = -\frac{\sqrt{2+\varphi}}{20} \sin 2\theta. \quad (3.7)$$

The Dirac phase δ in this Case is maximal, $|\sin \delta| = 1$. Up to first order in θ the quantity $\tan 2\theta \sim \sin 2\theta$ hence the sign of J_{CP} is related to the sign of θ , thus we expect two solutions since we do not impose any constraints on δ . The other invariants, defined in Appendix D, called I_1 and I_2 , are trivial ($I_1 = I_2 = 0$), thus the Majorana phases α and β are zero or π . The reactor mixing angle θ_{13} is proportional to $\sin^2 \theta$ thus in order to obtain $\theta_{13} \sim 9^\circ$ a small value of θ is needed. Assuming the best fit value for θ_{13} we get $\theta_{\text{bf}} = \pm 0.175$. Due to the sum rule in (3.6) $\sin^2 \theta_{12} \simeq 0.283$, which is within the 3σ allowed range.

A small value of θ means that $|y| \ll |x|, |z|$, see (3.4), and up to first order in y^2 we can expand $\sin^2 \theta$ as

$$\sin^2 \theta = \frac{(11\varphi + 7)y^2}{[2(1 + \varphi)x + (1 + 2\varphi)z]^2} + \mathcal{O}(y^4). \quad (3.8)$$

The neutrino masses can be obtained from the diagonalization of M_ν as

$$U_{\text{PMNS}}^T M_\nu U_{\text{PMNS}} = \text{diag}\{\tilde{m}_1, \tilde{m}_2, \tilde{m}_3\} \quad (3.9)$$

where \tilde{m}_j are the complex masses of the Majorana neutrinos. We indicate the absolute value of \tilde{m}_j as m_j . Starting from our PMNS matrix we have

$$m_1 = m_0 \left| s - \frac{x}{2} + z \frac{3\varphi - 2}{4} - \frac{3}{4}(\varphi - 2) \sqrt{[2(1 + \varphi)x + (1 + 2\varphi)z]^2 + (28 + 44\varphi)y^2} \right| \quad (3.10a)$$

$$m_2 = m_0 \left| s + x + z \left(1 - \frac{3}{2}\varphi \right) \right| \quad (3.10b)$$

$$m_3 = m_0 \left| s - \frac{x}{2} + z \frac{3\varphi - 2}{4} + \frac{3}{4}(\varphi - 2) \sqrt{[2(1 + \varphi)x + (1 + 2\varphi)z]^2 + (28 + 44\varphi)y^2} \right|. \quad (3.10c)$$

Notice that m_2 does not depend on y since it is the eigenvalue of the fixed column, see (2.71). Expressions for the atmospheric and solar mass differences, Δm_{31}^2 and Δm_{21}^2 , are not difficult to obtain from Eq. (3.10) but they are rather cumbersome (in principle they depend on four independent parameters) and the physical properties of the mass orderings are difficult to extract. For this reason, we prefer to show them in the following subsection using a perturbative expansion in the appropriate small parameter y .

For the reactor mixing angle θ_{13} , we notice that it is invariant under the replacement $\theta \rightarrow -\theta$, see Eq. (3.8), and therefore, thanks to (3.4), it is invariant under the exchange $y \rightarrow -y$. The neutrino masses are also invariant under the same transformation; we then expect at least two solutions $\{s, x, \pm y, z\}$ for each point of the parameter space compatible with the experimental data. On the other hand, the relations involving masses and angles are independent on the overall sign in the mass matrix; hence the solutions are invariant under $\{s, x, y, z\} \rightarrow -\{s, x, y, z\}$ and we expect two pairs of solution for each point.

3.1.1 Flavons of Case II

As a first step we want to compute the explicit form of the vacuum expectation values (vev) of the flavon fields in a given representation $\mathbf{r} \in A_5$. The vev of $\phi_{\nu, \mathbf{r}}$ is invariant under G_ν , then it is possible to use the following relations

$$\langle \phi_{\nu, \mathbf{r}} \rangle = Z \langle \phi_{\nu, \mathbf{r}} \rangle \quad (3.11)$$

which is the equation for the positive eigenvalue(s) of Z in the representation \mathbf{r} . If we assume a CP symmetry in the neutrino sector we have to impose the additional condition

$$\langle \phi_{\nu, \mathbf{r}} \rangle = X_{\mathbf{r}} \langle \phi_{\nu, \mathbf{r}} \rangle^*. \quad (3.12)$$

The CP matrices in representation \mathbf{r} are classified in Sec. 2.3.3. Using the conditions defined in (3.11) and (3.12) we can construct the flavon vevs. In the case of $G_\nu = Z_2 \otimes CP$ and $Z = T^2 S T^3 T^2$, $X = X_0$ we obtain

$$\langle \phi_{\nu, \mathbf{1}} \rangle = v_1 \quad (3.13a)$$

$$\langle \phi_{\nu, \mathbf{3}} \rangle = v \left(-\sqrt{2}\varphi^{-1}, 1, 1 \right)^T \quad (3.13b)$$

$$\langle \phi_{\nu, \mathbf{3}'} \rangle = w(\sqrt{2}\varphi, 1, 1)^T \quad (3.13c)$$

$$\langle \phi_{\nu, \mathbf{4}} \rangle = (y_r - iy_i, (1 + 2\varphi)y_r - iy_i, (1 + 2\varphi)y_r + iy_i, y_r + iy_i)^T \quad (3.13d)$$

$$\langle \phi_{\nu, \mathbf{5}} \rangle = \left(-\sqrt{\frac{2}{3}}(x_r + x_{r,2}), -x_r + i\varphi x_i, x_{r,2} - ix_i, x_{r,2} + ix_i, x_r + i\varphi x_i \right)^T \quad (3.13e)$$

where all coefficients are reals.

3.1.2 Two step symmetry breaking

To obtain a small value of θ it is possible to use a two-step symmetry breaking such as: $\mathcal{G}_\ell \rightarrow \mathcal{G}_\nu = Z_2 \otimes Z_2 \otimes CP \rightarrow Z_2 \otimes CP$. The Klein group and CP can be used to set the parameter y , which controls the size of θ , equal to zero. A possible choice is $y \propto y_r$ in (3.13d) and/or $y \propto x_i$ in (3.13e). In this case the parameter y is vanishing and only under $Z_2 \otimes CP$ it is non zero, therefore it is naturally the smallest parameter.

3.2 Constraints on neutrino masses

In the following we want to obtain testable predictions on the mass spectrum. This fact can be achieved reducing the number of independent parameters. The easiest way is to set some of the flavon vevs to zero: in several cases this fact is equivalent to leave out some flavons in a model; if not, due to reduced number of fields, we have to arrange for some vacuum alignment that leads to this.

Since we have four observables (three neutrino masses and one independent mixing angle because of (3.6)), we expect sum rules for neutrino masses and testable correlations, see Refs. [148–151]. These are worked out in each of the classes studied. Thus, in the following, we will start a classification reducing the number of independent parameters.

We assume two mechanisms to generate the light neutrino masses: Mechanism I involves the Weinberg operator [152] and Type II see-saw [153–155], while Mechanism II is based on Type I [156–159] and Type III [160] see-saw. Under the assumption of single type of new particles added to the SM, these three types of see-saw realizations exhaust all the possibilities of reproducing the Weinberg operator, see Ref. [161].

In our analysis we consider two realizations for the Type I (III): Mechanism II-1 where the Dirac mass matrix M_D is trivial, and Mechanism II-2 where the heavy Majorana mass matrix M_M is trivial. In this way we keep the number of independent parameters as small as possible.

We also assume different properties under A_5 for the matter field(s) in each mechanism: for Mechanism I we can have $L \sim \mathbf{3}$ or $\mathbf{3}'$ while for Mechanism II L and ν^c transform as $\mathbf{3}$ and/or $\mathbf{3}'$. A schematic representation of the classification used is shown in Fig. 3.1 where all the cases are summarized.

3.2.1 Equivalence between different mechanisms

The number of independent mechanisms discussed above can be reduced using the fact that the phenomenology of two (a priori) different cases is the same under the redefinition of the model parameters. In the following we use the same convention of Ref. [162] for the field content.

- **Weinberg and Type II see-saw**

The first observation is that the Weinberg operator and the Type II see-saw realization give us the same predictions. In fact, neglecting the A_5 contractions and flavour indices,

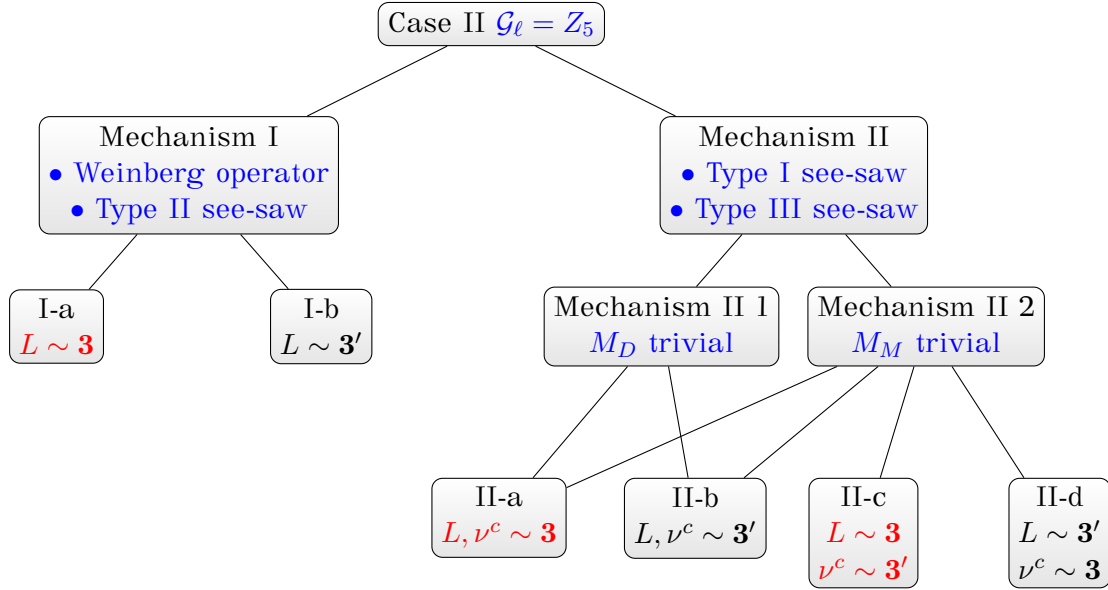


Figure 3.1: Scheme of the classification of neutrino masses used in this Chapter, see text for further details. We highlight in red the independent cases in our classification.

the effective operator for the Weinberg operator is

$$\mathcal{O}_{\text{Weinberg}} = y_W \frac{(L^T i \sigma_2 H) C (H^T i \sigma_2 L)}{\Lambda} \quad (3.14)$$

where Λ is the UV cutoff, C the charge conjugation operator, σ_2 the Pauli matrix, L is the usual lepton doublet and H the Higgs field. The relevant part of the Type II lagrangian is

$$\mathcal{L}_{\text{II}} \supset -y_{\text{II}} L^T C \sigma_2 \Delta L + h.c. \quad (3.15)$$

where Δ is a scalar that transforms as $(\mathbf{1}, \mathbf{2}, \mathbf{2})$ under the SM gauge group $SU(3)_c \otimes SU(2)_L \otimes U(1)_Y$. The scalar Δ can acquire a vev through the scalar potential

$$V_{\text{scalar}} = \mu H^T \sigma_2 \Delta^* H + m_\Delta^2 \text{Tr}\{\Delta \Delta\} + \dots \quad (3.16)$$

and thus $\langle \Delta \rangle \simeq \mu \langle H \rangle^2 / m_\Delta^2$. When Δ acquires a non-zero vev $m_\nu \neq 0$, and for $m_\Delta \gg \langle H \rangle$ and $\mu = \mathcal{O}(1)$ eV we get a light neutrino mass. Since we want to discuss the correlations in the mass spectrum it is sufficient to study only the Weinberg operator because the neutrino mass matrix M_ν is related to the one of Type II by the parameter redefinition

$$y_W \frac{\langle H \rangle^2}{\Lambda} \longleftrightarrow y_{\text{II}} \langle \Delta \rangle. \quad (3.17)$$

• Type I and Type III see-saw

A similar strategy is possible between Type I and Type III see-saw. In fact the lagrangian responsible for the Majorana mass in Type I is

$$\mathcal{L}_1 \supset -y_1 \bar{L} \sigma_2 H^* \nu^c + \frac{M_M}{2} \nu^c \nu^c + h.c. \quad (3.18)$$

where ν^c is the right-handed neutrino. The mass matrix for the light neutrinos can be obtained using the well know relation

$$M_\nu = -M_D^T M_M^{-1} M_D \quad (3.19)$$

where $M_D = y_D \langle H \rangle$ is the Dirac mass matrix and M_M is the mass of heavy Majorana particle. For Type III the additional field is \vec{T} , a fermionic triplet under $SU(2)_L$, and the lagrangian is

$$\mathcal{L}_{\text{III}} \supset y_{\text{III}} L^T C \sigma_2 \vec{\sigma} \cdot \vec{T} H + m_T \vec{T} \cdot \vec{T}. \quad (3.20)$$

In exactly the same manner as before in Type I, one gets a Type III see-saw for $m_T \gg \langle H \rangle$

$$M_\nu = y_{\text{III}}^T m_T^{-1} y_{\text{III}} \langle H \rangle^2 \quad (3.21)$$

and thus, without loss of generality, we can investigate only the Type I realizations since we are interesting on correlations about the mass spectrum and mixing angles.

• Mechanisms I-a and I-b

In the case of Mechanism I the predictions for $L \sim \mathbf{3}$ and $L \sim \mathbf{3}'$ are the same. Using the A_5 generators in representation $\mathbf{3}'$ the PMNS of Case II, defined in Eq. (3.1), can be obtained with a representative tuple $(Q, Z, X) = (T, S, X_0)$. The vev of the flavon invariant under the action of $Z = S$ in the five-dimensional representation is

$$\langle \phi_{\nu, \mathbf{5}} \rangle = \left(-\sqrt{\frac{2}{3}}(x_r + x_{r,2}), -x_r + i(1 - \varphi)x_i, x_{r,2} - ix_i, x_{r,2} + ix_i, x_r + i(1 - \varphi)x_i \right)^T. \quad (3.22)$$

We can recover the same phenomenology under the redefinition of the vevs

$$v_1 \longrightarrow v_1 \quad x_r \longleftrightarrow x_{r,2} \quad x_i \longrightarrow \varphi x_i \quad (3.23)$$

which is equivalent to a redefinition of the neutrino mass matrix parameter in (3.3): $s \longrightarrow s, x \longleftrightarrow z$ and $y \longrightarrow \varphi y$.

• Mechanisms II-a and II-b

Here we can have two possibilities: trivial M_D or trivial M_M .

- For a trivial Dirac mass matrix M_D the redefinition of the vevs is the same as before, (3.23). In this case we can perform a redefinition of the parameters in the heavy Majorana mass matrix M_M (indicated with capital letters) $S \longrightarrow S, X \longleftrightarrow Z$ and $Y \longrightarrow \varphi Y$.
- In the case of a trivial Majorana mass matrix M_M we have to consider the vev of flavons in representation $\mathbf{3}'$ invariant under $S = Z$. It is

$$\langle \phi_{\nu, \mathbf{3}'} \rangle = w \left(-\sqrt{2}\varphi^{-1}, 1, 1, \right)^T. \quad (3.24)$$

We notice that with respect to the case $L, \nu^c \sim \mathbf{3} \in A_5$, we have to change the vevs as

$$v \longrightarrow w \quad x_i \longrightarrow \varphi^{-1} x_i \quad x_r \longleftrightarrow x_{r,2} \quad (3.25)$$

to reproduce the same mass matrix.

• Mechanisms II-c and II-d

In this case we need to know the vev invariant under the action of $Z = S$ for the four-dimensional representation

$$\langle \phi_{\nu, \mathbf{4}} \rangle = (y_r - iy_i, (3 - 2\varphi)y_r - iy_i, (3 - 2\varphi)y_r + iy_i, y_r + iy_i)^T. \quad (3.26)$$

If we consider the light neutrino mass matrix M_ν we observe that it is invariant under the vevs redefinition

$$x_r \longleftrightarrow \pm x_{r,2} \quad x_i \longrightarrow \pm \varphi x_i \quad y_r \longrightarrow \pm(1 + 2\varphi)y_r \quad y_i \longrightarrow \mp y_i. \quad (3.27)$$

3.3 Analytic results

In this Section we discuss the main features for the mechanisms described above. In particular we investigate the mass spectrum and the sum rule Σ for the complex masses (further details in Appendix E). We also investigate the mass hierarchy, give predictions for the Majorana phases and the analytical relations among the flavon vevs to get the mass splittings and mixing angles in the allowed 3σ confidence region; a discussion on the sum of the neutrino masses and the parameters m_β and $m_{\beta\beta}$ is also included.

The strategy adopted to achieve this program is summarized as follows:

- from Eq. (3.4) we derive the expression of the internal angle θ and, using (3.8), we obtain a prediction for the mixing angle θ_{13} ; this allows to identify the parameter y in M_ν as the appropriate expansion parameter to be used in our analytical approximate estimates of the physical observables; notice that, in order to make θ_{13} numerically close to the experimental value, this requires a correlation among the same y and other parameters;
- masses and then mass differences are easily obtained from the mass spectrum at the appropriate perturbative order; with them, we can study the type of neutrino mass ordering imposing the following constraints:
 - $\Delta m_{21}^2 > 0$ and $\Delta m_{32}^2 > 0$ ($m_1 < m_2 < m_3$) for Normal Ordering (NO);
 - $\Delta m_{21}^2 > 0$ and $\Delta m_{31}^2 < 0$ ($m_3 < m_1 < m_2$) for Inverted Ordering (IO);
- in order to make the mass differences compatible with the experimental values, the ratio $r_\ell = \Delta m_{21}^2 / \Delta m_{3\ell}^2$ ($\ell = 1$ for NO or $\ell = 2$ for IO) is built for the allowed mass ordering and an ansatz of proportionality among the two remaining parameters is imposed: $p_1 = kp_2$; k is determined requiring r_ℓ and θ_{13} to be in the 3σ range; these ansatze have also been numerically verified. In the case of a small spread for k we quote only the value that accommodates well θ_{13} and the ratio r_ℓ ;
- finally, the prediction for mass sum rules, phases and effective masses are drawn when a natural expansion is possible.

In the following, we analyse more closely the relevant features of the sub-cases of each Mechanisms. To facilitate the comparison among the different cases, at the end of the sections we report two tables; the exact analytical predictions are highlighted in green.

3.3.1 Mechanism I

Field	L	H	$\phi_{\nu,1}$	$\phi_{\nu,5}$
A_5	3	1	1	5

Table 3.1: Quantum numbers of the fields involved in Mechanism I.

The effective lagrangian responsible for the neutrino masses is

$$\mathcal{L}^{eff} = y_1 \frac{[(LH)^2]_{\mathbf{1}} \phi_{\nu,1}}{\Lambda^2} + y_5 \frac{[(LH)^2]_{\mathbf{5}} \phi_{\nu,5}}{\Lambda^2}. \quad (3.28)$$

The quantum number of the matter, Higgs and flavon fields are reported in Tab. 3.1. Since the lepton fields L are in the same representation of A_5 only the contributions from

singlet and pentaplet flavons are relevant in the lagrangian ($[L \otimes L]_{\mathbf{3}} = (0, 0, 0)^T$). The Yukawa couplings are real, assuming our convention for the Clebsch-Gordan coefficients, see Appendix C for further details. After symmetry breaking (flavour and electroweak), we obtain a mass matrix M_ν for the neutrinos of the same form as in Eq. (3.3) with

$$s \equiv y_1 \frac{v_1}{\Lambda} \quad (3.29)$$

(contribution from the flavon singlet) and

$$x \equiv -y_5 \frac{x_{r,2}}{\Lambda} \sqrt{\frac{2}{3}} \quad y \equiv -y_5 \frac{x_i}{\Lambda} \sqrt{\frac{2}{3}} \quad z \equiv -y_5 \frac{x_r}{\Lambda} \sqrt{\frac{2}{3}}. \quad (3.30)$$

(contributions from the pentaplet). We notice that the parameter y comes from the pure imaginary part of the vev of the flavon in the representation $\mathbf{5}$. The absolute mass scale in this model can be set as

$$m_0 \equiv \frac{\langle H \rangle^2}{\Lambda}. \quad (3.31)$$

Here $\langle H \rangle^2 = 174$ GeV is the Higgs vacuum expectation value and Λ is the UV cutoff scale. In the case of $m_0 = \mathcal{O}(1)$ eV, the cutoff Λ is of order $\Lambda = \mathcal{O}(10^{13})$ GeV.

3.3.1.1 Mechanism I: $z = 0$

The reactor mixing angle, up to $\mathcal{O}(y^2)$, is given by

$$\sin^2 \theta_{13} = \frac{1 + \varphi y^2}{4 x^2} + \mathcal{O}(y^4). \quad (3.32)$$

The mass spectrum at NLO is

$$m_1 = m_0 \left| s + x + \frac{3}{4x} (2 + \varphi) y^2 + \mathcal{O}(y^4) \right| \quad (3.33a)$$

$$m_2 = m_0 |s + x| \quad (3.33b)$$

$$m_3 = m_0 \left| s - 2x - \frac{3}{4x} (2 + \varphi) y^2 + \mathcal{O}(y^4) \right|. \quad (3.33c)$$

We can now obtain a sum rule Σ for the complex masses \tilde{m}_j up to $\mathcal{O}(\sin^4 \theta_{13})$, which reads

$$\Sigma \equiv \tilde{m}_1 - \tilde{m}_2 + (3 - \varphi) (\tilde{m}_3 - \tilde{m}_2) \sin^2 \theta_{13} + \mathcal{O}(m \sin^4 \theta_{13}) \quad (3.34)$$

where the factor m is just the dimension scaling of the sum rule. From the mass spectrum, Eq. (3.33), we derive that IO is excluded and only the NO is acceptable for the mass spectrum, provided that $x > 0 \wedge s < -x$ or $x < 0 \wedge s > -x$.

Using the mass spectrum (3.33) we are able to predict the Majorana phases: under the assumption $m_1 > 0$, we have $\alpha = 0$ and $\beta = 0$.

The ratio between the solar and atmospheric mass-squared differences is given by

$$r_1 = \frac{2(3 - \varphi)(s + x)}{(2s - x)} \sin^2 \theta_{13} + \mathcal{O}(\sin^4 \theta_{13}). \quad (3.35)$$

where we used the relation defined in (3.32). To reproduce the experimental value of r_1 , we find that the linear relation $s = kx$, with $k = -20$ is quite a good ansatz. Consequently,

$$r_1 = 1.28 \sin^2 \theta_{13} + \mathcal{O}(\sin^4 \theta_{13}) \quad (3.36)$$

giving $r_1 = 0.031$ at θ_{bf} . It is important to observe that the previous correlation between s and x has been derived using the perturbative expansion in Eq. (3.35); however, it is well possible that this relation could be modified by higher order effects and/or cancellations between NLO and N²LO terms, visible in the numerical scan where all parameters are free and no correlation is imposed (see later). For this particular case, it turns out that $k = -6$ and $k \rightarrow -10^3$ also give good values of r_1 :

$$r_1 = \begin{cases} 1.38 \sin^2 \theta_{13} + \mathcal{O}(\sin^4 \theta_{13}) & s = -10^3 x \\ 1.06 \sin^2 \theta_{13} + \mathcal{O}(\sin^4 \theta_{13}) & s = -6x \end{cases} \quad (3.37)$$

For $k = -6$ we need a large value of θ_{13} in order to obtain a compatible value for r_1 , while assuming $k = -10^3$ the best fit point of θ_{13} gives $r_1 = 0.030$, in good agreement with the experimental data. Notice that the case $k = -10^3$, obtained in our numerical analysis is a good approximation for $k \rightarrow -\infty$, which corresponds to the limit of degenerate mass spectrum $m_j/m_0 = |s| + \mathcal{O}(y^2)$.

The sum of the neutrino masses is proportional to a non-trivial combination of the ratio r_1 and θ_{13}

$$\sum_j m_j \simeq \sqrt{\Delta m_{21}^2 \frac{5 \sin^2 \theta_{13} - r_1(\varphi + 2)}{r_1 \sin^2 \theta_{13}} \frac{r_1(\varphi + 1) + 2 \sin^2 \theta_{13}(\varphi + 2)}{2[5\varphi \sin^2 \theta_{13} - r_1(3\varphi + 1)]}} \quad (3.38)$$

which implies a lower bound $\sum_j m_j \gtrsim 0.155$ eV.

Using the ansatz $s = kx$, our estimates for m_β and $m_{\beta\beta}$ are:

$$m_\beta = \sqrt{-\frac{\Delta m_{31}^2 (k+1)^2}{6k-3} \left[1 + \frac{1}{2} \left(\frac{9}{(k+1)^2} + 2\varphi - 6 \right) \sin^2 \theta_{13} + \mathcal{O}(\sin^4 \theta_{13}) \right]} \quad (3.39)$$

which, taking into account the best fit values of the observables and the range of the allowed values of k , derived in (3.37), translates into the bound

$$3.86 \times 10^{-2} \text{ eV} \lesssim m_\beta \lesssim 6.20 \times 10^{-1} \text{ eV}, \quad (3.40)$$

and

$$m_{\beta\beta} = -\sqrt{\frac{\Delta m_{31}^2}{3-6k} (k+1) [1 - (3-\varphi) \sin^2 \theta_{13} + \mathcal{O}(\sin^4 \theta_{13})]} \quad (3.41)$$

from which

$$3.85 \times 10^{-2} \text{ eV} \lesssim m_{\beta\beta} \lesssim 6.20 \times 10^{-1} \text{ eV}. \quad (3.42)$$

In particular, for $k = -20$ we have $m_\beta \simeq m_{\beta\beta} \simeq 8.24 \times 10^{-2}$ eV.

3.3.1.2 Mechanism I: $x = 0$

For this case we have

$$\sin^2 \theta_{13} = \frac{y^2}{z^2} + \mathcal{O}(y^4). \quad (3.43)$$

At LO the mass spectrum is

$$m_1 = m_0 \left| s + \frac{1}{2}(3\varphi - 1)z + \mathcal{O}(y^2) \right| \quad (3.44a)$$

$$m_2 = m_0 \left| s - \left(\frac{3\varphi}{2} - 1 \right) z \right| \quad (3.44b)$$

$$m_3 = m_0 \left| \frac{1}{2}(2s - z) + \mathcal{O}(y^2) \right| \quad (3.44c)$$

which implies the following mass sum rule for the complex neutrino masses \tilde{m}_j

$$\Sigma = \tilde{m}_1 + (\varphi + 1)\tilde{m}_2 - (\varphi + 2)\tilde{m}_3 + \mathcal{O}(m \sin^2 \theta_{13}) \quad (3.45)$$

where m is a dimensionful factor needed to correctly reproduce the right dimension of Σ . The solar mass difference is

$$\Delta m_{21}^2/m_0^2 = -\frac{3(2\varphi - 1)}{4}z(4s + z) - 3\frac{s(4\varphi - 2) + (\varphi + 7)z}{2z}y^2 + \mathcal{O}(y^4). \quad (3.46)$$

Eq. (3.46) tells us that although the condition $z = -s/4$ makes zero the LO term it also causes negative coefficients of the y^2 terms in the expansion of the mass differences, for any value of the model parameters. Thus, the positiveness of the solar mass difference can only be obtained invoking a cancellation between LO and NLO terms. In particular, we get that only IO is allowed for this case, provided that $z > 0 \wedge -z(\varphi + 3)/4\varphi < s < -z/4$ or $z < 0 \wedge -z/4 < s < -z(\varphi + 3)/4\varphi$.

The Majorana phases could be predicted using the condition for a definite mass spectrum and Eq. (3.44) with the additional condition $m_1 > 0$. We have $\alpha = \pi$ and $\beta = \pi$.

The expression for r_2 as a function of θ_{13} is given by

$$r_2 = -\frac{(2\varphi - 1)(4s + z)}{4s(\varphi - 1) + (\varphi - 4)z} + \frac{4(4s^2(\varphi - 8) + s(11 - 7\varphi)z - 2(\varphi - 8)z^2)}{(4s(\varphi - 1) + (\varphi - 4)z)^2} \sin^2 \theta_{13} + \mathcal{O}(\sin^4 \theta_{13}) \quad (3.47)$$

and the ansatz $s \simeq -0.3z$ provides a good choice to reproduce the experimental value of r_2 ¹, $r_2 \simeq -0.14 + 4.33 \sin^2 \theta_{13} \sim -0.040$ for $\sin^2 \theta_{13} = 2.19 \times 10^{-2}$. Also in this case, we have observed that the coefficient of the (undisplayed) $\sin^4 \theta_{13}$ term can be as large as $\sim +8$, thus the corrections to the previous relations can be important and can partially destroy the correlation found above. For example, for $\theta = \theta_{\text{bf}}$, the N²LO computation gives $r_2 = -0.034$, a roughly 10% correction to the pure $\mathcal{O}(\sin^2 \theta_{13})$ contribution.

Using the relations derived above and the correlation between s and z we obtain for the sum of the neutrino masses

$$\sum_j m_j = \sqrt{-\Delta m_{32}^2} [2.71 + 7.49 \sin^2 \theta_{13} + \mathcal{O}(\sin^4 \theta_{13})] \simeq 1.42 \times 10^{-1} \text{ eV}. \quad (3.48)$$

For m_β and $m_{\beta\beta}$ we get

$$m_\beta \simeq \sqrt{-\Delta m_{32}^2} [1.08 + 2.40 \sin^2 \theta_{13} + \mathcal{O}(\sin^4 \theta_{13})] \simeq 5.61 \times 10^{-2} \text{ eV} \quad (3.49)$$

$$m_{\beta\beta} \simeq \sqrt{-\Delta m_{32}^2} [0.46 + 0.52 \sin^2 \theta_{13} + \mathcal{O}(\sin^4 \theta_{13})] \simeq 2.32 \times 10^{-2} \text{ eV} \quad (3.50)$$

where we used the best fit values of Δm_{32}^2 and θ_{13} [45].

3.3.1.3 Mechanism I: $s = 0$

The expression of $\tan 2\theta$ is the same as the one quoted in Eq. (3.4) (since this does not depend on s) and the reactor mixing angle θ_{13} fulfills Eq. (3.5) with the same $\sin^2 \theta$ defined

¹The other solution for k gives $s \simeq 0.9z$. However this solution reproduces the wrong sign of the solar mass difference, thus we exclude this possibility.

in (3.8). The mass eigenstates can be expressed at LO as

$$m_1 = m_0 \left| x + \frac{1}{2}(3\varphi - 1)z + \mathcal{O}(y^2) \right| \quad (3.51a)$$

$$m_2 = m_0 \left| x - \left(\frac{3\varphi}{2} - 1 \right) z \right| \quad (3.51b)$$

$$m_3 = m_0 \left| -\frac{1}{2}(4x + z) + \mathcal{O}(y^2) \right|. \quad (3.51c)$$

We have at LO the following exact mass sum rule for the complex neutrino masses \tilde{m}_j

$$\Sigma = \tilde{m}_1 + \tilde{m}_2 + \tilde{m}_3. \quad (3.52)$$

For NO, imposing $m_2 > m_1$ and $m_3 > m_2$ we get $x < 0 \wedge 0 < z < -2x/\varphi$ or $x > 0 \wedge -2x/\varphi < z < 0$, which tell us that the z parameter can be vanishingly small. Since there are no natural symmetry arguments behind this possibility, we will not discuss it more in detail. For IO, imposing again $m_2 > m_1$ but $m_3 < m_1$ we obtain $x < 0 \wedge -2x/\varphi < z < -4x$ or $x > 0 \wedge -4x < z < -2x/\varphi$, that, for a generic value of the x variable, does not set a strong restriction on the magnitude of z .

The Majorana phases are independent from the perturbative expansion and for NO (IO) are given by $\alpha = 0$ and $\beta = \pi$ ($\alpha = \pi$ and $\beta = 0$). From the sum rule Σ defined in (3.52) and assuming the best fit values for the solar and atmospheric squared-mass differences, we get in the case of NO $m_{\min} = m_1 = 2.77 \times 10^{-2}$ eV, and for IO $m_{\min} = m_3 = 7.64 \times 10^{-4}$ eV. The ratio r_2 is

$$r_2 = -\frac{(2\varphi - 1)z(4x + z)}{4x^2 + 4\varphi xz + (\varphi - 4)z^2} + \frac{4(2x^2 + xz + 2z^2) [4(\varphi - 2)x^2 - 4(\varphi - 1)xz - z^2] [(8\varphi + 6)x - (13\varphi + 6)z]}{[4x^2 + 4\varphi xz + (\varphi - 4)z^2]^2 (2(\varphi + 1)x + 2\varphi z + z)} \sin^2 \theta_{13} + \mathcal{O}(\sin^4 \theta_{13}). \quad (3.53)$$

The good ansatz in this case is $x = kz$ with $k \simeq -3/10$. For the sake of completeness, we also quote here the expression of θ_{13}

$$\sin^2 \theta_{13} = \frac{25(39\varphi + 34)}{961} \frac{y^2}{z^2} + \mathcal{O}(y^4) \quad x = -\frac{3}{10}z \quad (3.54)$$

from which we learn that $y/z \sim \pm 1/10$ must be fulfilled in order to reproduce the best fit value of θ_{13} . In this limit the ratio r_2 is given by

$$r_2 \simeq -0.11 + 2.33 \sin^2 \theta_{13} + \mathcal{O}(\sin^4 \theta_{13}) \quad (3.55)$$

thus in the 3σ CL region of experimental parameter space for $\theta \sim \theta_{\text{bf}}$. Using the relations among x, y and z discussed above, the sum of the neutrino masses can be expressed as

$$\sum_j m_j \simeq \sqrt{-\Delta m_{32}^2} [2.00 - 0.14 \sin^2 \theta_{13} + \mathcal{O}(\sin^4 \theta_{13})] \simeq 9.9 \times 10^{-2} \text{ eV} \quad (3.56)$$

whereas for m_β and $m_{\beta\beta}$ we have

$$m_\beta \simeq \sqrt{-\Delta m_{32}^2} [0.96 + 0.34 \sin^2 \theta_{13} + \mathcal{O}(\sin^4 \theta_{13})] \simeq 4.79 \times 10^{-2} \text{ eV} \quad (3.57)$$

and

$$m_{\beta\beta} \simeq \sqrt{-\Delta m_{32}^2} [0.41 + 0.03 \sin^2 \theta_{13} + \mathcal{O}(\sin^4 \theta_{13})] \simeq 2.01 \times 10^{-2} \text{ eV}, \quad (3.58)$$

where the numerical estimates are obtained for $\Delta m_{32}^2 = -2.449 \times 10^{-3} \text{ eV}^2$ and $\sin^2 \theta_{13} = 2.19 \times 10^{-2}$.

3.3.1.4 Mechanism I: summary tables

In this Section, we report all previous results in two different tables, to facilitate the comparison of the physics implied by the three cases analysed above. In particular, in Tab. 3.2 we report, for the allowed mass ordering, the predictions for the group theory parameter θ , the reactor angle and CP Majorana phases for Mechanism I. In Tab. 3.3, instead, we outline our results for the neutrino mass sum rules, for which we give the coefficients a, b and c of the complex masses \tilde{m}_j , for the assumed form $\Sigma(a, b, c) = a\tilde{m}_1 + b\tilde{m}_2 + c\tilde{m}_3$, and, given the somehow intricate analytical structure, the central numerical values of the sum of the neutrino masses and the effective masses m_β and $m_{\beta\beta}$ (for the case $z = 0$ instead we give a lower bound for $\sum_j m_j$ and an interval for the effective masses because the N²LO terms in the expression of the ratio r_1 turn out to be particularly important).

	$z = 0$	$x = 0$	$s = 0$
ordering	NO	IO	both
$\tan 2\theta$	$\sqrt{\varphi + 2} \frac{y}{x}$	$2\sqrt{3 - \varphi} \frac{y}{z}$	Eq. (3.4)
$\sin^2 \theta_{13}$	$\frac{1 + \varphi}{4} \frac{y^2}{x^2}$	$\frac{y^2}{z^2}$	$\frac{25(39\varphi + 34)}{961} \frac{y^2}{z^2}$
(α, β)	$(0, 0)$	(π, π)	$(0, \pi), (\pi, 0)$

Table 3.2: Leading order predictions for the group theory parameter θ , mixing angles and CP phases for Mechanism I. In the first line we also report the allowed ordering of the neutrino masses. The two values for (α, β) in the case $s = 0$ refer to NO and IO, respectively.

	$z = 0$	$x = 0$	$s = 0 - IO$
$\Sigma(a, b, c)$	$(1, -1 + (\varphi - 3)s_{13}^2, (3 - \varphi)s_{13}^2)$	$(1, \varphi + 1, -(2 + \varphi))$	$(1, 1, 1)$
$\sum_j m_j$ [eV]	$\gtrsim 0.155$	0.14	9.90×10^{-2}
m_β [eV]	$[3.86 \times 10^{-2}, 6.20 \times 10^{-1}]$	5.61×10^{-2}	4.79×10^{-2}
$m_{\beta\beta}$ [eV]	$[3.85 \times 10^{-2}, 6.20 \times 10^{-1}]$	2.32×10^{-2}	2.01×10^{-2}

Table 3.3: Leading order predictions for the neutrino mass sum rules and the numerical values of the sum of the neutrino masses and the effective masses m_β and $m_{\beta\beta}$ for Mechanism I. Here s_{13}^2 is a short-hand notation for $\sin^2 \theta_{13}$.

3.3.2 Mechanism II a-1

This section is devoted to the Type I see-saw mechanism with the lepton doublet and ν^c in the same A_5 representation and a trivial Dirac mass matrix. The quantum numbers of the matter, Higgs and flavon fields are reported in Tab. 3.4. With this assignment, the

Field	L	ν^c	H	$\phi_{\nu,1}$	$\phi_{\nu,5}$
A_5	3	3	1	1	5

Table 3.4: Quantum numbers of the fields involved in Mechanism II a-1.

Dirac mass matrix M_D is as simple as

$$M_D = m_D P_{23}, \quad (3.59)$$

where the matrix P_{23} is defined in (2.50) and $m_D \equiv y_D \langle H \rangle$, y_D is the Yukawa coupling and $\langle H \rangle$ is the Higgs vev. Assuming a Yukawa coupling of order one, the Dirac mass term is naturally of order $\mathcal{O}(10^2)$ GeV. The Majorana lagrangian is given by ²

$$\mathcal{L}_M = \frac{1}{2} \left\{ y_1 [(\nu^c \nu^c)_1 \phi_{\nu,1}]_1 + y_5 [(\nu^c \nu^c)_5 \phi_{\nu,5}]_1 \right\} + h.c. \quad (3.60)$$

and gives rise to a mass matrix with the same form of M_ν defined in (3.3). In order to avoid confusion we call with capital letters (S, X, Y and Z) the parameter of the heavy Majorana mass matrix. The absolute scale of the mass matrix is an arbitrary parameter that can be chosen as the scale of heavy Majorana particles. The matrix is

$$M_M = \bar{v} \begin{pmatrix} S + X + Z & \frac{3}{2\sqrt{2}}(Z + i\varphi Y) & \frac{3}{2\sqrt{2}}(Z - i\varphi Y) \\ \frac{3}{2\sqrt{2}}(Z + i\varphi Y) & \frac{3}{2}(X + iY) & S - \frac{X + Z}{2} \\ \frac{3}{2\sqrt{2}}(Z - i\varphi Y) & S - \frac{X + Z}{2} & \frac{3}{2}(X - iY) \end{pmatrix} \quad (3.61)$$

where

$$\bar{v} \equiv \max \left\{ |y_1 v_1|, |y_5 x_r|, |y_5 x_{r,2}|, |y_5 x_i| \right\} \sim \mathcal{O}(10^{13}) \text{ GeV} \quad (3.62)$$

and

$$S \equiv y_1 \frac{v_1}{\bar{v}} \quad (3.63)$$

which is the contribution from the flavon in representation $\mathbf{1}$, and

$$X \equiv -y_5 \frac{x_{r,2}}{\bar{v}} \sqrt{\frac{2}{3}} \quad Y \equiv -y_5 \frac{x_i}{\bar{v}} \sqrt{\frac{2}{3}} \quad Z \equiv -y_5 \frac{x_r}{\bar{v}} \sqrt{\frac{2}{3}}. \quad (3.64)$$

which are the contributions from the pentaplet.

The mass of the light neutrinos can be computed using the see-saw relation

$$M_\nu = -M_D^T M_M^{-1} M_D = -(M_M^{-1})^* m_D^2. \quad (3.65)$$

The parameters of M_M can be related to those of M_ν by

$$s = \frac{\bar{v}^3}{4 \det M_M} \left[4S^2 - 4X^2 - 6Y^2 - 2XZ - 4Z^2 - 3Y^2\varphi \right] \quad (3.66a)$$

$$x = -\frac{\bar{v}^3}{4 \det M_M} \left[4SX + 4X^2 + 4XZ + 3(Y^2 - Z^2 + Y^2\varphi) \right] \quad (3.66b)$$

$$y = -\frac{\bar{v}^3}{2 \det M_M} Y \left[2S + 2X + Z(2 - 3\varphi) \right] \quad (3.66c)$$

$$z = \frac{\bar{v}^3}{2 \det M_M} \left[-2SZ + 4XZ + Z^2 + 3Y^2\varphi \right] \quad (3.66d)$$

where the neutrino mass scale m_0 is

$$m_0 \equiv \frac{m_D^2}{\bar{v}} \quad (3.67)$$

²It is always possible to add in the Majorana lagrangian a direct mass term M . However the net effect is to rescale the coupling of the flavon in the representation $\mathbf{1}$ as $y_1 \phi_{\nu,1} \rightarrow M + y_1 \phi_{\nu,1}$. Thus the parameter S change as $S \rightarrow S + M/\bar{v}$.

and the determinant of the Majorana mass matrix reads

$$\det M_M = \frac{\bar{v}^3}{8} \left[-8S^3 + 6S(4X^2 + 2XZ + 3(\varphi + 2)Y^2 + 4Z^2) + 16X^3 + \right. \\ \left. + 12X^2Z + 6X(3(\varphi + 2)Y^2 - 7Z^2) - 63\varphi Y^2Z + 9Y^2Z - 11Z^3 \right]. \quad (3.68)$$

The scaling of the dimensionless parameters in M_ν is $\mathcal{O}(1)$ since the parameters of M_M are by construction $\lesssim 1$. The condition for $\det M_M \neq 0$, which gives us a constrain on the parameters S, X, Y and Z , guarantees the existence of M_M^{-1} .

The neutrino mass matrix M_ν can be diagonalized using U_{PMNS} of Case II with the additional condition on $\tan 2\theta$

$$\tan 2\theta = \frac{2\sqrt{11\varphi + 7}Y[2S + 2X - (3\varphi - 2)Z]}{2S(2(\varphi + 1)X + 2\varphi Z + Z) + 4(\varphi + 1)X^2 - 4\varphi XZ - (5\varphi + 4)Z^2} \quad (3.69)$$

where we notice that, with respect to the Weinberg operator, also the contribution from the singlet S appears. The expression for $\sin^2 \theta_{13}$ is the same as Eq. (3.5).

The light neutrino masses are fixed by the form of U_{PMNS} ; therefore we have formally the same expressions for the neutrino mass of the Weinberg operator, defined in (3.10) but with the parameters s, x, y and z now defined in (3.66). The spectrum of the heavy Majorana neutrinos are formally the same as those in (3.10) but evaluated with the parameters S, X, Y and Z .

3.3.2.1 Mechanism II a-1: $Z = 0$

The condition $Z = 0$ is equivalent to have $z \sim 0$ in the light neutrino mass matrix M_ν , because $z = \mathcal{O}(Y^2) = \mathcal{O}(x_i^2/\bar{v}^2)$, see (3.66). In this particular limit the relations for $\tan 2\theta$ and θ_{13} are the same as Mechanism I with $z = 0$ with the replacement $y \rightarrow Y$ and $x \rightarrow X$

$$\sin^2 \theta_{13} = \frac{1 + \varphi}{4} \frac{Y^2}{X^2} + \mathcal{O}(Y^4). \quad (3.70)$$

The neutrino mass spectrum at LO can be obtained from (3.33) with the transformation $m_j \rightarrow m_j^{-1}$. The spectrum is

$$m_1 = m_0 \left| -\frac{1}{S + X} + \mathcal{O}(Y^2) \right| \quad (3.71a)$$

$$m_2 = m_0 \left| -\frac{1}{S + X} \right| \quad (3.71b)$$

$$m_3 = m_0 \left| -\frac{1}{S - 2X} + \mathcal{O}(Y^2) \right|. \quad (3.71c)$$

We have the following mass sum rule for the complex masses \tilde{m}_j at NLO

$$\Sigma = \frac{1}{\tilde{m}_1} - \frac{1}{\tilde{m}_2} + (3 - \varphi) \left(\frac{1}{\tilde{m}_3} - \frac{1}{\tilde{m}_2} \right) \sin^2 \theta_{13} + \mathcal{O}(m^{-1} \sin^4 \theta_{13}) \quad (3.72)$$

where the factor m^{-1} is necessary to correctly reproduce the right mass dimension. Notice that we need to include the NLO contributions because at LO m_1 and m_2 are degenerate (we have $(m_2^{-1} - m_1^{-1})m_0 \propto \sin^2 \theta_{13}$).

Using the mass spectrum (3.71) we get that both NO and IO are allowed in this limit, provided that $X > 0 \wedge (X/2 < S < 2X \vee S > 2X)$ or $X < 0 \wedge (S < 2X \vee 2X < S < X/2)$ and $X > 0 \wedge (-X < S < X/2)$ or $X < 0 \wedge (X/2 < S < -X)$, respectively.

The value of the ratio r_ℓ , for both orderings, is given by

$$r_\ell = \frac{2(3-\varphi)(S-2X)^2}{(2S-X)(S+X)} \sin^2 \theta_{13} + \mathcal{O}(\sin^4 \theta_{13}). \quad (3.73)$$

As before, the ansatz $S = kX$ in the previous expression is used to correctly reproduce the best fit value of r_ℓ and θ_{13} ; we get two possible solutions: $S \simeq X$ and $S \simeq 44X$. For the first case, $S = X$, we obtain at LO $m_1/m_2 \sim 1$ and $m_3/m_2 \sim 2$ and non-trivial Majorana phases $\alpha = 0$ and $\beta = \pi$. Using the relations derived above and the relation between S and X the sum of the neutrino masses can be expressed as

$$\sum_j m_j = \sqrt{\frac{\Delta m_{31}^2}{3}} \left[4 + \frac{13}{2} \sqrt{5(2-\varphi)} \sin^2 \theta_{13} + \mathcal{O}(\sin^4 \theta_{13}) \right] \simeq 1.12 \times 10^{-1} \text{ eV}. \quad (3.74)$$

The effective masses are predicted to be

$$m_\beta = \sqrt{\frac{\Delta m_{31}^2}{3}} \left[1 - \frac{7}{2}(\varphi - 3) \sin^2 \theta_{13} + \mathcal{O}(\sin^4 \theta_{13}) \right] \simeq 3.16 \times 10^{-2} \text{ eV} \quad (3.75)$$

$$m_{\beta\beta} = \sqrt{\frac{\Delta m_{31}^2}{3}} \left[1 - \frac{1}{2}(12 - 7\varphi) \sin^2 \theta_{13} + \mathcal{O}(\sin^4 \theta_{13}) \right] \simeq 2.88 \times 10^{-2} \text{ eV} \quad (3.76)$$

where we used the explicit expression of the masses and the values of the Majorana phases, and in the numerical prediction we use the best fit values for θ_{13} and Δm_{31}^2 .

Now we consider the case $S = 44X$; a large value of S can be achieved if a direct mass term for the heavy neutrinos is possible, which means $M/\bar{v} = \mathcal{O}(10)$. This scenario is less interesting from the phenomenology point of view because the mass spectrum is quasi-degenerate; in fact, from (3.71) we have $m_j/m_0 = |S^{-1}| + \mathcal{O}(Y^2)$. Using Δm_{31}^2 we can express the sum of the neutrino masses as

$$\sum_j m_j \gtrsim \frac{945}{22} \sqrt{\frac{\Delta m_{31}^2}{29}} \simeq 0.38 \text{ eV} \quad (3.77)$$

which is still marginally compatible with the PLANCK data only (which imply $\sum_j m_j \leq 0.590 \text{ eV}$ @ 95% CL) but not with the CMB \oplus BAO data [53] (which give $\sum_j m_j \leq 0.230 \text{ eV}$ @ 95% CL). Both Majorana phases are vanishing $\alpha = 0$ and $\beta = 0$, whereas simple expressions m_β and $m_{\beta\beta}$ can be obtained

$$m_\beta = \frac{1}{420} \sqrt{\frac{\Delta m_{31}^2}{29}} \left[5580 + \frac{1}{2}(5908\varphi - 17681) \sin^2 \theta_{13} + \mathcal{O}(\sin^4 \theta_{13}) \right] \simeq 1.25 \times 10^{-2} \text{ eV} \quad (3.78)$$

$$m_{\beta\beta} = \frac{1}{15} \sqrt{\frac{\Delta m_{31}^2}{29}} \left[210 + \frac{1}{2}(211\varphi - 632) \sin^2 \theta_{13} + \mathcal{O}(\sin^4 \theta_{13}) \right] \simeq 1.25 \times 10^{-2} \text{ eV}. \quad (3.79)$$

Being $m_{\beta\beta} \simeq \sum_j m_j/3$, we have a lower bound $m_{\beta\beta} \gtrsim 0.12 \text{ eV}$.

The case of IO requires S , X and Y at the same order of magnitude; thus we will not consider such a possibility any more.

3.3.2.2 Mechanism II a-1: $X = 0$

Under the assumption of vanishing X the equation for $\sin^2 \theta_{13}$, Eq. (3.5), can be obtained from Mechanism I, $x = 0$, with the redefinition $y \rightarrow Y$ and $z \rightarrow Z$

$$\sin^2 \theta_{13} = \frac{Y^2}{Z^2} + \mathcal{O}(Y^4). \quad (3.80)$$

The light neutrino masses at LO are related to the spectrum (3.44) with the redefinition $m_j \rightarrow m_j^{-1}$

$$m_1 = m_0 \left| -\frac{2}{2S + (3\varphi - 1)Z} + \mathcal{O}(Y^2) \right| \quad (3.81a)$$

$$m_2 = m_0 \left| -\frac{2}{2(S + Z) - 3\varphi Z} \right| \quad (3.81b)$$

$$m_3 = m_0 \left| -\frac{2}{2S - Z} + \mathcal{O}(Y^2) \right|. \quad (3.81c)$$

In this case the sum of the complex masses \tilde{m}_j is

$$\Sigma = \frac{1}{\tilde{m}_1} + \frac{1 + \varphi}{\tilde{m}_2} - \frac{\varphi + 2}{\tilde{m}_3} + \mathcal{O}(m^{-1} \sin^2 \theta_{13}). \quad (3.82)$$

where the parameter m^{-1} is necessary to reproduce the correct mass dimension. The expressions for the mass-squared differences and the related ratio r_ℓ are quite cumbersome. From the ratios m_1/m_2 and m_3/m_2 we deduce that only the NO is allowed if $Z > 0 \wedge (3\varphi - 1)Z/4 > S > -Z/4$ or $(3\varphi - 1)Z/4 < 0 \wedge Z < S < -Z/4$. The experimental value of the (undisplayed) ratio r_1 is reproduced with the ansatz $S = kZ$ for three different values of the real parameter k , that is $k \simeq 1/3$, $k \simeq -1/4$ and $k \simeq 2/3$. (The case $k \simeq -1/4$ leads a natural suppression of the solar mass splitting.) Accordingly, we obtain $m_1/m_2 \sim 1/2$ and $m_3/m_2 \sim 13/2$ for $S = Z/3$, $m_1/m_2 \sim 1$ and $m_3/m_2 \sim \sqrt{5}$ for $S = -Z/4$ and we have $m_1/m_2 \sim 1/3$ and $m_3/m_2 \sim 9/2$ for $S = 2Z/3$.

The Majorana phases are fixed by (3.81) and the mass ordering. In the case $S/Z \sim 1/3$ and $S/Z \sim -1/4$ we get $\alpha = \pi$ and $\beta = \pi$ while in the case $S/Z \sim 2/3$ we obtain $\alpha = \pi$ and $\beta = 0$.

Also for $\sum_j m_j$, m_β and $m_{\beta\beta}$ we can draw three different predictions (obtained using the best fit values of atmospheric mass difference and the reactor mixing angle). For $S = Z/3$ we have

$$\sum_j m_j = \sqrt{\Delta m_{31}^2} [1.23 + 4.58 \sin^2 \theta_{13} + \mathcal{O}(\sin^4 \theta_{13})] \simeq 6.59 \times 10^{-2} \text{ eV} \quad (3.83)$$

$$m_\beta = \sqrt{\Delta m_{31}^2} [0.10 + 6.91 \sin^2 \theta_{13} + \mathcal{O}(\sin^4 \theta_{13})] \simeq 1.26 \times 10^{-2} \text{ eV} \quad (3.84)$$

and

$$m_{\beta\beta} = \sqrt{\Delta m_{31}^2} [-0.011 + 0.93 \sin^2 \theta_{13} + \mathcal{O}(\sin^4 \theta_{13})] \simeq 4.49 \times 10^{-4} \text{ eV}. \quad (3.85)$$

In the case $S = -Z/4$ we obtain

$$\sum_j m_j = \sqrt{\Delta m_{31}^2} \left[\frac{1 + 2\varphi}{2} + (9\varphi - 5) \sin^2 \theta_{13} + \mathcal{O}(\sin^4 \theta_{13}) \right] \simeq 1.11 \times 10^{-1} \text{ eV} \quad (3.86)$$

$$m_\beta = \frac{1}{10} \sqrt{\Delta m_{31}^2} [5 + (23\varphi - 9) \sin^2 \theta_{13} + \mathcal{O}(\sin^4 \theta_{13})] \simeq 2.78 \times 10^{-2} \text{ eV} \quad (3.87)$$

$$m_{\beta\beta} = \frac{1}{10} \sqrt{\Delta m_{31}^2} [2\varphi - 1 + (13\varphi - 9) \sin^2 \theta_{13} + \mathcal{O}(\sin^4 \theta_{13})] \simeq 9.78 \times 10^{-3} \text{ eV}. \quad (3.88)$$

Finally for $S = 2Z/3$ we have

$$\sum_j m_j = \sqrt{\Delta m_{31}^2} [1.23 - 5.91 \sin^2 \theta_{13} + \mathcal{O}(\sin^4 \theta_{13})] \simeq 5.73 \times 10^{-2} \text{ eV} \quad (3.89)$$

$$m_\beta = \sqrt{\Delta m_{31}^2} [0.13 + 1.30 \sin^2 \theta_{13} + \mathcal{O}(\sin^4 \theta_{13})] \simeq 7.74 \times 10^{-3} \text{ eV} \quad (3.90)$$

and

$$m_{\beta\beta} = \sqrt{\Delta m_{31}^2} [-0.014 + 1.16 \sin^2 \theta_{13} + \mathcal{O}(\sin^4 \theta_{13})] \simeq 5.63 \times 10^{-4} \text{ eV}. \quad (3.91)$$

3.3.2.3 Mechanism II a-1: $S = 0$

In this limit the reactor mixing angle becomes

$$\sin^2 \theta_{13} = \frac{(8\varphi + 5)[2X + (2 - 3\varphi)Z]^2}{[-4(\varphi + 1)X^2 + 4\varphi XZ + (5\varphi + 4)Z^2]^2} Y^2 + \mathcal{O}(Y^4). \quad (3.92)$$

Neglecting accidental cancellation in the numerator, we then expect $|Y| \ll |X|, |Z|$. We can obtain the LO expressions for the light neutrino masses

$$m_1 = m_0 \left| -\frac{2}{2X + (3\varphi - 1)Z} + \mathcal{O}(Y^2) \right| \quad (3.93a)$$

$$m_2 = m_0 \left| -\frac{2}{2X + (2 - 3\varphi)Z} \right| \quad (3.93b)$$

$$m_3 = m_0 \left| \frac{2}{4X + Z} + \mathcal{O}(Y^2) \right|. \quad (3.93c)$$

The sum for the complex masses \tilde{m}_j gives the exact (to all orders) sum rule

$$\Sigma = \frac{1}{\tilde{m}_1} + \frac{1}{\tilde{m}_2} + \frac{1}{\tilde{m}_3}. \quad (3.94)$$

From the mass spectrum (3.93) we observe that both orderings are in principle allowed: NO if $Z > 0 \wedge -Z/4 < X < -\varphi Z/2$ or $Z < 0 \wedge -\varphi Z/2 < X < -Z/4$ and IO for $Z < 0 \wedge 2(X + Z) < 3\varphi Z$ or $Z > 0 \wedge 2(X + Z) > 3\varphi Z$. Within this articulated parameter space, the limits $X \rightarrow 0$ and $Z \rightarrow 0$ give a particular simple expression for the ratio m_3/m_2 :

$$\frac{m_3}{m_2} = \left| -\frac{4X + Z}{2X + (2 - 3\varphi)Z} + \mathcal{O}(Y^2) \right| \rightarrow \begin{cases} 1/2 & Z \rightarrow 0 \\ 3\varphi - 2 & X \rightarrow 0 \end{cases} \quad (3.95)$$

so that X could be the smallest parameter in the case of NO while Z could be the smallest one for IO; however, there is no clear symmetry argument behind these possibilities that will not be addressed in the following. The Majorana phases are exact and are fixed by the mass spectrum and the explicit form of (3.93). In the case of NO we have $\alpha = \pi$ and $\beta = \pi$ while for IO we get $\alpha = 0$ and $\beta = \pi$.

Using the value of the Majorana phases we are able to obtain a prediction for the lightest neutrino mass m_{\min} from the sum rule Σ defined in (3.94). Assuming the best fit values for the solar and atmospheric squared mass differences (see Tab. 1.1) we obtain $m_{\min} = m_1 = 1.09 \times 10^{-2}$ eV for NO and $m_{\min} = m_3 = 2.84 \times 10^{-2}$ eV for IO.

3.3.2.4 Mechanism II a-1: summary tables

In this Section, we classify all previous results in two different tables: in Tab. 3.5 the allowed mass ordering, the predictions for the internal angle θ , $\sin^2 \theta_{13}$ and the CP Majorana phases. In Tab. 3.6 we summarize our results for the neutrino mass sum rules, for which we give the coefficients a, b and c of the complex masses \tilde{m}_i , for the assumed form $\Sigma(a, b, c) = a\tilde{m}_1^{-1} + b\tilde{m}_2^{-1} + c\tilde{m}_3^{-1}$, and the numerical values of $\sum_j m_j$ and the effective masses m_β and $m_{\beta\beta}$.

3.3.3 Mechanism II a-2

The cases contemplated here involve a trivial structure of the Majorana mass matrix and a more complicated Dirac mass matrix. The quantum numbers of the matter, Higgs and flavon fields are summarized in Tab. 3.7. The lagrangian responsible for the Dirac mass

	$Z = 0$	$X = 0$	$S = 0$
ordering	both	NO	both
$\tan 2\theta$	$\sqrt{\varphi+2}\frac{Y}{X}$	$2\sqrt{3-\varphi}\frac{Y}{Z}$	$-\frac{2\sqrt{11}\varphi+7[(3\varphi-2)Z-2X]Y}{4(\varphi+1)X^2-4\varphi XZ-(5\varphi+4)Z^2}$
$\sin^2 \theta_{13}$	$\frac{1+\varphi}{4}\frac{Y^2}{X^2}$	$\frac{Y^2}{Z^2}$	Eq. (3.92)
(α, β)	$(0, \pi)$	(π, π) ($S \simeq Z/3$ and $S \simeq -Z/4$) $(\pi, 0)$ ($S \simeq 2Z/3$)	$(\pi, \pi), (0, \pi)$

Table 3.5: Same as Tab. 3.2 but for Mechanism II a-1. The two values for (α, β) in the case $S = 0$ refer to NO and IO, respectively.

	$Z = 0 - \text{NO}$	$X = 0$	$S = 0$
$\Sigma(a, b, c)$	$(1, -1 + (\varphi - 3)s_{13}^2, (3 - \varphi)s_{13}^2)$	$(1, \varphi + 1, -(2 + \varphi))$	$(1, 1, 1)$
$\sum_j m_j$ [eV]	0.11 ($S \simeq X$) $\gtrsim 0.38$ ($S \simeq 44X$)	6.59×10^{-2} ($S \simeq Z/3$) 0.11 ($S \simeq -Z/4$) 5.73×10^{-2} ($S \simeq 2Z/3$)	-
m_β [eV]	3.16×10^{-2} ($S \simeq X$) 1.25×10^{-2} ($S \simeq 44X$)	1.26×10^{-2} ($S \simeq Z/3$) 2.78×10^{-2} ($S \simeq -Z/4$) 7.74×10^{-3} ($S \simeq 2Z/3$)	-
$m_{\beta\beta}$ [eV]	2.88×10^{-2} ($S \simeq X$) 1.25×10^{-2} ($S \simeq 44X$)	4.49×10^{-4} ($S \simeq Z/3$) 9.78×10^{-3} ($S \simeq -Z/4$) 5.63×10^{-4} ($S \simeq 2Z/3$)	-

Table 3.6: Same as Tab. 3.3 but for Mechanism II a-1.

Field	L	ν^c	H_u	$\phi_{\nu,1}$	$\phi_{\nu,3}$	$\phi_{\nu,5}$
A_5	3	3	1	1	3	5

Table 3.7: Quantum numbers of the fields involved in Mechanism II a-2.

matrix is

$$\mathcal{L}_D = Y_1(\nu^c L)_1 H_u + y_1 \left[(\nu^c L)_1 \frac{\phi_{\nu,1}}{\Lambda} \right]_1 H_u + y_3 \left[(\nu^c L)_3 \frac{\phi_{\nu,3}}{\Lambda} \right]_1 H_u + y_5 \left[(\nu^c L)_5 \frac{\phi_{\nu,5}}{\Lambda} \right]_1 H_u + h.c. \quad (3.96)$$

where Λ is the UV cutoff and the Yukawa couplings are real with our convention for the Kronecker products, see Appendix C. A direct mass term in the previous lagrangian can also be introduced; being proportional to the Yukawa coupling Y_1 , we simply redefine this coupling. For the Majorana mass matrix M_M we have

$$M_M = MP_{23} \quad (3.97)$$

where the matrix P_{23} is defined in (2.50). The heavy Majorana particles are degenerated in this framework. After the flavour and electroweak symmetry breakings we obtain a mass matrix for the Dirac neutrinos

$$M_D = M_D^1 + M_D^3 + M_D^5 \quad (3.98)$$

where the matrices have the following form

$$M_D^{\mathbf{1}} = \langle H \rangle \left(y_1 \frac{v_1}{\Lambda} + Y_1 \right) P_{23} \quad (3.99)$$

$$M_D^{\mathbf{3}} = i \frac{y_3 \langle H \rangle}{\Lambda} v \begin{pmatrix} 0 & -1 & 1 \\ 1 & 0 & \sqrt{2}\varphi^{-1} \\ -1 & -\sqrt{2}\varphi^{-1} & 0 \end{pmatrix} \quad (3.100)$$

$$M_D^{\mathbf{5}} = \frac{y_5 \langle H \rangle}{\Lambda} \begin{pmatrix} -\sqrt{\frac{2}{3}}(x_r + x_{r,2}) & -\frac{\sqrt{3}}{2}(x_r + ix_i\varphi) & -\frac{\sqrt{3}}{2}(x_r - ix_i\varphi) \\ -\frac{\sqrt{3}}{2}(x_r + ix_i\varphi) & -\sqrt{\frac{3}{2}}(ix_i + x_{r,2}) & \frac{x_r + x_{r,2}}{\sqrt{6}} \\ -\frac{\sqrt{3}}{2}(x_r - ix_i\varphi) & \frac{x_r + x_{r,2}}{\sqrt{6}} & \sqrt{\frac{3}{2}}(ix_i - x_{r,2}) \end{pmatrix}. \quad (3.101)$$

In order to reduce the number of parameters it is useful to introduce the following dimensionless quantities

$$f \equiv y_1 \frac{v_1}{\Lambda} + Y_1 \quad g \equiv y_3 \frac{v}{\Lambda} \quad (3.102)$$

for the flavons $\phi_{\nu,1}$ and $\phi_{\nu,3}$. We also define

$$h_r \equiv y_5 \frac{x_r}{\Lambda} \quad h_{r,2} \equiv y_5 \frac{x_{r,2}}{\Lambda} \quad h_i \equiv y_5 \frac{x_i}{\Lambda} \quad (3.103)$$

for the vevs components in the representation $\mathbf{5} \in A_5$.

The neutrino mass matrix M_ν can be obtained by

$$M_\nu = -M_D^T M_M^{-1} M_D = -\frac{1}{M} M_D^T P_{23} M_D \quad (3.104)$$

where we use the explicit expression for M_M . The form of M_ν is fixed by the symmetry, thus it is equivalent to (3.3) with parameters

$$s = \frac{1}{3} [4(\varphi - 3)g^2 - 3f^2 - 3(\varphi + 2)h_i^2 - 4h_r^2 - 2h_r h_{r,2} - 4h_{r,2}^2] \quad (3.105a)$$

$$x = \frac{1}{6\varphi} \left[4\varphi g^2 + 4\sqrt{3}(\varphi + 3)gh_i + \varphi \left(4h_{r,2} (\sqrt{6}f + h_{r,2}) - 3h_r^2 + 4h_r h_{r,2} \right) + (6\varphi + 3)h_i^2 \right] \quad (3.105b)$$

$$y = \frac{1}{3\varphi} \left[h_i \left(2\varphi (\sqrt{6}f + h_{r,2}) - (\varphi + 3)h_r \right) - 2\sqrt{3}g(\varphi h_r + 2h_{r,2}) \right] \quad (3.105c)$$

$$z = \frac{1}{6} \left[-8(\varphi - 1)g^2 + 8\sqrt{3}gh_i - 6\varphi h_i^2 - 2h_r \left(-2\sqrt{6}f + h_r + 4h_{r,2} \right) \right]. \quad (3.105d)$$

The neutrino mass scale m_0 is

$$m_0 \equiv \frac{\langle H \rangle^2}{M} \quad (3.106)$$

that is $m_0 = \mathcal{O}(1)$ eV. The relation between the vevs and θ can be expressed as

$$\begin{aligned} \tan 2\theta = & -\sqrt{58\varphi + 36} \left\{ 2\sqrt{6}g(\varphi h_r + 2h_{r,2}) + h_i \left(\sqrt{2}(\varphi + 3)h_r - 2\varphi \left(2\sqrt{3}f + \sqrt{2}h_{r,2} \right) \right) \right\} \times \\ & \times \left\{ 8\sqrt{3}g(7\varphi + 4)h_i + 2\sqrt{6}f[(5\varphi + 3)h_r + (6\varphi + 4)h_{r,2}] + \right. \\ & \left. - (14\varphi + 9)h_r^2 - (8\varphi + 4)h_r h_{r,2} + (12\varphi + 8)h_{r,2}^2 \right\}^{-1} \end{aligned} \quad (3.107)$$

hence we notice that the parameters g and h_i are relevant in the suppression of θ in order to obtain a small value of the reactor mixing angle θ_{13} , as shown in (3.5).

For this mechanism the Majorana phases are always vanishing, $\alpha = \beta = 0$.

3.3.3.1 Mechanism II a-2: $h_i = f = 0$

We start considering a vanishing singlet vev, $f = 0$ and vanishing complex part of the vev of the **5** representation, $h_i = 0$. In this limit the reactor angle is then

$$\sin^2 \theta_{13} = \frac{12(21\varphi + 13)g^2}{[h_r(9\varphi + 5) - 2h_{r,2}(3\varphi + 2)]^2} + \mathcal{O}(g^4). \quad (3.108)$$

The mass spectrum at LO is

$$m_1 = m_0 \left| -\frac{1}{6} ((1 - 3\varphi)h_r - 2h_{r,2})^2 + \mathcal{O}(g^2) \right| \quad (3.109a)$$

$$m_2 = m_0 \left| -\frac{1}{6} ((3\varphi - 2)h_r - 2h_{r,2})^2 \right| \quad (3.109b)$$

$$m_3 = m_0 \left| -\frac{1}{6} (h_r + 4h_{r,2})^2 + \mathcal{O}(g^2) \right| \quad (3.109c)$$

hence the following sum rule at LO for the complex masses \tilde{m}_j is fulfilled

$$\Sigma = (\tilde{m}_1 + \tilde{m}_2 - \tilde{m}_3)^2 - 4\tilde{m}_1\tilde{m}_2 + \mathcal{O}(m^2 \sin^2 \theta_{13}) \quad (3.110)$$

where m is a dimensionful parameter needed for consistency. Notice that the undisplayed coefficient of order $\sin^2 \theta_{13}$ is proportional to $h_r + 4h_{r,2} \propto \sqrt{m_3/m_0}$ hence we expect that the sum rule works better in the case of IO.

The solar mass-squared difference is

$$\Delta m_{21}^2/m_0^2 = -\frac{1}{12}(2\varphi - 1)h_r(h_r + 4h_{r,2}) (23h_r^2 + 4h_r h_{r,2} + 8h_{r,2}^2) + \mathcal{O}(g^2) \quad (3.111)$$

therefore a natural suppression is expected for $h_r \sim 0$ or for $h_r \sim -4h_{r,2}$. The second case is related to IO, because in this limit $m_3/m_2 \sim 0$, see (3.109c). Similar relations can be obtained for the atmospheric mass differences, which depend on a different combination of h_r and $h_{r,2}$ than that shown by the solar mass difference; we then expect $r_\ell \propto h_r(h_r + 4h_{r,2})$. In this case both hierarchies are allowed: NO if $h_{r,2} < 0 \wedge 0 < h_r < 2(2 - 3\varphi)h_{r,2}/11$ or $h_{r,2} > 0 \wedge 2(2 - 3\varphi)h_{r,2}/11 < h_r < 0$ and IO if $h_{r,2} < 0 \wedge (2 - 2\varphi)h_{r,2} < h_r < -4h_{r,2}$ or $h_{r,2} > 0 \wedge -4h_{r,2} < h_r < (2 - 2\varphi)h_{r,2}$.

If we assume that $h_r \sim 0$ (NO) we obtain for the reactor mixing angle

$$\sin^2 \theta_{13} = 3 \frac{g^2}{h_{r,2}^2} + \mathcal{O}(g^4) \quad h_r = 0 \quad (3.112)$$

thus we expect $g/h_{r,2} \sim \pm 1/10$ in order to recover the best fit value $\sin^2 \theta_{13} = 2.19 \times 10^{-2}$. In this limit we have $m_1/m_2 \sim 1$ and $m_3/m_2 \sim 4$. Assuming instead $h_r = -4h_{r,2}$ (IO), we have

$$\sin^2 \theta_{13} = \frac{1}{15} \frac{g^2}{h_{r,2}^2} + \mathcal{O}(g^4) \quad h_r = -4h_{r,2} \quad (3.113)$$

therefore we expect that $g/h_{r,2} \sim \pm 1/2$. In this limit we also expect that $m_1/m_2 \sim 1$ and $m_3/m_2 \sim 0$.

We can estimate $\sum_j m_j$, m_β and $m_{\beta\beta}$. We obtain for NO

$$\sum_j m_j = \sqrt{\Delta m_{31}^2} \left[2\sqrt{\frac{3}{5}} + \frac{26(\varphi - 1)}{5\sqrt{3}} \sin^2 \theta_{13} + \mathcal{O}(\sin^4 \theta_{13}) \right] \simeq 7.48 \times 10^{-2} \text{ eV} \quad (3.114)$$

$$m_\beta = \frac{1}{10} \sqrt{\frac{\Delta m_{31}^2}{3}} [4\varphi - 2 + (1 + 10\varphi) \sin^2 \theta_{13} + \mathcal{O}(\sin^4 \theta_{13})] \simeq 1.39 \times 10^{-2} \text{ eV} \quad (3.115)$$

and

$$m_{\beta\beta} = \frac{1}{5} \sqrt{\frac{\Delta m_{31}^2}{3}} [2\varphi - 1 - (4\varphi - 5) \sin^2 \theta_{13} + \mathcal{O}(\sin^4 \theta_{13})] \simeq 1.26 \times 10^{-2} \text{ eV} \quad (3.116)$$

where in the numerical evaluation we used the best fit values of Δm_{31}^2 and θ_{13} [45]. A similar analysis can be done for IO; we obtain

$$\sum_j m_j = \sqrt{-\Delta m_{32}^2} [2 + 2(3 - \varphi) \sin^2 \theta_{13} + \mathcal{O}(\sin^4 \theta_{13})] \simeq 1.02 \times 10^{-1} \text{ eV} \quad (3.117)$$

$$m_\beta = \sqrt{-\Delta m_{32}^2} \left[1 + \frac{3}{2} \sin^2 \theta_{13} + \mathcal{O}(\sin^4 \theta_{13}) \right] \simeq 5.11 \times 10^{-2} \text{ eV} \quad (3.118)$$

and

$$m_{\beta\beta} = \sqrt{-\Delta m_{32}^2} [1 + \sin^2 \theta_{13} + \mathcal{O}(\sin^4 \theta_{13})] \simeq 5.06 \times 10^{-2} \text{ eV}. \quad (3.119)$$

3.3.3.2 Mechanism II a-2: $h_i = h_r = 0$

The second possibility we explore is the case where, beside $h_i = 0$, one of the real vev of $\phi_{\nu,5}$ is null, $h_r = 0$. This case is quite similar to the Weinberg operator with $z = 0$ discussed in Sec. 3.3.1.1, because the mass matrix parameter z is almost close to zero (in fact $z = \mathcal{O}(g^2)$, see (3.105d)). The reactor mixing angle as a series in g has the following leading contribution

$$\sin^2 \theta_{13} = \frac{3g^2}{[\sqrt{6}f + h_{r,2}]^2} + \mathcal{O}(g^4). \quad (3.120)$$

In the limit $|g| \ll |f|, |h_{r,2}|$ we can obtain the mass spectrum at LO

$$m_1 = m_0 \left| -\frac{1}{3} \left(\sqrt{3}f - \sqrt{2}h_{r,2} \right)^2 + \mathcal{O}(g^2) \right| \quad (3.121a)$$

$$m_2 = m_0 \left| -\frac{1}{3} \left(\sqrt{3}f - \sqrt{2}h_{r,2} \right)^2 \right| \quad (3.121b)$$

$$m_3 = m_0 \left| -\frac{1}{3} \left(\sqrt{3}f + 2\sqrt{2}h_{r,2} \right)^2 + \mathcal{O}(g^2) \right| \quad (3.121c)$$

where we notice that $m_1 = m_2$ in the LO approximation. A different kind of neutrino mass sum rule can be obtained:

$$\begin{aligned} \Sigma &= (\tilde{m}_1 - \tilde{m}_2)^2 + 2(3 - \varphi) (\tilde{m}_1 - 3\tilde{m}_2) (\tilde{m}_1 - \tilde{m}_2) \sin^2 \theta_{13} + \\ &+ 20(\varphi - 2)\tilde{m}_2 (\tilde{m}_1 - 2\tilde{m}_2 + \tilde{m}_3) \sin^4 \theta_{13} + \mathcal{O}(m^2 \sin^6 \theta_{13}) \end{aligned} \quad (3.122)$$

In this case we need to include terms up to $\mathcal{O}(\sin^4 \theta_{13})$ since the difference $(m_2 - m_1)/m_0 \propto \sin^2 \theta_{13}$. To obtain the solar mass-squared difference we need to consider also the (undisplayed) NLO contributions for the masses. We obtain

$$\Delta m_{21}^2/m_0^2 = \frac{4(\varphi - 3) (3\sqrt{6}f^3 - 18f^2 h_{r,2} + 6\sqrt{6}f h_{r,2}^2 - 4h_{r,2}^3)}{3(\sqrt{6}f + h_{r,2})} g^2 + \mathcal{O}(g^4). \quad (3.123)$$

For the atmospheric mass differences $\Delta m_{3\ell}^2$ it is enough to consider only the LO term. Only NO is allowed, provided that $h_{r,2} < 0 \wedge \sqrt{2/3}h_{r,2} < f < -h_{r,2}/\sqrt{6}$ or $h_{r,2} > 0 \wedge -h_{r,2}/\sqrt{6} < f < \sqrt{2/3}h_{r,2}$.

As usual, the ratio r_1 can be expressed as a function of θ_{13} using the relation defined in (3.120)

$$r_1 = \frac{(\varphi - 3)(\sqrt{6}f + h_{r,2})(3\sqrt{6}f^3 - 18f^2h_{r,2} + 6\sqrt{6}fh_{r,2}^2 - 4h_{r,2}^3)}{3h_{r,2}(3\sqrt{6}f^3 + 9f^2h_{r,2} + 6\sqrt{6}fh_{r,2}^2 + 5h_{r,2}^3)} \sin^2 \theta_{13} + \mathcal{O}(\sin^4 \theta_{13}). \quad (3.124)$$

If we assume a linear relation between f and $h_{r,2}$ of the form $f = kh_{r,2}$ we can obtain the value of the coefficient k assuming both r_1 and θ_{13} in the 3σ confidence region. We obtain that the best value that accommodates both data with the constraint $\sum_j m_j \leq 0.23$ eV is $k \simeq -7/20$, for which $r_1 \simeq 1.19 \sin^2 \theta_{13}$. As in the case of Mechanism I with $z = 0$, discussed in Sec. 3.3.1.1, we have a large spread for k : it is constrained between $k \simeq -7/22$ and the values $k = -1/\sqrt{6}$, where the mass spectrum is degenerate at LO $m_j/m_0 = 3h_{r,2}^2/2 + \mathcal{O}(g^2)$. Another correlation between g and f can be found, again in the limit $f = -7/20h_{r,2}$, from the expression of the reactor angle:

$$\sin^2 \theta_{13} = \frac{600}{(347 - 140\sqrt{6})h_{r,2}^2} g^2 + \mathcal{O}(g^4) \quad f = -\frac{7}{20}h_{r,2} \quad (3.125)$$

thus we expect $g \sim \pm h_{r,2}/100$.

As a final remark we predict at LO and for $f = -7h_{r,2}/20$ that $m_1/m_2 \sim 1$ and $m_3/m_2 \sim 6/5$. The effective mass for β -decay and $0\nu\beta\beta$ -decay can be obtained under the same assumption. We have

$$m_\beta = \sqrt{\Delta m_{21}^2} \left[\frac{1.35}{\sin^2 \theta_{13}} + 0.04 \sin \theta_{13} + \mathcal{O}(\sin^2 \theta_{13}) \right] \simeq 7.88 \times 10^{-2} \text{ eV} \quad (3.126)$$

and

$$m_{\beta\beta} = \sqrt{\Delta m_{21}^2} \left[\frac{1.35}{\sin^2 \theta_{13}} + 0.01 \sin \theta_{13} + \mathcal{O}(\sin^2 \theta_{13}) \right] \simeq 7.88 \times 10^{-2} \text{ eV} \quad (3.127)$$

where the best fit values for Δm_{21}^2 and θ_{13} have been considered. Notice that the effective masses are constrained to be m_β ($m_{\beta\beta}$) $\gtrsim 5.49 \times 10^{-2}$ eV when $k \simeq -7/22$. A non-trivial relation for $\sum_j m_j$ as a function of r_1 , Δm_{31}^2 and θ_{13} exists, but it is quite cumbersome and we do not discuss it in details. We only mention the lower bound $\sum_j m_j \gtrsim 0.19$ eV.

3.3.3.3 Mechanism II a-2: $h_i = h_{r,2} = 0$

Starting from (3.5) we can obtain θ_{13}

$$\sin^2 \theta_{13} = \frac{24(21\varphi + 13)g^2}{[\sqrt{2}(9\varphi + 5)h_r - 4\sqrt{3}(3\varphi + 2)f]^2} + \mathcal{O}(g^4). \quad (3.128)$$

In the limit $|g| \ll |f|, |h_r|$ we can obtain the mass spectrum at LO

$$m_1 = m_0 \left| -\frac{1}{6} \left(\sqrt{6}f + (1 - 3\varphi)h_r \right)^2 + \mathcal{O}(g^2) \right| \quad (3.129a)$$

$$m_2 = m_0 \left| -\frac{1}{6} \left(\sqrt{6}f + (3\varphi - 2)h_r \right)^2 \right| \quad (3.129b)$$

$$m_3 = m_0 \left| -\frac{1}{6} \left(\sqrt{6}f + h_r \right)^2 + \mathcal{O}(g^2) \right|. \quad (3.129c)$$

At LO we can obtain the following sum rule for the complex masses \tilde{m}_j

$$\Sigma = (\tilde{m}_1 + (3\varphi + 2)\tilde{m}_2 - 5(\varphi + 1)\tilde{m}_3)^2 - 4(3\varphi + 2)\tilde{m}_1\tilde{m}_2 + \mathcal{O}(m^2 \sin^2 \theta_{13}) \quad (3.130)$$

where we notice that the coefficient in front of the masses are $\mathcal{O}(10)$, therefore we expect large deviation to the sum rule.

The solar mass difference is

$$\Delta m_{21}^2/m_0^2 = -\frac{1}{12}(2\varphi - 1)h_r \left(h_r - 2\sqrt{6}f \right) \left(12f^2 - 2\sqrt{6}fh_r + 23h_r^2 \right) + \mathcal{O}(g^2) \quad (3.131)$$

which is proportional to $h_r(h_r - 2\sqrt{6}f)$. The atmospheric mass differences are proportional to h_r . Therefore a possibility to suppress the ratio r_ℓ is to make the solar mass difference almost vanishing, that is to impose $h_r \simeq 2\sqrt{6}f$. The ansatz is compatible only for IO, for which the neutrino masses are $m_1 = m_2 = m_0 45f^2 + \mathcal{O}(g^2)$ and $m_3 = m_0 9f^2 + \mathcal{O}(g^2)$ and so $m_1/m_2 \sim 1$ and $m_3/m_2 \sim 1/5$. It is interesting to observe that m_3 could be close to zero if $f \simeq -h_r/\sqrt{6}$, see (3.129c), but this condition is not enough to obtain a small ratio r_2 , so we expect m_3 always different from zero.

The IO is the only hierarchy allowed in this case, for $f < 0 \wedge 2\sqrt{6}f < h_r < 2\sqrt{6}f/(3\varphi - 2)$ or $f > 0 \wedge 2\sqrt{6}f/(3\varphi - 2) < h_r < 2\sqrt{6}f$.

The relation $h_r \simeq 2\sqrt{6}f$ provides to be adequate to reproduce the (undisplayed) r_2 ; this in turn gives $\sin^2 \theta_{13}$ approximated by

$$\sin^2 \theta_{13} = \frac{1 + \varphi}{18} \frac{g^2}{f^2} + \mathcal{O}(g^4) \quad h_r = 2\sqrt{6}f; \quad (3.132)$$

so, to reproduce also its experimental value, we need $g \sim \pm 7/20f$. Simple predictions for $\sum_j m_j$, m_β and $m_{\beta\beta}$ are possible:

$$\sum_j m_j = \sqrt{-\frac{\Delta m_{32}^2}{6}} \left[\frac{11}{2} - \frac{163\varphi - 244}{36} \sin^2 \theta_{13} + \mathcal{O}(\sin^4 \theta_{13}) \right] \simeq 1.11 \times 10^{-1} \text{ eV} \quad (3.133)$$

$$m_\beta = \sqrt{-\frac{\Delta m_{32}^2}{6}} \left[\frac{5}{2} + \frac{\sqrt{188569 - 113295\varphi}}{60} \sin^2 \theta_{13} + \mathcal{O}(\sin^4 \theta_{13}) \right] \simeq 5.10 \times 10^{-2} \text{ eV} \quad (3.134)$$

and

$$m_{\beta\beta} = \sqrt{-\frac{\Delta m_{32}^2}{6}} \left[\frac{5}{2} - \frac{39\varphi - 68}{12} \sin^2 \theta_{13} + \mathcal{O}(\sin^4 \theta_{13}) \right] \simeq 5.07 \times 10^{-2} \text{ eV} \quad (3.135)$$

where we used $\sin^2 \theta_{13} = 2.19 \times 10^{-2}$ and $\Delta m_{32}^2 = -2.449 \times 10^{-3} \text{ eV}^2$.

3.3.3.4 Mechanism II a-2: $g = f = 0$

In this particular case the reactor angle is

$$\sin^2 \theta_{13} = \frac{(55\varphi + 34)h_i^2}{[(5\varphi + 3)h_r + (6\varphi + 4)h_{r,2}]^2} + \mathcal{O}(h_i^4). \quad (3.136)$$

Since the LO mass matrix M_ν is the same as the case $h_i = f = 0$, the mass spectrum is the same as Sec. 3.3.3.1. We emphasize that in this case the sum rule defined in (3.110) is exact (in the case of Sec. 3.3.3.1 we have $\mathcal{O}(\sin^2 \theta_{13})$ corrections), thus it is possible to use it to find the lightest neutrino mass m_{\min} assuming the best fit values for the solar and atmospheric mass differences. In the case of NO we get $m_{\min} = m_1 = 1.13 \times 10^{-2} \text{ eV}$, while in the case of IO we obtain $m_{\min} = m_3 = 2.97 \times 10^{-6} \text{ eV}$.

Since $m_3/m_0 \propto (h_r + 4h_{r,2})^2$ and $\Delta m_{21}^2/m_0^2 \propto h_r(h_r + 4h_{r,2})$, see (3.109c) and (3.111), we can argue that $h_r \sim 0$ for NO and $h_r \sim -4h_{r,2}$ for IO. In the first case we have

$$\sin^2 \theta_{13} = \frac{1 + \varphi}{4} \frac{h_i^2}{h_{r,2}^2} + \mathcal{O}(h_i^4) \quad h_r = 0 \quad (3.137)$$

therefore $h_i \sim \pm h_{r,2}/5$. We remind that in this case we expect $m_1/m_2 \sim 1$ and $m_3/m_2 \sim 4$. In the case of IO, starting from (3.136), we obtain

$$\sin^2 \theta_{13} = \frac{1 + \varphi}{20} \frac{h_i^2}{h_{r,2}^2} + \mathcal{O}(h_i^4) \quad h_r = -4h_{r,2} \quad (3.138)$$

thus for $\sin^2 \theta_{13} = 2.19 \times 10^{-2}$ we get $h_i \sim \pm 2h_{r,2}/5$. In this case we predict $m_1/m_2 \sim 1$ and $m_3/m_2 \sim 0$. We can obtain in this limit the values for $\sum_j m_j$, m_β and $m_{\beta\beta}$. In the case of NO, we get

$$\sum_j m_j = \frac{1}{10} \sqrt{3\Delta m_{31}^2} \left[\frac{2}{\sqrt{5}} + \frac{\varphi - 1}{5} \sin^2 \theta_{13} + \mathcal{O}(\sin^4 \theta_{13}) \right] \simeq 7.73 \times 10^{-2} \text{ eV} \quad (3.139)$$

$$m_\beta = \frac{1}{10} \sqrt{\frac{\Delta m_{31}^2}{3}} [4\varphi - 2 + (1 + 26\varphi) \sin^2 \theta_{13} + \mathcal{O}(\sin^4 \theta_{13})] \simeq 1.55 \times 10^{-2} \text{ eV} \quad (3.140)$$

and

$$m_{\beta\beta} = \frac{1}{5} \sqrt{\frac{\Delta m_{31}^2}{3}} [1 - 2\varphi - (4\varphi + 5) \sin^2 \theta_{13} + \mathcal{O}(\sin^4 \theta_{13})] \simeq 1.42 \times 10^{-2} \text{ eV} \quad (3.141)$$

A similar analysis can be done for IO, we obtain at NLO the same relations of the case $h_i = f = 0$ IO (see Sec. 3.3.3.1).

3.3.3.5 Mechanism II a-2: $g = h_r = 0$

Assuming $g = h_r = 0$ we obtain that the mixing angle θ_{13} can be expressed as

$$\sin^2 \theta_{13} = \frac{\varphi + 1}{4} \frac{h_i^2}{h_{r,2}^2} + \mathcal{O}(h_i^4). \quad (3.142)$$

We can then expand the observables as a series in the parameter h_i . At LO the mass spectrum and the sum rule for the neutrino complex masses are the same as $h_i = h_r = 0$, Sec. 3.3.3.2. The sum rule is formally the same as the case $h_i = h_r = 0$, which is defined in Eq. (3.122), with the same coefficients. However due to NLO corrections the value of the solar mass splitting is different

$$\Delta m_{21}^2/m_0^2 = \frac{(\varphi + 2) (3\sqrt{6}f^3 - 18f^2h_{r,2} + 6\sqrt{6}fh_{r,2}^2 - 4h_{r,2}^3)}{3h_{r,2}} h_i^2 + \mathcal{O}(h_i^4). \quad (3.143)$$

The atmospheric mass-squared difference at LO is the same as case $h_i = h_r = 0$ defined in Sec. 3.3.3.2. From then we infer that the only allowed mass hierarchy is the NO, when $h_{r,2} < 0 \wedge f < \sqrt{2/3}h_{r,2}$ or $h_{r,2} > 0 \wedge f > \sqrt{2/3}h_{r,2}$. At order h_i^2 the ratio r_1 can be expressed as a function of the reactor mixing angle using (3.142):

$$r_1 = \frac{(3 - \varphi) (3\sqrt{6}f^3 - 18f^2h_{r,2} + 6\sqrt{6}fh_{r,2}^2 - 4h_{r,2}^3)}{(3\sqrt{6}f^3 + 9f^2h_{r,2} + 6\sqrt{6}fh_{r,2}^2 + 5h_{r,2}^3)} \sin^2 \theta_{13} + \mathcal{O}(\sin^4 \theta_{13}). \quad (3.144)$$

The linear correlation $f = k h_{r,2}$ with $k \simeq 20$ allows to reproduce the experimental value of r_1 in the 3σ confidence region with the additional constraint $\sum_j m_j \leq 0.23$ eV, (in fact, we get $r_1 \simeq 1.14 \sin^2 \theta_{13} + \mathcal{O}(\sin^4 \theta_{13})$). As in the case $h_i = h_r = 0$, discussed in Sec. 3.3.3.2, there exists a spread for the parameter k : it is bounded between $k \simeq 17$ and $k \rightarrow \infty$ (that is $\mathcal{O}(10^3)$ in our numerical scan), where the mass spectrum at LO is degenerate, $m_j/m_0 = f^2 + \mathcal{O}(h_i^2)$.

As in the case of $h_i = h_r = 0$ we do not report the relation for the sum of the neutrino masses because it is a cumbersome function of $r_1, \Delta m_{21}^2$ and θ_{13} , nonetheless we get the

lower bound $\sum_j m_j \gtrsim 0.19$ eV. The effective masses m_β and $m_{\beta\beta}$ can be evaluated in this framework. We obtain

$$m_\beta = \sqrt{\Delta m_{31}^2} \left[1.27 - 1.70 \sin^2 \theta_{13} + \mathcal{O}(\sin^4 \theta_{13}) \right] \simeq 6.12 \times 10^{-2} \text{ eV} \quad (3.145)$$

and

$$m_{\beta\beta} = \sqrt{\Delta m_{31}^2} \left[1.27 - 1.75 \sin^2 \theta_{13} + \mathcal{O}(\sin^4 \theta_{13}) \right] \simeq 6.13 \times 10^{-2} \text{ eV} \quad (3.146)$$

where in the numerical evaluation we used the best fit values of Δm_{31}^2 and θ_{13} . Due to the spread in k we get the interval $5.53 \times 10^{-2} \text{ eV} \lesssim m_\beta$ ($m_{\beta\beta}$) $\lesssim 4.85 \times 10^{-1} \text{ eV}$.

3.3.3.6 Mechanism II a-2: $g = h_{r,2} = 0$

The reactor mixing angle is

$$\sin^2 \theta_{13} = \frac{h_i^2}{h_r^2} + \mathcal{O}(h_i^4). \quad (3.147)$$

In this case the LO expressions for the neutrino spectrum are the same as $h_i = h_{r,2} = 0$, Sec. 3.3.3.3, thus we do not report here the predictions for the mass ordering and Σ . In this case only IO is allowed, and we predict $m_1/m_2 \sim 1$ and $m_3/m_2 \sim 1/5$. The sum of the neutrino masses $\sum_j m_j$ and the parameters m_β and $m_{\beta\beta}$ are

$$\sum_j m_j = \sqrt{-\frac{\Delta m_{32}^2}{6}} \left[\frac{11}{2} + \frac{5(17+14\varphi)}{12} \sin^2 \theta_{13} + \mathcal{O}(\sin^4 \theta_{13}) \right] \simeq 1.18 \times 10^{-1} \text{ eV} \quad (3.148)$$

$$m_\beta = \sqrt{-\frac{\Delta m_{32}^2}{6}} \left[\frac{5}{2} + \frac{170\varphi + 143}{60} \sin^2 \theta_{13} + \mathcal{O}(\sin^4 \theta_{13}) \right] \simeq 5.36 \times 10^{-2} \text{ eV} \quad (3.149)$$

and

$$m_{\beta\beta} = \sqrt{-\frac{\Delta m_{32}^2}{6}} \left[\frac{5}{2} + \frac{19+34\varphi}{12} \sin^2 \theta_{13} + \mathcal{O}(\sin^4 \theta_{13}) \right] \simeq 5.32 \times 10^{-2} \text{ eV} \quad (3.150)$$

where we used $\sin^2 \theta_{13} = 2.19 \times 10^{-2}$ and $\Delta m_{32}^2 = -2.449 \times 10^{-3} \text{ eV}^2$.

3.3.3.7 Mechanism II a-2: summary tables

As done before we report all previous results in two different tables, to facilitate the comparison of physics implied by the six cases analysed above. In particular, in Tab. 3.8 we report the admitted mass ordering, the predictions for $\tan 2\theta$ and the reactor angle. The Majorana phases are always vanishing, $(\alpha, \beta) = (0, 0)$. In Tab. 3.9 we outline our results for the neutrino mass sum rules and the numerical values of $\sum_j m_j$ and the effective masses m_β and $m_{\beta\beta}$.

3.3.4 Mechanism II c-2

In this section we want to describe an alternative realization of the Type I see-saw where, with respect to the previous case, the right-handed neutrinos transform as a $\mathbf{3}'$, see Tab. 3.10. The lagrangian responsible for the Dirac mass is

$$\mathcal{L}_D = y_4 \left[(\nu^c L)_4 \frac{\phi_{\nu,4}}{\Lambda} \right]_1 H_u + y_5 \left[(\nu^c L)_5 \frac{\phi_{\nu,5}}{\Lambda} \right]_1 H_u + h.c. \quad (3.151)$$

where Λ is the UV cutoff scale.

$$M_D^5 = \frac{y_5 \langle H \rangle}{\Lambda} \begin{pmatrix} -\sqrt{\frac{2}{3}}(x_r + x_{r,2}) & \frac{x_r + ix_i \varphi}{\sqrt{3}} & \frac{x_r - ix_i \varphi}{\sqrt{3}} \\ \frac{ix_i + x_{r,2}}{\sqrt{3}} & \sqrt{\frac{2}{3}}(x_{r,2} - ix_i) & \sqrt{\frac{2}{3}}(x_r + ix_i \varphi) \\ \frac{x_{r,2} - ix_i}{\sqrt{3}} & \sqrt{\frac{2}{3}}(x_r - ix_i \varphi) & \sqrt{\frac{2}{3}}(ix_i + x_{r,2}) \end{pmatrix} \quad (3.153)$$

where the Yukawa couplings y_4 and y_5 are real. The total Dirac mass matrix is

$$M_D = M_D^4 + M_D^5. \quad (3.154)$$

In this case we assume that the heavy Majorana mass matrix is trivial as in (3.97), hence $M_M = MP_{23}$ where P_{23} is the matrix defined in Eq. (2.50) and M is the direct mass term of heavy neutrinos. Note that the three right-handed neutrinos are exactly degenerate. The light neutrino mass matrix is the same as (3.104), $M_\nu = -M_D^T P_{23} M_D / M$. We can estimate the scale of the light neutrinos as $\mathcal{O}(\langle H \rangle^2 v_i v_j / M \Lambda^2)$ where $v_i v_j$ are generic combination of the flavon vev.

It is convenient to redefine the parameters in M_ν introducing the following dimensionless quantities

$$f_r \equiv y_4 \frac{y_r}{\Lambda} \quad f_i \equiv y_4 \frac{y_i}{\Lambda} \quad (3.155)$$

for the flavon in the representation $\mathbf{4} \in A_5$. A similar position is possible for $\phi_{\nu,5}$

$$h_r \equiv y_5 \frac{x_r}{\Lambda} \quad h_{r,2} \equiv y_5 \frac{x_{r,2}}{\Lambda} \quad h_i \equiv y_5 \frac{x_i}{\Lambda}. \quad (3.156)$$

We expect that these parameters are of $\mathcal{O}(1)$. The neutrino mass matrix M_ν has the same form as (3.3) with

$$s = -\frac{2}{9} \left[(3(\varphi + 2)h_i^2 + 4h_r^2 + 2h_r h_{r,2} + 4h_{r,2}^2) + (9f_i^2 + (36\varphi + 27)f_r^2) \right] \quad (3.157a)$$

$$x = \frac{2}{9} \left[((5\varphi + 1)h_i^2 - h_{r,2}^2 - 4h_r h_{r,2}) + (4\sqrt{3}h_r f_i - 2\sqrt{3}h_{r,2} f_i + 2\sqrt{3}(4\varphi + 1)h_i f_r) - 6\varphi f_r^2 \right] \quad (3.157b)$$

$$y = \frac{4}{9} \left[h_i (2\varphi h_{r,2} - (\varphi - 2)h_r) + \sqrt{3}h_i f_i + f_r \left((\sqrt{3} + \sqrt{15})h_r - \sqrt{3}h_{r,2} \right) + 3(\varphi + 2)f_r f_i \right] \quad (3.157c)$$

$$z = -\frac{4}{9} \left[((\varphi - 1)h_i^2 - h_r^2 + h_{r,2}^2) - (2\sqrt{3}(\varphi + 1)h_i f_r - 2\sqrt{3}(h_r + h_{r,2})f_i) + (15\varphi + 9)f_r^2 \right]. \quad (3.157d)$$

As for Mechanism II a-2 discussed in Sec. 3.3.3 the absolute mass scale m_0 is $m_0 \equiv \langle H \rangle^2 / M$, see Eq. (3.106). The angle θ is related to the vevs by the relation

$$\begin{aligned} \tan 2\theta &= 2\sqrt{11\varphi + 7} \left\{ h_i \left(-(\varphi - 2)h_r + 2\varphi h_{r,2} + \sqrt{3}f_i \right) + \right. \\ &\quad \left. + f_r \left((\sqrt{3} + \sqrt{15})h_r - \sqrt{3}h_{r,2} + 3(\varphi + 2)f_i \right) \right\} \times \\ &\quad \times \left\{ h_i^2(\varphi + 2)(3\varphi + 1) + 4\sqrt{3}h_i(\varphi + 1)(3\varphi + 1)f_r + \varphi h_r^2 - 4(\varphi + 1)h_r h_{r,2} + \right. \\ &\quad \left. + 2\sqrt{3}h_r f_i - (2\varphi + 1)h_{r,2}^2 - 2\sqrt{3}(3\varphi + 2)h_{r,2} f_i - 3(3\varphi + 1)(4\varphi + 3)f_r^2 \right\}^{-1}. \quad (3.158) \end{aligned}$$

We need h_i or f_r (x_i and y_r in the vev language) small compared to the other vevs due to the fact that y can be vanishing when $h_i = 0$ and $f_r = 0$. Hence the relevant parameters for having a small θ , and thus a small reactor angle, are h_i and f_r . Notice that the case $h_i = 0$ is equivalent to $\phi_{\nu,5}$ invariant under $Z_2 \otimes Z_2 \otimes CP$, while $f_r = 0$ corresponds to $\phi_{\nu,4}$ invariant under $Z_2 \otimes Z_2 \otimes CP$, see Sec. 3.1.2.

As in Mechanism II a-2, Sec. 3.3.3, the Majorana CP phases are vanishing, $\alpha = \beta = 0$.

3.3.4.1 Mechanism II c-2: $h_i = f_i = 0$

In this limit the reactor mixing angle, up to corrections of order $\mathcal{O}(f_r^4)$, is

$$\sin^2 \theta_{13} = \frac{3(8\varphi + 5)(h_{r,2} - 2\varphi h_r)^2}{\left(-\varphi h_r^2 + 4(\varphi + 1)h_r h_{r,2} + (2\varphi + 1)h_{r,2}^2\right)^2} f_r^2 + \mathcal{O}(f_r^4). \quad (3.159)$$

We notice that θ_{13} could also be very small if $h_{r,2} \sim 2\varphi h_r$, but this possibility is not motivated by any symmetry argument based on residual symmetry for the flavon vevs and will not be considered any more. The masses of the light neutrinos are

$$m_1 = m_0 \left| -\frac{2}{3} \left((\varphi - 1)h_r + \varphi h_{r,2} \right)^2 + \mathcal{O}(f_r^2) \right| \quad (3.160a)$$

$$m_2 = m_0 \left| -\frac{2}{3} \left(\varphi h_r + (\varphi - 1)h_{r,2} \right)^2 \right| \quad (3.160b)$$

$$m_3 = m_0 \left| -\frac{2}{3} (h_r - h_{r,2})^2 + \mathcal{O}(f_r^2) \right|. \quad (3.160c)$$

The mass spectrum is the same as for Mechanism II a-2 with $h_i = f = 0$, discussed in Sec. 3.3.3.1, if we perform the vevs redefinition

$$h_r \rightarrow \pm \frac{1}{2}(h_r - 2h_{r,2}) \quad h_{r,2} \rightarrow \pm(h_r + h_{r,2}) \quad (3.161)$$

Using the expressions for the neutrino masses at LO we can obtain the same sum rule as for Mechanism II a-2 with $h_i = f = 0$ for the complex masses, defined in (3.110), $\Sigma = (\tilde{m}_1 + \tilde{m}_2 - \tilde{m}_3)^2 - 4\tilde{m}_1\tilde{m}_2 + \mathcal{O}(m^2 \sin^2 \theta_{13})$. It is interesting to notice that the (undisplayed) coefficient in front of $\sin^2 \theta_{13}$ is proportional to $(h_r - h_{r,2}) \sim \sqrt{m_3/m_0}$, see (3.160c), thus we expect that the sum rule works better in the case of IO.

The solar mass squared difference is

$$\Delta m_{21}^2/m_0^2 = \frac{4}{9}(2\varphi - 1)(h_r - h_{r,2})(h_r + h_{r,2})(3h_r^2 + 4h_r h_{r,2} + 3h_{r,2}^2) + \mathcal{O}(f_r^2) \quad (3.162)$$

thus a small value of the solar splitting can be achieved for $h_r \sim \pm h_{r,2}$. The possibility $h_r \sim +h_{r,2}$ is related to IO, because for the mass m_3 we have at LO $m_3/m_0 \propto (h_r - h_{r,2})^2$, hence it can be vanishing, see Eq. (3.160c). From the mass spectrum defined in (3.160) we see that both orderings are allowed: NO if $h_r < 0 \wedge h_r(\varphi - 2) < h_{r,2} < -h_r$ or $h_r > 0 \wedge -h_r < h_{r,2} < h_r(\varphi - 2)$, IO if $h_r < h_{r,2} < h_r/(2 + 3\varphi)$ or $h_r > 0 \wedge h_r/(2 + 3\varphi) < h_{r,2} < h_r$.

Using the fact that $h_r \sim \pm h_{r,2}$ we can obtain a simplified expression for θ_{13} . In the case of NO, $h_r \sim -h_{r,2}$, we have

$$\sin^2 \theta_{13} = \frac{13 + 21\varphi}{3} \frac{f_r^2}{h_r^2} + \mathcal{O}(f_r^4) \quad h_{r,2} = -h_r \quad (3.163)$$

hence we have $f_r \simeq \pm 2h_r/50$ to get a value of $\sin^2 \theta_{13}$ in the 3σ CL. While in the other case we have $h_r = +h_{r,2}$ (IO) and we obtain

$$\sin^2 \theta_{13} = \frac{3(1 + \varphi)}{5} \frac{f_r^2}{h_r^2} + \mathcal{O}(f_r^4) \quad h_{r,2} = +h_r \quad (3.164)$$

hence $f_r \sim \pm h_r/10$ to obtain a value of the reactor mixing angle compatible with the current data. It is possible to obtain the ratio of neutrino masses at LO assuming $h_r \sim \pm h_{r,2}$. With these assumptions we have $m_1/m_2 \sim 1$ for both orderings and $m_3/m_2 \sim 4$ for NO and $m_3/m_2 \sim 0$ for IO.

The sum of the neutrino masses $\sum_j m_j$ and the effective masses m_β and $m_{\beta\beta}$ can be obtained using the limits discussed above. We get for NO

$$\sum_j m_j = \sqrt{\Delta m_{31}^2} \left[2\sqrt{\frac{3}{5}} - \frac{17}{5} \sqrt{3(89 - 55\varphi)} \sin^2 \theta_{13} + \mathcal{O}(\sin^4 \theta_{13}) \right] \simeq 7.62 \times 10^{-2} \text{ eV} \quad (3.165)$$

$$m_\beta = \sqrt{\frac{\Delta m_{31}^2}{3}} \frac{1}{10} [4\varphi - 2 + (415 - 238\varphi) \sin^2 \theta_{13} + \mathcal{O}(\sin^4 \theta_{13})] \simeq 1.47 \times 10^{-2} \text{ eV} \quad (3.166)$$

and

$$m_{\beta\beta} = \sqrt{\frac{\Delta m_{31}^2}{3}} \frac{1}{5} [1 - 2\varphi + 4(32\varphi - 53) \sin^2 \theta_{13} + \mathcal{O}(\sin^4 \theta_{13})] \sim 1.34 \times 10^{-2} \text{ eV} \quad (3.167)$$

where we used the best fit values of Δm_{31}^2 and θ_{13} reported in Tab. 1.1. For IO we obtain similar results

$$\sum_j m_j = \sqrt{-\Delta m_{32}^2} [2 + 3(2 + \varphi) \sin^2 \theta_{13} + \mathcal{O}(\sin^4 \theta_{13})] \simeq 1.11 \times 10^{-2} \text{ eV} \quad (3.168)$$

$$m_\beta = \sqrt{-\Delta m_{32}^2} \left[1 + \frac{1}{2}(6\varphi + 5) \sin^2 \theta_{13} + \mathcal{O}(\sin^4 \theta_{13}) \right] \simeq 5.75 \times 10^{-2} \text{ eV} \quad (3.169)$$

and

$$m_{\beta\beta} = \sqrt{-\Delta m_{32}^2} [1 + (2 + 3\varphi) \sin^2 \theta_{13} + \mathcal{O}(\sin^4 \theta_{13})] \simeq 5.69 \times 10^{-2} \text{ eV} \quad (3.170)$$

where in the numerical evaluation $\Delta m_{32}^2 = -2.449 \times 10^{-3} \text{ eV}^2$ and $\sin^2 \theta_{13} = 2.19 \times 10^{-2}$.

3.3.4.2 Mechanism II c-2: $h_i = h_r = 0$

In this case, $h_r = 0$, the reactor mixing angle is

$$\sin^2 \theta_{13} = \frac{(8\varphi + 5) (\sqrt{3}h_{r,2} - 3(\varphi + 2)f_i)^2}{h_{r,2}^2 [(2\varphi + 1)h_{r,2} + 2\sqrt{3}(3\varphi + 2)f_i]^2 f_r^2 + \mathcal{O}(f_r^4)}. \quad (3.171)$$

A small reactor mixing angle can be obtained also for $h_{r,2} \sim \sqrt{3}(2 + \varphi)f_i$, but no clear symmetry argument can be invoked to explain such a relation.

The masses of the light neutrinos at LO are

$$m_1 = m_0 \left| -\frac{2}{3} (\varphi h_{r,2} + \sqrt{3}f_i)^2 + \mathcal{O}(f_r^2) \right| \quad (3.172a)$$

$$m_2 = m_0 \left| -\frac{2}{3} ((\varphi - 1)h_{r,2} - \sqrt{3}f_i)^2 \right| \quad (3.172b)$$

$$m_3 = m_0 \left| -\frac{2}{3} (h_{r,2} - \sqrt{3}f_i)^2 + \mathcal{O}(f_r^2) \right|. \quad (3.172c)$$

We can write the following sum rule for the complex masses as

$$\Sigma = (\tilde{m}_1 + (21\varphi + 13)\tilde{m}_2 - 5(3\varphi + 2)\tilde{m}_3)^2 - (84\varphi + 52)\tilde{m}_1\tilde{m}_2 + \mathcal{O}(m^2 \sin^2 \theta_{13}). \quad (3.173)$$

In this case the coefficient in front of $\sin^2 \theta_{13}$ can be large, thus we expect that the sum rule can be invalidated by NLO corrections.

The solar mass-squared difference is

$$\Delta m_{21}^2/m_0^2 = -\frac{4}{9}(2\varphi - 1)h_{r,2} \left(h_{r,2} + 2\sqrt{3}f_i \right) \left(3h_{r,2}^2 + 2\sqrt{3}h_{r,2}f_i + 6f_i^2 \right) + \mathcal{O}(f_r^2) \quad (3.174)$$

hence we expect a natural suppression for r_ℓ in the case of $f_i \sim -1/2\sqrt{3}h_{r,2}$ because $\Delta m_{3\ell}^2 \propto h_{r,2}$. This case is only compatible with NO, provided that $h_{r,2} > 0 \wedge f_i < -h_{r,2}/2\sqrt{3}$ or $h_{r,2} < 0 \wedge f_i > -h_{r,2}/2\sqrt{3}$.

From the expression of r_1 as a function of $\sin^2 \theta_{13}$, we need $f_i \sim -1/2\sqrt{3}h_{r,2}$ to reproduce the best fit values of both observables. Adopting this ansatz, we obtain

$$\sin^2 \theta_{13} = \frac{3}{4}(35\varphi + 26) \frac{f_r^2}{h_{r,2}^2} + \mathcal{O}(f_r^4) \quad f_i = -\frac{h_{r,2}}{2\sqrt{3}}. \quad (3.175)$$

and thus $f_r \sim \pm 1/50h_{r,2}$ if we want to reproduce $\sin^2 \theta_{13} = 2.19 \times 10^{-2}$.

From the mass spectrum, defined in (3.172), in the limit $f_i = -h_{r,2}/2\sqrt{3}$, we get $m_1/m_2 \sim 1$ and $m_3/m_2 \sim 9/5$. Using the relations derived above and the condition $f_i = -h_{r,2}/2\sqrt{3}$ we obtain

$$\sum_j m_j = \sqrt{\Delta m_{31}^2} [2.54 - 1.97 \sin^2 \theta_{13} + \mathcal{O}(\sin^4 \theta_{13})] \simeq 1.24 \times 10^{-1} \text{ eV} \quad (3.176)$$

$$m_\beta = \sqrt{\Delta m_{31}^2} [0.67 - 0.03 \sin^2 \theta_{13} + \mathcal{O}(\sin^4 \theta_{13})] \simeq 3.31 \times 10^{-2} \text{ eV} \quad (3.177)$$

and

$$m_{\beta\beta} = \sqrt{\Delta m_{31}^2} [0.67 - 0.25 \sin^2 \theta_{13} + \mathcal{O}(\sin^4 \theta_{13})] \simeq 3.29 \times 10^{-2} \text{ eV} \quad (3.178)$$

where in the numerical evaluations we used the best fit values for the atmospheric mass difference and reactor mixing angle [45].

3.3.4.3 Mechanism II c-2: $h_i = h_{r,2} = 0$

The reactor mixing angle is

$$\sin^2 \theta_{13} = \frac{(8\varphi + 5) (2\sqrt{3}\varphi h_r + 3(\varphi + 2)f_i)^2}{h_r^2 [\varphi h_r + 2\sqrt{3}f_i]^2} f_r^2 + \mathcal{O}(f_r^4). \quad (3.179)$$

From symmetry argument we expect that $|f_r| \ll 1$; however we could also have $h_r \simeq \sqrt{3}(1 - 2\varphi)f_i/2 \simeq -1.94f_i$, but this condition is not related to any symmetry argument. The masses at LO are

$$m_1 = m_0 \left| -\frac{2}{3} \left((\varphi - 1)h_r + \sqrt{3}f_i \right)^2 + \mathcal{O}(f_r^2) \right| \quad (3.180a)$$

$$m_2 = m_0 \left| -\frac{2}{3} \left(\varphi h_r - \sqrt{3}f_i \right)^2 \right| \quad (3.180b)$$

$$m_3 = m_0 \left| -\frac{2}{3} \left(h_r + \sqrt{3}f_i \right)^2 + \mathcal{O}(f_r^2) \right|. \quad (3.180c)$$

We obtain the following sum rule for the complex masses, which is exact at LO

$$\Sigma = (\tilde{m}_1 + (34 - 21\varphi)\tilde{m}_2 + 5(3\varphi - 5)\tilde{m}_3)^2 + (84\varphi - 136)\tilde{m}_1\tilde{m}_2 + \mathcal{O}(m^2 \sin^2 \theta_{13}) \quad (3.181)$$

where, as in the case $h_r = 0$ discussed in Sec. 3.3.4.2, the coefficient in front of $\sin^2 \theta_{13}$ is large.

We observe that the mass-squared differences are related, at LO, to the ones of the previous case ($h_r = 0$, discussed in Sec. 3.3.4.2); in fact

$$\begin{cases} h_{r,2} \longrightarrow h_r \\ f_i \longrightarrow -f_i \end{cases} \quad \text{and} \quad \begin{cases} \Delta m_{21}^2 \longrightarrow -\Delta m_{21}^2 \\ \Delta m_{31}^2 \longrightarrow +\Delta m_{32}^2 \end{cases} \quad (3.182)$$

Thus the allowed spectra in this case are both NO (for $h_r > 0 \wedge (\varphi - 1)/2\sqrt{3}h_r < f_i < h_r/2\sqrt{3}$ or $h_r < 0 \wedge (\varphi - 1)/2\sqrt{3}h_r > f_i > h_r/2\sqrt{3}$) and IO (for $h_r < 0 \wedge 6f_i > -\sqrt{3}\varphi h_r$ or $h_r > 0 \wedge 6f_i < -\sqrt{3}\varphi h_r$). In the following we will not deal with IO case since this hierarchy is realized at the price of having all the non-vanishing vevs at the same order of magnitude; thus there is no clear symmetry argument behind this realization.

To obtain a relation among h_r and f_i we need to consider the NLO corrections to the ratio r_1 expressed as a series in $\sin^2 \theta_{13}$. Fixing both r_1 and θ_{13} to their best fit values we get $h_r = 2\sqrt{3}f_i \simeq 3.46f_i$. Notice that this relation gives us a natural suppression for the solar mass splitting, see (3.174) and (3.182).

With this condition, we get

$$\sin^2 \theta_{13} = \frac{3(119\varphi + 74)}{4} \frac{f_r^2}{h_r^2} + \mathcal{O}(f_r^4) \quad f_i = \frac{h_r}{2\sqrt{3}} \quad (3.183)$$

and thus we need $f_r \sim \pm h_r/100$ to obtain a compatible value of the reactor angle.

We can obtain the relative hierarchy of the neutrino mass spectrum starting from the LO expression for the masses; for $f_i \simeq h_r/2\sqrt{3}$ we have $m_1/m_2 \sim 1$ and $m_3/m_2 \sim 9/5$. In this limit we get for NO the values of $\sum_j m_j$, m_β and $m_{\beta\beta}$. We have

$$\sum_j m_j = \sqrt{\Delta m_{31}^2} [2.54 - 3.03 \sin^2 \theta_{13} + \mathcal{O}(\sin^4 \theta_{13})] \simeq 1.23 \times 10^{-1} \text{ eV} \quad (3.184)$$

$$m_\beta = \sqrt{\Delta m_{31}^2} [0.67 - 0.50 \sin^2 \theta_{13} + \mathcal{O}(\sin^4 \theta_{13})] \simeq 3.26 \times 10^{-2} \text{ eV} \quad (3.185)$$

and

$$m_{\beta\beta} = \sqrt{\Delta m_{31}^2} [0.67 - 0.71 \sin^2 \theta_{13} + \mathcal{O}(\sin^4 \theta_{13})] \simeq 3.23 \times 10^{-2} \text{ eV} \quad (3.186)$$

where we used the best fit values for the atmospheric mass difference and reactor mixing angle [45]. As discussed above the IO gives all the vevs with the same order of magnitude thus we do not discuss here the analytical predictions.

3.3.4.4 Mechanism II c-2: $f_r = f_i = 0$

In this case only the flavon in representation $\mathbf{5} \in A_5$ is relevant for the Dirac mass. The light neutrino mass matrix is $M_\nu = -(M_D^{\mathbf{5}})^T P_{23} (M_D^{\mathbf{5}})/M$, where $M_D^{\mathbf{5}}$ is defined in (3.153). In this case the reactor angle θ_{13} is

$$\sin^2 \theta_{13} = \frac{(\varphi + 1)h_i^2 \left[(\varphi - 3)h_r - 2(3\varphi h_{r,2} + h_{r,2}) \right]^2}{\left[(1 - 2\varphi)h_r^2 + 4(\varphi + 2)h_r h_{r,2} + (3\varphi + 1)h_{r,2}^2 \right]^2} + \mathcal{O}(h_i^4) \quad (3.187)$$

where we neglect higher order terms in h_i . The mass spectrum at LO is the same as the case $h_i = f_i = 0$ discussed in Sec. 3.3.4.1, see (3.160). Also the sum rule Σ and the mass splittings are the same, so we can ignore the discussion regarding the mass spectrum in the following.

Using the fact that $h_r \sim -h_{r,2}$ for NO we have

$$\sin^2 \theta_{13} = \frac{(7\varphi + 10)}{9} \frac{h_i^2}{h_r^2} + \mathcal{O}(h_i^4) \quad h_r = -h_{r,2} \quad (3.188)$$

whereas for IO ($h_r \sim +h_{r,2}$) we obtain

$$\sin^2 \theta_{13} = \frac{(3\varphi + 2) h_i^2}{5 h_r^2} + \mathcal{O}(h_i^4) \quad h_r = +h_{r,2} \quad (3.189)$$

thus $h_i/h_r \sim \pm 1/10$ for values of θ_{13} compatible with the experimental determination, for both orderings.

For the sum of the neutrino masses and the effective masses, in the case of NO, we have

$$\sum_j m_j = \sqrt{\Delta m_{31}^2} [1.55 - 2.55 \sin^2 \theta_{13} + \mathcal{O}(\sin^4 \theta_{13})] \simeq 7.40 \times 10^{-2} \text{ eV} \quad (3.190)$$

$$m_\beta = \sqrt{\Delta m_{31}^2} [0.26 + 0.65 \sin^2 \theta_{13} + \mathcal{O}(\sin^4 \theta_{13})] \simeq 1.35 \times 10^{-2} \text{ eV} \quad (3.191)$$

and

$$m_{\beta\beta} \sqrt{\Delta m_{31}^2} [0.26 - 0.51 \sin^2 \theta_{13} + \mathcal{O}(\sin^4 \theta_{13})] \simeq 1.22 \times 10^{-2} \text{ eV} \quad (3.192)$$

where in the numerical evaluations we used the best fit values for Δm_{31}^2 and θ_{13} . For IO we have instead:

$$\sum_j m_j = \sqrt{-\Delta m_{32}^2} [2 - 3(4\varphi - 7) \sin^2 \theta_{13} + \mathcal{O}(\sin^4 \theta_{13})] \simeq 1.01 \times 10^{-1} \text{ eV} \quad (3.193)$$

$$m_\beta = \sqrt{-\Delta m_{32}^2} \left[1 + \frac{1}{2}(11 - 6\varphi) \sin^2 \theta_{13} + \mathcal{O}(\sin^4 \theta_{13}) \right] \simeq 5.02 \times 10^{-2} \text{ eV} \quad (3.194)$$

and

$$m_{\beta\beta} = \sqrt{-\Delta m_{32}^2} [1 + (5 - 3\varphi) \sin^2 \theta_{13} + \mathcal{O}(\sin^4 \theta_{13})] \simeq 4.96 \times 10^{-2} \text{ eV}. \quad (3.195)$$

3.3.4.5 Mechanism II c-2: $f_r = h_r = 0$

The reactor angle is

$$\sin^2 \theta_{13} = \frac{(5 + 8\varphi) (2\varphi h_{r,2} + \sqrt{3} f_i)^2}{h_{r,2}^2 [(2\varphi + 1) h_{r,2} + 2\sqrt{3}(3\varphi + 2) f_i]^2} h_i^2 + \mathcal{O}(h_i^4). \quad (3.196)$$

A possible partial cancellation occurs for $h_{r,2} \sim -\sqrt{3}(\varphi - 1) f_i/2 \simeq -0.54 f_i$ but no symmetry argument can be invoked to explain such a relation.

In the limit of small $|h_i|$ the LO terms for the solar and the atmospheric mass differences are the same as Sec. 3.3.4.2, therefore we discard the discussion about the mass ordering. Also the relation $f_i = k h_{r,2}$ invoked to get the ratio r_1 compatible with the data requires the same $k \simeq -1/2\sqrt{3}$. This in turn implies that

$$\sin^2 \theta_{13} = \frac{1}{4}(33\varphi + 25) \frac{h_i^2}{h_{r,2}^2} + \mathcal{O}(h_i^4) \quad f_i = -\frac{h_{r,2}}{2\sqrt{3}} \quad (3.197)$$

and then $h_i/h_{r,2} \sim \pm 3/100$ to get a compatible value of θ_{13} .

The value of m_β and $m_{\beta\beta}$ are different with respect to the case discussed in Sec. 3.3.4.2 because of the NLO corrections. We have

$$\sum_j m_j = \sqrt{\Delta m_{31}^2} [2.54 - 3.94 \sin^2 \theta_{13} + \mathcal{O}(\sin^4 \theta_{13})] \simeq 1.22 \times 10^{-1} \text{ eV} \quad (3.198)$$

$$m_\beta = \sqrt{\Delta m_{31}^2} [0.67 - 0.87 \sin^2 \theta_{13} + \mathcal{O}(\sin^4 \theta_{13})] \simeq 3.22 \times 10^{-2} \text{ eV} \quad (3.199)$$

and

$$m_{\beta\beta} = \sqrt{\Delta m_{31}^2} [0.67 - 1.10 \sin^2 \theta_{13} + \mathcal{O}(\sin^4 \theta_{13})] \simeq 3.19 \times 10^{-2} \text{ eV} \quad (3.200)$$

where we used the best fit values of Δm_{31}^2 and $\sin^2 \theta_{13}$ quoted in Ref. [45].

3.3.4.6 Mechanism II c-2: $f_r = h_{r,2} = 0$

In this case the reactor angle θ_{13} is

$$\sin^2 \theta_{13} = \frac{(5 + 8\varphi)h_i^2 (\sqrt{3}f_i - (\varphi - 2)h_r)^2}{h_r^2 [\varphi h_r + 2\sqrt{3}f_i]^2} + \mathcal{O}(h_i^4). \quad (3.201)$$

As for the previous case ($h_r = 0$) the predictions for the LO terms in the solar and atmospheric mass-squared differences are the same as $\phi_{\nu,5}$ invariant under $Z_2 \otimes Z_2 \otimes CP$, because M_ν has the same form at LO, thus the relations for the mass spectrum and Σ are the same as Sec. 3.3.4.3 when $h_{r,2} = h_i = 0$.

We can obtain a relation between f_i and h_r of the form $f_i = kh_r$ in the limit of small h_i using the NLO expression for r_1 as series of θ_{13} . We get that $k \sim 1/2\sqrt{3}$ assures a natural suppression in the ratio r_1 . Under this assumption the reactor angle reads

$$\sin^2 \theta_{13} = \frac{13 - 3\varphi}{4} \frac{h_i^2}{h_r^2} + \mathcal{O}(h_i^4) \quad f_i = \frac{h_r}{2\sqrt{3}} \quad (3.202)$$

hence we need $h_i \sim \pm h_r/10$ to obtain $\sin^2 \theta_{13} = 2.19 \times 10^{-2}$. The mass spectrum in this limit is constrained to have $m_1/m_2 \sim 1$ and $m_3/m_2 \sim 9/5$, as discussed in the case of NO in Sec. 3.3.4.3. The value of $\sum_j m_j$, m_β and $m_{\beta\beta}$ are:

$$\sum_j m_j = \sqrt{\Delta m_{31}^2} [2.54 - 7.64 \sin^2 \theta_{13} + \mathcal{O}(\sin^4 \theta_{13})] \simeq 1.18 \times 10^{-1} \text{ eV} \quad (3.203)$$

$$m_\beta = \sqrt{\Delta m_{31}^2} [0.67 - 2.28 \sin^2 \theta_{13} + \mathcal{O}(\sin^4 \theta_{13})] \simeq 3.06 \times 10^{-2} \text{ eV} \quad (3.204)$$

and

$$m_{\beta\beta} \sqrt{\Delta m_{31}^2} [0.67 - 2.50 \sin^2 \theta_{13} + \mathcal{O}(\sin^4 \theta_{13})] \simeq 3.04 \times 10^{-2} \text{ eV} \quad (3.205)$$

where we used the best fit values of Δm_{31}^2 and $\sin^2 \theta_{13}$.

3.3.4.7 Mechanism II c-2: summary table

Differently to the other mechanisms we report our results in one table only because of cumbersome formulae for $\tan 2\theta$ and θ_{13} . In Tab. 3.11 we summarize our numerical results for the neutrino mass sum rules and the numerical values of $\sum_j m_j$ and the effective masses m_β and $m_{\beta\beta}$.

3.4 Numerical results

In this Section we discuss the validity of our analytical estimates, discussed in Sec. 3.3, with respect to the numerical evaluation. The results for the observables m_β and $m_{\beta\beta}$ are discussed in Sec. 3.5. In the following we outline the procedure used to get our numerical results for the neutrino observables ³:

- We generate the parameters of M_ν with a flat distribution in the range $[-1, +1]$. The overall scale m_0 is left as a free parameter and will be determined later on.
- We diagonalize the product $M_\nu^\dagger M_\nu$ and we check that the numerical PMNS matrix is in the 3σ allowed region, for both orderings, referring to the matrix in Eq. (1.16).

³We double checked the obtained results with independent codes written in `Mathematica` and `C`.

	$h_i = f_i = 0$	$h_i = h_r = 0$	$h_i = h_{r,2} = 0$
Σ	$(\tilde{m}_1 + \tilde{m}_2 - \tilde{m}_3)^2 - 4\tilde{m}_1\tilde{m}_2$	Eq. (3.173)	Eq. (3.181)
$\sum_j m_j$ [eV]	7.62×10^{-2} (NO), 1.11×10^{-2} (IO)	1.24×10^{-1}	1.23×10^{-1}
m_β [eV]	1.47×10^{-2} (NO), 5.75×10^{-2} (IO)	3.31×10^{-2}	3.26×10^{-2}
$m_{\beta\beta}$ [eV]	1.34×10^{-2} (NO), 5.69×10^{-2} (IO)	3.29×10^{-2}	3.23×10^{-2}
	$f_r = f_i = 0$	$f_r = h_r = 0$	$f_r = h_{r,2} = 0$
Σ	$(\tilde{m}_1 + \tilde{m}_2 - \tilde{m}_3)^2 - 4\tilde{m}_1\tilde{m}_2$	Eq. (3.173)	Eq. (3.181)
$\sum_j m_j$ [eV]	7.40×10^{-2} (NO), 1.01×10^{-1} (IO)	1.22×10^{-1}	1.18×10^{-1}
m_β [eV]	1.35×10^{-2} (NO), 5.02×10^{-2} (IO)	3.22×10^{-2}	3.06×10^{-2}
$m_{\beta\beta}$ [eV]	1.22×10^{-2} (NO), 4.96×10^{-2} (IO)	3.19×10^{-2}	3.04×10^{-2}

Table 3.11: Same as Tab. 3.3 but for Mechanism II c-2.

- Since the mass ordering is fixed by the form of U_{PMNS} we can construct the spectrum and the squared-mass differences. We can determine the ordering and test if the obtained r_ℓ is inside the 3σ regions reported in Eq. (1.18) for NO and (1.19) for IO.
- We can now fix the value of m_0 comparing the best fit value of Δm_{21}^2 with our numerical estimate (whose overall undetermined scale is precisely m_0) thus we can obtain the mass spectrum.
- Using the values of mixing angles and mass splittings we compute the χ^2 for the allowed orderings. We use the same definition of (2.119) and the data of Ref. [45].

In our numerical scan we generate $\mathcal{O}(10^8)$ points and the sampling efficiency is $\mathcal{O}(10^{-(3\div 4)})$ for four (or more) free parameters and $\mathcal{O}(10^{-(5\div 6)})$ for three free parameters.

For a given observable q we can define an associated error as

$$\Delta q \equiv \frac{q^{\text{Full}} - q^{(\text{N})\text{LO}}}{q^{\text{Full}}} \quad (3.206)$$

where the superscript Full refers to the full numerical evaluation obtained in the numerical scan while (N)LO refers to the order of the analytical quantity q . We observe that the error on the reactor mixing angle θ_{13} is a linear function of its full numerical value. In fact, in terms of the small variable y , $\sin^2 \theta_{13}$ can be written as a series of the form $s_{13}^2 \text{LO} y^2 + s_{13}^2 \text{NLO} y^4 + \mathcal{O}(y^6)$, thus

$$\Delta \sin^2 \theta_{13} \simeq \frac{s_{13}^2 \text{NLO}}{s_{13}^2 \text{LO}} y^2 \propto \sin^2 \theta_{13}. \quad (3.207)$$

At the beginning of each subsection we report the tables with the best fit values for the χ^2 obtained in our numerical scan with the additional constraint $\sum_j m_j \leq 0.23$ eV (except in Tab 3.13 for Mechanism II a-1 with $Z = 0$ and $|S| \gg |X|$ where this constraint cannot be satisfied. In this case we show the χ^2 with the constraint $\sum_j m_j \leq 0.59$ eV). To quantify the contribution of the mixing angles and the mass splittings in the total χ^2 we introduce the parameters χ_a^2 and χ_m^2 which are defined as

$$\chi_a^2 \equiv \sum_{i \neq j} \chi_{\sin^2 \theta_{ij}}^2 \quad \chi_m^2 \equiv \chi_{\Delta m_{21}^2}^2 + \chi_{\Delta m_{3\ell}^2}^2 \quad (3.208)$$

where $\ell = 1$ for NO and $\ell = 2$ for IO. For the sake of completeness we also report the χ^2 for cases that cannot be expressed as a series in the natural small parameter not considered

in the analytical part. These are marked with $\boldsymbol{\times}$.

3.4.1 Mechanism I

	$z = 0$	$x = 0$	$s = 0 - \text{NO}$	$s = 0 - \text{IO } \boldsymbol{\times}$
χ_a^2	11.78	5.62	4.90	5.76
χ_m^2	1.19	0.32	1.63	0.90
χ^2	12.97	5.94	6.53	6.66

Table 3.12: Minimum of the χ^2 in the case of Mechanism I.

3.4.1.1 Mechanism I: $z = 0$

The model discussed in Sec. 3.3.1.1 has many interesting features. In particular, as discussed in (3.37), the proportionality between the two parameters x and s is not fixed to a single relation but different values of the proportionality constant k are possible. To confirm this analytic result and to better quantify the whole range of correlation between x and s , we have reported the results of our numerical scan (for the allowed points only) in the left panel in Fig. 3.2, where we also indicated the analytic correlations found in Sec. 3.3.1.1. Interestingly enough, for these points, we confirm the bound $r_1 \gtrsim (3 - \varphi) \sin^2 \theta_{13} \simeq 1.38 \sin^2 \theta_{13}$ (right panel of Fig. 3.2), related to the limit $x \rightarrow 0$ discussed in (3.37), where the mass spectrum at LO is degenerate, $m_j/m_0 = |s| + \mathcal{O}(y^2)$.

As shown in Fig. 3.3 we cannot have both r_1 and θ_{13} close to the experimental best fit points if we require that the sum of the neutrino masses is lower than the cosmological upper bound using the PLANCK \oplus BAO data. Notice that the behaviour of $\sum_j m_j$ is in agreement with the prediction discussed in (3.38).

As a final remark, we can quantify the goodness of the expansion in the small $|y|$. We observe that the corrections for r_1 and $\sin^2 \theta_{13}$ are roughly 10% for the whole parameter space. For θ_{13} we observe a linear correlation as discussed in (3.207).

3.4.1.2 Mechanism I: $x = 0$

In this case the prediction discussed in Sec. 3.3.1.2 are in good agreement with our numerical scan. In particular we observe a strong correlation between s and z , as discussed in (3.47). This happens for all the points in the allowed 3σ confidence region for mass splittings and mixing angles. We observe that the corrections to the mixing angle θ_{13} and the ratio r_2 using (3.43) and (3.47) with respect to the full numerical evaluation are of order 10% and 15% \div 20 % in the whole parameter space.

3.4.1.3 Mechanism I: $s = 0$

In this case the analysis performed for IO in Sec. 3.3.1.3 is in good agreement with our numerical scan. In particular, we observe the strong correlation between x and z discussed in (3.53). The values for $\Delta \sin^2 \theta_{13}$ ($|\Delta r_2|$) are of order 10% (5%).

On the other hand, we also found points compatible with NO, but the smallest parameter in the neutrino mass matrix M_ν turns out to be z , *i.e.* $|z| \ll |y|$. However, there are no (clear) symmetry arguments behind this possibility that we do not investigate anymore.

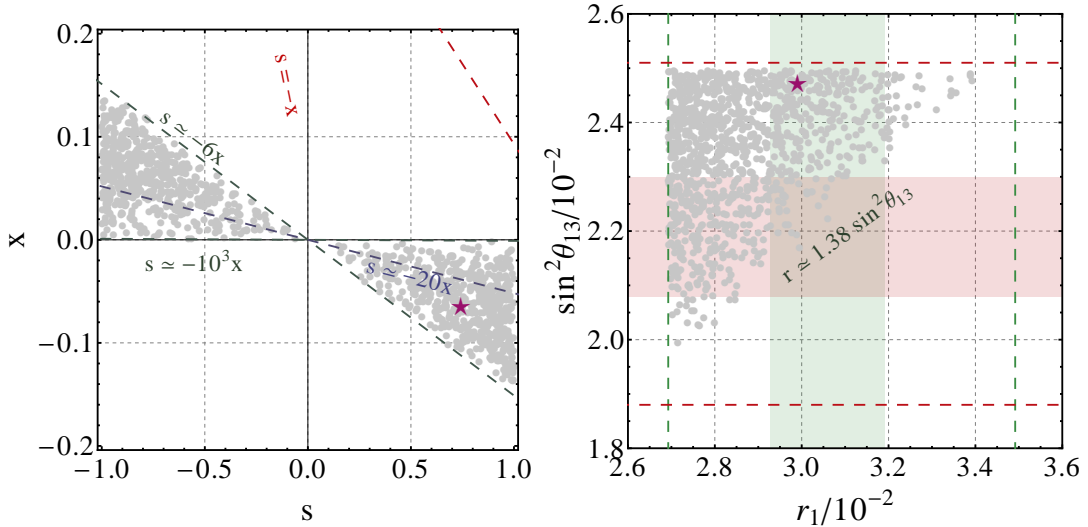


Figure 3.2: (Left plot) Distribution of the parameter s and x in the plane (s, x) for Mechanism I with $z = 0$. The points satisfy the experimental constraints on mixing angles and mass splittings at 3σ CL. The red dashed line is the theoretical expectation for the excluded region at order y^2 and the blue dashed line is the theoretical expectation between s and x given by (3.36). The green dashed lines are the upper and lower limit on k , see Eq. (3.37). (Right plot) Scatter plot in the plane $(r_1, \sin^2 \theta_{13})$. The red (green) region indicates the 1σ confidence region on $\sin^2 \theta_{13}$ (r_1) and the dashed red (green) lines the 3σ confidence region on the same parameter extracted from Ref. [45]. The green dashed line is the lower bound obtained from (3.37) where the mass spectrum is degenerate. The purple star indicates the minimum of the χ^2 in Tab. 3.12.

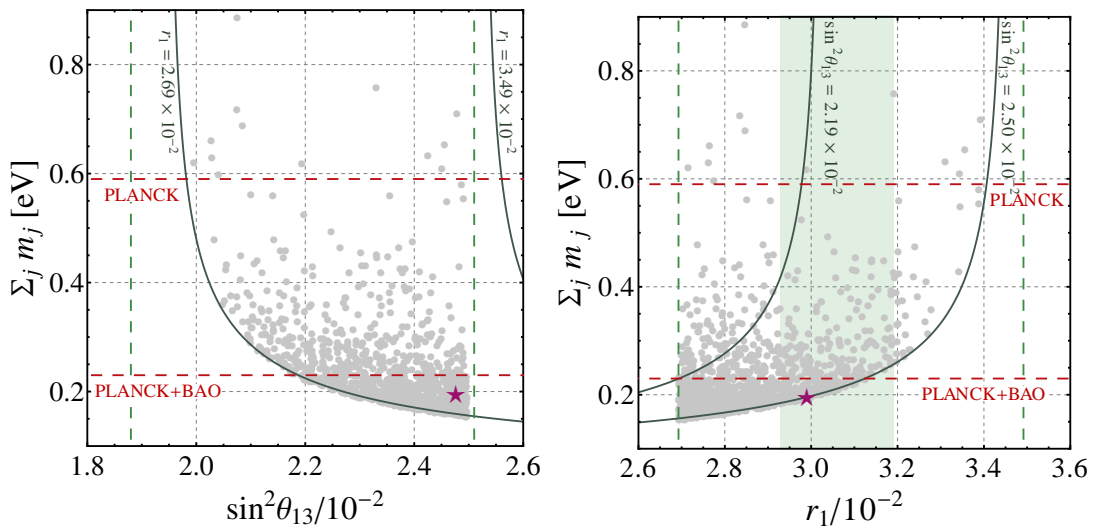


Figure 3.3: Scatter plots in the plane $(\sin^2 \theta_{13}, \sum_j m_j)$ (left plot) and $(r_1, \sum_j m_j)$ (right plot) assuming Mechanism I and $z = 0$. The horizontal dashed red line indicates the upper bound on the sum of neutrino masses by PLANCK Collaboration @ 95% CL [53], the green region indicates the 1σ confidence region and the vertical dashed green line the 3σ confidence region on $\sin^2 \theta_{13}$ (r_1) extracted from Ref. [45]. The purple star indicates the minimum of the χ^2 under the assumption $\sum_j m_j \leq 0.23$ eV. The green lines indicate the region of the planes which are admitted using the predictions of (3.38) for the compatible values of r_1 and θ_{13} .

3.4.2 Mechanism II a-1

	$Z = 0$ (NO)		$Z = 0$		$X = 0$ (NO)		$S = 0$	
	$ S = X $	$ S \gg X $	IO \times	$S \simeq Z/3$	$S \simeq -Z/4$	$X \simeq 2Z/3$	NO \times	IO \times
χ_a^2	4.38	6.09	5.51	4.37	4.38	4.36	4.36	7.91
χ_m^2	0.02	8.56	0.16	0.09	0.00	0.02	0.01	1.06
χ^2	4.40	14.65	5.67	4.46	4.38	4.38	4.37	8.96

Table 3.13: Minimum of the χ^2 in the case of Mechanism II a-1.

3.4.2.1 Mechanism II a-1: $Z = 0$

In Sec. 3.3.2.1 we found that two correlations are possible between S and X , namely $S \simeq X$ and $|S| \gg |X|$. Our numerical scan confirms these analytical estimates. The corrections to the analytical expression of r_1 and θ_{13} given in Sec. 3.3.2.1 turn out to be roughly 10% for both observables assuming $|S| \simeq |X|$ or $|S| \gg |X|$. In particular, the case $|S| \gg |Z|$ has a positive Δr_1 while $S \simeq X$ has a negative Δr_1 . We also observe IO, but in this case the parameters $|S|, |X|$ and $|Y|$ have the same order of magnitude.

3.4.2.2 Mechanism II a-1: $X = 0$

As discussed in Sec. 3.3.2.2 it is possible to have three different correlations between S and Z . This is also confirmed to a very good accuracy by the numerical scan. We observe that there is not a specific pattern in the plane $(r_1, \sin^2 \theta_{13})$ for the different correlations between S and Z , see also Tab. 3.13 where the values for χ_{\min}^2 are similar. This also reflects on the fact that the NLO corrections to r_1 are not completely negligible; in fact, we found that at LO in the expansion parameter Y $|\Delta r_1| \sim 50\%$ while $\Delta \sin^2 \theta_{13} \sim 10\%$.

3.4.2.3 Mechanism II a-1: $S = 0$

This possibility was not discussed analytically in detail since it is related to patterns with a non-natural hierarchy among the vevs. In fact for NO we get from our numerical scan $|Z| \gg |Y| \gg |X|$ while for IO $|X| \gg |Y| \gg |Z|$, see Sec. 3.3.2.3. We do not discuss this situation any more.

3.4.3 Mechanism II a-2

	$h_i = f = 0$		$h_i = h_r = 0$		$h_i = h_{r,2} = 0$		$g = f = 0$		$g = h_r = 0$		$g = h_{r,2} = 0$	
	NO \times	IO	NO	NO \times	IO	NO \times	IO	NO	IO	NO	IO	
χ_a^2	4.36	5.76	11.73	4.71	5.71	4.37	5.52	12.05	6.20	12.05	6.20	
χ_m^2	0.01	0.14	4.64	0.01	0.01	0.00	0.01	6.06	0.00	6.06	0.00	
χ^2	4.37	5.90	16.37	4.72	5.72	4.47	5.53	18.11	6.20	18.11	6.20	

Table 3.14: Minimum of the χ^2 in the case of Mechanism II a-2.

3.4.3.1 Mechanism II a-2: $h_i = f = 0$

The analytical predictions, performed in Sec. 3.3.3.1, for the strong correlation between h_r and $h_{r,2}$ are well confirmed. Also the prediction for the mixing angles are confirmed by

our numerical scan because $\Delta \sin^2 \theta_{13} \sim 10\%$. For the mass splittings the LO predictions (discussed in Sec. 3.3.3.1) do not correctly reproduce the numerical results. For NO we observe that $|h_r| \ll |g|$ (this condition is necessary to have a small r_1 , see (3.111)), where g is the naturally smallest parameter, and we get $|\Delta r_1| \sim 40\%$ with our analytical predictions. For IO the NLO corrections to mass splittings are important, *e.g.* the solar mass-squared difference is $\mathcal{O}(10^2)$ larger with respect to the experimental value. However these were cumbersome and we did not report the full expansion in our analytical discussion. If we include the undisplayed NLO corrections for the mass splittings, these are in agreement with the full numerical evaluation at $10\% \div 20\%$ level.

3.4.3.2 Mechanism II a-2: $h_i = h_r = 0$

This particular realization, discussed in detail in Sec. 3.3.3.2, has a similar phenomenology as Mechanism I with $z = 0$. In fact there exists a lower bound for the allowed region in the plane $(r_1, \sin^2 \theta_{13})$, as in the right plot of Fig. 3.2. The lower bound is a consequence of the limit $f = -h_{r,2}/\sqrt{6}$, where the mass spectrum is degenerate at LO, $m_j/m_0 = 3h_{r,2}^2/2 + \mathcal{O}(g^2)$. In this case the relation between r_1 and θ_{13} is the same as $k \simeq -10^3$ discussed in (3.37): $r_1 = (3 - \varphi) \sin^2 \theta_{13} + \mathcal{O}(\sin^4 \theta_{13})$. Also the scans of $\sum_j m_j$ as a function of r_1 or θ_{13} are similar to those shown in Fig. 3.3. In fact there exists a lower bound $\sum_j m_j \gtrsim 0.19$ eV for θ_{13} close to the upper limit at 3σ CL, (in the case of Mechanism I with $z = 0$ the lower bound is $\sum_j m_j \gtrsim 0.155$ eV). This is a consequence of a non trivial relation among $\sum_j m_j$, θ_{13} , Δm_{31}^2 and the ratio r_1 , as discussed in Sec. 3.3.3.2. Also the parameters $\Delta \sin^2 \theta_{13}$ and $|\Delta r_1|$ are similar to those discussed in the case of Mechanism I with $z = 0$.

3.4.3.3 Mechanism II a-2: $h_i = h_{r,2} = 0$

The predictions for the mixing angles discussed in Sec. 3.3.3.3 are in agreement with our numerical discussion; however our numerics also shows that NO is allowed for the mass spectrum of quasi-degenerate type. This is realized when $|h_r| \ll |g| \ll |f|$, thus with h_r as the smallest parameter. This possibility cannot be explained using symmetry arguments. For the case discussed in the analytical Section we observe that the corrections for the mixing angles are of $\mathcal{O}(10\%)$ with respect to the full numerical evaluation: instead the corrections for the solar mass difference, and then r_1 , are important. We observe $|\Delta \Delta m_{21}^2| \sim |\Delta r_1| \sim 50\% \div 90\%$. The NLO effects (that we did not report in Sec. 3.3.3.3) reduce the discrepancy between the analytical prediction and the full numerical scan at the level of 10% .

3.4.3.4 Mechanism II a-2: $g = f = 0$

We observe a strong correlation between h_r and $h_{r,2}$, as discussed in the analytical part. The analytical predictions, assuming IO, for the mixing angles performed in Sec. 3.3.3.4 are in good agreement with our numerical scan. The error for θ_{13} is roughly 10% , while $|\Delta r_1| \sim 60\% \div 90\%$ using the LO expansions for the mass-squared differences. If we include the NLO corrections for the mass splittings we obtain $|\Delta r_1| \sim 10\%$. For NO we observe that $|h_r| \ll |h_i|$, as discussed in Sec. 3.3.3.4.

3.4.3.5 Mechanism II a-2: $g = h_r = 0$

As discussed in details in Sec. 3.3.3.5 this case is quite similar to $h_i = h_r = 0$ because the LO predictions are the same. Also this case is in good agreement with our numerical scan in the parameter space, with similar results for $\Delta \sin^2 \theta_{13}$ and $|\Delta r_1|$, see Sec. 3.4.3.2.

3.4.3.6 Mechanism II a-2: $g = h_{r,2} = 0$

This realization, discussed in Sec. 3.3.3.6, has a phenomenology similar to the case $h_i = h_{r,2} = 0$ discussed above in Sec. 3.4.3.2. The numerics confirms that only IO is allowed. The LO results for θ_{13} are in agreement with the numerical evaluation to a high degree of precision while for the mass splittings we obtain $\Delta m_{21}^2 = \mathcal{O}(10^{-4}) \text{ eV}^2$ and thus we need to consider also the NLO corrections to correctly reproduce the full numerical evaluation. Using the NLO formulae we obtain $|\Delta \Delta m_{21}^2| \sim |\Delta r_2| \sim 20\%$.

3.4.4 Mechanism II c-2

	$h_i = f_i = 0$		$h_i = h_r = 0$		$h_i = h_{r,2} = 0$		$f_r = f_i = 0$		$f_r = h_r = 0$		$f_r = h_{r,2} = 0$	
	NO	IO	NO	NO	IO \times	NO	IO	NO	NO	NO	NO	
χ_a^2	4.36	5.55	4.37	8.81	5.80	4.36	5.51	5.55	4.39			
χ_m^2	0.00	0.01	0.01	0.00	0.02	0.00	0.01	0.31	0.05			
χ^2	4.36	5.56	4.38	8.81	5.82	4.36	5.52	5.86	4.44			

Table 3.15: Minimum of the χ^2 in the case of Mechanism II c-2.

3.4.4.1 Mechanism II c-2: $h_i = f_i = 0$

The numerical scan in the parameter space for NO is in good agreement with the analytical expansions performed in Sec. 3.3.4.2, in particular we observe the strong correlation between h_r and $h_{r,2}$. We observe that the corrections are roughly 3% (13%) for $\sin^2 \theta_{13}$ (r_1) in the whole parameter space. Assuming IO the NLO corrections to the mass splitting are important and cannot be neglected. For instance in the case of the solar mass splitting at LO we get a negative value $\Delta m_{21} = -\mathcal{O}(10^{-4}) \text{ eV}^2$ while at NLO we get $\Delta m_{21} = \mathcal{O}(10^{-5}) \text{ eV}^2$.

3.4.4.2 Mechanism II c-2: $h_i = h_r = 0$

The analysis performed in Sec. 3.3.4.2 is compatible with the numerical analysis performed in our numerical scan: we observed that the approximations correctly reproduce the numerical values, being the deviations roughly 5% for $|\Delta r_1|$ and $\Delta \sin^2 \theta_{13}$.

3.4.4.3 Mechanism II c-2: $h_i = h_{r,2} = 0$

For NO the analytical expansion for small values of $|f_r|$ correctly reproduces the reactor angle: the corrections are roughly $\Delta \sin^2 \theta_{13} \sim 10\%$ in the whole 3σ region for θ_{13} , while for $|\Delta r_1|$ we observe a $35 \div 60\%$ deviation with respect to the full numerical evaluation. Including the NLO corrections we obtain a good agreement because $|\Delta r_1| \sim 5\% \div 10\%$.

3.4.4.4 Mechanism II c-2: $f_r = f_i = 0$

The prediction for mixing angles discussed in Sec. 3.3.4.4 are in agreement with our numerical analysis. In particular, the reactor mixing angle obtained using the analytical expansion is about $15\% \div 20\%$ different with respect to the full numerical evaluation for NO while it is only 5% for IO. At LO the predictions for the mass splittings partially reproduce the numerical values, because $\Delta r_1 \sim 40\% \div 60\%$ for NO and $\Delta m_{21}^2 = \mathcal{O}(10^{-4}) \text{ eV}^2$ for IO. If we include the NLO correction we reduce the discrepancy between the full numerical result and the analytical prediction. As an example of the NLO corrections for

the ratio r_ℓ we shown in Fig. 3.4 the results of $|\Delta r_\ell|$ as a function of r_ℓ . We notice that the corrections to the NLO predictions of r_ℓ are about $5 \div 10\%$ ($5 \div 15\%$) for NO (IO).

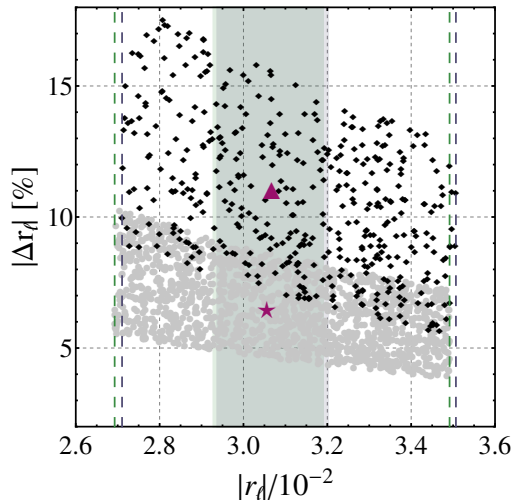


Figure 3.4: Distribution of the corrections with respect to the full numerical evaluation in the planes $(r_\ell, |\Delta r_\ell|)$ in the case of Type I see-saw Mechanism II c-2 with $f_r = f_i = 0$ using the NLO relations. The green (blue) region indicates the 1σ CL for r_1 ($|r_2|$) extracted from Ref. [45]. The points satisfy the experimental constraints on mixing angles and mass splittings at 3σ CL. The purple star indicates the values with χ_{\min}^2 assuming NO while the purple triangle assuming IO, see Tab. 3.15.

3.4.4.5 Mechanism II c-2: $f_r = h_r = 0$

The predictions discussed in Sec. 3.3.4.5 are in agreement with our numerical scan. However, we have observed that also other realizations with all the parameters in M_ν with the same order of magnitude are possible. In this case no clear symmetry arguments can be invoked to explain the absence of hierarchy. Concerning the validity of the analytical formulae, the correction are of order 10% for $\sin^2 \theta_{13}$, while their impact on r_1 is roughly $45 \div 80\%$ in the admitted confidence region. Just to make a comparison, in the case of Mechanism II c-2 ($h_i = h_r = 0$) that has the same LO prediction for the mass spectrum, as discussed in the analytical part, the corrections to r_1 are roughly at the 5% level. A possible explanation for these differences can be found using the NLO coefficients of r_1 . In the limit $f_i/h_{r,2} = -1/2\sqrt{3}$ we have

$$\frac{\text{NLO coefficient } r_1 \text{ Mechanism II c: } h_i = h_r = 0}{\text{NLO coefficient } r_1 \text{ Mechanism II c: } f_r = h_r = 0} = (15 - 9\varphi) \frac{f_r^2}{h_i^2} = (15 - 9\varphi) \frac{9}{25} \simeq 0.15757 \quad (3.209)$$

where we used the approximate relations among f_r and $h_{r,2}$ obtained after (3.175) and that among h_i and $h_{r,2}$ derived after (3.197). Hence the corrections in the case of Mechanism II c-2 $h_i = h_r = 0$ are smaller than those of the Mechanism II c-2 $f_r = h_r = 0$, thus we expect a qualitative difference between these two realizations.

3.4.4.6 Mechanism II c-2: $f_r = h_{r,2} = 0$

This case was discussed in Sec. 3.3.4.6. In our numerical scan we found that also other configurations of NO with all the parameters at the same order of magnitude are allowed, but these cannot be predicted using symmetry arguments and were not discussed in the analytic part. The predictions for the natural case, $|h_i| \ll 1$, are in agreement with our numerical scan. In fact $\Delta \sin^2 \theta_{13} \sim 30 \div 45\%$ and $|\Delta r_1| \sim 5\% \div 15\%$. With respect to the

case $h_i = h_{r,2} = 0$, which has the same LO predictions for the mass spectrum, discussed in Sec. 3.4.4.3 we observe a different behaviour. Using the NLO coefficients of r_1 (in the limit $f_i/h_r = 1/2\sqrt{3}$) we have

$$\frac{\text{NLO coefficient } r_1 \text{ Mechanism II c: } h_i = h_{r,2} = 0}{\text{NLO coefficient } r_1 \text{ Mechanism II c: } f_r = h_{r,2} = 0} = (39 + 63\varphi) \frac{f_r^2}{h_i^2} = \frac{39 + 63\varphi}{100} \simeq 1.40936 \quad (3.210)$$

where we used the approximate relation among f_r and h_r obtained after (3.183) and that among h_i and h_r derived after (3.202), thus the corrections in the case of model with $h_i = h_{r,2} = 0$ are larger than those of $f_r = h_{r,2} = 0$.

3.5 Predictions for m_β and $m_{\beta\beta}$

In this Section we discuss our results for the effective masses m_β and $m_{\beta\beta}$. The analytical estimates are summarized in Tabs. 3.3, 3.6, 3.9 and 3.11. We show our results in several plots in the planes $(m_{\min}, m_{\beta\beta})$ and $(m_\beta, m_{\beta\beta})$ where we also indicate the bounds on m_{\min} with red vertical dashed lines. These are obtained from the cosmological data [53]: $m_{\min} < 0.19$ eV assuming PLANCK data and $m_{\min} < 0.07$ eV using PLANCK \oplus BAO data. For m_β we indicate with a red vertical dashed line the expected sensitivity for the KATRIN experiment: 0.2 eV @ 90% CL [50]. The excluded region for $m_{\beta\beta}$, in both planes, is the area over the horizontal purple dashed line, $m_{\beta\beta} \geq 0.19$ eV obtained using the 90% CL limit on the half-life of ^{76}Ge [61]. A recent result using the ^{136}Xe , $T_{1/2}^{0\nu}(^{136}\text{Xe}) > 1.07 \times 10^{26}$ years @ 90% CL [66], gives the lower bound for the excluded region $m_{\beta\beta} \geq 0.083$ eV ($g_A = 1.269$), but this result has a large uncertainty due to the bad knowledge on the nuclear matrix element.

3.5.1 Mechanism I

In the case of Mechanism I, discussed in Sec. 3.3.1, we obtain different predictions for $m_{\beta\beta}$ or m_β assuming a particular vacuum alignment for the flavon fields (see Tab. 3.3). In Fig. 3.5 we show our results for $m_{\beta\beta}$ as a function of m_{\min} (left panel) and m_β (right panel) assuming $s = 0$, $x = 0$ or $z = 0$.

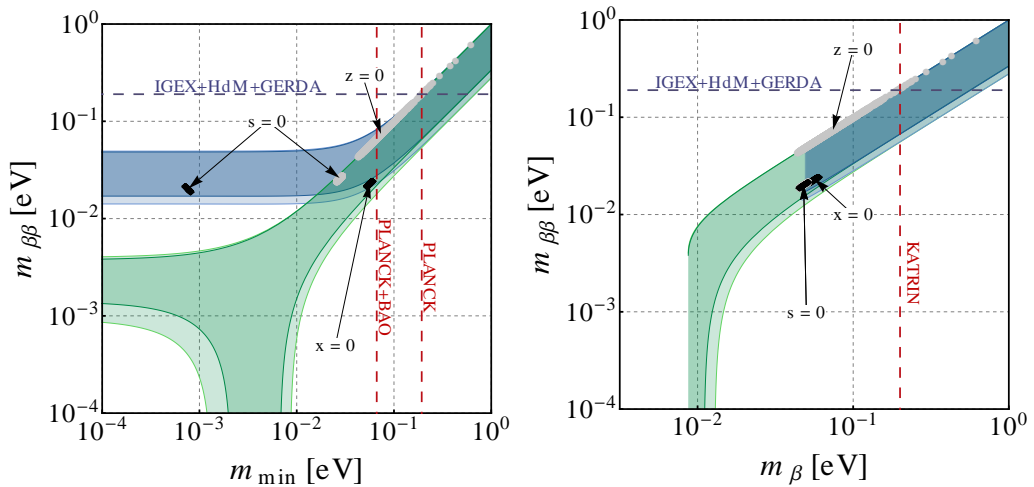


Figure 3.5: Effective mass $m_{\beta\beta}$ for the neutrinoless double beta decay as a function of m_{\min} (left plot) and m_β (right plot) in the case of Mechanism I. Gray circles are for NO while black diamonds for IO. The green (blue) region is the allowed area for $m_{\beta\beta}$ at 3σ CL of mixing parameters [45] assuming NO (IO) while the green (blue) lines contain the region at 1σ .

The predictions, summarized in Tab. 3.3, for the cases $z = 0$, $x = 0$ and $s = 0$ (IO) are in agreement with the numerical evaluation performed in our numerical scan. We also show the results for the case $s = 0$, assuming NO, where it does not exist a natural expansion in the small parameter y .

We observe that the high mass region in the case $z = 0$ is already excluded by cosmology and the current experiments on neutrinoless double decay. Future experiments, discussed in Sec. 1.2.1, could probe the IO and quasi-degenerate region with a sensitivity $m_{\beta\beta} \sim 0.01 \div 0.05$ eV (for a recent review see Ref. [59]). Thus we expect to confirm or reject different realizations of Mechanism I using neutrinoless double beta decay experiments, while m_{β} is far from the expected sensitivity of the KATRIN experiment except for the case $z = 0$.

3.5.2 Mechanism II a-1

In the case of Mechanism II a-1, discussed in Sec. 3.3.2, we have many predictions because of different vacuum alignments, see for instance Tab. 3.6. Our results are shown in Fig. 3.6 where we use the same conventions as Fig. 3.5.

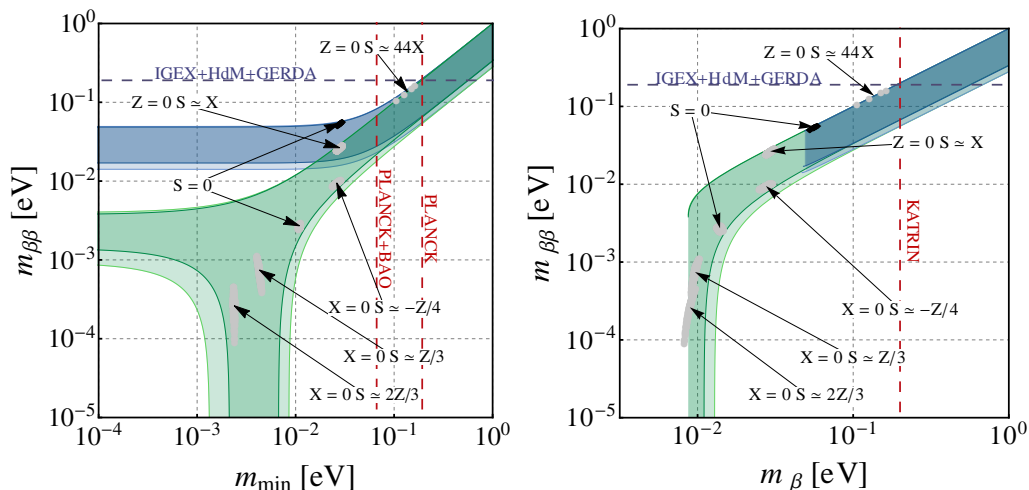


Figure 3.6: Same as Fig. 3.5 but in the case of Mechanism II a-1.

The predictions discussed in the various cases are in agreement with our numerical scan, even for the case $S = 0$ where we only discussed the value of the lightest neutrino mass m_{\min} because no simple expansion in the natural smallest parameter Y is possible. The case $Z = 0$ with $|S| \gg |X|$ is close to the excluded region and already excluded using the $\text{PLANCK} \oplus \text{BAO}$ data, as discussed in Sec. 3.3.2.1. In this Mechanism of $A_5 \otimes CP$ the future neutrinoless double beta decay experiments could probe only the cases $Z = 0$ and $S = 0$ (IO), while the realizations for $X = 0$ and $S = 0$ (NO) are beyond the expected sensitivity. For m_{β} only the case $Z = 0$ and $|S| \gg |X|$ is close to the KATRIN sensitivity.

3.5.3 Mechanism II a-2

In the case of Mechanism II a-2, described in Sec. 3.3.3, the situation is quite intricate because several realizations for the vacuum alignment are possible. In Fig. 3.7 we show our results for the numerical scan in the parameter space (we also show the results for $h_i = h_{r,2} = 0$ with NO, which does not have an expansion in small $|g|$). We indicate as “1” the cluster made by the cases $h_i = f = 0$ NO (grey) and $g = f = 0$ NO (pink); “2”: $g = f = 0$ IO (green); “3”: $h_i = f = 0$ IO (black); “4” $g = h_{r,2} = 0$ IO (green) and $h_i = h_{r,2} = 0$ IO (black); “5”: $g = h_r = 0$ NO (pink), $h_i = h_r = 0$ NO (grey) and $h_i = h_{r,2} = 0$ NO (grey). We observe that the predictions for $m_{\beta\beta}$ in the cases marked as 2, 3 and 4 are quite similar, thus it

is difficult, from the experimental point of view, to distinguish among these realizations. The results are in agreement with the analytical predictions discussed above in Sec. 3.3.3, see Tab. 3.9.

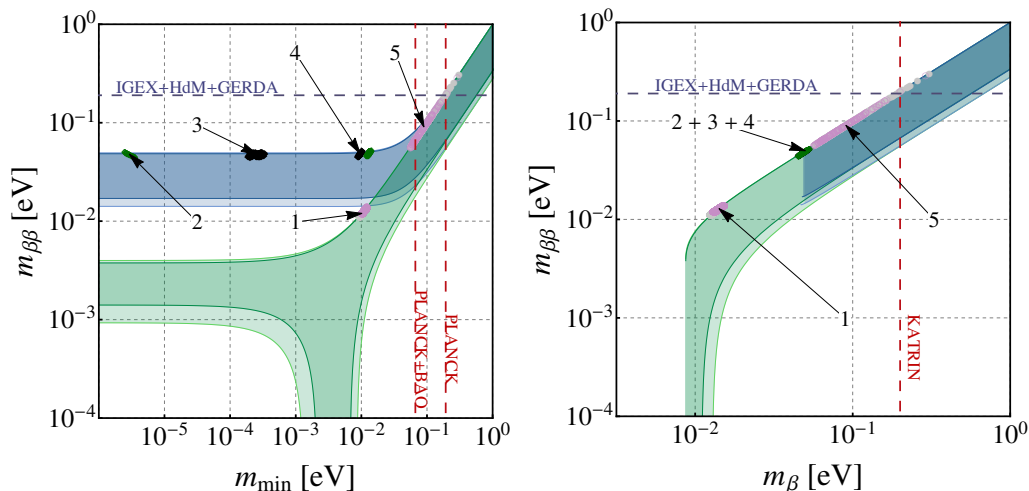


Figure 3.7: Same as Fig. 3.5 but in the case of Mechanism II a-2. See text for further details.

For both cases $h_i = h_r = 0$ and $g = h_r = 0$ (marked as 5) the predictions for $m_{\beta\beta}$ are quite similar to those of Mechanism I with $z = 0$, see Sec. 3.5.1, thus it is impossible to distinguish among these cases. In the plane $(m_\beta, m_{\beta\beta})$ we observe that the predictions for the cases with $g = 0$ or $h_i = 0$ are the same, so there is no way to disentangle these two cases. However, the predictions for the lightest neutrino mass m_{\min} are quite different in cases with $g = f = 0$ assuming IO with respect to the other IO realizations (see clusters 2, 3 and 4), thus we expect that the next cosmological experiments, such as EUCLID [54] combined with the PLANCK data, could improve the knowledge on m_{\min} , because the expected sensitivity on the sum of the neutrino masses is $\mathcal{O}(10^{-2})$ eV.

3.5.4 Mechanism II c-2

This Mechanism, discussed in Sec. 3.3.4, contains six different realizations of the vacuum alignment. The results for the numerical scan over the parameter space are shown in Fig. 3.8 where we observe that the data are in agreement with our analytical predictions, summarized in Tab. 3.11. We also show the results for $h_i = h_{r,2}$ with IO, that does not have a natural expansion in the parameter $|f_r|$. We indicate with “1” the cluster with $h_i = f_i = 0$ NO (pink) and $f_r = f_i = 0$ NO (grey); label “2”: $h_i = f_i = 0$ IO (green) and $f_r = f_i = 0$ IO (black); label “3”: $h_i = h_r = 0$ NO (pink), $h_i = h_{r,2} = 0$ NO (pink), $f_r = h_r = 0$ NO (grey) and $f_r = h_{r,2} = 0$ NO (grey); label “4”: $h_i = h_{r,2} = 0$ IO (green).

This realization is similar to the Mechanism II a-2 discussed above in Sec. 3.5.3 because the prediction in the plane $(m_\beta, m_{\beta\beta})$ is the same in the two cases with $f_r = 0$ and $h_i = 0$, see clusters 1,2 and 3 (while in Mechanism II a-2 for $g = 0$ and $h_i = 0$) and far from the expected KATRIN sensitivity, thus it is difficult to distinguish among different realizations. Also the predictions for m_{\min} are similar for the cases with $f_i = 0$, $h_r = 0$ or $h_{r,2} = 0$, thus it is difficult to disentangle these cases.

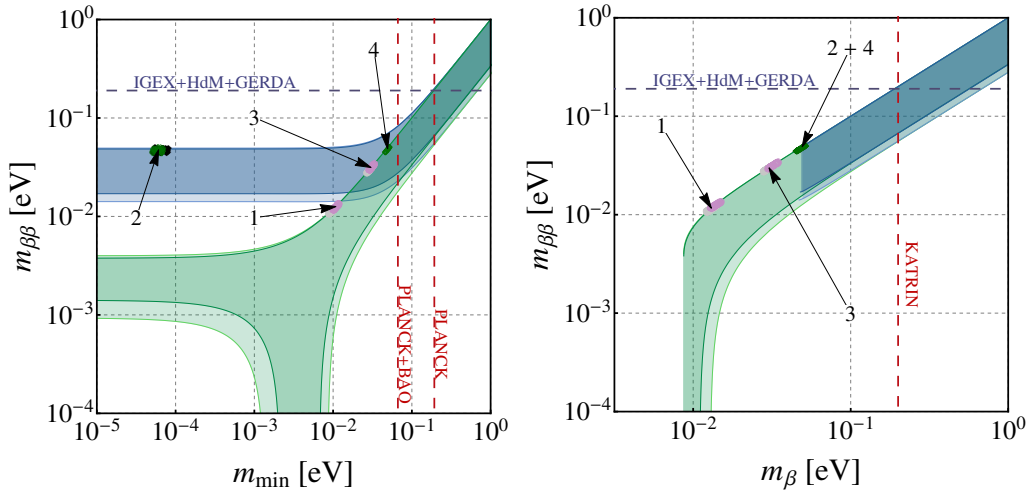


Figure 3.8: Same as Fig. 3.7 but in the case of Mechanism II c-2.

3.6 Model for Mechanism II c-2: $f_r = f_i = 0$

In this Section we want to construct an explicit realization for the neutrino mass spectrum based on the classification discussed above in Sec. 3.3. We concentrate our investigation on Mechanism II c-2 with $f_r = f_i = 0$, discussed in Sec. 3.3.4.4, where the lepton doublet transforms as a $\mathbf{3} \in A_5$ while the right-handed neutrino as a $\mathbf{3}'$. This realization is equivalent to have only a flavon in the pentaplet representation.

The prototype model of how a non-Abelian discrete symmetry can reproduce a given mixing pattern is the model of Altarelli and Feruglio based on A_4 [163]. We consider a SUSY realization to generate the neutrino and charged lepton masses in the $A_5 \otimes CP$ framework. However additional symmetries are needed to correctly reproduce the right vacuum alignment and prevent some unwanted couplings. We consider an abelian Z_3 symmetry (see Appendix B for more details about abelian groups) and an abelian charge, the Froggatt-Nielsen (FN) charge $U(1)_{\text{FN}}$ [147] spontaneously broken through the vev of a scalar field Θ_1 . As usual in SUSY, we also take into account the continuous R-symmetry $U(1)_R$ that has the usual R-parity as a subgroup; terms in a superpotential should always have total R-charge equal to two, see Ref. [164] for further details. The quantum numbers for the matter fields are summarized in Tab. 3.16.

Field	L	ν^c	E	H_d	H_u	$\phi_{\nu,5}$	$\phi_{\nu,3}$	$\phi_{\nu,3'}$	φ_5	χ_5	$\chi_{3'}$	$\tilde{\varphi}_5$	$\tilde{\chi}_5$	$\tilde{\chi}_{3'}$
A_5	$\mathbf{3}$	$\mathbf{3}'$	$\mathbf{3}$	$\mathbf{1}$	$\mathbf{1}$	$\mathbf{5}$	$\mathbf{3}$	$\mathbf{3}'$	$\mathbf{5}$	$\mathbf{5}$	$\mathbf{3}'$	$\mathbf{5}$	$\mathbf{5}$	$\mathbf{3}'$
Z_3	ω_3	ω_3^0	ω_3	ω_3^0	ω_3^0	ω_3^2	ω_3	ω_3	ω_3	ω_3^2	ω_3^0	ω_3	ω_3^2	ω_3^0
$U(1)_{\text{FN}}$	0	0	1/3	0	0	0	0	0	-1/3	-2/3	-1	-1/12	-1/6	-1/4
$U(1)_R$	1	1	1	0	0	0	0	0	0	0	0	0	0	0

Table 3.16: Quantum numbers of the fields involved in the Model.

In the flavon sector, we would like to build a potential for the field $\phi_{\nu,5}$ such that the minimum is as in (3.13e) and $|x_i| \ll |x_r|, |x_{r,2}|$. The method of the *driving fields* is the appropriate one. They do not get vevs but merely help the other flavons to do so. In the following we present a SUSY case in which the $U(1)_{\text{FN}}$ is gauged such that a field Θ_1 gets its vev through a D -term. The quantum numbers of the driving fields and Θ_1 are summarized in Tab. 3.17.

Field	$\phi_{\nu,5}^0$	$\phi_{\nu,1}^0$	χ_5^0	$\chi_{3'}^0$	χ_1^0	$\tilde{\chi}_5^0$	$\tilde{\chi}_{3'}^0$	$\tilde{\chi}_1^0$	Θ_1
A_5	5	1	5	3'	1	5	3'	1	1
Z_3	ω_3	ω_3	ω_3	ω_3^0	ω_3^0	ω_3	ω_3^0	ω_3^0	ω_3^0
$U(1)_{\text{FN}}$	0	0	2/3	1	1	1/6	1/4	1/4	-2
$U(1)_{\text{R}}$	2	2	2	2	2	2	2	2	0

Table 3.17: Quantum numbers of the driving fields and Θ_1 involved in the Model.

The scalar potential can be written as

$$V_{\text{scalar}} = V_F + V_D \quad (3.211)$$

where the F -term and D -term are

$$V_F = \sum_{\text{fields}} \left| \frac{\partial \mathcal{W}}{\partial \Phi} \right|^2 \quad V_D = \frac{1}{2} (M_{FI}^2 - g_{\text{FN}} |\Theta_1|^2)^2. \quad (3.212)$$

The D -term can be constructed in the same way as Refs. [165,166]. In V_D the parameter g_{FN} is the $U(1)_{\text{FN}}$ charge and M_{FI} is the contribution of the Fayet-Iliopoulos term. There are SUSY minima such that $V_F = V_D = 0$. The vanishing of V_D requires

$$|\langle \Theta_1 \rangle|^2 = \frac{M_{FI}^2}{g_{\text{FN}}}. \quad (3.213)$$

The superpotential can be written as

$$\mathcal{W} = \mathcal{W}_\nu + \mathcal{W}_\ell \quad (3.214)$$

where $\mathcal{W}_{\nu(\ell)}$ is the relevant part for the neutrino (charged lepton) driving fields. These can be expressed as series of Λ^{-1} , where Λ is the UV cutoff scale

$$\mathcal{W} = (\mathcal{W}_\nu^{\text{LO}} + \mathcal{W}_\ell^{\text{LO}}) + (\delta \mathcal{W}_\nu + \delta \mathcal{W}_\ell) + \dots \quad (3.215)$$

3.6.1 LO superpotential

At LO we can study $\mathcal{W}_\nu^{\text{LO}}$ and $\mathcal{W}_\ell^{\text{LO}}$ separately because of FN charges.

3.6.1.1 Neutrino superpotential: $\mathcal{W}_\nu^{\text{LO}}$

The superpotential is

$$\begin{aligned} \mathcal{W}_\nu^{\text{LO}} = & \mu_5 [\phi_{\nu,5}^0 \phi_{\nu,5}]_{\mathbf{1}} + \lambda [\phi_{\nu,5}^0 (\phi_{\nu,3} \phi_{\nu,3'})]_{\mathbf{1}} + \lambda_3 [\phi_{\nu,5}^0 (\phi_{\nu,3} \phi_{\nu,3})]_{\mathbf{1}} + \\ & + \lambda_{3'} [\phi_{\nu,5}^0 (\phi_{\nu,3'} \phi_{\nu,3'})]_{\mathbf{1}} + g_3 [\phi_{\nu,1}^0 (\phi_{\nu,3} \phi_{\nu,3})]_{\mathbf{1}} + g_{3'} [\phi_{\nu,1}^0 (\phi_{\nu,3'} \phi_{\nu,3'})]_{\mathbf{1}} \end{aligned} \quad (3.216)$$

where $\mu_5, \lambda, \lambda_3, \lambda_{3'}, g_3, g_{3'} \in \mathbb{R}$ as a consequence of the Clebsh-Gordan coefficients, see Appendix C. The components of the $\langle \phi_{\nu,5} \rangle$ in (3.13e) can be parametrized as

$$x_i = \bar{x}_i + \delta x_i \quad x_r = \bar{x}_r + \delta x_r \quad x_{r,2} = \bar{x}_{r,2} + \delta x_{r,2}. \quad (3.217)$$

The terms $\delta x_i, \delta x_r$ and $\delta x_{r,2}$ are the quantum corrections, that we ignore at this order in the Λ^{-1} expansion. The equations for the minimum, $V_F = 0$, give us the following vevs

$$w = i \sqrt{\frac{g_3}{g_{3'}}} (\varphi - 1) v \quad (3.218)$$

where v is unconstrained. Since we need v and w real the parameters in the potential fulfill the condition $g_3 g_{3'} < 0$; similar bounds hold in other models with CP , see for instance Ref. [74]. The other vevs are

$$\bar{x}_i = 0 \quad (3.219a)$$

$$\bar{x}_r = \frac{3w^2 \lambda_{3'} - 6v^2 \lambda_3 (\varphi - 1) - 2wv \lambda (\varphi + 1)}{\sqrt{6} \mu_5} \quad (3.219b)$$

$$\bar{x}_{r,2} = \frac{6w^2 \lambda_{3'} \varphi + 3v^2 \lambda_3 + 2wv \lambda (\varphi - 2)}{\sqrt{6} \mu_5}. \quad (3.219c)$$

Using (3.218), (3.219b) and (3.219c) we get

$$\frac{x_r}{x_{r,2}} \simeq \frac{\bar{x}_r}{\bar{x}_{r,2}} = \frac{2\sqrt{-g_3 g_{3'}} \lambda (3\varphi - 4) + 3[2g_3 \lambda_{3'} (1 - 2\varphi) + g_{3'} \lambda_3 (2 + \varphi)]}{2\sqrt{-g_3 g_{3'}} \lambda (1 + 3\varphi) - 3[2g_3 \lambda_{3'} (1 - 2\varphi) + g_{3'} \lambda_3 (\varphi - 3)]} \quad (3.220)$$

which is compatible with $x_r/x_{r,2} \simeq \pm 1$, see Sec. 3.3.4.4, assuming a tuning among the parameters in $\mathcal{W}_\nu^{\text{LO}}$.

3.6.1.2 Charged lepton superpotential: $\mathcal{W}_\ell^{\text{LO}}$

This analysis is similar to the one discussed in Ref. [113]. The superpotential at the renormalizable level is

$$\begin{aligned} \mathcal{W}_\ell^{\text{LO}} = & \eta [\chi_1^0 (\chi_5 \varphi_5)_1]_1 + m_{3'} [\chi_{3'}^0 \chi_{3'}]_1 + \rho_{3'} [\chi_{3'}^0 (\chi_5 \varphi_5)_{3'}]_1 + m_5 [\chi_5^0 \chi_5]_1 + \\ & + \rho_a [\chi_5^0 (\varphi_5 \varphi_5)_{5^1}]_1 + \rho_b [\chi_5^0 (\varphi_5 \varphi_5)_{5^2}]_1 + \\ & + \tilde{\eta} [\tilde{\chi}_1^0 (\tilde{\chi}_5 \tilde{\varphi}_5)_1]_1 + \tilde{m}_{3'} [\tilde{\chi}_{3'}^0 \tilde{\chi}_{3'}]_1 + \tilde{\rho}_{3'} [\tilde{\chi}_{3'}^0 (\tilde{\chi}_5 \tilde{\varphi}_5)_{3'}]_1 + \tilde{m}_5 [\tilde{\chi}_5^0 \tilde{\chi}_5]_1 + \\ & + \tilde{\rho}_a [\tilde{\chi}_5^0 (\tilde{\varphi}_5 \tilde{\varphi}_5)_{5^1}]_1 + \tilde{\rho}_b [\tilde{\chi}_5^0 (\tilde{\varphi}_5 \tilde{\varphi}_5)_{5^2}]_1 \end{aligned} \quad (3.221)$$

where all coefficients are real. A particular solution for the vevs at LO is

$$\langle \chi_{3'} \rangle = (0, 0, 0)^T \quad \langle \tilde{\chi}_{3'} \rangle = (0, 0, 0)^T \quad (3.222a)$$

$$\langle \chi_5 \rangle = (0, 0, 0, 0, v_\chi)^T \quad \langle \tilde{\chi}_5 \rangle = (0, 0, 0, 0, \tilde{v}_\chi)^T \quad (3.222b)$$

$$\langle \varphi_5 \rangle = (0, 0, v_\varphi, 0, 0)^T \quad \langle \tilde{\varphi}_5 \rangle = (0, 0, \tilde{v}_\varphi, 0, 0)^T \quad (3.222c)$$

where

$$v_\chi = \frac{2\rho_a + 3\rho_b}{\sqrt{6}} \frac{v_\varphi^2}{m_5} \quad \tilde{v}_\chi = \frac{2\tilde{\rho}_a + 3\tilde{\rho}_b}{\sqrt{6}} \frac{\tilde{v}_\varphi^2}{\tilde{m}_5} \quad (3.223)$$

and $v_\varphi, \tilde{v}_\varphi$ are unconstrained.

3.6.2 NLO corrections

3.6.2.1 Neutrino superpotential: $\delta\mathcal{W}_\nu$

Due to Z_3 and $U(1)_{\text{FN}}$ charges the corrections in the sector with the neutrino driving fields do not contain $\chi_5, \tilde{\chi}_5, \varphi_5, \tilde{\varphi}_5, \chi_{3'}$ and $\tilde{\chi}_{3'}$. We have two possible contractions with the driving fields $\phi_{\nu,5}^0$ and $\phi_{\nu,1}^0$: $\phi_{\nu,5} \phi_{\nu,5} \phi_{\nu,3}$ and $\phi_{\nu,5} \phi_{\nu,5} \phi_{\nu,3'}$, so in principle four kinds of operators, up to contractions, are possible. Since we have two identical fields we can use the antisymmetry of the Clebsh-Gordan coefficients in order to reduce the number of non-vanishing operators. We get only six independent operators, collected in Appendix F.1. Notice that there are no correction to the driving field $\phi_{\nu,1}^0$ at NLO

$$\frac{\partial \mathcal{W}_\nu}{\partial \phi_{\nu,1}^0} = \frac{\partial \mathcal{W}_\nu^{\text{LO}}}{\partial \phi_{\nu,1}^0} + \dots = 0 \quad (3.224)$$

where dots indicate N²LO corrections, thus δv and δw satisfy the LO relation, see Eq. (3.218). With the above operators we could find the corrections to the vevs defined in (3.219). We get

$$\delta x_i \propto \frac{1}{\Lambda} \frac{v^5}{\mu_5^3} \quad \delta x_r = -\delta x_{r,2} \quad (3.225)$$

where δx_i is a function of the couplings $g_j^{3(3')}$ and the LO vevs (3.218) and (3.219), hence $\delta x_i = \mathcal{O}(v^2/\Lambda)$ with the natural condition $v = \mathcal{O}(\mu_5)$. Thus we get the required hierarchy $|x_i| \ll |x_r|, |x_{r,2}|$. In order to obtain the correct size of θ_{13} , see Eq. (3.187), we can assume

$$\frac{w}{\Lambda} \sim \frac{v}{\Lambda} \sim \frac{\bar{x}_r}{\Lambda} \sim \frac{\bar{x}_{r,2}}{\Lambda} \sim \lambda_C \quad \frac{x_i}{\Lambda} = \frac{\delta x_i}{\Lambda} \sim \lambda_C^2 \quad (3.226)$$

where λ_C is the sine of the Cabibbo angle, $\lambda_C \simeq 0.22$ [167]. From the see-saw mechanism we could predict the scale of the heavy Majorana particles

$$m_\nu \sim \frac{\langle H_u \rangle^2}{M} \frac{v_i v_j}{\Lambda^2} \sim \frac{\langle H_u \rangle^2}{M} \lambda_C^2 = \sin^2 \beta \frac{\langle H \rangle^2}{M} \lambda_C^2 \quad (3.227)$$

thus for $m_\nu = 0.1$ eV and $\sin \beta \sim 1$ we get $M = \mathcal{O}(10^{13})$ GeV.

3.6.2.2 Charged lepton superpotential: $\delta \mathcal{W}_\ell$

In $\delta \mathcal{W}_\ell$ it is possible to have contractions among the driving fields χ_5^0 , $\chi_{3'}^0$ and χ_1^0 and all the scalar flavon fields. We get twenty-eight operators with the pentaplet χ_5^0 , sixteen with $\chi_{3'}^0$, seven with χ_1^0 , twelve with $\tilde{\chi}_5^0$, seven with $\tilde{\chi}_{3'}^0$ and only four with $\tilde{\chi}_1^0$. These are discussed in Appendix F.I. Thus we have $28 + 16 + 7 + 12 + 7 + 4 = 74$ operators at NLO. The effect of these operators is to modify the vacuum alignment of (3.222). We get

$$\langle \chi_{3'} \rangle = (\delta \chi_{3'}^1, \delta \chi_{3'}^2, \delta \chi_{3'}^3)^T \quad (3.228a)$$

$$\langle \chi_5 \rangle = (\delta \chi_5^1, \delta \chi_5^2, \delta \chi_5^3, \delta \chi_5^4, v_\chi + \delta v_\chi)^T \quad (3.228b)$$

$$\langle \varphi_5 \rangle = (\delta \varphi_5^1, \delta \varphi_5^2, v_\varphi + \delta v_\varphi, \delta \varphi_5^4, \delta \varphi_5^5)^T \quad (3.228c)$$

$$\langle \tilde{\chi}_{3'} \rangle = (\delta \tilde{\chi}_{3'}^1, \delta \tilde{\chi}_{3'}^2, \delta \tilde{\chi}_{3'}^3)^T \quad (3.228d)$$

$$\langle \tilde{\chi}_5 \rangle = (\delta \tilde{\chi}_5^1, \delta \tilde{\chi}_5^2, \delta \tilde{\chi}_5^3, \delta \tilde{\chi}_5^4, \tilde{v}_\chi + \delta \tilde{v}_\chi)^T \quad (3.228e)$$

$$\langle \tilde{\varphi}_5 \rangle = (\delta \tilde{\varphi}_5^1, \delta \tilde{\varphi}_5^2, \tilde{v}_\varphi + \delta \tilde{v}_\varphi, \delta \tilde{\varphi}_5^4, \delta \tilde{\varphi}_5^5)^T \quad (3.228f)$$

where all $\delta \chi_r^i$ are different from zero. Note that not all variations are independent because we have more $\delta \chi_r^i$, (twenty-six) than equations (sixteen) thus ten vevs are functions of the others. Notice that the fields $\chi_{3'}$ and $\tilde{\chi}_{3'}$ are needed to obtain a solution for the NLO equations. The expressions for the field variations are quite cumbersome and thus we do not include them here.

3.6.3 Neutrino mass spectrum

At LO the model is the one discussed in Mechanism II c-2 with $f_r = f_i = 0$ (this is equivalent to no flavon in representation $\mathbf{4} \in A_5$) and the light neutrino mass matrix is $M_\nu = -M_D^5 P_{23} M_D^5 / M$ where M_D^5 is defined in Eq. (3.153). At LO $h_i = 0$ thus $\theta_{13} = 0$.

3.6.3.1 NLO corrections

The Dirac lagrangian at NLO can be written as

$$\mathcal{L}_D^{\text{NLO}} = H_u \left\{ y_{33'}^4 \left[(\nu^c L)_4 \left(\frac{\phi_{\nu, \mathbf{3}} \phi_{\nu, \mathbf{3}'}}{\Lambda^2} \right)_4 \right]_1 + y_{33'}^5 \left[(\nu^c L)_5 \left(\frac{\phi_{\nu, \mathbf{3}} \phi_{\nu, \mathbf{3}'}}{\Lambda^2} \right)_5 \right]_1 + \right.$$

$$+ y_{33}^5 \left[(\nu^c L)_5 \left(\frac{\phi_{\nu,3} \phi_{\nu,3}}{\Lambda^2} \right)_{5_s} \right]_1 + y_{3'3'}^5 \left[(\nu^c L)_5 \left(\frac{\phi_{\nu,3'} \phi_{\nu,3'}}{\Lambda^2} \right)_{5_s} \right]_1 \Big\}. \quad (3.229)$$

The Yukawa couplings are real. The Dirac mass can be written as

$$M_D = M_D^{\text{LO}} + M_D^{\text{NLO}} + \dots \quad (3.230)$$

where we expect the naive scaling $M_D^{\text{LO}} \sim \langle H_u \rangle v_i / \Lambda$ and $M_D^{\text{NLO}} \sim \langle H_u \rangle v_i v_j / \Lambda^2$ and v_i is a generic vev defined as in (3.226). We obtain that $(\text{Im } M_D^{\text{NLO}})_{ij} = 0$, thus this term does not contribute to θ_{13} . The matrix is

$$M_D^{\text{NLO}} \sim \langle H_u \rangle \frac{v_i v_j}{\Lambda^2} \begin{pmatrix} a & e & e \\ d & b & c \\ d & c & b \end{pmatrix} \quad (3.231)$$

where a, b, c, d are $\mathcal{O}(1)$ real coefficients.

The Majorana lagrangian at NLO is ⁴

$$\mathcal{L}_M^{\text{NLO}} = \lambda_{53}^5 \left[(\nu^c \nu^c)_5 \left(\frac{\phi_{\nu,3} \phi_{\nu,5}}{\Lambda} \right)_{5_1} \right] + \lambda_{53'}^5 \left[(\nu^c \nu^c)_5 \left(\frac{\phi_{\nu,3'} \phi_{\nu,5}}{\Lambda} \right)_{5_1} \right] \quad (3.232)$$

where λ_{53}^5 and $\lambda_{53'}^5$ are real parameters. The mass matrix for the heavy Majorana particles can be written as

$$M_M = M_M^{\text{LO}} + M_M^{\text{NLO}} + \dots = M_{P_{23}} + M_M^{\text{NLO}} + \dots \quad (3.233)$$

where we used Eq. (3.97) for M_M^{LO} . From the NLO corrections we get

$$M_M^{\text{NLO}} \sim i \frac{vw}{\Lambda} \begin{pmatrix} 0 & -\tilde{f} & \tilde{f} \\ -\tilde{f} & f & 0 \\ \tilde{f} & 0 & -f \end{pmatrix} \quad (3.234)$$

where $\tilde{f} = \sqrt{2}\varphi f$ and $f = \mathcal{O}(1)$. The light neutrino mass matrix can be obtained as

$$M_\nu = M_\nu^{\text{LO}} + M_\nu^{\text{NLO}} + \dots \quad (3.235)$$

where the LO term is discussed in Sec. 3.3.4.4 and the NLO term can be written as

$$M_\nu^{\text{NLO}} = -\frac{1}{M} \left[\left(M_D^{\text{NLO}T} P_{23} M_D^{\text{LO}} + M_D^{\text{LO}T} P_{23} M_D^{\text{NLO}} \right) - M_D^{\text{LO}T} M_M^{\text{NLO}} M_D^{\text{LO}} \right]. \quad (3.236)$$

The term in parentheses is real, thus it does not contribute to θ_{13} (see the discussion after Eq. (3.3)), while the last term has the following structure

$$\frac{1}{M} M_D^{\text{LO}T} M_M^{\text{NLO}} M_D^{\text{LO}} = i \langle H_u \rangle^2 \frac{v_i v_j v_k (\bar{x}_r - \bar{x}_{r,2})}{\Lambda^3 M} \begin{pmatrix} 0 & -\tilde{g} & \tilde{g} \\ -\tilde{g} & g & 0 \\ \tilde{g} & 0 & -g \end{pmatrix} \quad (3.237)$$

where $\tilde{g} = \sqrt{2}\varphi g$ and $g = \mathcal{O}(1)$. This part of the neutrino mass matrix is important to get $\theta_{13} \neq 0$. Notice that in the case of IO this term is negligible because $x_r - x_{r,2} \simeq \bar{x}_r - \bar{x}_{r,2} \simeq 0$, see Sec. 3.3.4.4, and a non-zero reactor angle is a consequence of δx_i defined in (3.225). The form of M_ν is the same M_ν^{LO} thus the neutrino phenomenology does not change at this order.

⁴Notice that terms proportional to one flavon fields are forbidden by Z_3 and $U(1)_{\text{FN}}$ charges.

3.6.4 Charged lepton masses

At LO the Yukawa lagrangian responsible of the lepton mass is the following

$$\begin{aligned} \mathcal{L}_Y = & y_\tau H_d \left[(E^c L)_5 \frac{\varphi_5}{\Lambda} \right]_1 + y_\mu^1 H_d \left[(E^c L)_5 \frac{(\tilde{\chi}_5 \tilde{\chi}_5)_{5_s^1}}{\Lambda^2} \right]_1 + y_\mu^2 H_d \left[(E^c L)_5 \frac{(\tilde{\chi}_5 \tilde{\chi}_5)_{5_s^2}}{\Lambda^2} \right]_1 + \\ & + y_3 H_d \left[(E^c L)_3 \frac{(\tilde{\chi}_{3'} \tilde{\varphi}_5)_3}{\Lambda^2} \right]_1 + y_5 H_d \left[(E^c L)_5 \frac{(\tilde{\chi}_{3'} \tilde{\varphi}_5)_5}{\Lambda^2} \right]_1 + h.c. \end{aligned} \quad (3.238)$$

therefore $m_\tau = y_\tau \sqrt{3/2} \langle H_d \rangle v_\varphi / \Lambda$, $m_\mu = y_\mu^1 \langle H_d \rangle \tilde{v}_\chi^2 / 2\Lambda^2$ and $m_e = 0$. Including the effect of the vevs shifts, (3.228), in the Yukawa lagrangian (3.238) we obtain corrections for the charged lepton mass matrix M_ℓ . We get

$$M_\ell = \langle H_d \rangle \text{diag} \left\{ 0, y_\mu^1 \frac{\tilde{v}_\chi^2}{2\Lambda^2}, y_\tau \sqrt{\frac{3}{2}} \frac{v_\varphi}{\Lambda} \right\} + \langle H_d \rangle \frac{y_\tau}{\Lambda} \begin{pmatrix} -\delta\varphi_5^1 & \frac{\sqrt{3}}{2} \delta\varphi_5^5 & -\frac{\sqrt{3}}{2} \delta\varphi_5^2 \\ \frac{\sqrt{3}}{2} \delta\varphi_5^5 & \sqrt{\frac{3}{2}} \delta\varphi_5^4 & \frac{1}{2} \delta\varphi_5^1 \\ -\frac{\sqrt{3}}{2} \delta\varphi_5^2 & \frac{1}{2} \delta\varphi_5^1 & \sqrt{\frac{3}{2}} \delta v_\varphi \end{pmatrix} \quad (3.239)$$

where the mass matrix at NLO is symmetric because of the Kronecker products. We get corrections for U_{PMNS} by charged leptons through U_ℓ^\dagger , see Sec. 2.3. These corrections can change the LO prediction $\theta_{23} = \pi/4$ and are useful to accommodate the recent hint by $\text{NO}\nu\text{A}$ of a deviation from a maximal atmospheric mixing. To obtain the right hierarchy we need $\delta\varphi_5^1 \simeq 0$, which is a particular solution for (3.228). As discussed in Ref. [113] the correction $\delta\varphi_5^1$ can be smaller than the others $\delta\varphi_5^{j \neq 1}$. In fact, embedding A_5 to its double cover \mathcal{I}' it is possible to solve this issue because \mathcal{I}' has a doublet representation that can be used for the right-handed charged leptons. This approach was used in Ref. [168] to reproduce the mass hierarchy in the quark sector.

The matrix U_ℓ can be written as

$$U_\ell \simeq \begin{pmatrix} 1 & \left(\frac{m_{12} V}{m_{22} \Lambda}\right)^* & \left(\frac{m_{13} V}{m_{33} \Lambda}\right)^* \\ -\frac{m_{12} V}{m_{22} \Lambda} & 1 & -\left(\frac{m_{11}/2 V^2}{m_{33} \Lambda^2}\right)^* \\ -\frac{m_{13} V}{m_{33} \Lambda} & \frac{m_{11}/2 V^2}{m_{33} \Lambda^2} & 1 \end{pmatrix} \quad (3.240)$$

where we indicate as $m_{ij} \equiv (M_\ell)_{ij}$ the matrix elements of M_ℓ and V is the scale of the vevs, defined through the relation (3.223) at LO. The ratio between the vevs and the cutoff scale is fixed by phenomenology

$$\lambda_C^2 \simeq \frac{m_\mu}{m_\tau} \sim \frac{V}{\Lambda} \quad (3.241)$$

where $\lambda_C \simeq 0.22$ is the Cabibbo angle. However, a certain degree of fine-tuning is needed in this model to have $m_e/m_\mu \simeq \lambda_C^{3\frac{1}{2}}$. The estimate in (3.241) is also useful to investigate the size of the reactor angle. The PMNS matrix is the product $U_\ell^\dagger U_\nu$, where, at this order in Λ^{-1} expansion, U_ν is defined as in (3.1). To quantify the effect of U_ℓ we can assume $\theta = 0$, so the Golden Ratio (GR) mixing angle θ_{12} is modified by a factor $\mathcal{O}(\lambda_C^2)$ while the reactor and atmospheric angles change at $\mathcal{O}(\lambda_C^4)$ [113]

$$\sin^2 \theta_{12} = \frac{3-\varphi}{5} [1 + \mathcal{O}(\lambda_C^2)] \quad \sin^2 \theta_{13} = \mathcal{O}(\lambda_C^4) \quad \sin^2 \theta_{23} = \frac{1}{2} [1 + \mathcal{O}(\lambda_C^4)]. \quad (3.242)$$

At order Λ^{-2} no operators are relevant for the lepton masses. We have $4 + 11 + 19 = 34$ operators at order Λ^{-3} , four with $E^c \otimes L \sim \mathbf{1}$, eleven with $E^c \otimes L \sim \mathbf{3}$ and nineteen with $E^c \otimes L \sim \mathbf{5}$, see Sec. F.2. In general these operators give a mass for e and also corrections to m_τ and m_μ . All these operators are suppressed at least as λ_C^4 due to (3.226) and (3.241), thus we could ignore the effects on the PMNS matrix.

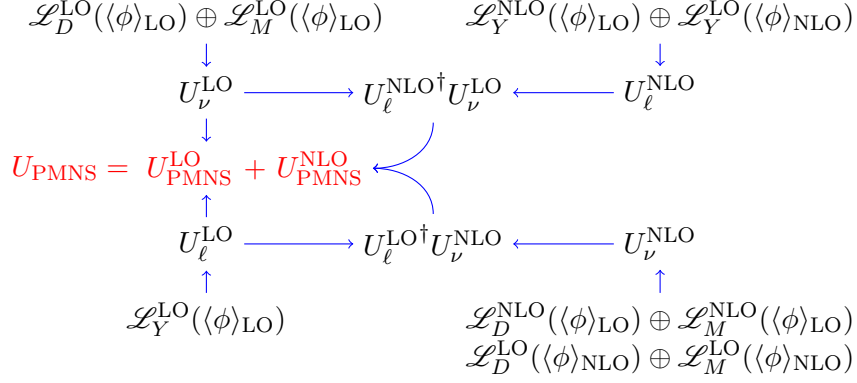


Figure 3.9: Scheme of the contributions to the PMNS matrix from the charged lepton and neutrino sector.

3.6.5 PMNS matrix summary

We want to summarize the results discussed above, in particular the order of magnitude of the mixing angles. Each angle has four contributions at NLO, as shown in Fig. 3.9. These corrections come from:

- the neutrino matrix U_ν , which is obtained from
 - 1 the neutrino lagrangian (3.151) (with $y_4 = 0$), using $\langle\phi_{\nu,r}\rangle$ evaluated at NLO (3.225);
 - 2 the effective operators for neutrino masses, defined in the Dirac (3.229) and Majorana (3.232) lagrangians, using $\langle\phi_{\nu,r}\rangle$ at LO, see Eqs. (3.218) and (3.219);
- the charged-lepton matrix U_ℓ , which is obtained from
 - 3 the Yukawa lagrangian (3.238), using $\langle\chi_r\rangle$ at NLO (3.228);
 - 4 the effective operators for charged-leptons masses (F.9a),(F.10) and (F.11), with $\langle\chi_r\rangle$ and $\langle\phi_{\nu,r}\rangle$ evaluated at LO, see (3.218), (3.219) and (3.222).

In this model the LO prediction for U_{PMNS} is the Golden Ratio matrix, which has $\theta_{13} = 0$, a maximal atmospheric angle and a non-trivial value of θ_{12} (see the discussion after Eq. (2.19) in Chapter 2). Only at NLO the reactor angle acquires a non-zero value as summarized above. Using the formula for $\sin^2 \theta_{13}$ as a function of the neutrino flavons vevs, Eq. (3.187), and the corrections from U_ℓ^\dagger we get

$$\sin^2 \theta_{13} \simeq \frac{2 + \varphi}{5} \left| \sin \theta + i \sqrt{\frac{3 - \varphi}{2}} \left(\frac{m_{12}^*}{m_{22}^*} - \frac{m_{13}^*}{m_{33}^*} \right) \frac{V}{\Lambda} \right|^2 \quad (3.243)$$

where $\sin \theta = \mathcal{O}(\lambda_C)$, see Eq. (3.226), and V/Λ is $\mathcal{O}(\lambda_C^2)$, see Eq. (3.241). Thus we expect that the phenomenology of θ_{13} is the same as $A_5 \otimes CP$ assuming $\mathcal{O}(1)$ coefficients in M_ℓ . The atmospheric angle θ_{23} receives corrections at order λ_C^3 , as discussed above

$$\sin^2 \theta_{23} \simeq \frac{1}{2} \left[1 + \sqrt{\frac{4 + 2\varphi}{5}} \sin \theta \frac{\text{Im}\{(V/\Lambda)(m_{13}m_{22} + m_{12}m_{33})m_{22}^*m_{33}^*\}}{|m_{22}m_{33}|^2} \right] \quad (3.244)$$

hence to get $\theta_{23} \neq \pi/4$ we need large coefficients in M_ℓ . The solar angle θ_{12} is

$$\sin^2 \theta_{12} \simeq \frac{3 - \varphi}{5} \left[1 + \frac{\sin^2 \theta}{5} - \frac{1}{\sqrt{10}} \left(\frac{m_{12}}{m_{22}} + \frac{m_{13}}{m_{33}} + c.c. \right) \frac{V}{\Lambda} \right]. \quad (3.245)$$

Note that the sum rule between the solar and reactor angles, defined in (3.6), is broken by the quantum corrections. Using the above relations we could obtain a mixing pattern that is in agreement at the level of 3σ with the current experimental data: $\theta_{23} \neq \pi/2$ and $\theta_{13} \sim 9^\circ$.

4

New Physics at Neutrino Facilities

After the discovery of the non-vanishing reactor mixing angle θ_{13} in 2012 and its measurement in the Double Chooz [39], Daya Bay [40] and RENO [41] reactor experiments, experimental efforts in the neutrino sector are now devoted to establishing the presence of CP violation in the lepton sector, the neutrino mass ordering and the absolute mass scale.

The large value of the reactor angle, θ_{13} about 9° , allows to search for the CP Dirac phase δ in Long Baseline (LBL) neutrino experiments, such as Tokai to Kamioka (T2K) [35], NO ν A [138] and in future LBL experiments such as Hyper-Kamiokande [42], the Deep Underground Neutrino Experiment (DUNE) [169] and the proposed ESS ν SB [170].

The observation of 28 electron neutrino events in T2K [35] confirmed the $\nu_\mu \rightarrow \nu_e$ transition at more than 7σ and provided a first weak indication for the value of the CP Dirac phase δ . In fact, a combined analysis of the appearance and disappearance channels in T2K, which also includes the reactor constraints on the reactor angle [171], disfavors $\delta/\pi \in [0.15, 0.83]$ for NO and $[-0.18, 1.09]$ for IO at 90% CL, with a best fit point around maximal CP violation, $\delta \simeq 3\pi/2$. This shows the large increase of sensitivity in the determination of δ when performing a combined analysis of reactor and super-beam data, see Refs. [45, 47, 48, 110].

The strength of such a procedure can also be used to test the presence of physics beyond the Standard Model (SM) in the neutrino sector that affects neutrino oscillation probabilities, and to investigate its impact on the determination of the standard oscillation parameters. This analysis was performed in Ref. [172].

In this Chapter, we consider two possible scenarios, discussed in Section 4.1, in the effective field theory approach: the so called *Large Extra Compactified Dimensions* (LED) model, where sterile neutrinos can propagate in a larger than three-dimensional space whereas the SM left-handed neutrinos are confined to a four-dimensional space-time brane; and *Non-Standard Neutrino Interactions* (NSI), where the neutrino interactions with ordinary matter are parametrized at low energy in terms of effective flavour-dependent couplings. In Section 4.2 we discuss the statistical procedure adopted in our analysis while in Section 4.3 we show our results assuming SM, LED or NSI oscillation probabilities.

4.1 Effective Theory

In this Section we want to review the two models and their impact on neutrino oscillation probabilities. In our work, following similar analysis performed in Refs. [173, 174], we use

an effective field theory approach, which means that the theory is valid up to a certain energy scale Λ . We assume that this scale is far from the usual electroweak scale, *i.e.* $\Lambda \gg m_W$, and we can write an effective lagrangian \mathcal{L}^{eff} that contains the effect of New Physics for each specific model. In both models we can consider the effect of NP on oscillation phenomena as a perturbation of the SM neutrino amplitude

$$\mathcal{A}(\nu_\alpha \rightarrow \nu_\beta) = \mathcal{A}_{SM}(\nu_\alpha \rightarrow \nu_\beta) + \delta\mathcal{A}(\nu_\alpha \rightarrow \nu_\beta). \quad (4.1)$$

4.1.1 Large Extra Dimensions

This is a model of sterile neutrinos that propagate in LED giving rise to Kaluza-Klein (KK) modes. The Standard Model LH neutrinos are confined to a 4D spacetime brane [175–177]. In this case the right-handed neutrinos, as gravity, can propagate in the bulk.

There exist several bounds on the number of extra dimensions in the context of LED from astrophysics experiments [167]. We focus our attention to a 6D picture. The extra dimensions are compactified, the fifth (sixth) is a circle of radius R (R'). We use, in practice, a 5D approach, because we consider the limit $R \gg R'$ [178–182]. From torsion experiment on Newton's law we have the following bound on the radius [183]

$$R \leq 37 \mu\text{m} @ 95\% \text{ CL}. \quad (4.2)$$

We consider a framework where we have a Dirac mass term for the three active neutrinos. This model is often indicated as the (3,3) LED model. The action of 5D massless bulk neutrinos $\Psi^\alpha(x_\mu, y)$, interacting with the standard LH neutrinos ν_α is

$$S = i \int d^4x \, dy \, \bar{\Psi}^\alpha(x_\mu, y) \Gamma_A \partial^A \Psi^\alpha(x_\mu, y) + \int d^4x \, \left[i \bar{\nu}_L^\alpha \not{\partial} \nu_L^\alpha + \lambda_{\alpha\beta} H \bar{\nu}_L^\alpha \psi_R^\beta(x_\mu, 0) + \text{hc} \right] + S_I \quad (4.3)$$

where Γ_A are the Dirac matrices in five dimensions $A = 0, 1, 2, 3, 4$, $\lambda_{\alpha\beta}$ the Yukawa couplings and H the Higgs doublet. S_I is the part of the action responsible for neutrino interaction with matter. After electroweak symmetry breaking the neutrino mass matrix can be extracted from the Lagrangian. Following the conventions of Ref. [184] the effective lagrangian in 4D is

$$\mathcal{L}_{LED}^{eff} = \mathcal{L}_M + \mathcal{L}_{CC} \quad (4.4)$$

where

$$\mathcal{L}_M = \sum_{\alpha,\beta} m_{\alpha\beta} \left\{ \bar{\nu}_{\alpha,L}^{(0)} \nu_{\alpha,R}^{(0)} + \sqrt{2} \sum_{k=1}^{\infty} \bar{\nu}_{\alpha,L}^{(0)} \nu_{\alpha,R}^{(k)} \right\} + \sum_{\alpha} \sum_{k=1}^{\infty} \frac{k}{R} \bar{\nu}_{\alpha,L}^{(k)} \nu_{\alpha,R}^{(k)} \quad (4.5a)$$

$$\mathcal{L}_{CC} = \frac{g}{\sqrt{2}} \sum_{\alpha} \bar{\ell}_\alpha \gamma^\mu (\mathbb{1} - \gamma_5) \nu_{\alpha,L}^{(0)} W_\mu + h.c. \quad (4.5b)$$

Here we have indicated with $\alpha = e, \mu, \tau$ the flavour eigenstates, $i = 1, 2, 3$ the mass eigenstates and $k \in \mathbb{N} \setminus \{0\}$ the KK modes. In this lagrangian the zero mode is the SM left-handed neutrino and the KK modes are the particles of New Physics. The matrix $m_{\alpha\beta}$ is the Dirac mass matrix.

In this framework $\nu_{\alpha,L}^{(k)}$ and $\nu_{\alpha,R}^{(k)}$ are massive linear combinations of the bulk fermion fields, which are coupled to SM neutrinos $\nu_{\alpha,L}^{(0)}$.

To evaluate the probability amplitude $\mathcal{A}(\nu_\alpha \rightarrow \nu_\beta)$ in this model we need to know the mass eigenstates $m_j^{(k)}$ and the matrix elements of transition between the zero mode and the tower of KK states $W_j^{(k)}$. In Appendix G we report further details about the evaluation of

these terms. This diagonalization can be done by a unitary transformation with respect to the active flavours

$$\nu_{\alpha,L}^{(0)} = \sum_i U_{\alpha i} \nu_{i,L}^{(0)} \quad (4.6a)$$

$$\nu_{\alpha,R}^{(0)} = \sum_i R_{\alpha i} \nu_{i,R}^{(0)} \quad (4.6b)$$

$$\nu_{\alpha,R}^{(k)} = \sum_i R_{\alpha i} \nu_{i,R}^{(k)} \quad k \geq 1 \quad (4.6c)$$

where $U_{\alpha i}$ are the PMNS matrix elements. The condition

$$\sum_{\alpha,\beta} U_{\alpha i}^* m_{\alpha\beta} R_{\beta j} = \delta^{ij} M_\nu^j \iff \left(U^\dagger m R \right)_{ij} = \text{diag} \left(M_\nu^j \right) \quad (4.7)$$

must be satisfied. Notice that this is not a matrix product, but only a condition on matrix elements. In this model the oscillation amplitude is

$$\mathcal{A}(\nu_\alpha \rightarrow \nu_\beta) = \sum_{i,j,l} \sum_{k=0}^{\infty} U_{\alpha i} U_{\beta j}^* W_{ij}^{(0k)} W_{lj}^{(0k)} \exp \left[i \frac{(\lambda_j^{(k)})^2 L}{2R^2 E_\nu} \right]. \quad (4.8)$$

In vacuum we have a diagonal matrix element of transition, $W_{ij} \propto \delta_{ij}$ (see Appendix G.1), thus we get

$$\mathcal{A}(\nu_\alpha \rightarrow \nu_\beta) = \sum_j \sum_{k=0}^{\infty} U_{\alpha j} U_{\beta j}^* |W_j^{(k)}|^2 \exp \left[i \frac{(\lambda_j^{(k)})^2 L}{2R^2 E_\nu} \right]. \quad (4.9)$$

Thus the probability is

$$\mathcal{P}(\nu_\alpha \rightarrow \nu_\beta) = \left| \mathcal{A}(\nu_\alpha \rightarrow \nu_\beta) \right|^2 = \sum_{i,j} \sum_{k,k'=0}^{\infty} U_{\alpha j} U_{\alpha i}^* U_{\beta i} U_{\beta j}^* |W_j^{(k)}|^2 |W_i^{(k')}|^2 \exp \left[i \frac{(\lambda_j^{(k)})^2 - (\lambda_i^{(k')})^2}{2R^2 E_\nu} L \right]. \quad (4.10)$$

This means that the SM probability is slightly modified by the extra dimensions, in fact the mass of new particles is heavier than zero modes and the matrix elements are suppressed: $W_j^{(k \geq 1)} \sim k^{-1}$. We can recover the SM probability in the limit of $R, m_0 \rightarrow 0$, as shown in Fig. 4.4, for the channel $\nu_\mu \rightarrow \nu_\mu$ for a baseline of $L = 295$ km and $E_\nu = 1$ GeV.

The deformed probability depends on two parameters: the radius R of the extra dimension and the mass of lightest neutrino m_0 through the dimensionless perturbative parameter ξ , defined as ¹

$$\xi_j \equiv \sqrt{2} R m_j, \quad j = 1, 2, 3. \quad (4.11)$$

In the case of reactor experiments, the above-mentioned procedure allows to calculate the LED contribution to the total amplitude $\mathcal{A}(\nu_\alpha \rightarrow \nu_\beta) = \mathcal{A}_{\text{SM}}(\nu_\alpha \rightarrow \nu_\beta) + \delta \mathcal{A}_{\text{LED}}(\nu_\alpha \rightarrow \nu_\beta)$ as discussed in [184]

$$\begin{aligned} \delta \mathcal{A}_{\text{LED}}(\bar{\nu}_e \rightarrow \bar{\nu}_e) &\simeq \xi_1^2 |U_{e1}|^2 + \xi_2^2 |U_{e2}|^2 + \xi_3^2 |U_{e3}|^2 \simeq \\ &\simeq \xi_1^2 \cos^2 \theta_{12} \cos^2 \theta_{13} + \xi_2^2 \cos^2 \theta_{13} \sin^2 \theta_{12} + \xi_3^2 \sin^2 \theta_{13}. \end{aligned} \quad (4.12)$$

In the NO case ($m_3 > m_2 > m_1 = m_0$), $\delta \mathcal{A}_{\text{LED}}(\bar{\nu}_e \rightarrow \bar{\nu}_e)$ is dominated by the last term, in fact $\xi_3^2 \propto m_3^2$, and thus suppressed by the small reactor angle θ_{13} . For the IO case

¹Notice that $m_j \equiv m_j^{(k=0)}$, which are the mass eigenstates that we observe in current experiments.

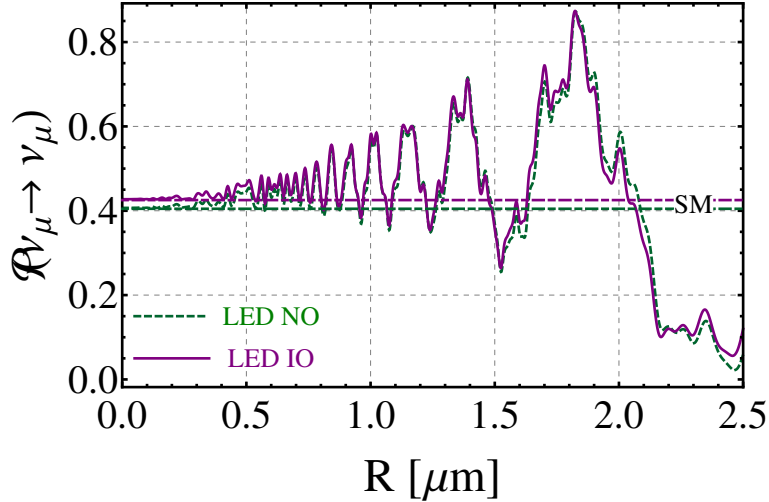


Figure 4.1: In this plot we show the limit $R \rightarrow 0$ for the LED oscillation probabilities assuming NO (dashed green) or IO (solid purple). These reproduce the SM probabilities for both mass ordering (small dashed lines). The LED probabilities are obtained for a baseline $L = 295$ km, $m_0 = 0$ eV and $E_\nu = 1$ GeV.

($m_2 > m_1 > m_3 = m_0$) the first two terms dominate the amplitude and no suppressing factor is at work; we then expect the IO scenario to give us better constraints on R and m_0 than the NO case. The situation is quite different for the $\nu_\mu \rightarrow \nu_\mu$ and $\nu_\mu \rightarrow \nu_e$ channels. Indeed for the disappearance channel we have

$$\begin{aligned} \delta\mathcal{A}_{\text{LED}}(\nu_\mu \rightarrow \nu_\mu) &\simeq \xi_1^2 |U_{\mu 1}|^2 + \xi_2^2 |U_{\mu 2}|^2 + \xi_3^2 |U_{\mu 3}|^2 \simeq \\ &\simeq \xi_1^2 \cos^2 \theta_{23} \sin^2 \theta_{12} + \xi_2^2 \cos^2 \theta_{12} \cos^2 \theta_{23} + \xi_3^2 \cos^2 \theta_{13} \sin^2 \theta_{23} + \\ &+ 2(\xi_1^2 - \xi_2^2) \cos \theta_{12} \cos \theta_{23} \sin \theta_{12} \sin \theta_{13} \sin \theta_{23} \cos \delta + \mathcal{O}(\sin^2 \theta_{13}) \end{aligned} \quad (4.13)$$

and, due to the absence of the $\sin \theta_{13}$ suppression in the ξ_3^2 term, we do not expect a significant difference in sensitivity between NO and IO. This channel is also expected to give better constraints than the $\nu_\mu \rightarrow \nu_e$ appearance one; in fact, in this last case the amplitude reads

$$\begin{aligned} \delta\mathcal{A}_{\text{LED}}(\nu_\mu \rightarrow \nu_e) &\simeq \xi_1^2 U_{e1} U_{\mu 1}^* + \xi_2^2 U_{e2} U_{\mu 2}^* + \xi_3^2 U_{e3} U_{\mu 3}^* \simeq \\ &\simeq (\xi_2^2 - \xi_1^2) \cos \theta_{12} \sin \theta_{12} \cos \theta_{13} \cos \theta_{23} + \xi_3^2 \sin \theta_{13} \cos \theta_{13} \sin \theta_{23} e^{-i\delta} + \\ &- \sin \theta_{13} \sin \theta_{23} \cos \theta_{13} e^{-i\delta} (\xi_1^2 \cos^2 \theta_{12} + \xi_2^2 \sin^2 \theta_{12}) \end{aligned} \quad (4.14)$$

and every term is suppressed by either $\xi_2^2 - \xi_1^2 \propto \Delta m_{21}^2$ or $\sin \theta_{13}$.

The global effects are reported in Fig. 4.2 for the channels $\bar{\nu}_e \rightarrow \bar{\nu}_e$ and $\nu_\mu \rightarrow \nu_e$ as a function of the neutrino energy. In our numerical study we used only the first five KK resonances since the effects for more particles is meaningless.

4.1.2 Non Standard Interactions

In this Section we want to describe a model of interaction for neutrino in the low energy regime called NSI which can describe NP effects in a model independent way. The importance of NSI in the context of neutrino oscillations has pointed out in [185] and there exists a large literature about this topic, see Ref. [186] for a recent review. We follow the conventions of Ref. [187] (see also Refs. [173,174] for a similar analysis).

If we consider only lepton number conserving operators, $\Delta L = 0$, the most general NSI

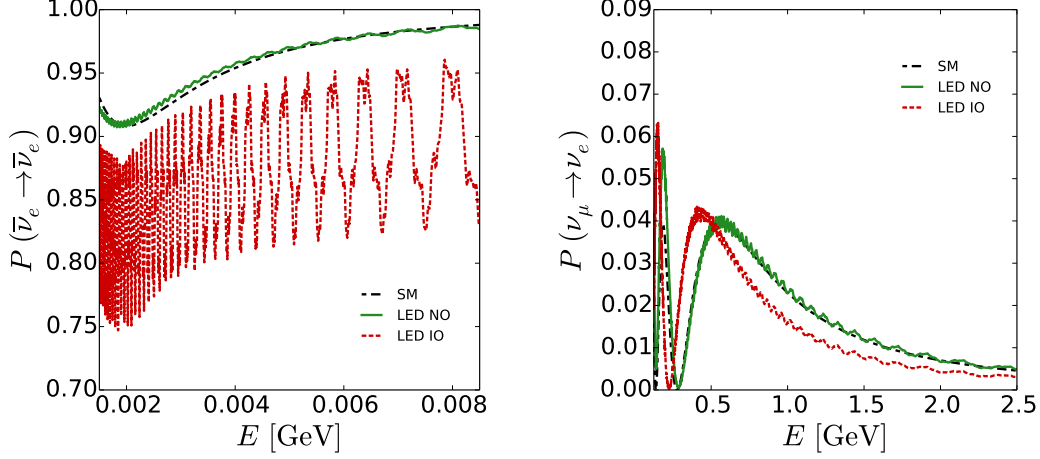


Figure 4.2: Probability of oscillation as a function of the neutrino energy in the channel $\bar{\nu}_e \rightarrow \bar{\nu}_e$ at $L = 1$ km (left) or $\nu_\mu \rightarrow \nu_e$ at $L = 275$ km (right) using the LED probabilities. These are obtained fixing $m_0 = 0$ eV, $R = 0.5$ μm , $\delta = 0$, $\sin^2 2\theta_{13} = 0.09$, $\sin^2 \theta_{12} = 3.08 \times 10^{-2}$ and $\Delta m_{21}^2 = 7.54 \times 10^{-5}$ eV². For NO we use $\Delta m_{31}^2 = 2.5 \times 10^{-3}$ eV² and $\sin^2 \theta_{23} = 4.37 \times 10^{-2}$, while for IO $\Delta m_{31}^2 = -2.3 \times 10^{-3}$ eV² and $\sin^2 \theta_{23} = 4.55 \times 10^{-2}$.

effective lagrangian reads

$$\mathcal{L}_{\text{NSI}}^{\text{eff}} = \mathcal{L}_{V\pm A} + \mathcal{L}_{S\pm P} + \mathcal{L}_T \quad (4.15)$$

where the subscripts indicated the Lorentz structure of the operator

$$\begin{aligned} \mathcal{L}_{V\pm A} = & \frac{G_F}{\sqrt{2}} \sum_{\alpha,\beta} \sum_{f,f'} (\varepsilon_{V\pm A}^v)_{\alpha\beta}^{f,f'} \left[\bar{\nu}_\beta \gamma^\sigma (\mathbb{1} - \gamma_5) \ell_\alpha \right] \left[\bar{f}' \gamma_\sigma (\mathbb{1} \pm \gamma_5) f \right] + \\ & + \frac{G_F}{\sqrt{2}} \sum_{\alpha,\beta} \sum_{f,f'} (\varepsilon_{V\pm A}^m)_{\alpha\beta}^f \left[\bar{\nu}_\beta \gamma^\sigma (\mathbb{1} - \gamma_5) \ell_\alpha \right] \left[\bar{f} \gamma_\sigma (\mathbb{1} \pm \gamma_5) f \right] \end{aligned} \quad (4.16a)$$

$$\mathcal{L}_{S\pm P} = \frac{G_F}{\sqrt{2}} \sum_{\alpha,\beta} \sum_{f,f'} (\varepsilon_{S\pm P}^v)_{\alpha\beta}^{f,f'} \left[\bar{\nu}_\beta (\mathbb{1} - \gamma_5) \ell_\alpha \right] \left[\bar{f}' (\mathbb{1} \mp \gamma_5) f \right] \quad (4.16b)$$

$$\mathcal{L}_T = \frac{G_F}{\sqrt{2}} \sum_{\alpha,\beta} \sum_{f,f'} (\varepsilon_T^v)_{\alpha\beta}^{f,f'} \left[\bar{\nu}_\beta \sigma^{\rho\tau} \ell_\alpha \right] \left[\bar{f}' \sigma_{\rho\tau} f \right]. \quad (4.16c)$$

Here α is the index of generations, $\alpha = \{e, \mu, \tau\}$ and f, f' are the component of an arbitrary weak doublet which is a partner of the neutrinos. In the tensor operator $\sigma_{\rho\tau} = i[\gamma_\rho, \gamma_\tau]/2$. The dimensionless tensor ε in flavour space gives the strength of non-standard interaction relative to G_F , the Fermi constant. The superscript v stands for vacuum effects and m for matter effects. We expect that these effects are suppressed as

$$|\varepsilon| \sim \frac{m_W^2}{m_{\text{NSI}}^2} \quad (4.17)$$

where m_{NSI} is the typical mass of New Physics, $m_{\text{NSI}} \lesssim \Lambda$ and Λ is the UV cutoff scale. Since there are many free parameters to constraint, we can use several arguments in order to reduce their number [187]:

1. In experiments for neutrino oscillations in vacuum we can set $f, f' = u, d$, therefore we can write $(\varepsilon^v)_{\alpha\beta}^{ff'} = (\varepsilon^v)_{\alpha\beta}$ without loss of generality. The same consideration holds for matter oscillations, so that $(\varepsilon^m)_{\alpha\beta}^{ff'} = (\varepsilon^m)_{\alpha\beta}$.

2. For the non-standard matter effects only couplings to electrons, up and down quarks are important.
3. The lepton τ in detector beam source can be neglected because τ production is almost impossible in reactor and beam experiments, thus $(\varepsilon_{V\pm A}^v)_{\tau\beta} = (\varepsilon_{S\pm P}^v)_{\tau\beta} = (\varepsilon_T^v)_{\tau\beta} = 0$ for all $\beta = \{e, \mu, \tau\}$. For the same reason we can neglect muons in reactor experiments and electrons in superbeam since they are the subdominant background.
4. In muon interaction there is still room for non $(V - A)(V - A)$ interactions [188].
5. Tensor interactions are forbidden in pion decay because the operator must have a parity odd in the interaction.
6. In the detection processes involving muons the $(S + P)(S \pm P)$ and TT interactions are suppressed by a factor $m_\mu/E_\nu = \mathcal{O}(10^{-3})$ for neutrino energy of $\mathcal{O}(1)$ GeV. We also neglect possible interference effects that can strongly modify the oscillation amplitude.
7. Interaction of the type $(V - A)(V + A)$ may in general be important in cross sections, so we cannot neglect them.
8. The measurements of angular distribution in nuclear β decay strongly constrained the TT and $(S + P)(S \pm P)$ operators, thus we can set $(\varepsilon_{S\pm P}^v)_{e\beta} = (\varepsilon_T^v)_{e\beta} = 0$ for all $\beta = \{e, \mu, \tau\}$.
9. In electron interactions there is still room for $(V - A)(V + A)$ operators with electrons because these terms are chirally suppressed, thus the coefficient could be large. It is possible to obtain bounds on the effective axial and vector couplings using proton and neutron data, but due to the fact of non perturbative nature of low energy QCD these are strongly model dependent, see Ref. [189].

Using these arguments we can write a more compact expression for the oscillation probability in vacuum because we consider only interactions with $(V - A)(V \pm A)$ Lorentz structure. Therefore in our analysis effects of NSI can appear at low energy through vacuum couplings, defined as $\varepsilon_{\alpha\beta}^v \equiv \varepsilon_{\alpha\beta} = |\varepsilon_{\alpha\beta}| \exp i\phi_{\alpha\beta}$.

Notice that these new couplings can affect neutrino production and detection [10,190,191], so the neutrino at production s and detection d states are a superposition of the orthonormal flavour eigenstates $|\nu_\alpha\rangle$, see for instance Refs. [186,192,193]. We have

$$|\nu_\alpha^s\rangle = |\nu_\alpha\rangle + \sum_{\beta=e,\mu,\tau} \varepsilon_{\alpha\beta}^s |\nu_\beta\rangle = \left[(1 + \varepsilon^s) |\nu\rangle \right]_\alpha \quad (4.18a)$$

$$\langle \nu_\beta^d | = \langle \nu_\beta | + \sum_{\alpha=e,\mu,\tau} \varepsilon_{\alpha\beta}^d \langle \nu_\alpha | = \left[\langle \nu | (1 + \varepsilon^d) \right]_\beta. \quad (4.18b)$$

The oscillation probability can be obtained by squaring the amplitude $\langle \nu_\beta^d | e^{-iHL} | \nu_\alpha^s \rangle$, where H is the hamiltonian in the mass eigenstates basis:

$$\mathcal{P}(\nu_\alpha^s \rightarrow \nu_\beta^d) = |\langle \nu_\beta^d | e^{-iHL} | \nu_\alpha^s \rangle|^2 = \left| (1 + \varepsilon^d)_{\gamma\beta} (e^{-iHL})_{\gamma\delta} (1 + \varepsilon^s)_{\alpha\delta} \right|^2. \quad (4.19)$$

We can obtain a numerical expression for the probability but is more useful to introduce a perturbative formalism to understand the dependence of NP on the parameters. All those expressions are reported in Appendix H. Notice that the states $|\nu_\alpha^s\rangle$ and $\langle \nu_\beta^d |$, in general, do not form a complete set of states, so the norm is not automatically set to one

$$\sum_\alpha |\nu_\alpha^s\rangle \langle \nu_\alpha^s| \neq \mathbb{1} \quad \langle \nu_\alpha^s | \nu_\beta^s \rangle \neq \delta_{\alpha\beta} \quad \sum_\beta |\nu_\beta^d\rangle \langle \nu_\beta^d| \neq \mathbb{1} \quad \langle \nu_\alpha^d | \nu_\beta^d \rangle \neq \delta_{\alpha\beta}. \quad (4.20)$$

This implies effects which occur when $L = 0$, they are the so-called *zero distance effects*. In this way the disappearance channel may have large deviations with respect to the SM prediction.

For $\varepsilon_{\alpha\beta}$ there exist model independent bounds, derived in Ref. [194], which at 90% CL read

$$|\varepsilon_{ee}| < 0.041, \quad |\varepsilon_{e\mu}| < 0.025, \quad |\varepsilon_{e\tau}| < 0.041, \quad |\varepsilon_{\mu e}^{s,d}| < 0.026, \quad |\varepsilon_{\mu\mu}^{s,d}| < 0.078, \quad |\varepsilon_{\mu\tau}^{s,d}| < 0.013. \quad (4.21)$$

For a more recent review on the NSI bounds see for instance Ref. [195]. In Fig. 4.3 we show the $\mathcal{P}(\bar{\nu}_e \rightarrow \bar{\nu}_e)$ and $\mathcal{P}(\nu_\mu \rightarrow \nu_\mu)$ oscillation probabilities. The effect of NSI is shown for a particular choice of the parameters.

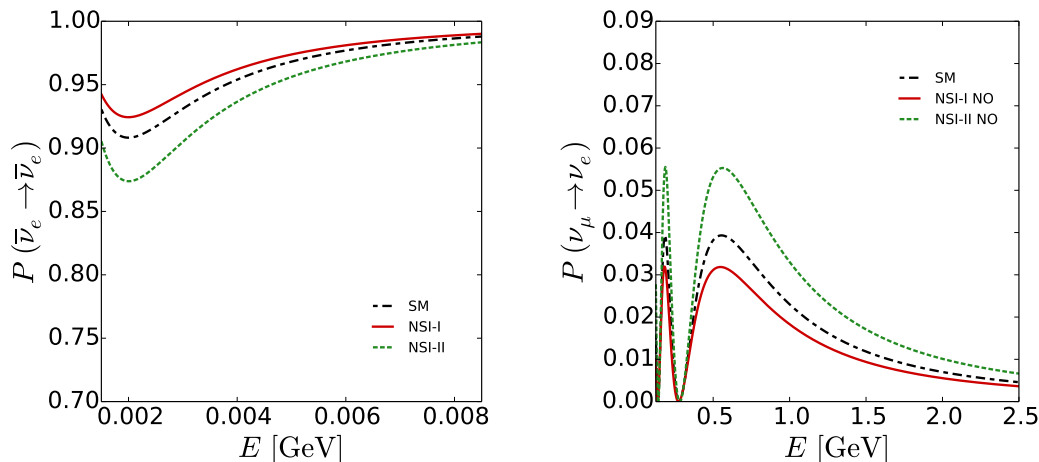


Figure 4.3: Probability of oscillation as a function of the neutrino energy in the channel $\bar{\nu}_e \rightarrow \bar{\nu}_e$ at $L = 1$ km (left) or $\nu_\mu \rightarrow \nu_\mu$ at $L = 275$ km (right) assuming NSI probabilities obtained fixing $\delta = 0$, the mixing angles $\sin^2 2\theta_{13} = 0.09$, $\sin^2 \theta_{12} = 3.08 \times 10^{-2}$ and $\sin^2 \theta_{23} = 4.37 \times 10^{-2}$. The mass splittings are $\Delta m_{21}^2 = 7.54 \times 10^{-5}$ eV², $\Delta m_{31}^2 = 2.5 \times 10^{-3}$ eV². For NSI-I we fixed $\varepsilon_{\mu e}^s = \varepsilon_{e\mu} = \varepsilon_{e\tau} = 10^{-2}$ and all the phases are zero, while in the case NSI-II $\varepsilon_{e\tau} = 4 \times 10^{-2}$ and $\phi_{e\tau} = 0$.

4.2 Statistical Analysis

In this Section we want to summarize the main features of the T2K and Daya Bay experiments and the statistical procedure that we use in our study. We analyze the data using a modified version of the software GLOBES, see Refs. [196,197] as well as the documentation at the following URL: <https://www.mpi-hd.mpg.de/personalhomes/globes/index.html>. The software is designed to simulate the oscillation experiments taking into account all the systematics and uncertainties.

4.2.1 T2K Experiment

T2K (Tokai to Kamioka) is a long-baseline neutrino experiment in Japan, and is studying neutrino oscillations. The T2K experiment sends an intense beam of muon neutrinos from Tokai, which is on the east coast of Japan, to Kamioka at a distance of $L_{SK} = 295$ km in western Japan. The neutrino beam is made in collisions between a proton beam and a graphite target; these collisions produce pions, which decay to muon neutrinos².

²Technical details are available at <http://t2k-experiment.org/t2k/>

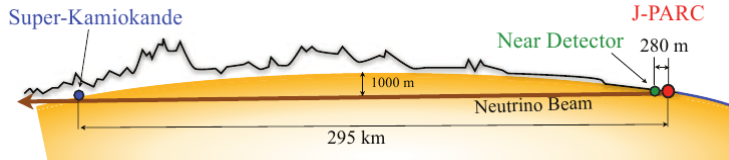


Figure 4.4: Schematic layout of T2K experiment.

T2K studies neutrino oscillations with two separate detectors, both of which are 2.5 degrees away from the centre of the neutrino beam. The ND280 near detector is $L_{\text{ND280}} = 280$ metres from the target, and measures the number of muon neutrinos in the beam before any oscillations occur. The off-axis configuration allows to obtain an almost monochromatic neutrino energy by the relation ³

$$E_\nu = \frac{m_\pi^2 - m_\mu^2}{2(E_\pi - p_\pi \cos \theta)} \simeq 0.68 \text{ GeV} \quad (4.22)$$

where θ is the angle respect to the neutrino beam, and the numerical value is the energy peak, at $p_\pi = m_\pi \cot \theta$. In the left panel of Fig. 4.5 we report the neutrino energy E_ν as a function of the pion momentum p_π for different axis configuration.

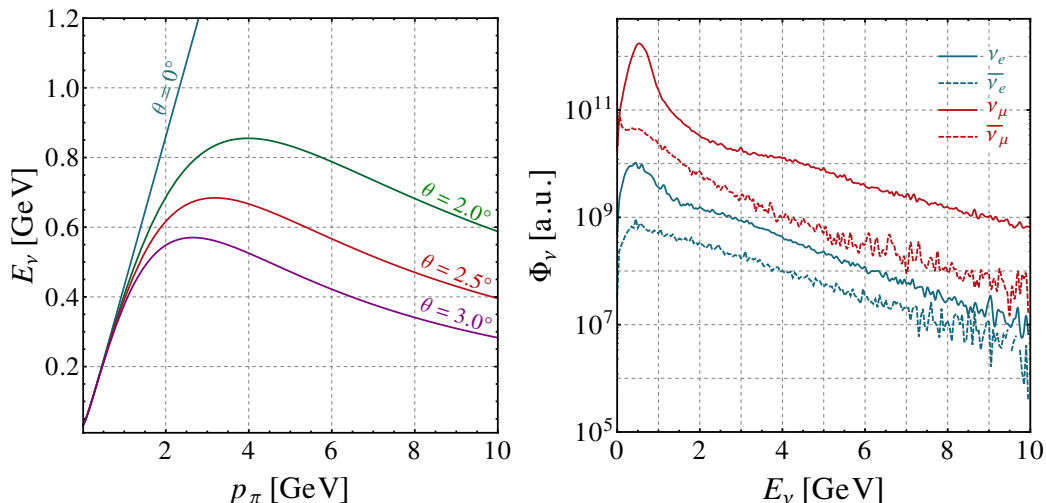


Figure 4.5: (Left) Energy of neutrino products by pion decay as a function of pion momentum. Are reported several angles, in red the off-axis configuration at T2K. (Right) Flux of T2K experiment as a function of neutrino energy for various flavour for Run I+II, data taken from [198].

For the analysis we used the public data for the disappearance channel [34], for the appearance ones [35] at the far detector and the data collected at the near detector [198]. During Run I-IV in disappearance Super-Kamiokande (SK) has 120 events and 28 in appearance, see Ref. [34,35] while the ND280 has collected 17369 events of CCQE with zero pions in the final state [198]. Important parameters of the experiment are the fiducial mass of near and far detectors. We have ⁴

$$FM_{\text{ND280}} = 1529 \text{ kg} \quad FM_{\text{SK}} = 22.5 \text{ kton}. \quad (4.23)$$

The measured event rates at the near detector have been estimated rescaling the non oscillated measured event rates at the far detector using the scale factor $L_{\text{SK}}^2/L_{\text{ND280}}^2 \times$

³The neutrinos are mainly produced from pions and kaon decay. In the off-axis configuration the pions are the most relevant contribution.

⁴Private communication, see Ref. [199].

$FM_{\text{ND280}}/FM_{\text{SK}}$, *i.e.* we use Gauss theorem for the flux of the experiment, constrained with the 17369 observed events. The neutrino flux has been estimated from Ref. [198], see the right panel in Fig. 4.5. ⁵ We normalize all the events with a bin-to-bin normalization constant, N_j^d , extracted using the T2K best fit for each channel. The energy bin pre-smearing is performed assuming a resolution function of gaussian form

$$R(E_\nu, E'_\nu) = \frac{1}{\sigma_E \sqrt{2\pi}} \exp \left[-\frac{(E_\nu - E'_\nu)^2}{2\sigma_E^2} \right] \quad (4.24)$$

where E'_ν is the energy after the smearing processes. The energy resolution is assumed to be [200]

$$\frac{\sigma_E}{E_\nu} = \frac{0.085 \text{ GeV}}{E_\nu}. \quad (4.25)$$

This value is based on the programmatic report of T2K [201]. In our simulation we see that this values does not influence the analysis since the main contribution comes from the normalization of each bin N_j^d , extracted from the best fit. Besides other functional dependences for σ_E give us consistent results. The post-smearing efficiency is evaluated in the same way.

All these effects are subleading because of low statistics, but can be important when we combine the analysis of T2K with other experiments, as for example the reactor Daya Bay experiment.

We have simulated the systematics of the experiment, which are summarized in the upper panel of Tab. 4.3. All the σ 's are the standard deviations of the systematic parameters, which are expressed as gaussians with zero means. The parameter σ_{ρ_c} contains the systematics uncertainties in the c -th channel, corresponds to $(\sigma_{\rho_1}, \sigma_{\rho_2}) = (8.8\%, 8.1\%)$, which values extracted from Table II of Ref. [35] and Table I of Ref. [34], σ_{Ω_d} is the fiducial mass uncertainty for the d -th detector (σ_{Ω_d} and σ_{Ω_N} have been estimated to be of the order of 1% for the far and the near detectors similarly to [202]), α_d and α_N are free parameters which represent the energy scale for predicted signal events with uncertainty σ_{α_d} and σ_{α_N} , ($\sigma_{\alpha_d}, \sigma_{\alpha_N} = 1\%$ [203]).

4.2.2 Daya Bay Experiment

The Daya Bay (DB) Reactor Neutrino Experiment is a China-based multinational particle physics project studying neutrinos. It is situated at Daya Bay, approximately 52 kilometers northeast of Hong Kong and 45 kilometers east of Shenzhen. At present time the experiment consists of eight Antineutrino Detectors (AD), clustered in three locations within 1.9 km of six nuclear reactors. Each detector consists of 20 ton of liquid scintillator (linear alkylbenzene doped with gadolinium) surrounded by photomultiplier tubes and shielding. ⁶

The Daya Bay experimental setup that we take into account consists of six reactors [40], emitting $\bar{\nu}_e$. The flux of arriving $\bar{\nu}_e$ has contributions from the isotopes ^{235}U , ^{238}U , ^{239}Pu , and ^{241}Pu , with weights reported in Tab. 4.1, whose spectra have been recently estimated in Refs. [205, 206].

The total flux of arriving $\bar{\nu}_e$ at the six ADs has been estimated using the convenient parametrization discussed in Ref. [205] and taking into account all the distances between

⁵Available at <http://t2k-experiment.org/results/nd280data-numu-cc-inc-xs-on-c-2013>

⁶Further details can be found at <http://dayabay.ihep.ac.cn/twiki/bin/view/Public/>

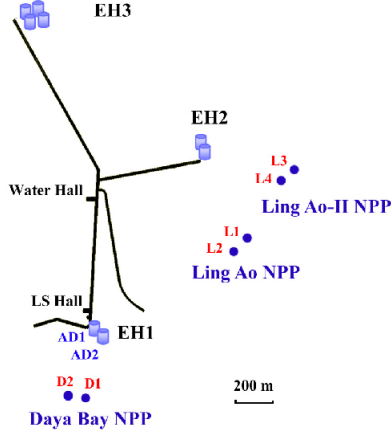


Figure 4.6: Schematic layout of DB experiment, from Ref. [204].

	^{235}U	^{238}U	^{239}Pu	^{241}Pu
AD1	63.3	12.2	19.5	4.8
AD2	63.3	12.2	19.5	4.8
AD3	61.0	12.5	21.5	4.9
AD4	61.5	12.4	21.5	4.9
AD5	61.5	12.4	21.5	4.9
AD6	61.5	12.4	21.5	4.9

Table 4.1: Ratio of $\bar{\nu}_e$ from isotope in percentage. See the presentation at NuFact 2013 by S. Jetter (link).

the detectors and the reactors, see Tab. 4.2. For this analysis we use the data set accumulated during 217 days extracted from Fig. 2 of Ref. [207]. The antineutrino energy E_ν is reconstructed by the prompt energy deposited by the positron E_{prompt} using the approximated relation [40] $E_\nu \simeq E_{\text{prompt}} + 0.8 \text{ MeV}$. The energy resolution function is a Gaussian function, as discussed in the case of the T2K experiment, see (4.24), parametrized according to

$$\sigma_E = \begin{cases} \gamma \sqrt{E_\nu / \text{MeV} - 0.8} & E_\nu > 1.8 \text{ MeV} \\ \gamma & E_\nu \leq 1.8 \text{ MeV} \end{cases} \quad (4.26)$$

with $\gamma = 0.08 \text{ MeV}$. The cross section for the inverse beta decay (IBD) $\bar{\nu}_e + p \rightarrow e^+ + n$ process has been taken from Ref. [208].

We use the following systematics, see Tab. 4.3 for a summary. The parameter σ_ε is the reactor flux uncertainty ($\sigma_\varepsilon \simeq 3\%$), the parameter σ_d is the uncorrelated detection uncertainty ($\sigma_d = 0.2\%$) and σ_{B_d} is the background uncertainty of the d -th detector obtained using the information given in Ref. [207]: $\sigma_{B_1} = \sigma_{B_2} = 8.21$, $\sigma_{B_3} = 5.95$, $\sigma_{B_4} = \sigma_{B_5} = \sigma_{B_6} = 1.15$ and $\sigma_r = 0.8\%$ is the correlated reactor uncertainties. The corresponding pull parameters are $(\varepsilon, \varepsilon_d, \eta_d, \alpha_r)$. With this choice of nuisance parameters we are able to reproduce the 1σ , 2σ and 3σ confidence level results presented in Fig. 3 of Ref. [207] with high accuracy. The differences are at the level of few percent (see for instance Tab. I and Tab. II of Ref. [173] where this analysis was already performed).

	D1	D2	L1	L2	L3	L4
AD1	362	372	903	817	1354	1265
AD2	358	368	903	817	1354	1266
AD3	1332	1358	468	490	558	499
AD4	1920	1894	1533	1534	1551	1525
AD5	1918	1892	1535	1535	1555	1528
AD6	1925	1900	1539	1539	1556	1530

Table 4.2: Baselines from antineutrino detectors AD1-6 to reactors D1, D2, and L1-4 in meters, the data are summarised in Tab. 2 of Ref. [40].

4.2.3 Definition of $\Delta\chi^2$

We introduce the systematics in the signal through priors and we perform a minimization of these in the χ^2 using the software GLoBES [196,197]. Our analysis is performed by the so-called *pull method*, see Refs. [200,209]. We construct the total χ^2 as the sum of T2K, χ_{T2K}^2 , and DB, χ_{DB}^2 , contributions

$$\chi^2(\boldsymbol{\theta}) \equiv \min_{\boldsymbol{\rho}} [\chi_{\text{T2K}}^2(\boldsymbol{\theta}; \boldsymbol{\rho}) + \chi_{\text{DB}}^2(\boldsymbol{\theta}; \boldsymbol{\rho})] \quad (4.27)$$

where $\boldsymbol{\theta} = \{\sin^2 \theta_{13}, \sin^2 \theta_{23}, \delta, \Delta m_{31}^2\}$ is the vector of parameters that we want to estimate and $\boldsymbol{\rho}$ is the vector of the fifteen systematics considered in our analysis and discussed above. See Tab. 4.3 for a complete list. In the following O_j^d is the observed event in the j -th bin of detector d and T_j^d is the test event. The test events rate in each energy bin, of width ΔE_j , is calculated using GLoBES by the relation

$$T_j^d(\boldsymbol{\theta}, \boldsymbol{\rho}) = \frac{1}{N_j^d} \int_{\Delta E_j(\boldsymbol{\rho})} dE \Phi_{\nu_\alpha}(E) \mathcal{P}(\nu_\alpha \rightarrow \nu_\beta)(E; \boldsymbol{\theta}) \sigma_{\nu_\beta}(E) \epsilon(E) \quad (4.28)$$

where Φ_{ν_α} is the neutrino flux, $\mathcal{P}(\nu_\alpha \rightarrow \nu_\beta)$ the probability of oscillations, σ_{ν_β} the cross section of the processes and ϵ the detector efficiency. As discussed above N_j^d is the normalization, which is extracted from the best fit in the case of T2K, or from the unoscillated events in the case of Daya Bay. In the χ^2 the sum is performed over all c -th channel and d -th detectors.

The T2K χ^2 is given by a Poisson function [203]

$$\begin{aligned} \chi_{\text{T2K}}^2(\boldsymbol{\theta}; \boldsymbol{\rho}) = & \sum_{c=1}^2 \sum_{i=1}^{n_{bins}^c} 2 \left[O_i^c - T_j^c(\boldsymbol{\theta}, \boldsymbol{\rho}) \cdot (1 + \rho_c + \Omega_c) + O_i^c \log \frac{O_i^c}{T_j^c(\boldsymbol{\theta}, \boldsymbol{\rho}) \cdot (1 + \rho_c + \Omega_c)} \right] + \\ & + \sum_{i=1}^{n_{bins}^N} 2 \left[O_i^N - T_j^N(\boldsymbol{\theta}, \boldsymbol{\rho}) \cdot (1 + \rho_1 + \rho_2 + \Omega_N) + O_i^N \log \frac{O_i^N}{T_j^N(\boldsymbol{\theta}, \boldsymbol{\rho}) \cdot (1 + \rho_1 + \rho_2 + \Omega_N)} \right] + \\ & + \sum_{d=1}^2 \left(\frac{\rho_d^2}{\sigma_{\rho_d}^2} + \frac{\Omega_d^2}{\sigma_{\Omega_d}^2} \right) + \frac{\Omega_N^2}{\sigma_{\Omega_N}^2} + \text{Priors} \end{aligned} \quad (4.29)$$

where n_{bins}^c is the number of bins in c -th channel at SK, while n_{bins}^N at ND280.

The Daya Bay χ^2 is a gaussian function. Its definition can be found in Ref. [40]

$$\chi_{\text{DB}}^2(\boldsymbol{\theta}; \boldsymbol{\rho}) = \sum_{d=1}^6 \sum_{i=1}^{26} \frac{[O_i^d - T_i^d(\boldsymbol{\theta}, \boldsymbol{\rho}) \cdot (1 + \varepsilon + \sum_r \omega_r^d \alpha_r + \varepsilon_d) + \eta_d]^2}{O_i^d + B_i^d} + \frac{\varepsilon^2}{\sigma_\varepsilon^2} + \sum_r \frac{\alpha_r^2}{\sigma_r^2} +$$

Name	Pull	Error	Value	Reference
Appearance Systematic	ρ_1	σ_{ρ_1}	0.088	[35]
Disappearance Systematic	ρ_2	σ_{ρ_2}	0.081	[34]
Fiducial mass SK [†]	Ω_d	σ_{Ω_d}	0.01	[202]
Fiducial mass ND280 [†]	Ω_N	σ_{Ω_N}	0.01	[202]
Energy SK [†]	α_d	σ_{α_d}	0.01	[203]
Energy ND280 [†]	α_N	σ_{α_N}	0.01	[203]
Reactor Flux	ε	σ_ε	0.03	[207]
Uncorrelated Energy	ε_d	σ_d	0.02	[207]
Correlated Energy [◇]	α_r	σ_r	0.08	[207]
Background AD1	η_1	σ_{B_1}	8.21	[207]
Background AD2	η_2	σ_{B_2}	8.21	[207]
Background AD3	η_3	σ_{B_3}	5.95	[207]
Background AD4	η_4	σ_{B_4}	1.15	[207]
Background AD5	η_5	σ_{B_5}	1.15	[207]
Background AD6	η_6	σ_{B_6}	1.15	[207]

Table 4.3: Systematics uncertainties used in our simulation for T2K (upper panel) and DB (lower panel). The values taken from T2K collaboration are estimated for $\sin^2(2\theta_{13}) = 0.1$ by Monte Carlo simulation. The values with [†], instead, are considered in a conservative scenario. The value with [◇] is obtained at $E_\nu \sim 1$ MeV.

$$+ \sum_{d=1}^6 \left[\frac{\varepsilon_d^2}{\sigma_d^2} + \frac{\eta_d^2}{\sigma_{B_d}^2} \right] + \text{Priors} \quad (4.30)$$

where O_i^d are the measured IBD events of the d -th detector ADs in the i -th bin, B_i^d the corresponding background. The parameter ω_r^d is the fraction of IBD contribution of the r -th reactor to the d -th detector AD, determined by the approximated relation $\omega_r^d \sim L_{rd}^{-2}/(\sum_{r=1}^6 1/L_{rd}^2)$, where L_{rd} is the distance between the d -th detector and the r -th reactor which are reported in Tab. 4.2.

4.2.4 Priors

In our analysis we marginalized over the parameters not shown in the plots, unless explicitly stated. In particular we considered θ_{13} , θ_{23} , δ and Δm_{31}^2 as free parameters completely unconstrained; we used gaussian priors on the solar mixing angle and mass difference defined through the mean value and the 1σ error as follows: $\sin^2\theta_{12} = 0.306 \pm 20\%$ and $\Delta m_{21}^2 = (7.6 \pm 5\%) \times 10^{-5} \text{ eV}^2$, according to Ref. [110]. The software GLoBES searches for the parameters in the allowed 3σ range using a gaussian distribution. The same scan is performed for the nuisance parameters quoted in Tab. 4.4.

The NSI parameters are considered as free parameters constrained by the upper limits, Eq. (4.21), while in the case of LED we impose the additional constraint to be in the perturbative regime, *i.e.* $\xi_j < 0.2$ and R fulfils the condition (4.2).

4.3 Results

In this Section we want to summarize the main results of our procedure. In particular in Section 4.3.1 we discuss the analysis performed using the T2K \oplus Daya Bay data for the standard oscillation parameters assuming SM, LED or NSI oscillation probabilities. In the Sections 4.3.2 and 4.3.3, we discuss the bounds that we obtained for the NP scenarios.

4.3.1 Standard oscillation parameters

We show our results for SM oscillation probabilities in Fig. 4.7 after performing a combined fit to the Daya Bay [207] and T2K [34,35] data. We show the 1σ , 2σ , 3σ confidence regions of $\Delta\chi^2 \equiv \chi^2 - \chi_{\min}^2$ for 1 degree of freedom (dof) in the $(\delta, \sin^2\theta_{13})$, $(\delta, \sin^2\theta_{23})$, $(\sin^2\theta_{13}, \sin^2\theta_{23})$, $(\Delta m_{31}^2, \sin^2\theta_{23})$ and $(\Delta m_{31}^2, \sin^2 2\theta_{13})$ planes in the case of NO (IO) with dotted, dashed and solid lines (red, orange and yellow), respectively. We cut the χ^2 at 1 dof as done in Ref. [110] in order to easily compare our results.

The obtained best fit points are indicated with a circle for NO and with a cross for IO. The figures have been obtained using the standard oscillation probabilities relevant for the $\bar{\nu}_e \rightarrow \bar{\nu}_e$, $\nu_\mu \rightarrow \nu_e$ and $\nu_\mu \rightarrow \nu_\mu$ channels (these were computed using the software GLoBES) see Appendix A for the appropriate formulae.

The obtained best fit points and the 3σ confidence level regions are summarized in Tab. 4.4. The results that we obtained are in agreement with Ref. [110] and we observe that the recent hint for maximal CP violation in the leptonic sector, $\delta \simeq 3\pi/2$, is achieved mainly using the latest Daya Bay and T2K results, however due to the low statistics of the T2K experiment these results are very preliminary.

Notice that the definition $\Delta\chi^2$ that we use is based on Wilks' theorem, which is not applicable to discrete choices (such as NO vs IO, see for instance Ref. [210]) or to cyclic variables (such as the Dirac CP phase δ , see a detailed discussion in the global analysis of Ref. [48]). In the hierarchy tests, it has been observed that the above $\Delta\chi^2$ prescription is useful to investigate the statistical difference between normal or inverted ordering with good approximation [211]. For CP violation tests, the prescription appears to lead (in general) to more conservative bounds on δ , as compared with the results obtained from numerical experiments, see Refs. [212,213].

As it can be seen from Fig. 4.7 and in Tab. 4.4 the differences between the two mass ordering schemes is small and therefore the hierarchy cannot be established. We would like to remark that our results are in agreement with the ones obtained with a more sophisticated technique taking into account all the available data from neutrino oscillation experiments in [45,47,110], see also the analysis performed by the T2K Collaboration in Ref. [171].

Parameter	SM		LED		NSI	
	Best-fit	3σ range	Best-fit	3σ range	Best-fit	3σ range
$ \Delta m_{31}^2 /10^{-3}$ [eV ²]	$2.51^{+0.06}_{-0.06}$	2.34 – 2.69	$2.53^{+0.07}_{-0.05}$	2.37 – 2.73	$2.56^{+0.06}_{-0.09}$	2.31 – 2.74
	$2.54^{+0.06}_{-0.06}$	2.37 – 2.73	$2.54^{+0.07}_{-0.07}$	2.35 – 2.71	$2.56^{+0.09}_{-0.08}$	2.32 – 2.77
$\sin^2\theta_{23}/10^{-1}$	$5.3^{+0.4}_{-0.6}$	4.0 – 6.3	$5.3^{+0.4}_{-0.5}$	4.1 – 6.3	$5.2^{+0.6}_{-0.8}$	3.8 – 6.5
	$5.3^{+0.4}_{-0.5}$	4.1 – 6.2	$5.3^{+0.4}_{-0.5}$	4.1 – 6.3	$5.2^{+0.6}_{-0.8}$	3.9 – 6.5
$\sin^2\theta_{13}/10^{-2}$	$2.3^{+0.3}_{-0.2}$	1.6 – 3.0	$2.3^{+0.2}_{-0.4}$	1.4 – 3.0	$3.9^{+0.4}_{-2.6}$	0.7 – 5.1
	$2.4^{+0.2}_{-0.3}$	1.6 – 3.0	$2.2^{+0.1}_{-0.1}$	1.3 – 2.9	$3.8^{+0.5}_{-2.6}$	0.7 – 5.1
δ/π	$1.53^{+0.33}_{-0.37}$	-	$1.47^{+0.35}_{-0.31}$	-	$1.65^{+0.55}_{-0.78}$	-
	$1.48^{+0.36}_{-0.35}$	-	$1.59^{+0.30}_{-0.36}$	-	$1.35^{+0.75}_{-0.49}$	-

Table 4.4: Best fit ($\pm 1\sigma$) and 3σ errors of the standard parameters obtained in the fit of T2K \oplus Daya Bay data, using the SM, LED and NSI probabilities. If two values are given, the upper one corresponds to Normal Ordering and the lower one to Inverted Ordering.

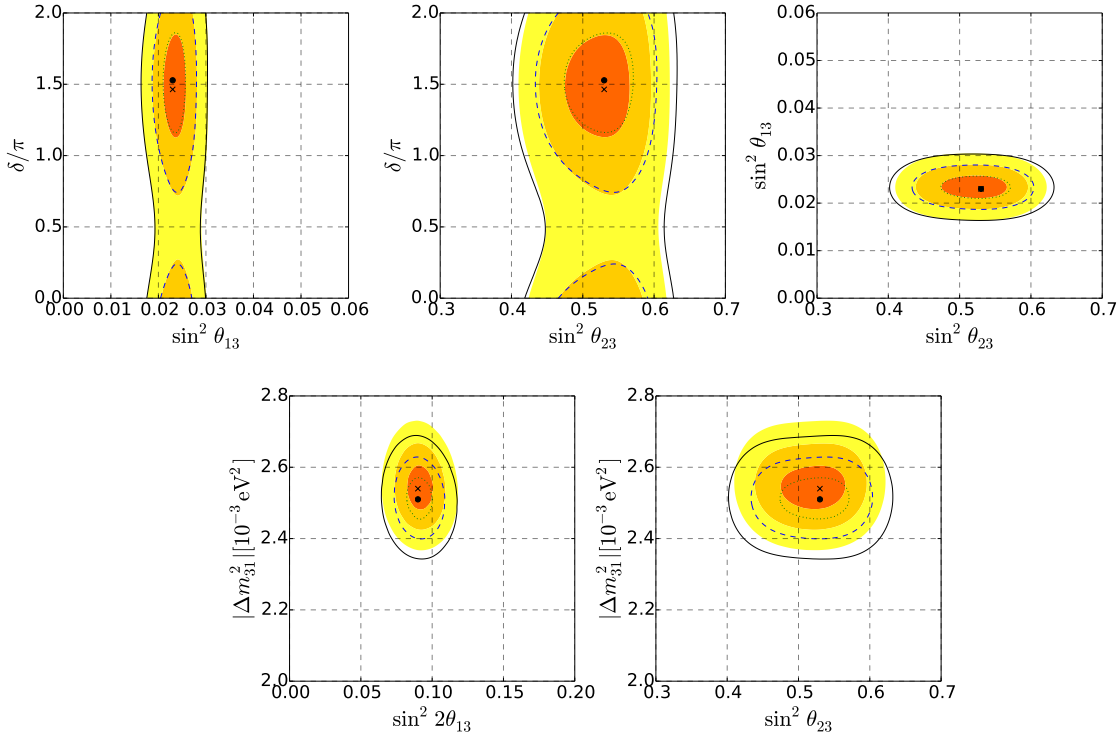


Figure 4.7: Best fit points and 1σ , 2σ and 3σ confidence region obtained from the T2K and Daya Bay data using the SM oscillation probabilities in the planes $(\delta, \sin^2 \theta_{13})$, $(\delta, \sin^2 \theta_{23})$ and $(\sin^2 \theta_{13}, \sin^2 \theta_{23})$ (upper panel), $(\Delta m_{31}^2, \sin^2 2\theta_{13})$ and $(\Delta m_{31}^2, \sin^2 \theta_{23})$ (lower panel) in the case of NO (IO) with dotted, dashed and solid lines (red, orange and yellow), respectively. The best fit point is marked with a circle for NO and a cross for IO.

We show our results in Fig. 4.8 for LED and in Fig. 4.9 for NSI after performing a combined fit to the Daya Bay [207] and T2K [34,35] data. Fig. 4.8 and Fig. 4.9 have been obtained using the LED and the NSI oscillation probabilities relevant for the interesting channels, see Section 4.1.1 for LED and Section 4.1.2 for NSI. The obtained best fit points and confidence level regions at 3σ are summarized in Tab. 4.4 for both models.

We show the best fit points, a circle for NO and a cross for IO, and the 2σ , 3σ confidence regions for 1 degree of freedom (dof) in the $(\delta, \sin^2 \theta_{13})$, $(\delta, \sin^2 \theta_{23})$, $(\sin^2 \theta_{13}, \sin^2 \theta_{23})$, $(\Delta m_{31}^2, \sin^2 \theta_{23})$ and $(\Delta m_{31}^2, \sin^2 2\theta_{13})$ planes assuming NO (IO) with dashed and solid lines (orange and yellow), respectively.

We do not show the 1σ confidence regions due to the low sensitivity in the NSI case to the CP violation phase as it can be understood from the one dimensional projections of the $\Delta\chi^2 = \chi^2 - \chi_{\min}^2$ function, shown in Fig 4.10 for NO and in Fig. 4.11 for IO.

The presence of LED parameters in the oscillation formulae does not affect too much the shape of the contours, see Fig. 4.7 and Fig. 4.8, as well as Tab. 4.4; in this respect, the importance of including the T2K data in our analysis is mainly visible in the determination of Δm_{31}^2 . In fact, in the analysis of the Daya Bay data only performed in Ref. [173], the 3σ confidence region for the atmospheric mass splitting was roughly 5% larger with respect to the SM determination, whereas in the present analysis this difference is reduced to roughly 1%. The reactor angle θ_{13} is strongly constrained from the Daya Bay data, see Ref. [173], and it is very close to the SM result as shown in the one dimensional projections of $\Delta\chi^2$ in Figs. 4.10 and 4.11.

In the NSI scenario the presence of the new complex couplings $\varepsilon_{\alpha\beta}$ enlarges the confi-

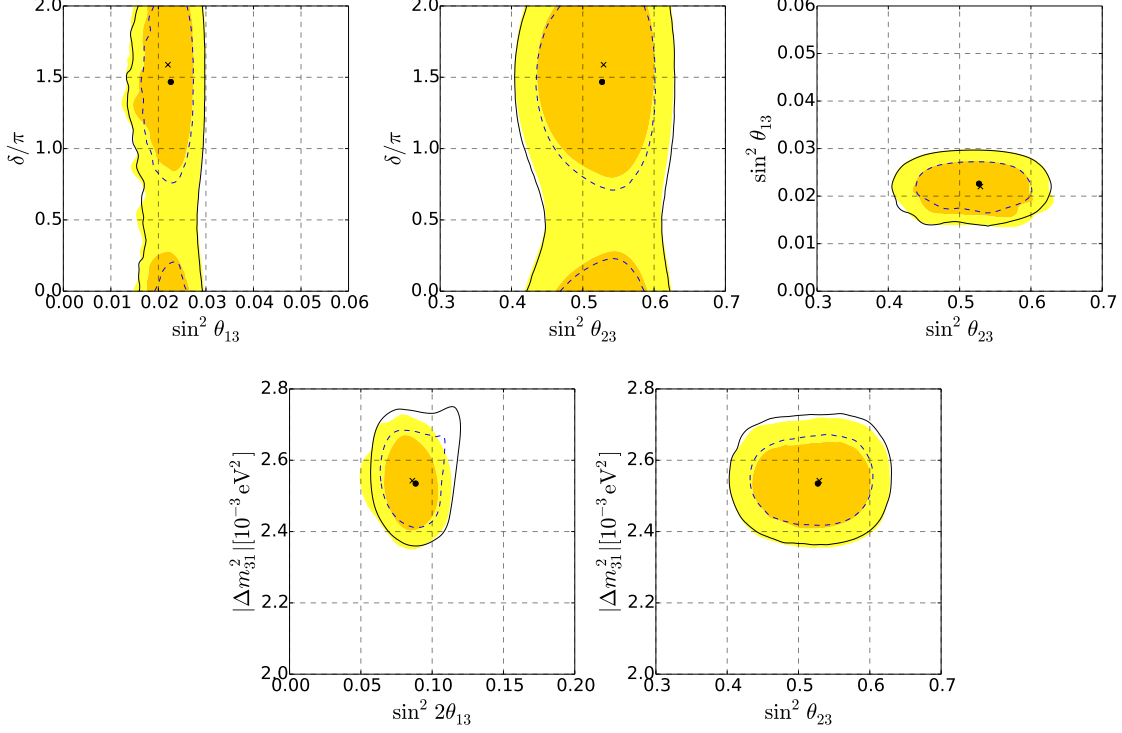


Figure 4.8: Same as Fig. 4.7 but using the LED oscillation probabilities.

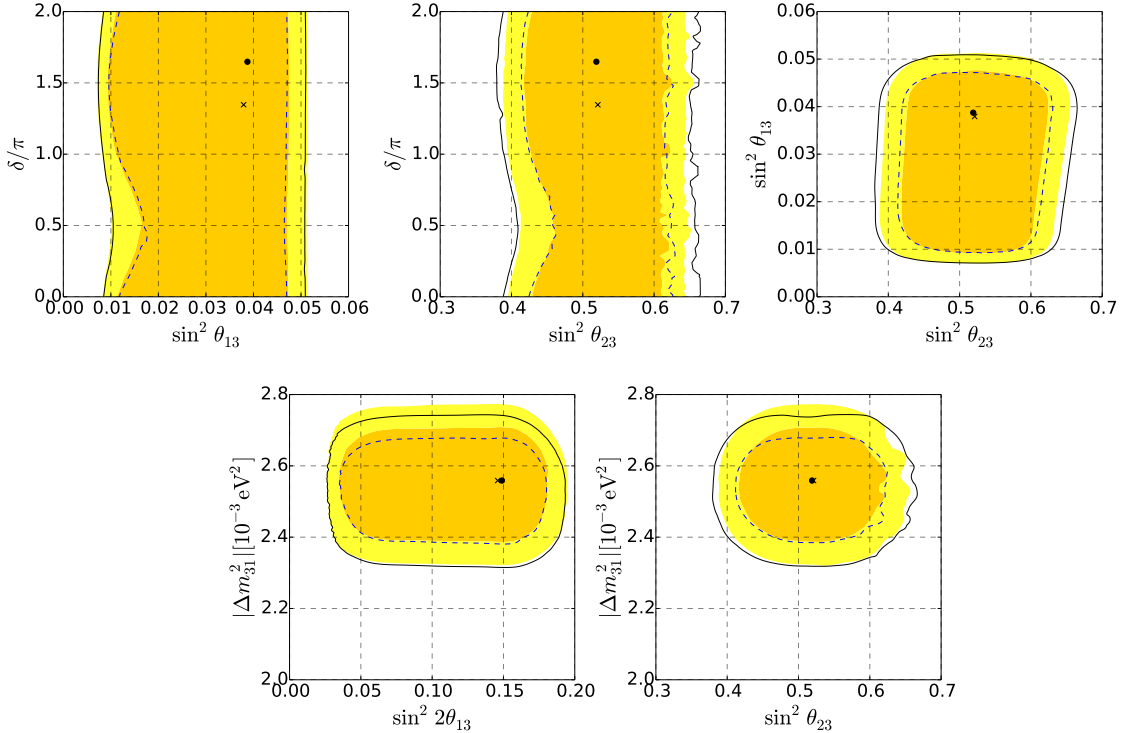


Figure 4.9: Same as Fig. 4.7 but using the NSI oscillation probabilities.

dence regions of the standard oscillation parameters and, in particular, reduces the hints for maximal CP violation since the whole $[0, 2\pi]$ range for the Dirac phase δ is allowed at 2σ confidence level, see the one dimensional projections in Figs. 4.10 and 4.11. This effect is caused by the new sources of the CP violation, encoded in the unconstrained

phases $\phi_{\alpha\beta}$ in the oscillation probabilities, see Appendix H for the relevant probabilities. A large effect is also found in the determination of the reactor angle θ_{13} . Indeed, in the NSI case, the 3σ confidence region of $\sin^2 \theta_{13}$ is roughly twice as large as in the SM case, as can be observed from Tab. 4.4. The main reason for such a behaviour is the strong correlation among the reactor angle and the NSI parameters: for large enough $\varepsilon_{\mu e}^s$ and/or $\varepsilon_{e\mu,\tau}$ (and an appropriate choice of the related CP phases), huge cancellations can occur with the standard part of the probability, thus causing an increase of the allowed θ_{13} ; the opposite can also happen: positive interferences can decrease the expected value of the reactor angle, see for instance Ref. [173].

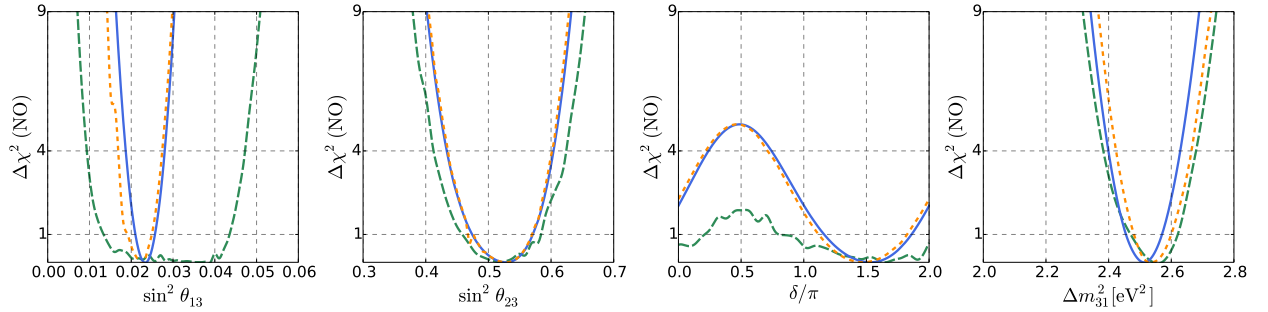


Figure 4.10: $\Delta\chi^2$ as a function of $\sin^2 \theta_{13}$ (left panel), $\sin^2 \theta_{23}$ (middle-left panel), δ (middle-right panel) and Δm_{31}^2 (right panel) using the SM (solid blue line), LED (small dashed orange line) and NSI (large dashed green line) oscillation probabilities assuming NO neutrino mass spectrum.

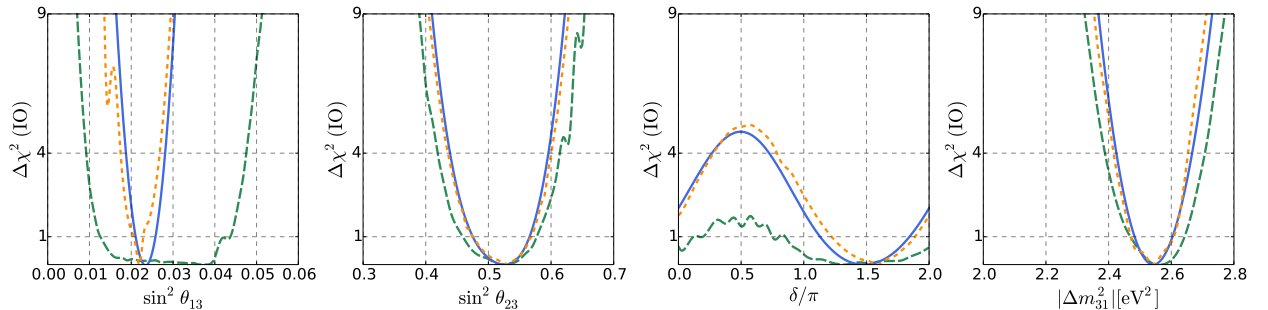


Figure 4.11: Same as Fig. 4.10, but assuming IO neutrino mass spectrum.

We can easily notice in the one dimensional projections, Figs. 4.10 and 4.11 that the atmospheric mixing angle θ_{23} is close to SM result for both models of NP. The same happens for the mass splitting Δm_{31}^2 .

4.3.2 LED fit

We consider the bounds on the size of the largest extra dimension R after performing a fit with the T2K data only or with a combined analysis of the T2K and the Daya Bay data, our results are shown in Fig. 4.12. The purple horizontal dashed line represent the expected sensitivity on the lightest neutrino mass from the KATRIN experiment [51]. In Fig. 4.12 we show the 2σ and 3σ exclusion limits with dashed and solid lines for NO and with orange and yellow regions for IO neutrino mass spectrum. The circles and the stars represent the 2σ bounds obtained using the IceCube IC-40 and IC-79 data set [214], respectively, from which we have the following constraints: $R \leq 0.54 \mu\text{m}$ ($R \leq 0.34 \mu\text{m}$)

using the IC-40 (IC-79) data set at 1 dof ⁷.

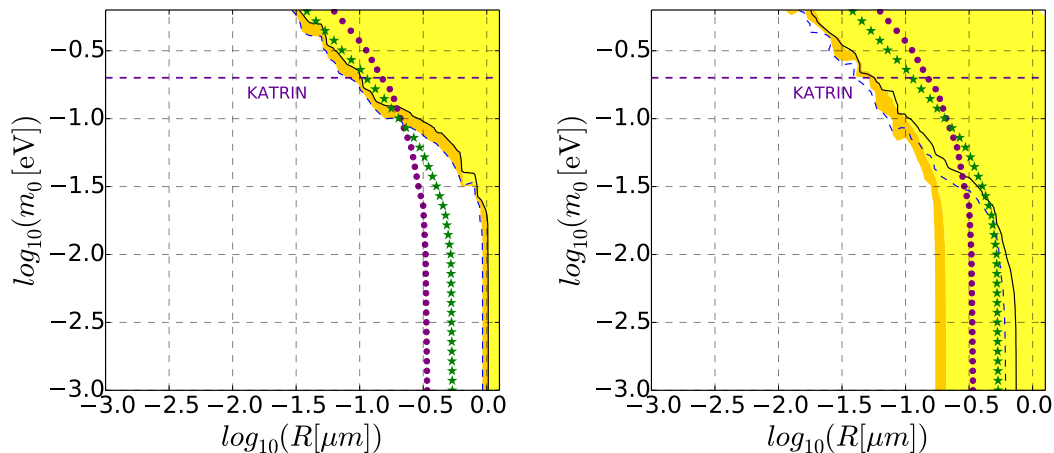


Figure 4.12: Exclusion regions at 2σ and 3σ confidence level for 1 dof with the dashed and solid lines for NO and with the orange and yellow regions for IO neutrino mass spectrum for the LED model in the $(\log_{10}(R), \log_{10}(m_0))$ -plane, where m_0 is the lightest neutrino mass and R the large extra dimension size, obtained fitting the data of T2K experiment (left panel) and the Daya Bay and the T2K experiments (right panel). The circles and the stars represent the 2σ bounds obtained using the IceCube IC-40 and IC-79 data set [214] at 1 dof, respectively.

In our analysis we obtain an upper bound on the size of the largest extra dimension R for T2K $R \leq 0.93 \mu\text{m}$ for normal and inverted ordering at 2σ CL and $R \leq 0.60 \mu\text{m}$ for NO and $R \leq 0.17 \mu\text{m}$ for IO at 2σ CL in the combined analysis. All these bounds are summarised in Tab. 4.5. We do not show the obtained best fit points for m_0 and R since the χ^2 is almost flat in the allowed region (white areas in Fig. 4.12), they are meaningless.

The T2K data we used in the analysis consist on 28 appearance events and 120 disappearance events, but the relevant constraint in T2K on the size of the largest extra dimension R comes mainly from the $\nu_\mu \rightarrow \nu_\mu$ channel, see (4.13) and the relative discussion, which is more sensitive. The combined analysis is dominated by the Daya Bay experiment, as expected due to the higher statistics, see (4.12) for $\bar{\nu}_e \rightarrow \bar{\nu}_e$ and (4.14) for $\nu_\mu \rightarrow \nu_e$.

	DB	T2K	T2K \oplus DB	IC-40	IC-79
Ref.	[173]	[172]	[172]	[214]	[214]
NO	0.57	0.93	0.60	0.54	0.34
IO	0.19	0.93	0.17	0.54	0.34

Table 4.5: Upper bounds on R in μm at 2σ using different datasets.

4.3.3 NSI fit

Finally we analyze the bounds on the new couplings $\varepsilon_{\alpha\beta}$ arising from the latest data of the T2K and the Daya Bay experiments. In Fig. 4.13 we show the 2σ and 3σ confidence regions for $\delta = 0$ for the zero distance terms in the $\nu_\mu \rightarrow \nu_\mu$ oscillation probability in

⁷We thank A. Esmaili, O. L. G. Peres and Z. Tabrizi for providing us the χ^2 function of their LED analysis with the IceCube data.

which the NSI parameters not shown in the plots are set to zero. The relevant parameters in $\mathcal{P}(\bar{\nu}_e \rightarrow \bar{\nu}_e)$ are discussed in Ref. [173] (see also Ref. [195] for a recent review). The results for other values of the CP violation phase δ are similar to the case $\delta = 0$ because these couplings enter as a constant shift of the neutrino flux, see Appendix H.

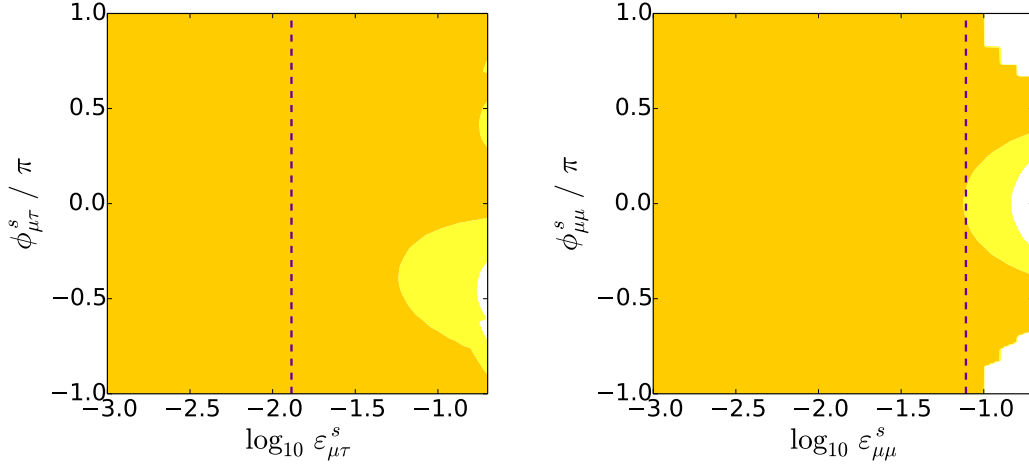


Figure 4.13: Allowed regions at 2σ and 3σ confidence level for 1 dof within the planes $(\varepsilon_{\mu\tau}^s, \phi_{\mu\tau}^s)$ (left panel) $(\varepsilon_{\mu\mu}^s, \phi_{\mu\mu}^s)$ (right panel). The dashed vertical lines are $\varepsilon_{\mu\tau}^s = 0.013$ and $\varepsilon_{\mu\mu}^s = 0.078$, see (4.21).

Similarly we show in Fig. 4.14 the confidence regions for the other NSI couplings but fixing $\delta = 0, \pi, 3\pi/2$ in the upper, middle and lower panels, respectively. As shown in Fig. 4.14 the confidence regions depend on the choice of δ because this parameter is not well defined at 1σ confidence level, as discussed above, see for instance Fig. 4.10 and 4.11 for the one dimensional projections of $\Delta\chi^2$. For this reason we have to show the results for fixed values of δ . The other parameters are marginalized over. Thus we can obtain a bound for the absolute values of $\varepsilon_{\alpha\beta}$ that are correlated to the values of the relative phases $\phi_{\alpha\beta}$, see Tab. 4.6.

$\phi_{e\mu}/\pi$	δ/π	Upper bound @ 2σ CL	$\phi_{\mu e}^s/\pi$	δ/π	Upper bound @ 2σ CL
0	0	4.85×10^{-3}	0	0	6.28×10^{-3}
1	1	9.94×10^{-3}	1	1	9.96×10^{-3}
-1/2	3/2	3.50×10^{-2}	1/2	3/2	3.12×10^{-2}

Table 4.6: Upper bounds on the parameter $\varepsilon_{e\mu}$ and $\varepsilon_{\mu e}^s$ at 2σ CL for particular choices of the phases $\phi_{e\mu}$ and $\phi_{\mu e}^s$ and δ , the values are obtained from Fig. 4.14.

For example at $\delta = 0$ in the range $\phi_{e\mu} \in [-1.41, 1.33]$ we have $\varepsilon_{e\mu} \leq 0.025$ at 3σ CL (the bound quoted in Ref. [194]), and for $\phi_{e\mu} = 0$ we obtain $\varepsilon_{e\mu} < 4.9 \times 10^{-3}$ at 3σ CL which are stronger bounds respect to what found in Ref. [194]. However, for maximal CP violation, $\delta = 3\pi/2$ we obtain a less stringent bound for the same parameter. The same analysis is possible for $\varepsilon_{e\tau}$ and $\varepsilon_{\mu e}^s$. For this last parameter we obtain in the region $\phi_{\mu e}^s \in [-1.17, 1.50]$ that $\varepsilon_{\mu e}^s \leq 0.026$ at 3σ CL (the bound quoted in Ref. [194]) and in particular for $\delta = 0$ and $\phi_{\mu e}^s = 0.20$ we have $\varepsilon_{\mu e}^s < 6.2 \times 10^{-3}$ at 3σ confidence level. Again the bound obtained for $\delta = 3\pi/2$ is less relevant compared to the analysis of Ref. [194]. See Tab. 4.6 for a summary of the bounds that we obtained for the NSI couplings.

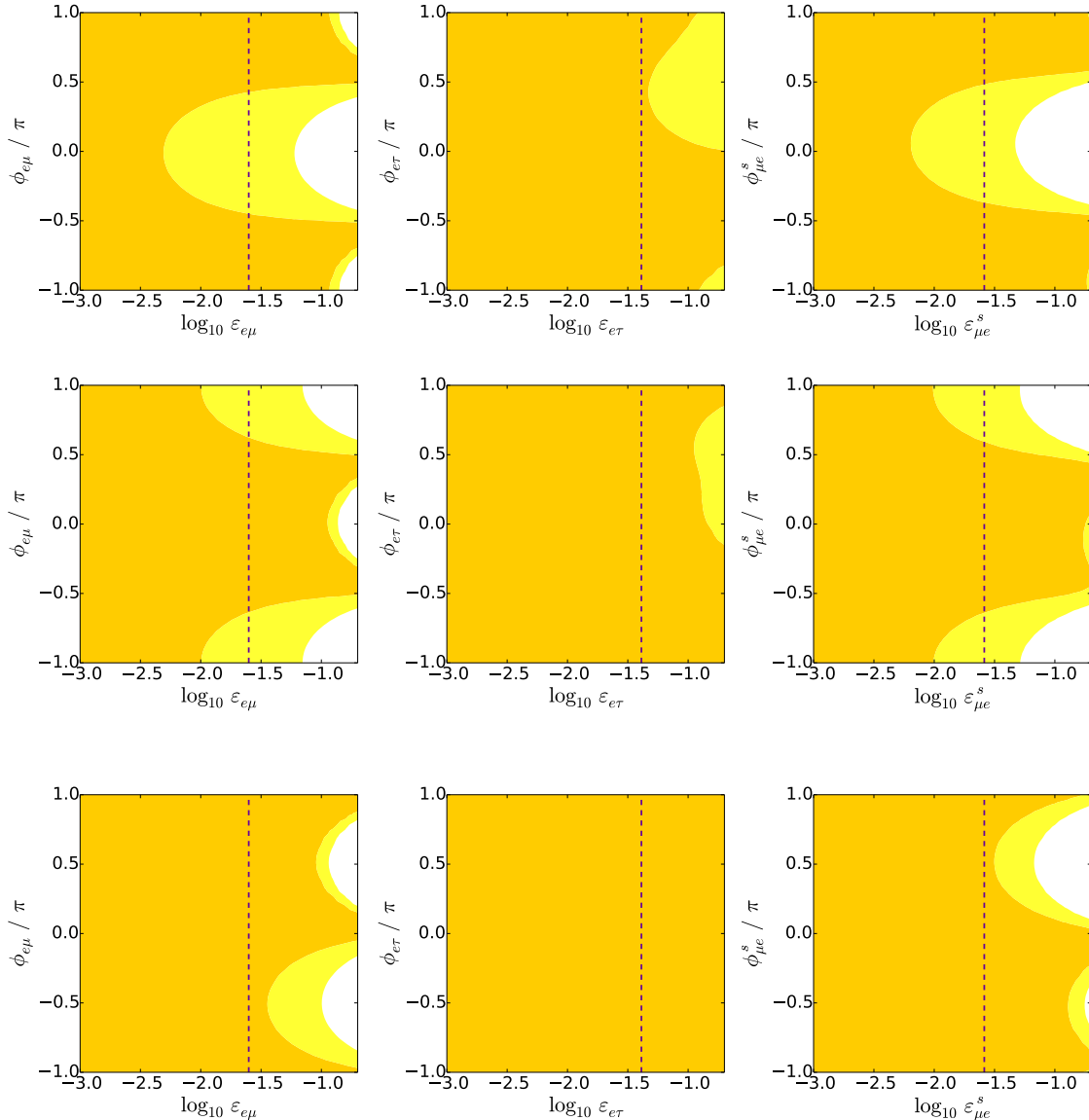


Figure 4.14: Allowed regions in the $(\varepsilon_{\alpha\beta}, \phi_{\alpha\beta})$ -planes at 2σ and 3σ confidence level for 1 dof and $\delta = 0, \pi, 3\pi/2$ in the upper, middle and lower panels, respectively. The vertical lines are at $\varepsilon_{e\mu} = 0.025$, $\varepsilon_{e\tau} = 0.041$ and $\varepsilon_{\mu e}^s = 0.026$, see (4.21).

4.4 Discussion

While the impact of LED on the best fit values and 1σ errors of the standard oscillation parameters is almost negligible (the largest difference is found for $\sin^2 \theta_{13}$ where the 3σ LED confidence region is almost 10% larger than the standard model), this is not the case for the NSI scenario, where particularly the allowed values of θ_{13} and δ are different from the standard determination. Indeed the 1σ confidence region for θ_{13} is roughly six times larger than the standard model analysis.

The situation is similar for the Dirac phase δ , where the presence of new phases from the NSI complex couplings $\varepsilon_{\alpha\beta}$ reduces the sensitivity with respect to the standard physics. In fact, although the best fit is still around the standard solution $\delta \simeq 3\pi/2$ (as found in [45,47,48,110]), the presence of NSI effects makes this value statistically less significant. As for the bounds on the parameters of the LED and NSI models at 2σ CL (1 dof), we have found the following results:

- using the T2K data only we obtain $R \leq 0.93 \mu\text{m}$ for both NO and IO.
- in the combined analysis of the T2K \oplus Daya Bay data we obtain $R \leq 0.60 \mu\text{m}$ for NO and $R \leq 0.17 \mu\text{m}$ for IO
- for $|\varepsilon_{e\mu}| < 4.85 \times 10^{-3}$ and $|\varepsilon_{\mu e}^s| < 6.28 \times 10^{-3}$ (for $\delta = 0$); $|\varepsilon_{e\mu}| < 9.94 \times 10^{-3}$ and $|\varepsilon_{\mu e}^s| < 9.96 \times 10^{-3}$ (for $\delta = \pi$).

Following the discussion of the previous Section, the current bounds on the NSI parameters are expected to be improved after a better determination of the standard CP phase δ . For the LED parameters, an effort must be done in order to constrain the absolute mass m_0 and, consequently, the value of R .

5

Conclusions

After the discovery of a non-zero reactor angle θ_{13} in 2012 we are entering in the age of CP discovery. However, from a theoretical point of view, we do not know yet the origin of the lepton mixing and why the neutrino masses are lighter compared to others leptons. The models of NP that we investigated in this Thesis deal with these topics. In particular we analysed three different realizations of physics beyond the SM that are interesting for neutrino phenomenology: generalized CP symmetry, Large Extra Dimensions and Non-Standard neutrino Interactions.

In the first part (Chapter 2) we studied a mechanism to generate the lepton mixing based on non-abelian discrete symmetry combined with the so-called generalized CP symmetry. The PMNS matrix is given by the misalignment between the residual symmetries in the charged and neutrino sector. We assumed the group of even permutations of five elements, A_5 , as a symmetry in the full leptonic sector. The predictions based on this approach lead to mixing angles that are functions of a single parameter, the internal angle θ . We have found that four mixing patterns, based on different residual symmetries, accommodate well the mixing angles in the experimental allowed range, for a particular choice of the free parameter θ .

In Chapter 3 we constructed several realizations of the neutrino mass spectrum based on the residual symmetry Z_5 in the charged lepton sector. In this approach the flavour structure of the model is given by additional scalar fields, the flavons, with non-zero vacuum expectations values. We performed a classification, reducing the number of independent parameters in the neutrino mass matrix, to obtain testable relations among the mixing parameters. These relations can be checked at present and future neutrino facilities. We also showed the predictions for the low energy observables, the effective masses m_β and $m_{\beta\beta}$. As a last point of our analysis we discussed a particular scenario, based on Type I see-saw mechanism, with a particular vacuum alignment with only three independent parameters. We discussed the origin of the charged lepton masses and the corrections to U_{PMNS} from the charged sector.

The effect of NP in the neutrino sector can modify the oscillation phenomenology and might produce a bias in the extraction of the oscillation parameters. In Chapter 4 we studied this phenomenon in the context of two extension of the SM: Large Extra Dimensions and Non-Standard Interactions. We used the data of the Daya Bay reactor and T2K

beam experiments to investigate how these models of NP can modify the oscillation amplitude. We found that LED slightly modifies our knowledge on mixing parameters with respect to the SM. In the NSI scenario the reactor angle and the Dirac phase δ are not well defined at the level of 1σ due to the new complex couplings ε that enter in the oscillation amplitude. We also use the experimental data to constraint the parameter space of NP: the radius of the largest extra dimensions in LED and the absolute values of the complex couplings for NSI.

In conclusion, we are in an exciting era for neutrino physics. Several experiments are ongoing and many others are planned. In the next years we will be able to obtain information about the mixing parameters with higher accuracy and, probably, we can get information on the absolute mass scale from β -decay, $0\nu\beta\beta$ -decay and cosmology experiments. In the spirit of this impressive progress we expect that the mechanism of NP described in this Thesis can be confirmed or rejected at a certain confidence level.



SM oscillation probabilities

In this Appendix we summarized the SM oscillation probabilities that are relevant in the analysis performed in Chapter 4. These can be found in Ref. [215], where the Authors perform a complete analysis studying the matter effect on neutrino oscillation. Since the experiments T2K and Daya Bay (DB) have a small baseline we could ignore the matter effects at this level. The formulae can be expressed as a series in the small parameters $\sin \theta_{13}$ and $\Delta m_{21}^2 \ll |\Delta m_{3\ell}^2|$.

The approximated formula $\mathcal{P}_{\text{SM}}(\nu_\mu \rightarrow \nu_\mu)$ (relevant to T2K experiment) can be found in Ref. [216]. It reads

$$\begin{aligned} \mathcal{P}_{\text{SM}}(\nu_\mu \rightarrow \nu_\mu) \simeq & 1 - [\sin^2 2\theta_{23} - \sin^2 \theta_{23} \sin^2 2\theta_{13} \cos 2\theta_{23}] \sin^2 \left(\frac{\Delta m_{23}^2 L}{4E_\nu} \right) + \\ & - \left(\frac{\Delta m_{12}^2 L}{4E_\nu} \right) [\sin^2 \theta_{12} \sin^2 2\theta_{23} + \tilde{J} \sin^2 \theta_{23} \cos \delta] \sin \left(\frac{\Delta m_{23}^2 L}{2E_\nu} \right) + \\ & - \left(\frac{\Delta m_{12}^2 L}{4E_\nu} \right)^2 \left[\cos^4 \theta_{23} \sin^2 2\theta_{12} + \sin^2 \theta_{12} \sin^2 2\theta_{23} \cos \left(\frac{\Delta m_{23}^2 L}{4E_\nu} \right) \right]. \end{aligned} \quad (\text{A.1})$$

Here $\tilde{J} \equiv \cos \theta_{13} \sin 2\theta_{12} \sin 2\theta_{13} \sin 2\theta_{23}$ is the Jarlskog-like invariant. The other relevant channel is $\nu_\mu \rightarrow \nu_e$. The probability is

$$\begin{aligned} \mathcal{P}_{\text{SM}}(\nu_\mu \rightarrow \nu_e) \simeq & \sin^2 \theta_{23} \sin^2 2\theta_{13} \sin^2 \left(\frac{\Delta m_{31}^2 L}{4E_\nu} \right) + \\ & - \sin \delta \frac{\sin 2\theta_{12} \sin 2\theta_{23}}{2 \sin \theta_{13}} \sin^2 2\theta_{13} \sin \left(\frac{\Delta m_{21}^2 L}{4E_\nu} \right) \sin^2 \left(\frac{\Delta m_{31}^2 L}{4E_\nu} \right) \end{aligned} \quad (\text{A.2})$$

For the DB experiment

$$\begin{aligned} \mathcal{P}_{\text{SM}}(\bar{\nu}_e \rightarrow \bar{\nu}_e) \simeq & 1 - \cos^4 \theta_{13} \sin^2 2\theta_{12} \sin^2 \left(\frac{\Delta m_{21}^2 L}{4E_\nu} \right) + \\ & - \sin^2 2\theta_{13} \left[\cos^2 \theta_{12} \sin^2 \left(\frac{\Delta m_{31}^2 L}{4E_\nu} \right) + \sin^2 \theta_{12} \sin^2 \left(\frac{\Delta m_{32}^2 L}{4E_\nu} \right) \right]. \end{aligned} \quad (\text{A.3})$$

Notice that $|\Delta m_{21}^2| \ll |\Delta m_{3\ell}^2|$ and $\ell = 1, 2$, thus at the DB detector the argument of the square bracket in the second line can be approximated with an effective mass Δm_{ee}^2 , see for instance Ref. [217]. This is the parameter measured by the DB collaboration.

B

Non abelian discrete groups

In this Appendix we recapitulate some basic facts about group theory, in particular we focus on non abelian discrete symmetries, which are used in our analysis developed in Chapter 2.

B.1 Group theory

We want to recall some basic definitions about group theory. We follow Refs. [218–220] and [67]. The couple $\{\mathcal{G}, \cdot\}$, where \mathcal{G} is a generic set and \cdot some operation well defined, is called a *group* if the following four properties are satisfied

1. **Closure:** $\forall g_1, g_2 \in \mathcal{G}, g_1 \cdot g_2 = g_3 \in \mathcal{G}$
2. **Associativity:** $\forall g_1, g_2, g_3 \in \mathcal{G}, g_1 \cdot (g_2 \cdot g_3) = (g_1 \cdot g_2) \cdot g_3$
3. **Identity:** $\exists! e \in \mathcal{G} : e \cdot g = g \cdot e = g, \forall g \in \mathcal{G}$
4. **Inverse:** $\forall g \in \mathcal{G} \exists g^{-1} : g \cdot g^{-1} = g^{-1} \cdot g = e.$

The *order* is the number of the elements in \mathcal{G} ; the order of a *finite* group is finite. The group is called *abelian* if all of their elements are commutable each others. *i.e.* $g_1 \cdot g_2 = g_2 \cdot g_1$ for all elements of the group. If all elements do not satisfy the commutativity the group is called *non-abelian*.

The simplest example of finite groups are the cyclic group of order N , called Z_N , which consists of

$$\{e, \omega_N, \omega_N^2, \dots, \omega_N^{N-1}\} \in Z_N \quad (\text{B.1})$$

where $\omega_N^N = e$. The Z_N group can be represented as discrete rotations, whose generator ω_N corresponds to $2\pi/N$ rotation, see Fig. B.1.

In the case of non-abelian groups a simple example is given by the groups of permutations of N objects, S_N , with order $N!$. For instance we consider here the group of permutations of three elements S_3 . We call the elements $\mathcal{G} = \{1, 2, 3\}$ and the $3! = 6$ operations are

$$e \equiv \gamma_{123} = (1, 2, 3) \quad \gamma_{23} = (1, 3, 2) \quad \gamma_{12} = (2, 1, 3) \quad (\text{B.2})$$

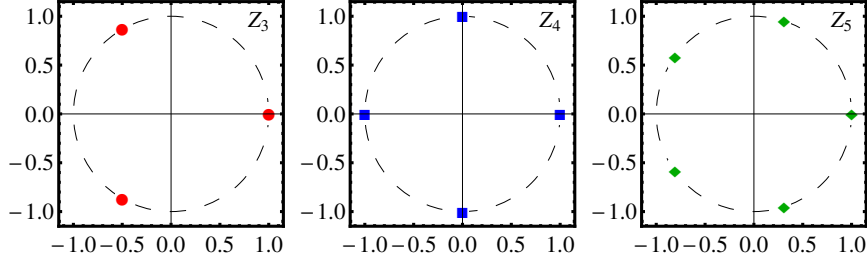


Figure B.1: Elements of Z_N for $N = 3, 4, 5$ on the unitary circle.

$$\gamma_{312} = (3, 1, 2) \quad \gamma_{13} = (3, 2, 1) \quad \gamma_{231} = (2, 3, 1). \quad (\text{B.3})$$

These operations form a group. Therefore the product of elements is still an element of \mathcal{G}

$$\gamma_{12}\gamma_{312}(1, 2, 3) = \gamma_{12}(3, 1, 2) = (1, 3, 2) \in \mathcal{G} \quad (\text{B.4a})$$

$$\gamma_{312}\gamma_{12}(1, 2, 3) = \gamma_{312}(2, 1, 3) = (3, 2, 1) \in \mathcal{G} \quad (\text{B.4b})$$

and so on. Notice that the group is non-abelian, in fact $\gamma_{312}\gamma_{12} \neq \gamma_{12}\gamma_{312}$.

If a subset \mathcal{H} of the group \mathcal{G} is also a group, \mathcal{H} is called the *subgroup* of \mathcal{G} . The Lagrange's theorem tells us that the order of the subgroup \mathcal{H} must be a divisor of the order of \mathcal{G} (for a modern proof see Ref. [67]).

If a subgroup \mathcal{N} of \mathcal{G} satisfies $g^{-1}\mathcal{N}g = \mathcal{N}$ for any element $g \in \mathcal{G}$, the subgroup \mathcal{N} is called a *normal subgroup* or an invariant subgroup. The subgroup \mathcal{H} and normal subgroup \mathcal{N} of \mathcal{G} satisfy $\mathcal{H}\mathcal{N} = \mathcal{N}\mathcal{H}$ and it is a subgroup of \mathcal{G} , where

$$\mathcal{N}\mathcal{H} = \{n_j \cdot h_j \text{ such that } n_j \in \mathcal{N}, h_j \in \mathcal{H}\} \quad (\text{B.5})$$

and similar for $\mathcal{H}\mathcal{N}$.

When $g^h = e$ for an element $g \in \mathcal{G}$, the number h is called the order of g . The elements, $\{e, g, g^2, \dots, g^{h-1}\}$, form a subgroup, which is the abelian Z_h group with the order h .

The elements $g^{-1} \cdot a \cdot g$ for $g \in \mathcal{G}$ are called elements *conjugate* to the element a . The set including all elements to conjugate to an element a of \mathcal{G} , $\{g^{-1} \cdot a \cdot g, \forall g \in \mathcal{G}\}$, is called a *conjugacy class*. All of elements in a conjugacy class have the same order because

$$(g \cdot a \cdot g^{-1})^h = \underbrace{g \cdot a(g^{-1} \cdot g) \cdot a \cdot (g^{-1} \cdot g) \dots a \cdot g^{-1}}_h = g \cdot a^h \cdot g^{-1} = g \cdot e \cdot g^{-1} = g \cdot g^{-1} = e. \quad (\text{B.6})$$

The conjugacy class including the identity e consists of the single element e .

B.2 Representations and characters

In the following we need to know the action of the group elements $g \in \mathcal{G}$ in the vectorial space \mathbb{V} . The *representation* r is the omomorphism

$$r : \begin{cases} \mathcal{G} \longrightarrow GL(\mathbb{V}) \\ g \in \mathcal{G} \longmapsto r(g) \in GL(\mathbb{V}) \end{cases} \quad (\text{B.7})$$

such that

$$r(g_1 \cdot g_2) = r(g_1)r(g_2) \quad \forall g_1, g_2 \in \mathcal{G} \quad (\text{B.8a})$$

$$r(e) = \mathbb{1}. \quad (\text{B.8b})$$

where C_i denotes the conjugacy class of g_i and n_i denotes the number of elements in the conjugacy class C_i .

If there are d_n n -dimensional irreducible representations, the elements of the group in a given representation $r(g)$ are represented by $(n \times n)$ matrices. The identity e is always represented by the $(n \times n)$ identity matrix $\mathbb{1}_n$ and the character of $\chi^{[r(g)]}(C_1)$ for the conjugacy class $C_1 = e$ is found to be n for the n -dimensional representation. It is possible to show that the number of unitary irreducible representations should be equal to the number of conjugacy classes, thus

$$\sum_n d_n = \text{number of conjugacy classes.} \quad (\text{B.15})$$

Using the (B.14) and the results quoted above it is possible to show that

$$\sum_p |\chi^{[r_q(g_i)]}(C_1)|^2 = \sum_n d_n n^2 = d_1 + 4d_2 + 9d_3 + \dots = N_G \quad (\text{B.16})$$

where n is a natural number.

B.3 The group S_4

The group S_4 is the permutation group of order four, it has $4! = 24$ elements and it is isomorphic to the symmetry group of the cube. The algebra, introduced in (2.7), contains two generators, S and T , that satisfied the condition $S^2 = T^4 = (ST)^3 = \mathbb{1}$.

S_4	C_1	$3C_2^{[2]}$	$6C_3^{[2]}$	$6C_4^{[4]}$	$8C_5^{[3]}$
$\chi^{[1]}$	1	1	1	1	1
$\chi^{[1']}$	1	1	-1	-1	1
$\chi^{[2]}$	2	2	0	0	-1
$\chi^{[3]}$	3	-1	1	-1	0
$\chi^{[3']}$	3	-1	-1	1	0

Table B.1: Characters of the S_4 group.

The group contain five irreducible representations, two singlet $\mathbf{1}$ and $\mathbf{1}'$, one doublet $\mathbf{2}$ and two triplets $\mathbf{3}$ and $\mathbf{3}'$. The (non trivial) tensor products are

$$\mathbf{1}' \otimes \mathbf{1}' = \mathbf{1} \quad (\text{B.17a})$$

$$\mathbf{1}' \otimes \mathbf{2} = \mathbf{2} \quad (\text{B.17b})$$

$$\mathbf{1}' \otimes \mathbf{3} = \mathbf{3}' \quad (\text{B.17c})$$

$$\mathbf{1}' \otimes \mathbf{3}' = \mathbf{3} \quad (\text{B.17d})$$

$$\mathbf{2} \otimes \mathbf{2} = \mathbf{1}_s \oplus \mathbf{2}_s \oplus \mathbf{1}'_a \quad (\text{B.17e})$$

$$\mathbf{2} \otimes \mathbf{3} = \mathbf{2} \otimes \mathbf{3}' = \mathbf{3} \oplus \mathbf{3}' \quad (\text{B.17f})$$

$$\mathbf{3} \otimes \mathbf{3} = \mathbf{3}' \otimes \mathbf{3}' = \mathbf{1}_s \oplus \mathbf{2}_s \oplus \mathbf{3}'_s \oplus \mathbf{3}_a \quad (\text{B.17g})$$

$$\mathbf{3} \otimes \mathbf{3}' = \mathbf{1}' \oplus \mathbf{2} \oplus \mathbf{3} \oplus \mathbf{3}' \quad (\text{B.17h})$$

where the subscript s (a) denotes symmetric (antisymmetric) combinations. The S_4 elements can be classified by the order h of each element, where $\omega^h = e$. These are classified in Tab. B.1 where the five conjugacy classes are summarized with their characters. We have $1 + 3 + 6 + 6 + 8 = 24$ elements in each class and the superscript indicates the order of each element in the conjugacy classes. The same classification is adopted for A_5 in the main text, see for instance Tab. 2.2.



Kronecker products of A_5

We report here the complete list of the Kronecker products for the group $A_5 \otimes CP$. With respect to the simple group A_5 we need the to impose additional condition

$$\left[X(\mathbf{r} \otimes \mathbf{r}')^* \right]_{\mathbf{r}''} = \left[X(\mathbf{r})^* \otimes X(\mathbf{r}')^* \right]_{\mathbf{r}''} \quad \forall \mathbf{r}, \mathbf{r}', \mathbf{r}'' \in A_5 \quad (\text{C.1})$$

where X is the CP matrix for the representation $\mathbf{r} \in A_5$.

We report the Kronecker products in the case of $X = X_0$. We assigne $a = (a_1, a_2, a_3)^T$ and $b = (b_1, b_2, b_3)^T$ to the $\mathbf{3}$ representation, while $a' = (a'_1, a'_2, a'_3)^T$ and $b' = (b'_1, b'_2, b'_3)^T$ belong to the $\mathbf{3}'$ representation, $c = (c_1, c_2, c_3, c_4, c_5)^T$ and $d = (d_1, d_2, d_3, d_4, d_5)^T$ are pentaplets; $f = (f_1, f_2, f_3, f_4)^T$ and $g = (g_1, g_2, g_3, g_4)^T$ are tetraplets.

- $\mathbf{3} \otimes \mathbf{3} = \mathbf{1}_s \oplus \mathbf{3}_a \oplus \mathbf{5}_s$

$$\mathbf{1} = a_1 b_1 + a_2 b_3 + a_3 b_2 \quad (\text{C.2a})$$

$$\mathbf{3} = i \left(a_2 b_3 - a_3 b_2, a_1 b_2 - a_2 b_1, a_3 b_1 - a_1 b_3 \right)^T \quad (\text{C.2b})$$

$$\mathbf{5} = \left(a_1 b_1 - \frac{a_2 b_3}{2} - \frac{a_3 b_2}{2}, \frac{\sqrt{3}}{2} (a_1 b_2 + a_2 b_1), -\sqrt{\frac{3}{2}} a_2 b_2, -\sqrt{\frac{3}{2}} a_3 b_3, -\frac{\sqrt{3}}{2} (a_1 b_3 + a_3 b_1) \right)^T \quad (\text{C.2c})$$

- $\mathbf{3}' \otimes \mathbf{3}' = \mathbf{1}_s \oplus \mathbf{3}'_a \oplus \mathbf{5}_s$

$$\mathbf{1} = a'_1 b'_1 + a'_2 b'_3 + a'_3 b'_2 \quad (\text{C.3a})$$

$$\mathbf{3}' = i \left(a'_2 b'_3 - a'_3 b'_2, a'_1 b'_2 - a'_2 b'_1, a'_3 b'_1 - a'_1 b'_3 \right)^T \quad (\text{C.3b})$$

$$\mathbf{5} = \left(a'_1 b'_1 - \frac{a'_2 b'_3}{2} - \frac{a'_3 b'_2}{2}, \sqrt{\frac{3}{2}} a'_3 b'_3, -\frac{\sqrt{3}}{2} (a'_1 b'_2 + a'_2 b'_1), -\frac{\sqrt{3}}{2} (a'_1 b'_3 + a'_3 b'_1), -\sqrt{\frac{3}{2}} a'_2 b'_2 \right)^T \quad (\text{C.3c})$$

- $\mathbf{3} \otimes \mathbf{3}' = \mathbf{4} \oplus \mathbf{5}$

$$\mathbf{4} = i \left(a_2 b'_1 - \frac{a_3 b'_2}{\sqrt{2}}, -a_1 b'_2 + \frac{a_3 b'_3}{\sqrt{2}}, a_1 b'_3 - \frac{a_2 b'_2}{\sqrt{2}}, -a_3 b'_1 + \frac{a_2 b'_3}{\sqrt{2}} \right)^T \quad (\text{C.4a})$$

$$\mathbf{5} = \left(a_1 b'_1, -\frac{a_2 b'_1 + \sqrt{2} a_3 b'_2}{\sqrt{3}}, \frac{a_1 b'_2 + \sqrt{2} a_3 b'_3}{\sqrt{3}}, \frac{a_1 b'_3 + \sqrt{2} a_2 b'_2}{\sqrt{3}}, \frac{a_3 b'_1 + \sqrt{2} a_2 b'_3}{\sqrt{3}} \right)^T \quad (\text{C.4b})$$

• $\mathbf{3} \otimes \mathbf{4} = \mathbf{3}' \oplus \mathbf{4} \oplus \mathbf{5}$

$$\mathbf{3}' = i \left(a_2 g_4 - a_3 g_1, \frac{1}{\sqrt{2}} (\sqrt{2} a_1 g_2 + a_2 g_1 + a_3 g_3), -\frac{1}{\sqrt{2}} (\sqrt{2} a_1 g_3 + a_2 g_2 + a_3 g_4) \right)^T \quad (\text{C.5a})$$

$$\mathbf{4} = i \left(a_1 g_1 + \sqrt{2} a_3 g_2, -a_1 g_2 + \sqrt{2} a_2 g_1, a_1 g_3 - \sqrt{2} a_3 g_4, -a_1 g_4 - \sqrt{2} a_2 g_3 \right)^T \quad (\text{C.5b})$$

$$\mathbf{5} = \left(a_3 g_1 + a_2 g_4, \sqrt{\frac{2}{3}} (\sqrt{2} a_1 g_1 - a_3 g_2), \frac{1}{\sqrt{6}} (\sqrt{2} a_1 g_2 - 3 a_3 g_3 + a_2 g_1), \frac{1}{\sqrt{6}} (\sqrt{2} a_1 g_3 - 3 a_2 g_2 + a_3 g_4), \sqrt{\frac{2}{3}} (-\sqrt{2} a_1 g_4 + a_2 g_3) \right)^T \quad (\text{C.5c})$$

• $\mathbf{3}' \otimes \mathbf{4} = \mathbf{3} \oplus \mathbf{4} \oplus \mathbf{5}$

$$\mathbf{3} = i \left(a'_2 g_3 - a'_3 g_2, \frac{1}{\sqrt{2}} (\sqrt{2} a'_1 g_1 + a'_2 g_4 - a'_3 g_3), \frac{1}{\sqrt{2}} (-\sqrt{2} a'_1 g_4 + a'_2 g_2 - a'_3 g_1) \right)^T \quad (\text{C.6a})$$

$$\mathbf{4} = i \left(a'_1 g_1 + \sqrt{2} a'_3 g_3, a'_1 g_2 - \sqrt{2} a'_3 g_4, -a'_1 g_3 + \sqrt{2} a'_2 g_1, -a'_1 g_4 - \sqrt{2} a'_2 g_2 \right)^T \quad (\text{C.6b})$$

$$\mathbf{5} = \left(a'_3 g_2 + a'_2 g_3, \frac{1}{\sqrt{6}} (\sqrt{2} a'_1 g_1 - 3 a'_2 g_4 - a'_3 g_3), -\sqrt{\frac{2}{3}} (\sqrt{2} a'_1 g_2 + a'_3 g_4), -\sqrt{\frac{2}{3}} (\sqrt{2} a'_1 g_3 + a'_2 g_1), \frac{1}{\sqrt{6}} (-\sqrt{2} a'_1 g_4 + 3 a'_3 g_1 + a'_2 g_2) \right)^T \quad (\text{C.6c})$$

• $\mathbf{3} \otimes \mathbf{5} = \mathbf{3} \oplus \mathbf{3}' \oplus \mathbf{4} \oplus \mathbf{5}$

$$\mathbf{3} = \left(\frac{2 a_1 c_1}{\sqrt{3}} + a_3 c_2 - a_2 c_5, -\frac{a_2 c_1}{\sqrt{3}} + a_1 c_2 - \sqrt{2} a_3 c_3, -\frac{a_3 c_1}{\sqrt{3}} - a_1 c_5 - \sqrt{2} a_2 c_4 \right)^T \quad (\text{C.7a})$$

$$\mathbf{3}' = \left(a_1 c_1 + \frac{a_2 c_5 - a_3 c_2}{\sqrt{3}}, \frac{a_1 c_3 + \sqrt{2} (a_3 c_4 - a_2 c_2)}{\sqrt{3}}, \frac{a_1 c_4 + \sqrt{2} (a_2 c_3 + a_3 c_5)}{\sqrt{3}} \right)^T \quad (\text{C.7b})$$

$$\mathbf{4} = \left(4 a_1 c_2 + 2 \sqrt{3} a_2 c_1 + \sqrt{2} a_3 c_3, 2 a_1 c_3 - 2 \sqrt{2} a_2 c_2 - 3 \sqrt{2} a_3 c_4, 2 a_1 c_4 - 3 \sqrt{2} a_2 c_3 + 2 \sqrt{2} a_3 c_5, -4 a_1 c_5 + \sqrt{2} a_2 c_4 + 2 \sqrt{3} a_3 c_1 \right)^T \quad (\text{C.7c})$$

$$\mathbf{5} = i \left(a_2 c_5 + a_3 c_2, a_2 c_1 - \frac{a_1 c_2 + \sqrt{2} a_3 c_3}{\sqrt{3}}, -\frac{2 a_1 c_3 + \sqrt{2} a_2 c_2}{\sqrt{3}}, \frac{2 a_1 c_4 - \sqrt{2} a_3 c_5}{\sqrt{3}}, a_3 c_1 + \frac{a_1 c_5 - \sqrt{2} a_2 c_4}{\sqrt{3}} \right)^T \quad (\text{C.7d})$$

• $\mathbf{3}' \otimes \mathbf{5} = \mathbf{3} \oplus \mathbf{3}' \oplus \mathbf{4} \oplus \mathbf{5}$

$$\mathbf{3} = \left(a'_1 c_1 + \frac{a'_3 c_3 + a'_2 c_4}{\sqrt{3}}, \frac{-a'_1 c_2 + \sqrt{2} (a'_3 c_4 + a'_2 c_5)}{\sqrt{3}}, \frac{a'_1 c_5 + \sqrt{2} (a'_2 c_3 - a'_3 c_2)}{\sqrt{3}} \right)^T \quad (\text{C.8a})$$

$$\mathbf{3}' = \left(\frac{2 a'_1 c_1}{\sqrt{3}} - a'_3 c_3 - a'_2 c_4, -\frac{a'_2 c_1}{\sqrt{3}} - a'_1 c_3 - \sqrt{2} a'_3 c_5, -\frac{a'_3 c_1}{\sqrt{3}} - a'_1 c_4 + \sqrt{2} a'_2 c_2 \right)^T \quad (\text{C.8b})$$

$$\mathbf{4} = \left(2 a'_1 c_2 + 3 \sqrt{2} a'_2 c_5 - 2 \sqrt{2} a'_3 c_4, -4 a'_1 c_3 + 2 \sqrt{3} a'_2 c_1 + \sqrt{2} a'_3 c_5, -4 a'_1 c_4 - \sqrt{2} a'_2 c_2 + 2 \sqrt{3} a'_3 c_1, -2 a'_1 c_5 - 2 \sqrt{2} a'_2 c_3 - 3 \sqrt{2} a'_3 c_2 \right)^T \quad (\text{C.8c})$$

$$\mathbf{5} = i \left(a'_2 c_4 - a'_3 c_3, \frac{2 a'_1 c_2 + \sqrt{2} a'_3 c_4}{\sqrt{3}}, -a'_2 c_1 - \frac{a'_1 c_3 - \sqrt{2} a'_3 c_5}{\sqrt{3}}, a'_3 c_1 + \frac{a'_1 c_4 + \sqrt{2} a'_2 c_2}{\sqrt{3}}, \frac{-2 a'_1 c_5 + \sqrt{2} a'_2 c_3}{\sqrt{3}} \right)^T \quad (\text{C.8d})$$

- $4 \otimes 4 = \mathbf{1}_s \oplus \mathbf{3}_a \oplus \mathbf{3}'_a \oplus \mathbf{4}_s \oplus \mathbf{5}_s$

$$\mathbf{1} = f_1 g_4 + f_2 g_3 + f_3 g_2 + f_4 g_1 \quad (\text{C.9a})$$

$$\mathbf{3} = i \left(f_1 g_4 - f_4 g_1 + f_3 g_2 - f_2 g_3, \sqrt{2}(f_2 g_4 - f_4 g_2), \sqrt{2}(f_1 g_3 - f_3 g_1) \right)^T \quad (\text{C.9b})$$

$$\mathbf{3}' = i \left(f_1 g_4 - f_4 g_1 + f_2 g_3 - f_3 g_2, \sqrt{2}(f_3 g_4 - f_4 g_3), \sqrt{2}(f_1 g_2 - f_2 g_1) \right)^T \quad (\text{C.9c})$$

$$\mathbf{4} = i \left(f_3 g_3 - f_4 g_2 - f_2 g_4, f_1 g_1 + f_3 g_4 + f_4 g_3, -f_4 g_4 - f_1 g_2 - f_2 g_1, \right. \\ \left. - f_2 g_2 + f_1 g_3 + f_3 g_1 \right)^T \quad (\text{C.9d})$$

$$\mathbf{5} = \left(f_1 g_4 + f_4 g_1 - f_3 g_2 - f_2 g_3, -\sqrt{\frac{2}{3}}(2f_3 g_3 + f_2 g_4 + f_4 g_2), \sqrt{\frac{2}{3}}(-2f_1 g_1 + f_3 g_4 + f_4 g_3), \right. \\ \left. \sqrt{\frac{2}{3}}(-2f_4 g_4 + f_2 g_1 + f_1 g_2), \sqrt{\frac{2}{3}}(2f_2 g_2 + f_1 g_3 + f_3 g_1) \right)^T \quad (\text{C.9e})$$

- $4 \otimes 5 = \mathbf{3} \oplus \mathbf{3}' \oplus \mathbf{4} \oplus \mathbf{5}_1 \oplus \mathbf{5}_2$

$$\mathbf{3} = \left(4f_1 c_5 - 4f_4 c_2 - 2f_3 c_3 - 2f_2 c_4, -2\sqrt{3}f_1 c_1 - \sqrt{2}(2f_2 c_5 - 3f_3 c_4 + f_4 c_3), \right. \\ \left. \sqrt{2}(-f_1 c_4 + 3f_2 c_3 + 2f_3 c_2) - 2\sqrt{3}f_4 c_1 \right)^T \quad (\text{C.10a})$$

$$\mathbf{3}' = \left(2f_1 c_5 - 2f_4 c_2 + 4f_3 c_3 + 4f_2 c_4, -2\sqrt{3}f_2 c_1 + \sqrt{2}(2f_4 c_4 + 3f_1 c_2 - f_3 c_5), \right. \\ \left. \sqrt{2}(f_2 c_2 - 3f_4 c_5 + 2f_1 c_3) - 2\sqrt{3}f_3 c_1 \right)^T \quad (\text{C.10b})$$

$$\mathbf{4} = \left(3f_1 c_1 + \sqrt{6}(f_2 c_5 + f_3 c_4 - 2f_4 c_3), -3f_2 c_1 + \sqrt{6}(f_4 c_4 - f_1 c_2 + 2f_3 c_5), \right. \\ \left. -3f_3 c_1 + \sqrt{6}(f_1 c_3 + f_4 c_5 - 2f_2 c_2), 3f_4 c_1 + \sqrt{6}(f_2 c_3 - f_3 c_2 - 2f_1 c_4) \right)^T \quad (\text{C.10c})$$

$$\mathbf{5}_1 = i \left(f_1 c_5 + 2f_2 c_4 - 2f_3 c_3 + f_4 c_2, -2f_1 c_1 + \sqrt{6}f_2 c_5, f_2 c_1 + \sqrt{\frac{3}{2}}(-f_1 c_2 - f_3 c_5 + 2f_4 c_4), \right. \\ \left. -f_3 c_1 - \sqrt{\frac{3}{2}}(f_2 c_2 + f_4 c_5 + 2f_1 c_3), -2f_4 c_1 - \sqrt{6}f_3 c_2 \right)^T \quad (\text{C.10d})$$

$$\mathbf{5}_2 = i \left(f_2 c_4 - f_3 c_3, -f_1 c_1 + \frac{2f_2 c_5 - f_3 c_4 - f_4 c_3}{\sqrt{6}}, -\sqrt{\frac{2}{3}}(f_1 c_2 + f_3 c_5 - f_4 c_4), \right. \\ \left. -\sqrt{\frac{2}{3}}(f_1 c_3 + f_2 c_2 + f_4 c_5), -f_4 c_1 - \frac{2f_3 c_2 + f_1 c_4 + f_2 c_3}{\sqrt{6}} \right)^T \quad (\text{C.10e})$$

- $5 \otimes 5 = \mathbf{1}_s \oplus \mathbf{3}_a \oplus \mathbf{3}'_a \oplus \mathbf{4}_a \oplus \mathbf{4}_s \oplus \mathbf{5}_{1,s} \oplus \mathbf{5}_{2,s}$

$$\mathbf{1} = c_1 d_1 + c_3 d_4 + c_4 d_3 - c_2 d_5 - c_5 d_2 \quad (\text{C.11a})$$

$$\mathbf{3} = i \left(2(c_4 d_3 - c_3 d_4) + c_2 d_5 - c_5 d_2, \sqrt{3}(c_2 d_1 - c_1 d_2) + \sqrt{2}(c_3 d_5 - c_5 d_3), \right. \\ \left. \sqrt{3}(c_5 d_1 - c_1 d_5) + \sqrt{2}(c_4 d_2 - c_2 d_4) \right)^T \quad (\text{C.11b})$$

$$\mathbf{3}' = i \left(2(c_2 d_5 - c_5 d_2) + c_3 d_4 - c_4 d_3, \sqrt{3}(c_3 d_1 - c_1 d_3) + \sqrt{2}(c_4 d_5 - c_5 d_4), \right. \\ \left. \sqrt{3}(c_1 d_4 - c_4 d_1) + \sqrt{2}(c_3 d_2 - c_2 d_3) \right)^T \quad (\text{C.11c})$$

$$\mathbf{4}_s = i \left((c_1 d_2 + c_2 d_1) - \frac{(c_3 d_5 + c_5 d_3) - 4c_4 d_4}{\sqrt{6}}, -(c_1 d_3 + c_3 d_1) - \frac{(c_4 d_5 + c_5 d_4) - 4c_2 d_2}{\sqrt{6}}, \right. \\ \left. (c_1 d_4 + c_4 d_1) - \frac{(c_2 d_3 + c_3 d_2) + 4c_5 d_5}{\sqrt{6}}, (c_1 d_5 + c_5 d_1) - \frac{(c_2 d_4 + c_4 d_2) + 4c_3 d_3}{\sqrt{6}} \right)^T \quad (\text{C.11d})$$

$$\begin{aligned}
\mathbf{4}_a = i & \left((c_1 d_2 - c_2 d_1) + \sqrt{\frac{3}{2}}(c_3 d_5 - c_5 d_3), (c_1 d_3 - c_3 d_1) + \sqrt{\frac{3}{2}}(c_4 d_5 - c_5 d_4), \right. \\
& \left. (c_4 d_1 - c_1 d_4) + \sqrt{\frac{3}{2}}(c_3 d_2 - c_2 d_3), (c_1 d_5 - c_5 d_1) + \sqrt{\frac{3}{2}}(c_4 d_2 - c_2 d_4) \right)^T
\end{aligned} \tag{C.11e}$$

$$\begin{aligned}
\mathbf{5}_1 = & \left(c_1 d_1 + c_2 d_5 + c_5 d_2 + \frac{c_3 d_4 + c_4 d_3}{2}, -(c_1 d_2 + c_2 d_1) + \sqrt{\frac{3}{2}}c_4 d_4, \right. \\
& \frac{1}{2}(c_1 d_3 + c_3 d_1 - \sqrt{6}(c_4 d_5 + c_5 d_4)), \\
& \left. \frac{1}{2}(c_1 d_4 + c_4 d_1 + \sqrt{6}(c_2 d_3 + c_3 d_2)), -(c_1 d_5 + c_5 d_1) - \sqrt{\frac{3}{2}}c_3 d_3 \right)^T
\end{aligned} \tag{C.11f}$$

$$\begin{aligned}
\mathbf{5}_2 = & \left(\frac{2c_1 d_1 + c_2 d_5 + c_5 d_2}{2}, \frac{-3(c_1 d_2 + c_2 d_1) + \sqrt{6}(2c_4 d_4 + c_3 d_5 + c_5 d_3)}{6}, \right. \\
& \left. - \frac{2c_4 d_5 + 2c_5 d_4 + c_2 d_2}{\sqrt{6}}, \right. \\
& \left. \frac{2c_2 d_3 + 2c_3 d_2 - c_5 d_5}{\sqrt{6}}, \frac{-3(c_1 d_5 + c_5 d_1) + \sqrt{6}(-2c_3 d_3 + c_2 d_4 + c_4 d_2)}{6} \right)^T
\end{aligned} \tag{C.11g}$$

D

CP invariants

The mixing angles can be extracted using the PMNS matrix defined in (1.2). Using the PMNS matrix elements we get

$$\sin^2 \theta_{12} = \frac{|U_{12}|^2}{1 - |U_{13}|^2} \quad \sin^2 \theta_{13} = |U_{13}|^2 \quad \sin^2 \theta_{23} = \frac{|U_{23}|^2}{1 - |U_{13}|^2}. \quad (\text{D.1})$$

With this convention we can define the Jarlskog invariant J_{CP} [109] as

$$J_{\text{CP}} \equiv \text{Im} \left[U_{11} U_{13}^* U_{31}^* U_{33} \right] = \frac{1}{8} \sin 2\theta_{12} \sin 2\theta_{23} \sin 2\theta_{13} \cos \theta_{13} \sin \delta. \quad (\text{D.2})$$

Similar invariants, called I_1 and I_2 , can be defined for the Majorana phases

$$I_1 \equiv \text{Im} \left[U_{12} U_{12} U_{11}^* U_{11}^* \right] = \sin^2 \theta_{12} \cos^2 \theta_{12} \cos^4 \theta_{13} \sin \alpha \quad (\text{D.3})$$

$$I_2 \equiv \text{Im} \left[U_{13} U_{13} U_{11}^* U_{11}^* \right] = \sin^2 \theta_{13} \cos^2 \theta_{12} \cos^2 \theta_{13} \sin \beta. \quad (\text{D.4})$$

A third non-independent invariant can also be introduced

$$I_3 \equiv \text{Im} \left[U_{13} U_{13} U_{12}^* U_{12}^* \right] = \cos^2 \theta_{12} \sin^2 \theta_{13} \cos^2 \theta_{13} \sin(\beta - \alpha). \quad (\text{D.5})$$

Notice that the Dirac phase δ has a physical meaning only if all mixing angles are different from 0 and $\pi/2$. Analogously, the vanishing of the invariants $I_{1,2}$ only implies $\sin \alpha = 0$, $\sin \beta = 0$, if solutions with $\sin 2\theta_{12} = 0$, $\cos \theta_{13} = 0$ or $\sin 2\theta_{13} = 0$, $\cos \theta_{12} = 0$ are discarded. Furthermore, notice that one of the Majorana phases becomes unphysical, if the lightest neutrino mass vanishes.

The Dirac *CP* phase can be extracted from (D.2) and the mixing angles (D.1) as

$$\sin \delta = \frac{8J_{\text{CP}}}{\sin 2\theta_{12} \sin 2\theta_{23} \sin 2\theta_{13} \cos \theta_{13}}. \quad (\text{D.6})$$

We can extract the Majorana phases from the numerical PMNS mixing matrix taking into the account that there exist unphysical phases, $\delta_{e,\mu,\tau}$, parametrized by a diagonal matrix $\text{diag}\{\exp i\delta_e, \exp i\delta_\mu, \exp i\delta_\tau\}$ that multiplies U_{PMNS} from the left. These can be eliminated with a redefinition of the charged lepton fields. A similar procedure is discussed in [221]

using a different parametrization for the PMNS matrix.¹ We can obtain the Majorana phases

$$\alpha = 2 \arg \left\{ \frac{U_{12}}{U_{11}} \right\} \quad (\text{D.7})$$

$$\beta = 2 \arg \left\{ \frac{U_{13}}{U_{11}} \right\}. \quad (\text{D.8})$$

For the sake of completeness we report how to extract the values of the unphysical phases

$$\delta_e = \arg\{U_{11}\} \quad (\text{D.9})$$

$$\delta_\mu = \arg \left\{ U_{23} e^{-i(\beta/2+\delta)} \right\} \quad (\text{D.10})$$

$$\delta_\tau = \arg \left\{ U_{33} e^{-i(\beta/2+\delta)} \right\}. \quad (\text{D.11})$$

¹For further details see the webpage <http://reapmpt.hepforge.org/>.



Neutrino mass sum rules

In the models we have considered we can define a sum rule Σ , *i.e.* a relation for the complex masses \tilde{m}_j . The complex masses are defined as

$$\tilde{m}_1 \equiv m_1 \quad \tilde{m}_2 \equiv m_2 e^{i\alpha} \quad \tilde{m}_3 \equiv m_3 e^{i\beta} \quad (\text{E.1})$$

where we use the same convention of Ref. [148] (see also Refs. [149–151]). In this case m_j are the absolute values of the light neutrino masses and α and β are the Majorana phases, see (1.2) for our PMNS convention. The sum rule is a generic function of the complex masses, $\Sigma = \Sigma(\tilde{m}_1, \tilde{m}_2, \tilde{m}_3)$ that is equal to zero in a given model. In general the masses appear as \tilde{m}_j^p where $p \in \mathbb{Z}$ depends on the type of neutrino masses. For instance in the case of Mechanism I $p = 1$, in Mechanism II with trivial Dirac mass matrix $p = -1$ and otherwise $p = 2$.

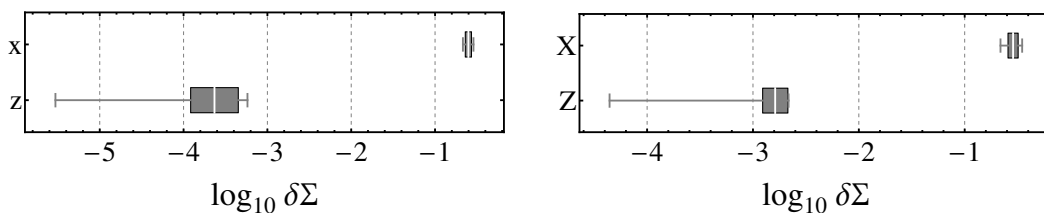


Figure E.1: Distribution of the of $\log_{10} \delta\Sigma$ for Mechanism I (left plot) and Mechanism II a-1 (right plot). We show only the results for x (X) and z (Z) equal to zero in the case of Mechanism I (Mechanism II a-1) because for $s = 0$ ($S = 0$) the parameter $\delta\Sigma$ is zero. The gray lines indicate the range for the parameter $\delta\Sigma$, the white line is the mean of the distribution while the gray region is the 1σ range.

Notice that the sum rule is defined as series in the expansion parameter, which depends on the particular model. In order to quantify the deviation of the LO (or NLO/N²LO for some particular sum rules) prediction we introduce the following dimensionless parameter, evaluated for the full numerical values of the neutrino masses

$$\delta\Sigma \equiv \left| \frac{\Sigma}{\sum_j m_j^p / 3} \right| \quad (\text{E.2})$$

which is independent on the absolute scale of the neutrino masses. An alternative definition could be $\delta\Sigma = \Sigma / [(\sum_j m_j)^p / 3]$; in this case the value of $\delta\Sigma$ can be different with respect

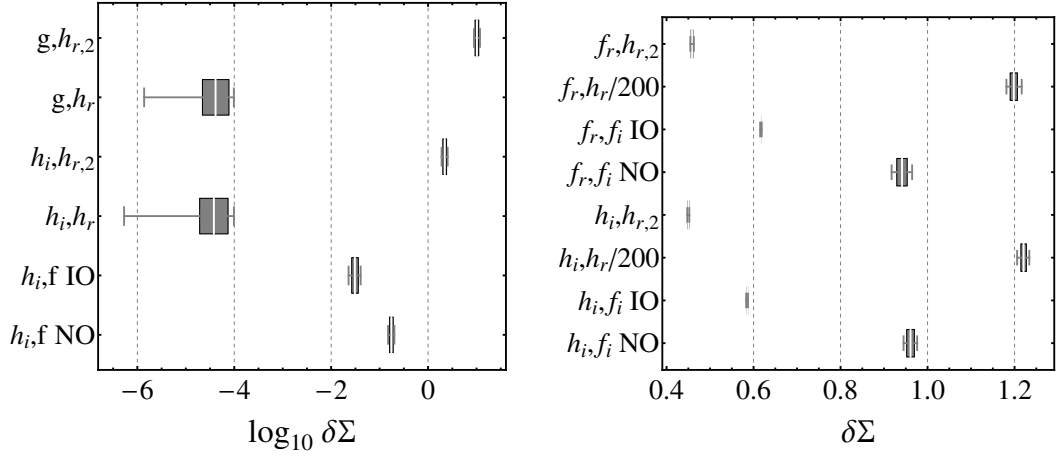


Figure E.2: Same as Fig. E.1 but for Mechanism II a-2 (left plot) and Mechanism II c-2 (right plot). In the left panel for $h_r = 0$ we rescaled the distribution by a factor 200 because the NLO corrections are important, as discussed in the main text, see Sec. 3.3.4.

to those obtained with the previous definition, however the relative goodness among the sum rules in the various cases is conserved.

For the sake of completeness we show our results for $\delta\Sigma$ obtained from our numerical scans. The results are shown in Figs E.1 and E.2 where we observe that the relative goodness of the different cases in each Mechanism is in agreement with the prediction of Chapter 3. In particular for Mechanism II a-2 (c-2) we observe that in the case of $h_i = f = 0$ ($h_i = f_i = 0$ and $f_r = f_i = 0$) IO has a smaller value of $\delta\Sigma$ with respect to NO.

F

Effective operators

We collect the operators that are relevant for the model discussed in Sec. 3.6.

F.1 Superpotential $\delta\mathcal{W}$

• NLO operators in $\delta\mathcal{W}_\nu$

We have six operators for $\delta\mathcal{W}_\nu$ at NLO

$$\frac{g_4^3}{\Lambda} \left\{ \phi_{\nu,5}^0 [(\phi_{\nu,5}\phi_{\nu,5})_{4_s}\phi_{\nu,3}]_5 \right\}_1 \quad \frac{g_{5_1}^3}{\Lambda} \left\{ \phi_{\nu,5}^0 [(\phi_{\nu,5}\phi_{\nu,5})_{5_s^1}\phi_{\nu,3}]_5 \right\}_1 \quad \frac{g_{5_2}^3}{\Lambda} \left\{ \phi_{\nu,5}^0 [(\phi_{\nu,5}\phi_{\nu,5})_{5_s^2}\phi_{\nu,3}]_5 \right\}_1 \quad (\text{F.1a})$$

$$\frac{g_4^{3'}}{\Lambda} \left\{ \phi_{\nu,5}^0 [(\phi_{\nu,5}\phi_{\nu,5})_{4_s}\phi_{\nu,3'}]_5 \right\}_1 \quad \frac{g_{5_1}^{3'}}{\Lambda} \left\{ \phi_{\nu,5}^0 [(\phi_{\nu,5}\phi_{\nu,5})_{5_s^1}\phi_{\nu,3'}]_5 \right\}_1 \quad \frac{g_{5_2}^{3'}}{\Lambda} \left\{ \phi_{\nu,5}^0 [(\phi_{\nu,5}\phi_{\nu,5})_{5_s^2}\phi_{\nu,3'}]_5 \right\}_1. \quad (\text{F.1b})$$

• NLO operators in $\delta\mathcal{W}_\ell$

We get twenty-eight operators with the pentaplet χ_5^0

$$\begin{aligned} & \frac{\tilde{a}_{1,5}^{55}}{\Lambda} \left\{ \chi_5^0 [(\tilde{\chi}_5\tilde{\chi}_5)_3\tilde{\varphi}_5]_5 \right\}_1 \quad \frac{\tilde{a}_{5_1,4}^{55}}{\Lambda} \left\{ \chi_5^0 [(\tilde{\chi}_5\tilde{\chi}_5)_{4_s}\tilde{\varphi}_5]_{5_1} \right\}_1 \quad \frac{\tilde{a}_{5_2,4}^{55}}{\Lambda} \left\{ \chi_5^0 [(\tilde{\chi}_5\tilde{\chi}_5)_{4_s}\tilde{\varphi}_5]_{5_2} \right\}_1 \\ & \frac{\tilde{a}_{5_1,5_1}^{55}}{\Lambda} \left\{ \chi_5^0 [(\tilde{\chi}_5\tilde{\chi}_5)_{5_s^1}\tilde{\varphi}_5]_{5_1} \right\}_1 \quad \frac{\tilde{a}_{5_2,5_1}^{55}}{\Lambda} \left\{ \chi_5^0 [(\tilde{\chi}_5\tilde{\chi}_5)_{5_s^2}\tilde{\varphi}_5]_{5_2} \right\}_1 \\ & \frac{\tilde{a}_{5_1,5_2}^{55}}{\Lambda} \left\{ \chi_5^0 [(\tilde{\chi}_5\tilde{\chi}_5)_{5_s^2}\tilde{\varphi}_5]_{5_1} \right\}_1 \quad \frac{\tilde{a}_{5_2,5_2}^{55}}{\Lambda} \left\{ \chi_5^0 [(\tilde{\chi}_5\tilde{\chi}_5)_{5_s^2}\tilde{\varphi}_5]_{5_2} \right\}_1 \end{aligned} \quad (\text{F.2a})$$

$$\begin{aligned} & \frac{a_{3,5}^3}{\Lambda} \left\{ \chi_5^0 [(\phi_{\nu,5}\phi_{\nu,3})_3\chi_5]_5 \right\}_1 \quad \frac{a_{3',5}^3}{\Lambda} \left\{ \chi_5^0 [(\phi_{\nu,5}\phi_{\nu,3})_{3'}\chi_5]_5 \right\}_1 \quad \frac{a_{4,5_1}^3}{\Lambda} \left\{ \chi_5^0 [(\phi_{\nu,5}\phi_{\nu,3})_4\chi_5]_{5_1} \right\}_1 \\ & \frac{a_{4,5_2}^3}{\Lambda} \left\{ \chi_5^0 [(\phi_{\nu,5}\phi_{\nu,3})_4\chi_5]_{5_2} \right\}_1 \quad \frac{a_{5,5_1}^3}{\Lambda} \left\{ \chi_5^0 [(\phi_{\nu,5}\phi_{\nu,3})_5\chi_5]_{5_1} \right\}_1 \quad \frac{a_{5,5_2}^3}{\Lambda} \left\{ \chi_5^0 [(\phi_{\nu,5}\phi_{\nu,3})_5\chi_5]_{5_2} \right\}_1 \end{aligned} \quad (\text{F.2b})$$

$$\begin{aligned} & \frac{a_{3,5}^{3'}}{\Lambda} \left\{ \chi_5^0 [(\phi_{\nu,5}\phi_{\nu,3'})_3\chi_5]_5 \right\}_1 \quad \frac{a_{3',5}^{3'}}{\Lambda} \left\{ \chi_5^0 [(\phi_{\nu,5}\phi_{\nu,3'})_{3'}\chi_5]_5 \right\}_1 \quad \frac{a_{4,5_1}^{3'}}{\Lambda} \left\{ \chi_5^0 [(\phi_{\nu,5}\phi_{\nu,3'})_4\chi_5]_{5_1} \right\}_1 \\ & \frac{a_{4,5_2}^{3'}}{\Lambda} \left\{ \chi_5^0 [(\phi_{\nu,5}\phi_{\nu,3'})_4\chi_5]_{5_2} \right\}_1 \quad \frac{a_{5,5_1}^{3'}}{\Lambda} \left\{ \chi_5^0 [(\phi_{\nu,5}\phi_{\nu,3'})_5\chi_5]_{5_1} \right\}_1 \quad \frac{a_{5,5_2}^{3'}}{\Lambda} \left\{ \chi_5^0 [(\phi_{\nu,5}\phi_{\nu,3'})_5\chi_5]_{5_2} \right\}_1 \end{aligned} \quad (\text{F.2c})$$

$$\begin{aligned} & \frac{\tilde{a}_{3,5}^{53'}}{\Lambda} \left\{ \chi_5^0 [(\tilde{\varphi}_5 \tilde{\chi}_{3'})_3 \chi_5]_5 \right\}_1 & \frac{\tilde{a}_{3',5}^{53'}}{\Lambda} \left\{ \chi_5^0 [(\tilde{\varphi}_5 \tilde{\chi}_{3'})_{3'} \chi_5]_5 \right\}_1 & \frac{\tilde{a}_{4,51}^{53'}}{\Lambda} \left\{ \chi_5^0 [(\tilde{\varphi}_5 \tilde{\chi}_{3'})_4 \chi_5]_{5^1} \right\}_1 \\ & \frac{\tilde{a}_{4,52}^{53'}}{\Lambda} \left\{ \chi_5^0 [(\tilde{\varphi}_5 \tilde{\chi}_{3'})_4 \chi_5]_{5^2} \right\}_1 & \frac{\tilde{a}_{5,51}^{53'}}{\Lambda} \left\{ \chi_5^0 [(\tilde{\varphi}_5 \tilde{\chi}_{3'})_5 \chi_5]_{5^1} \right\}_1 & \frac{\tilde{a}_{5,52}^{53'}}{\Lambda} \left\{ \chi_5^0 [(\tilde{\varphi}_5 \tilde{\chi}_{3'})_5 \chi_5]_{5^2} \right\}_1 \end{aligned} \quad (\text{F.2d})$$

$$\frac{\tilde{a}_1^{3'3'}}{\Lambda} \left\{ \chi_5^0 [(\tilde{\chi}_{3'} \tilde{\chi}_{3'})_1 \tilde{\chi}_5]_{5^2} \right\}_1 & \frac{\tilde{a}_{51}^{3'3'}}{\Lambda} \left\{ \chi_5^0 [(\tilde{\chi}_{3'} \tilde{\chi}_{3'})_5 \tilde{\chi}_{5^1}]_{5^1} \right\}_1 & \frac{\tilde{a}_{52}^{3'3'}}{\Lambda} \left\{ \chi_5^0 [(\tilde{\chi}_{3'} \tilde{\chi}_{3'})_5 \tilde{\chi}_{5^2}]_{5^2} \right\}_1. \quad (\text{F.2e})$$

We have sixteen operators with $\chi_{3'}^0$

$$\begin{aligned} & \frac{\tilde{b}_1^{3'}}{\Lambda} \left\{ \chi_{3'}^0 [(\tilde{\varphi}_5 \chi_5)_1 \tilde{\chi}_{3'}]_{3'} \right\}_1 & \frac{\tilde{b}_{3'}^{3'}}{\Lambda} \left\{ \chi_{3'}^0 [(\tilde{\varphi}_5 \chi_5)_{3'} \tilde{\chi}_{3'}]_{3'} \right\}_1 & \frac{\tilde{b}_{41}^{3'}}{\Lambda} \left\{ \chi_{3'}^0 [(\tilde{\varphi}_5 \chi_5)_{4_1} \tilde{\chi}_{3'}]_{3'} \right\}_1 \\ & \frac{\tilde{b}_{42}^{3'}}{\Lambda} \left\{ \chi_{3'}^0 [(\tilde{\varphi}_5 \chi_5)_{4_2} \tilde{\chi}_{3'}]_{3'} \right\}_1 & \frac{\tilde{b}_{51}^{3'}}{\Lambda} \left\{ \chi_{3'}^0 [(\tilde{\varphi}_5 \chi_5)_{5_1} \tilde{\chi}_{3'}]_{3'} \right\}_1 & \frac{\tilde{b}_{52}^{3'}}{\Lambda} \left\{ \chi_{3'}^0 [(\tilde{\varphi}_5 \chi_5)_{5_2} \tilde{\chi}_{3'}]_{3'} \right\}_1 \end{aligned} \quad (\text{F.3a})$$

$$\frac{b_4^5}{\Lambda} \left\{ \chi_{3'}^0 [(\varphi_5 \varphi_5)_{4_s} \varphi_5]_{3'} \right\}_1 & \frac{b_{51}^5}{\Lambda} \left\{ \chi_{3'}^0 [(\varphi_5 \varphi_5)_{5_s^1} \varphi_5]_{3'} \right\}_1 & \frac{b_{52}^5}{\Lambda} \left\{ \chi_{3'}^0 [(\varphi_5 \varphi_5)_{5_s^2} \varphi_5]_{3'} \right\}_1 \quad (\text{F.3b})$$

$$\frac{\tilde{b}_4^5}{\Lambda} \left\{ \chi_{3'}^0 [(\tilde{\chi}_5 \tilde{\chi}_5)_{4_s} \chi_5]_{3'} \right\}_1 & \frac{\tilde{b}_{51}^5}{\Lambda} \left\{ \chi_{3'}^0 [(\tilde{\chi}_5 \tilde{\chi}_5)_{5_s^1} \chi_5]_{3'} \right\}_1 & \frac{\tilde{b}_{52}^5}{\Lambda} \left\{ \chi_{3'}^0 [(\tilde{\chi}_5 \tilde{\chi}_5)_{5_s^2} \chi_5]_{3'} \right\}_1 \quad (\text{F.3c})$$

$$\frac{b_4^3}{\Lambda} \left\{ \chi_{3'}^0 [(\phi_{\nu,3} \chi_{3'})_4 \phi_{\nu,5}]_{3'} \right\}_1 & \frac{b_5^3}{\Lambda} \left\{ \chi_{3'}^0 [(\phi_{\nu,3} \chi_{3'})_5 \phi_{\nu,5}]_{3'} \right\}_1 \quad (\text{F.3d})$$

$$\frac{b_{3'}^{3'}}{\Lambda} \left\{ \chi_{3'}^0 [(\phi_{\nu,3'} \chi_{3'})_{3'} \phi_{\nu,5}]_{3'} \right\}_1 & \frac{b_5^{3'}}{\Lambda} \left\{ \chi_{3'}^0 [(\phi_{\nu,3'} \chi_{3'})_5 \phi_{\nu,5}]_{3'} \right\}_1. \quad (\text{F.3e})$$

In the case of χ_1^0 we have only seven non vanishing operators

$$\frac{c_{51}^5}{\Lambda} \left\{ \chi_1^0 [(\varphi_5 \varphi_5)_{5_s^1} \varphi_5]_1 \right\}_1 & \frac{c_{51}^5}{\Lambda} \left\{ \chi_1^0 [(\varphi_5 \varphi_5)_{5_s^2} \varphi_5]_1 \right\}_1 \quad (\text{F.4a})$$

$$\frac{\tilde{c}_{51}^5}{\Lambda} \left\{ \chi_1^0 [(\tilde{\chi}_5 \tilde{\chi}_5)_{5_s^1} \chi_5]_1 \right\}_1 & \frac{\tilde{c}_{51}^5}{\Lambda} \left\{ \chi_1^0 [(\tilde{\chi}_5 \tilde{\chi}_5)_{5_s^2} \chi_5]_1 \right\}_1 \quad (\text{F.4b})$$

$$\frac{c_5^3}{\Lambda} \left\{ \chi_1^0 [(\phi_{\nu,3} \chi_{3'})_5 \phi_{\nu,5}]_1 \right\}_1 \quad (\text{F.4c})$$

$$\frac{c_5^{3'}}{\Lambda} \left\{ \chi_1^0 [(\phi_{\nu,3'} \chi_{3'})_5 \phi_{\nu,5}]_1 \right\}_1 \quad (\text{F.4d})$$

$$\frac{\tilde{c}_{3'}^{3'}}{\Lambda} \left\{ \chi_1^0 [(\chi_5 \tilde{\varphi}_5)_{3'} \tilde{\chi}_{3'}]_1 \right\}_1. \quad (\text{F.4e})$$

We get twelve operators with the pentaplet $\tilde{\chi}_5^0$

$$\begin{aligned} & \frac{\tilde{d}_{3,5}^3}{\Lambda} \left\{ \tilde{\chi}_5^0 [(\phi_{\nu,5} \phi_{\nu,3})_3 \tilde{\chi}_5]_5 \right\}_1 & \frac{\tilde{d}_{3',5}^3}{\Lambda} \left\{ \tilde{\chi}_5^0 [(\phi_{\nu,5} \phi_{\nu,3})_{3'} \tilde{\chi}_5]_5 \right\}_1 & \frac{\tilde{d}_{4,51}^3}{\Lambda} \left\{ \tilde{\chi}_5^0 [(\phi_{\nu,5} \phi_{\nu,3})_4 \tilde{\chi}_5]_{5^1} \right\}_1 \\ & \frac{\tilde{d}_{4,52}^3}{\Lambda} \left\{ \tilde{\chi}_5^0 [(\phi_{\nu,5} \phi_{\nu,3})_4 \tilde{\chi}_5]_{5^2} \right\}_1 & \frac{\tilde{d}_{5,51}^3}{\Lambda} \left\{ \tilde{\chi}_5^0 [(\phi_{\nu,5} \phi_{\nu,3})_5 \tilde{\chi}_5]_{5^1} \right\}_1 & \frac{\tilde{d}_{5,52}^3}{\Lambda} \left\{ \tilde{\chi}_5^0 [(\phi_{\nu,5} \phi_{\nu,3})_5 \tilde{\chi}_5]_{5^2} \right\}_1 \end{aligned} \quad (\text{F.5a})$$

$$\begin{aligned} & \frac{\tilde{d}_{3,5}^{3'}}{\Lambda} \left\{ \tilde{\chi}_5^0 [(\phi_{\nu,5} \phi_{\nu,3'})_3 \tilde{\chi}_5]_5 \right\}_1 & \frac{\tilde{d}_{3',5}^{3'}}{\Lambda} \left\{ \tilde{\chi}_5^0 [(\phi_{\nu,5} \phi_{\nu,3'})_{3'} \tilde{\chi}_5]_5 \right\}_1 & \frac{\tilde{d}_{4,51}^{3'}}{\Lambda} \left\{ \tilde{\chi}_5^0 [(\phi_{\nu,5} \phi_{\nu,3'})_4 \tilde{\chi}_5]_{5^1} \right\}_1 \\ & \frac{\tilde{d}_{4,52}^{3'}}{\Lambda} \left\{ \tilde{\chi}_5^0 [(\phi_{\nu,5} \phi_{\nu,3'})_4 \tilde{\chi}_5]_{5^2} \right\}_1 & \frac{\tilde{d}_{5,51}^{3'}}{\Lambda} \left\{ \tilde{\chi}_5^0 [(\phi_{\nu,5} \phi_{\nu,3'})_5 \tilde{\chi}_5]_{5^1} \right\}_1 & \frac{\tilde{d}_{5,52}^{3'}}{\Lambda} \left\{ \tilde{\chi}_5^0 [(\phi_{\nu,5} \phi_{\nu,3'})_5 \tilde{\chi}_5]_{5^2} \right\}_1. \end{aligned} \quad (\text{F.5b})$$

We have seven operators with $\chi_{3'}^0$

$$\frac{b_4^5}{\Lambda} \left\{ \chi_{3'}^0 [(\varphi_5 \varphi_5)_{4_s} \varphi_5]_{3'} \right\}_1 & \frac{b_{51}^5}{\Lambda} \left\{ \chi_{3'}^0 [(\varphi_5 \varphi_5)_{5_s^1} \varphi_5]_{3'} \right\}_1 & \frac{b_{52}^5}{\Lambda} \left\{ \chi_{3'}^0 [(\varphi_5 \varphi_5)_{5_s^2} \varphi_5]_{3'} \right\}_1 \quad (\text{F.6a})$$

$$\frac{b_4^3}{\Lambda} \left\{ \chi_{3'}^0 [(\phi_{\nu,3} \chi_{3'})_4 \phi_{\nu,5}]_{3'} \right\}_1 \quad \frac{b_5^3}{\Lambda} \left\{ \chi_{3'}^0 [(\phi_{\nu,3} \chi_{3'})_5 \phi_{\nu,5}]_{3'} \right\}_1 \quad (\text{F.6b})$$

$$\frac{b_{3'}^3}{\Lambda} \left\{ \chi_{3'}^0 [(\phi_{\nu,3'} \chi_{3'})_{3'} \phi_{\nu,5}]_{3'} \right\}_1 \quad \frac{b_5^3}{\Lambda} \left\{ \chi_{3'}^0 [(\phi_{\nu,3'} \chi_{3'})_5 \phi_{\nu,5}]_{3'} \right\}_1. \quad (\text{F.6c})$$

We have seven operators with $\tilde{\chi}_{3'}^0$,

$$\frac{\tilde{e}_4^5}{\Lambda} \left\{ \tilde{\chi}_{3'}^0 [(\tilde{\varphi}_5 \tilde{\varphi}_5)_{4_s} \tilde{\varphi}_5]_{3'} \right\}_1 \quad \frac{\tilde{e}_{5_1}^5}{\Lambda} \left\{ \tilde{\chi}_{3'}^0 [(\tilde{\varphi}_5 \tilde{\varphi}_5)_{5_1^s} \tilde{\varphi}_5]_{3'} \right\}_1 \quad \frac{\tilde{e}_{5_2}^5}{\Lambda} \left\{ \tilde{\chi}_{3'}^0 [(\tilde{\varphi}_5 \tilde{\varphi}_5)_{5_2^s} \tilde{\varphi}_5]_{3'} \right\}_1 \quad (\text{F.7a})$$

$$\frac{\tilde{e}_4^3}{\Lambda} \left\{ \tilde{\chi}_{3'}^0 [(\phi_{\nu,3} \tilde{\chi}_{3'})_4 \phi_{\nu,5}]_{3'} \right\}_1 \quad \frac{\tilde{e}_5^3}{\Lambda} \left\{ \tilde{\chi}_{3'}^0 [(\phi_{\nu,3} \tilde{\chi}_{3'})_5 \phi_{\nu,5}]_{3'} \right\}_1 \quad (\text{F.7b})$$

$$\frac{\tilde{e}_{3'}^3}{\Lambda} \left\{ \tilde{\chi}_{3'}^0 [(\phi_{\nu,3'} \tilde{\chi}_{3'})_{3'} \phi_{\nu,5}]_{3'} \right\}_1 \quad \frac{\tilde{e}_{5'}^3}{\Lambda} \left\{ \tilde{\chi}_{3'}^0 [(\phi_{\nu,3'} \tilde{\chi}_{3'})_5 \phi_{\nu,5}]_{3'} \right\}_1. \quad (\text{F.7c})$$

In the case of $\tilde{\chi}_1^0$ we have only four non vanishing operators

$$\frac{\tilde{f}_{5_1}^5}{\Lambda} \left\{ \tilde{\chi}_1^0 [(\tilde{\varphi}_5 \tilde{\varphi}_5)_{5_1^s} \tilde{\varphi}_5]_1 \right\}_1 \quad \frac{\tilde{f}_{5_2}^5}{\Lambda} \left\{ \tilde{\chi}_1^0 [(\tilde{\varphi}_5 \tilde{\varphi}_5)_{5_2^s} \tilde{\varphi}_5]_1 \right\}_1 \quad (\text{F.8a})$$

$$\frac{\tilde{f}_5^3}{\Lambda} \left\{ \tilde{\chi}_1^0 [(\phi_{\nu,3} \tilde{\chi}_{3'})_5 \phi_{\nu,5}]_1 \right\}_1 \quad (\text{F.8b})$$

$$\frac{\tilde{f}_{5'}^3}{\Lambda} \left\{ \tilde{\chi}_1^0 [(\phi_{\nu,3'} \tilde{\chi}_{3'})_5 \phi_{\nu,5}]_1 \right\}_1. \quad (\text{F.8c})$$

F.2 Operators for charged lepton masses

With three flavons we have four operators with $E^c \otimes L \sim \mathbf{1}$

$$y_{3,3}^1 H_d \left\{ (E^c L)_1 \left[\left(\frac{\phi_{\nu,5} \varphi_5}{\Lambda^2} \right)_3 \frac{\phi_{\nu,3}}{\Lambda} \right]_1 \right\}_1 \quad y_{3',3'}^1 H_d \left\{ (E^c L)_1 \left[\left(\frac{\phi_{\nu,5} \varphi_5}{\Lambda^2} \right)_{3'} \frac{\phi_{\nu,3'}}{\Lambda} \right]_1 \right\}_1 \quad (\text{F.9a})$$

$$\tilde{y}_{5_1}^1 H_d \left\{ (E^c L)_1 \left[\left(\frac{\tilde{\varphi}_5 \tilde{\varphi}_5}{\Lambda^2} \right)_{5_1^s} \frac{\tilde{\chi}_5}{\Lambda} \right]_1 \right\}_1 \quad \tilde{y}_{5_2}^1 H_d \left\{ (E^c L)_1 \left[\left(\frac{\tilde{\varphi}_5 \tilde{\varphi}_5}{\Lambda^2} \right)_{5_2^s} \frac{\tilde{\chi}_5}{\Lambda} \right]_1 \right\}_1. \quad (\text{F.9b})$$

We also have

$$y_{3,1}^3 H_d \left\{ (E^c L)_3 \left[\left(\frac{\phi_{\nu,5} \varphi_5}{\Lambda^2} \right)_1 \frac{\phi_{\nu,3}}{\Lambda} \right]_3 \right\}_1 \quad y_{3,3}^3 H_d \left\{ (E^c L)_3 \left[\left(\frac{\phi_{\nu,5} \varphi_5}{\Lambda^2} \right)_3 \frac{\phi_{\nu,3}}{\Lambda} \right]_3 \right\}_1$$

$$y_{3,5_1}^3 H_d \left\{ (E^c L)_3 \left[\left(\frac{\phi_{\nu,5} \varphi_5}{\Lambda^2} \right)_{5_1} \frac{\phi_{\nu,3}}{\Lambda} \right]_3 \right\}_1 \quad y_{3,5_2}^3 H_d \left\{ (E^c L)_3 \left[\left(\frac{\phi_{\nu,5} \varphi_5}{\Lambda^2} \right)_{5_2} \frac{\phi_{\nu,3}}{\Lambda} \right]_3 \right\}_1 \quad (\text{F.10a})$$

$$y_{3',4_s}^3 H_d \left\{ (E^c L)_3 \left[\left(\frac{\phi_{\nu,5} \varphi_5}{\Lambda^2} \right)_{4_s} \frac{\phi_{\nu,3'}}{\Lambda} \right]_3 \right\}_1 \quad y_{3',4_a}^3 H_d \left\{ (E^c L)_3 \left[\left(\frac{\phi_{\nu,5} \varphi_5}{\Lambda^2} \right)_{4_a} \frac{\phi_{\nu,3'}}{\Lambda} \right]_3 \right\}_1$$

$$y_{3',5_1}^3 H_d \left\{ (E^c L)_3 \left[\left(\frac{\phi_{\nu,5} \varphi_5}{\Lambda^2} \right)_{5_1} \frac{\phi_{\nu,3'}}{\Lambda} \right]_3 \right\}_1 \quad y_{3',5_2}^3 H_d \left\{ (E^c L)_3 \left[\left(\frac{\phi_{\nu,5} \varphi_5}{\Lambda^2} \right)_{5_2} \frac{\phi_{\nu,3'}}{\Lambda} \right]_3 \right\}_1 \quad (\text{F.10b})$$

$$\tilde{y}_4^3 H_d \left\{ (E^c L)_3 \left[\left(\frac{\tilde{\varphi}_5 \tilde{\varphi}_5}{\Lambda^2} \right)_{4_s} \frac{\tilde{\chi}_5}{\Lambda} \right]_3 \right\}_1 \quad \tilde{y}_{5_1}^3 H_d \left\{ (E^c L)_3 \left[\left(\frac{\tilde{\varphi}_5 \tilde{\varphi}_5}{\Lambda^2} \right)_{5_1^s} \frac{\tilde{\chi}_5}{\Lambda} \right]_3 \right\}_1$$

$$\tilde{y}_{5_2}^3 H_d \left\{ (E^c L)_3 \left[\left(\frac{\tilde{\varphi}_5 \tilde{\varphi}_5}{\Lambda^2} \right)_{5_2^s} \frac{\tilde{\chi}_5}{\Lambda} \right]_3 \right\}_1. \quad (\text{F.10c})$$

therefore we have eleven operators with $E^c \otimes L \sim \mathbf{3}$. We also have nineteen operators with $E^c \otimes L \sim \mathbf{5}$

$$\begin{aligned}
& y_{3,3_a}^5 H_d \left\{ (E^c L)_5 \left[\left(\frac{\phi_{\nu,5}\varphi_5}{\Lambda^2} \right)_3 \frac{\phi_{\nu,3}}{\Lambda} \right]_5 \right\}_1 & y_{3,3'_a}^5 H_d \left\{ (E^c L)_5 \left[\left(\frac{\phi_{\nu,5}\varphi_5}{\Lambda^2} \right)_{3'} \frac{\phi_{\nu,3}}{\Lambda} \right]_5 \right\}_1 \\
& y_{3,4_s}^5 H_d \left\{ (E^c L)_5 \left[\left(\frac{\phi_{\nu,5}\varphi_5}{\Lambda^2} \right)_{4_s} \frac{\phi_{\nu,3}}{\Lambda} \right]_5 \right\}_1 & y_{3,4_a}^5 H_d \left\{ (E^c L)_5 \left[\left(\frac{\phi_{\nu,5}\varphi_5}{\Lambda^2} \right)_{4_a} \frac{\phi_{\nu,3}}{\Lambda} \right]_5 \right\}_1 \\
& y_{3,5_1}^5 H_d \left\{ (E^c L)_5 \left[\left(\frac{\phi_{\nu,5}\varphi_5}{\Lambda^2} \right)_{5_1} \frac{\phi_{\nu,3}}{\Lambda} \right]_5 \right\}_1 & y_{3,5_2}^5 H_d \left\{ (E^c L)_5 \left[\left(\frac{\phi_{\nu,5}\varphi_5}{\Lambda^2} \right)_{5_2} \frac{\phi_{\nu,3}}{\Lambda} \right]_5 \right\}_1 \quad (F.11a)
\end{aligned}$$

$$\begin{aligned}
& y_{3',3_a}^5 H_d \left\{ (E^c L)_5 \left[\left(\frac{\phi_{\nu,5}\varphi_5}{\Lambda^2} \right)_3 \frac{\phi_{\nu,3'}}{\Lambda} \right]_5 \right\}_1 & y_{3',3'_a}^5 H_d \left\{ (E^c L)_5 \left[\left(\frac{\phi_{\nu,5}\varphi_5}{\Lambda^2} \right)_{3'} \frac{\phi_{\nu,3'}}{\Lambda} \right]_5 \right\}_1 \\
& y_{3',4_s}^5 H_d \left\{ (E^c L)_5 \left[\left(\frac{\phi_{\nu,5}\varphi_5}{\Lambda^2} \right)_{4_s} \frac{\phi_{\nu,3'}}{\Lambda} \right]_5 \right\}_1 & y_{3',4_a}^5 H_d \left\{ (E^c L)_5 \left[\left(\frac{\phi_{\nu,5}\varphi_5}{\Lambda^2} \right)_{4_a} \frac{\phi_{\nu,3'}}{\Lambda} \right]_5 \right\}_1 \\
& y_{3',5_1}^5 H_d \left\{ (E^c L)_5 \left[\left(\frac{\phi_{\nu,5}\varphi_5}{\Lambda^2} \right)_{5_1} \frac{\phi_{\nu,3'}}{\Lambda} \right]_5 \right\}_1 & y_{3',5_2}^5 H_d \left\{ (E^c L)_5 \left[\left(\frac{\phi_{\nu,5}\varphi_5}{\Lambda^2} \right)_{5_2} \frac{\phi_{\nu,3'}}{\Lambda} \right]_5 \right\}_1 \quad (F.11b)
\end{aligned}$$

$$\begin{aligned}
& \tilde{y}_{5_1,4}^5 H_d \left\{ (E^c L)_1 \left[\left(\frac{\tilde{\varphi}_5 \tilde{\varphi}_5}{\Lambda^2} \right)_{4_s} \frac{\tilde{\chi}_5}{\Lambda} \right]_{5_1} \right\}_1 & \tilde{y}_{5_2,4}^3 H_d \left\{ (E^c L)_1 \left[\left(\frac{\tilde{\varphi}_5 \tilde{\varphi}_5}{\Lambda^2} \right)_{4_s} \frac{\tilde{\chi}_5}{\Lambda} \right]_{5_2} \right\}_1 \\
& \tilde{y}_{5_1,5_1}^5 H_d \left\{ (E^c L)_5 \left[\left(\frac{\tilde{\varphi}_5 \tilde{\varphi}_5}{\Lambda^2} \right)_{5_1^!} \frac{\tilde{\chi}_5}{\Lambda} \right]_{5_1} \right\}_1 & \tilde{y}_{5_2,5_1}^3 H_d \left\{ (E^c L)_5 \left[\left(\frac{\tilde{\varphi}_5 \tilde{\varphi}_5}{\Lambda^2} \right)_{5_1^!} \frac{\tilde{\chi}_5}{\Lambda} \right]_{5_2} \right\}_1 \\
& \tilde{y}_{5_1,5_2}^5 H_d \left\{ (E^c L)_5 \left[\left(\frac{\tilde{\varphi}_5 \tilde{\varphi}_5}{\Lambda^2} \right)_{5_1^!} \frac{\tilde{\chi}_5}{\Lambda} \right]_{5_1} \right\}_1 & \tilde{y}_{5_2,5_2}^3 H_d \left\{ (E^c L)_5 \left[\left(\frac{\tilde{\varphi}_5 \tilde{\varphi}_5}{\Lambda^2} \right)_{5_2^!} \frac{\tilde{\chi}_5}{\Lambda} \right]_{5_2} \right\}_1 \\
& & \tilde{y}_1^3 H_d \left\{ (E^c L)_5 \left[\left(\frac{\tilde{\varphi}_5 \tilde{\varphi}_5}{\Lambda^2} \right)_{1_s} \frac{\tilde{\chi}_5}{\Lambda} \right]_5 \right\}_1 \quad (F.11c)
\end{aligned}$$



LED mass eigenstates and matrix elements

In this Appendix we want to discuss how to compute the mass eigenstates for the neutrinos in the LED framework. We use the same conventions of Ref. [184]. The mass matrix follows Eq. (4.7), and can be written as

$$RM_j = \lim_{k \rightarrow \infty} \begin{pmatrix} m_j R & 0 & 0 & \dots & 0 \\ \sqrt{2} m_j R & 1 & 0 & \dots & 0 \\ \sqrt{2} m_j R & 0 & 2 & \dots & 0 \\ & & & \ddots & \\ \sqrt{2} m_j R & 0 & 0 & \dots & k \end{pmatrix} = \lim_{k \rightarrow \infty} \begin{pmatrix} 2^{-1/2} \xi_j & 0 & 0 & \dots & 0 \\ \xi_j & 1 & 0 & \dots & 0 \\ \xi_j & 0 & 2 & \dots & 0 \\ & & & \ddots & \\ \xi_j & 0 & 0 & \dots & k \end{pmatrix} \quad (\text{G.1})$$

where we used the definition of ξ_j , given in Eq. (4.11), $\xi_j \equiv \sqrt{2} m_j R$. Notice that the matrix M_j has two indices in the KK subspace. We can define two vectors, for mass and flavour eigenstates

$$\boldsymbol{\nu}_\alpha \equiv \begin{pmatrix} \nu_\alpha^{(0)} \\ \nu_\alpha^{(1)} \\ \vdots \end{pmatrix} \quad \boldsymbol{\nu}_i \equiv \begin{pmatrix} \nu_i^{(0)} \\ \nu_i^{(1)} \\ \vdots \end{pmatrix} \quad \alpha = e, \mu, \tau \quad i = 1, 2, 3. \quad (\text{G.2})$$

We can also define a unitary matrix to rotate the two vectors using the relation

$$\boldsymbol{\nu}_\alpha = \mathbf{U}_{\alpha i} \boldsymbol{\nu}_i \quad (\text{G.3})$$

so \mathbf{U} is

$$\mathbf{U}_{\alpha i} \equiv \begin{pmatrix} U_{\alpha i} & 0 \\ 0 & R_{\alpha i} \end{pmatrix} \quad (\text{G.4})$$

where the matrices U and R are defined by Eq. (4.6). To diagonalize the mass matrix M we need two rotations, so we need to diagonalize both $M^\dagger M$ and MM^\dagger . Since we are interested only on SM fields we can diagonalize only the product $M^\dagger M$.

The neutrino evolution equation is

$$i \frac{d}{dt} \boldsymbol{\nu}_{i,L} = \mathcal{H}_{ij} \boldsymbol{\nu}_{i,L} \quad (\text{G.5})$$

where the hamiltonian \mathcal{H} is

$$\mathcal{H}_{ij} = \frac{\delta_{ij}}{2E_\nu} M_i^\dagger M_j + \left(\mathbf{U}^\dagger \mathbf{V} \mathbf{U} \right)_{ij}. \quad (\text{G.6})$$

Here \mathbf{V} is the matter matrix, defined as

$$\mathbf{V} = \delta_{\alpha\beta} \mathcal{V}_\alpha = \text{diag}\{\mathcal{V}_e, \mathcal{V}_\mu, \mathcal{V}_\tau\}. \quad (\text{G.7})$$

As the matrix \mathbf{U} , the matter matrix \mathbf{V} lives in a 2×2 subspace; in fact we have

$$\mathcal{V}_{\alpha i} = \begin{pmatrix} V_{\alpha i} & 0 \\ 0 & 0 \end{pmatrix} = \begin{pmatrix} \delta_{\alpha e} V_{CC} + V_{NC} & 0 \\ 0 & 0 \end{pmatrix} \quad (\text{G.8})$$

where the interaction with matter produces the potentials $V_{CC} = \sqrt{2}G_F n_e$ and $V_{NC} = -2^{-1/2}G_F n_n$. With this definition we can reformulate the hamiltonian \mathcal{H} as the sum of two contributions, the mass $M^\dagger M$ and the mixing \mathbb{V} , defined as

$$\mathbb{V}_{ij} \equiv 2R^2 E_\nu \sum_\alpha U_{\alpha i}^* U_{\alpha j} V_\alpha. \quad (\text{G.9})$$

The squared mass matrix is then

$$\mathbb{M}^2 \equiv R^2 M_j^\dagger M_j = \lim_{k \rightarrow \infty} \begin{pmatrix} (k + 1/2)\xi_j^2 & \xi_j & 2\xi_j & \dots & k\xi_j \\ \xi_j & 1 & 0 & \dots & 0 \\ 2\xi_j & 0 & 4 & \dots & 0 \\ & & & \ddots & \\ k\xi_j & 0 & 0 & \dots & k^2 \end{pmatrix} \quad (\text{G.10})$$

that can be written as

$$\mathbb{M}^2 = \lim_{k \rightarrow \infty} \begin{pmatrix} \eta_j & \mathbf{v}_j^T \\ \mathbf{v}_j & \mathbf{K}^2 \end{pmatrix} \quad (\text{G.11})$$

with the following definitions

$$\eta_j = \left(k + \frac{1}{2}\right)\xi_j^2 \quad \mathbf{v}_j = \xi_j \begin{pmatrix} 1 \\ 2 \\ \vdots \\ k \end{pmatrix} \quad \mathbf{K}^2 = \text{diag}\{1, 4, 9, \dots, k^2\}. \quad (\text{G.12})$$

We can separate the zero mode and the KK modes using a rescaling hamiltonian $\overline{\mathcal{H}}$ such that

$$\overline{\mathcal{H}} = \begin{pmatrix} \left(\eta_j \delta^{ij} + \mathbb{V}_{ij}\right)_{00} & \left(\mathbf{v}_j^T\right)_{0k} \\ \left(\mathbf{v}_j\right)_{k'0} & \left(\mathbf{K}^2\right)_{kk'} \end{pmatrix} \quad (\text{G.13})$$

where the subscript indices live in KK space. To diagonalize this hamiltonian, *i.e.* to solve the secular problem, we need to solve

$$\det \left(2R^2 E_\nu \overline{\mathcal{H}} - \lambda^2 \mathbb{1} \right) = 0. \quad (\text{G.14})$$

We can use the Gauss algorithm for triangularization. We find for a finite k

$$\left[\left(X_{00} - \lambda^2 \right) - \sum_{n=1}^k \frac{X_{0n} X_{n0}}{X_{nn} - \lambda^2} \right] \prod_{n=1}^k \left(X_{nn} - \lambda^2 \right) = 0 \quad (\text{G.15})$$

where $X = 2R^2 E_\nu \overline{\mathcal{H}}$ and it has three indices in mass space, one over KK modes and two in flavour space

$$X_{00} = 2R^2 E_\nu \left[\delta^{ij} \left(k + \frac{1}{2} \right) \xi_j^2 + \mathbb{V}_{ij} \right] \quad (\text{G.16a})$$

$$X_{0k} = X_{k0} = \delta^{ij} 2R^2 E_\nu k \quad (\text{G.16b})$$

$$X_{kk} = \delta^{ij} 2R^2 E_\nu k^2 \quad (\text{G.16c})$$

therefore Eq. (G.15) becomes

$$2R^2 E_\nu \left[\delta^{ij} \left(k + \frac{1}{2} \right) \xi_j^2 - \lambda^2 + \mathbb{V}_{ij} - \delta^{ij} \xi_j^2 \sum_{n=1}^k \frac{n^2}{n^2 - \lambda^2} \right] \prod_{n=1}^k (n^2 - \lambda^2) = 0. \quad (\text{G.17})$$

Using the fact that $k = \sum_{n=1}^k 1$ we have

$$\left[\mathbb{V}_{ij} + \delta^{ij} \xi_j^2 \left(\frac{1}{2} - \lambda^2 - \sum_{n=1}^k \frac{\lambda^2}{n^2 - \lambda^2} \right) \right] \prod_{n=1}^k (n^2 - \lambda^2) = 0. \quad (\text{G.18})$$

Taking the limit $k \rightarrow \infty$ and using the Taylor series for the cotangent function

$$- \sum_{n=1}^{\infty} \frac{\lambda^2}{n^2 - \lambda^2} = \frac{1}{2} \left(\pi \lambda \cot(\pi \lambda) - 1 \right) \quad (\text{G.19})$$

we find that the secular problem is the same as to solve

$$\det T = 0 \quad T_{ij} \equiv \mathbb{V}_{ij} + \delta^{ij} \xi_j^2 \left(\pi \lambda \cot(\pi \lambda) - \lambda^2 \right). \quad (\text{G.20})$$

The solution of this equation gives the mass of KK modes; in fact we have that $\lambda_j^{(k)} = Rm_j^{(k)}$. To find the eigenvectors $w_j^{(k)}$ we have to solve

$$\mathcal{H} w_j^{(k)} = \left(\lambda_j^{(k)} \right)^2 w_j^{(k)}. \quad (\text{G.21})$$

We can define the component of the vector as

$$\left(w_i^{(k)} \right)_j^{(k')} \equiv W_{ij}^{(kk')} \quad (\text{G.22})$$

so for $k' = 0$ we have

$$\eta_j W_{ij}^{(k0)} + \sum_{n=1}^k n \xi_j W_{ij}^{(kn)} + \sum_{p=1}^3 \mathbb{V}_{jp} W_{ip}^{(k0)} - \left(\lambda_i^{(k)} \right)^2 W_{ij}^{(k0)} = 0 \quad (\text{G.23})$$

and for $k' \neq 0$

$$k' \xi_j W_{ij}^{(k0)} - \left[k'^2 - \left(\lambda_i^{(k)} \right)^2 \right] W_{ij}^{(kk')} = 0. \quad (\text{G.24})$$

We notice that the equation for the matrix element of transition between the zero mode and the KK is of the form of Eq. (G.18), so in the limit $k \rightarrow \infty$ we have, for each value of $\lambda_i^{(k)}$, the equation

$$\sum_{p=1}^3 T_{ip} W_{ip}^{(k0)} = 0. \quad (\text{G.25})$$

To obtain the correct normalization for the eigenvectors $w_i^{(k)}$ we need to use the condition

$$w_i^{(k)} \cdot w_j^{(k')} = \delta^{ij} \delta^{kk'} \quad (\text{G.26})$$

thus

$$\sum_{p=1}^3 W_{ip}^{(k0)} W_{jp}^{(k'0)} = \delta^{ij} \delta^{kk'}. \quad (\text{G.27})$$

In this way we must solve the following equation

$$\sum_{p=1}^3 \left(W_{ip}^{(k0)} \right)^2 \left[1 + \xi_p^2 \left(\frac{\pi^2 \cot^2 \pi \lambda_p^{(k)}}{4} - \frac{\pi \cot \pi \lambda_p^{(k)}}{4 \lambda_p^{(k)}} + \frac{\pi^2}{4} \right) \right] = 1 \quad (\text{G.28})$$

that we obtained using Eq. (G.25) into the normalization condition Eq. (G.27). It is also possible to find the non diagonal element in the KK space with the same procedure

$$W_j^{(kk')} = \frac{k \xi_j}{\lambda_i^{(k')^2 - k^2} } W_i^{0k} \quad (\text{G.29})$$

the details of the calculation can be found in Ref. [182].

G.1 Oscillation in vacuum

In vacuum we can set $\mathbb{V}_{ij} = 0$, in this way

$$\det T = -\frac{\left(\lambda_j^{(k)} \right)^3}{8} \prod_{j=1}^3 \left(2 \lambda_j^{(k)} - \pi \xi_j^2 \cot \pi \lambda_j^{(k)} \right) = 0. \quad (\text{G.30})$$

This is a transcendental equation, but we can use a perturbative expansion in the region of parameter space $R^{-1} \gg m_j$, which means $\xi_j \ll 1$.

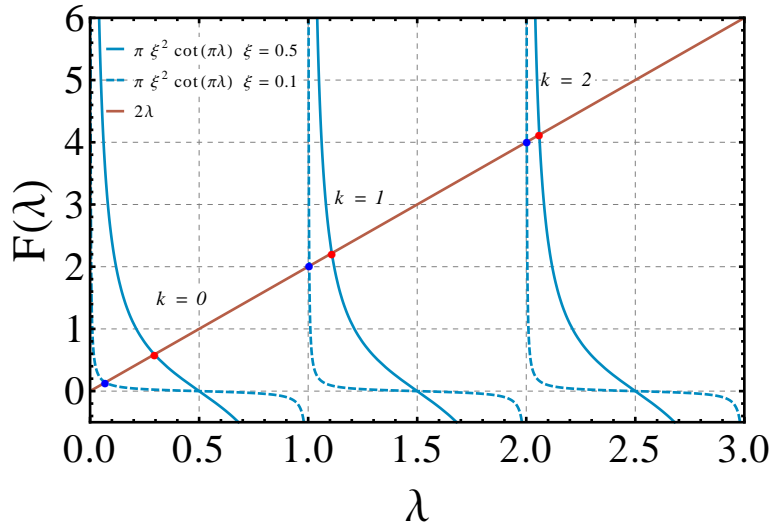


Figure G.1: Numerical solution of Eq. (G.30). The KK tower are the dots in the plot for different values of ξ .

First of all we can write the master equation in the form

$$\pi \lambda_j^{(k)} = \arctan \frac{\pi \xi_j^2}{2 \lambda_j^{(k)}} + k \pi \quad k \in \mathbb{N}. \quad (\text{G.31})$$

Using the fact that $\arctan x \simeq x$ we can rewrite as

$$\lambda_j^{(k)} = \frac{\xi_j^2}{2\lambda_j^{(k)}} + k + \mathcal{O}(\xi_j^3) \quad k \in \mathbb{N}. \quad (\text{G.32})$$

Now we assume a perturbative expansion in the form

$$\lambda_j^{(k)} = \lambda_j^{\bar{0}} + \xi_j \lambda_j^{\bar{1}} + \xi_j^2 \lambda_j^{\bar{2}} + \mathcal{O}(\xi_j^3) \quad (\text{G.33})$$

where the bar over the number means the perturbative order, not the KK index. In this way we get

$$\lambda_j^{(0)} = \frac{\xi_j}{\sqrt{2}} \left[1 - \frac{\pi^2 \xi_j^2}{12} + \frac{11 \pi^4 \xi_j^4}{16 \cdot 90} + \mathcal{O}(\xi_j^6) \right] \quad (\text{G.34a})$$

$$\lambda_j^{(k \geq 1)} = k + \frac{\xi_j^2}{2k} - \frac{\xi_j^4}{4k^3} + \mathcal{O}(\xi_j^3). \quad (\text{G.34b})$$

Using the Eq. (G.28) we obtain

$$W_j^{(00)} = 1 - \frac{\pi^2 \xi_j^2}{12} + \frac{7 \pi^4 \xi_j^4}{16 \cdot 90} + \mathcal{O}(\xi_j^6) \quad (\text{G.35a})$$

$$W_j^{(0k \geq 1)} = \frac{\xi_j}{k} - \frac{3\xi_j^3}{4k^3} + \mathcal{O}(\xi_j^4) \quad (\text{G.35b})$$

In Tab. G.1 we report some values for the eigenvalues and for the matrix elements of transition evaluated numerically and using the approximate relations at first order in ξ_j . It is clear that the relations are in good agreement with the true numerical values.

	k	$\xi = 0.5$		$\xi = 0.1$		$\xi = 0.05$	
$\lambda_j^{(k)}$	0	0.2949	0.2809	0.0701	0.0701	0.0353	0.0353
	1	1.1084	1.1250	1.0050	1.0050	1.0013	1.0013
	2	2.0600	2.0625	2.0025	2.0025	2.0004	2.0006
	3	3.0409	3.0417	3.0017	3.0016	3.0003	3.0004
	4	4.0309	4.0312	4.0013	4.0013	4.0003	4.0003
$W_j^{(0k)}$	0	0.8262	0.7944	0.9918	0.9912	0.9979	0.9979
	1	0.4072	0.5000	0.0992	0.1000	0.0499	0.0500
	2	0.2351	0.2500	0.0499	0.0500	0.0171	0.0250
	3	0.1620	0.1667	0.0342	0.0333	0.0134	0.0167
	4	0.1230	0.1250	0.0250	0.0250	0.0125	0.0125

Table G.1: Values of $\lambda_j^{(k)}$ and $W_j^{(0k)}$ calculated numerically using the software Mathematica (left columns) and with the perturbative relations at order ξ_j of Eq. (G.34) and (G.35) (right columns).

G.2 Sum rule for probability

In our code we use some test for the probability we evaluated numerically. In particular we used the fact that

$$\sum_{\alpha} \mathcal{P}(\nu_{\alpha} \rightarrow \nu_{\beta}) = \sum_{\beta} \mathcal{P}(\nu_{\alpha} \rightarrow \nu_{\beta}) = 1 \quad (\text{G.36})$$

as in SM. We can easily test the relation in vacuum starting from Eq. (4.10). At order ξ^2 we have

$$\begin{aligned} \sum_{\beta} \mathcal{P}(\nu_{\alpha} \rightarrow \nu_{\beta}) &= \sum_{\beta} \sum_{i,j} \sum_{k,k'=0}^{\infty} U_{\alpha j} U_{\alpha i}^* U_{\beta i} U_{\beta j}^* |W_j^{(k)}|^2 |W_i^{(k')}|^2 \exp \left[i \frac{(\lambda_j^{(k)})^2 - (\lambda_i^{(k')})^2}{2R^2 E} L \right] = \\ &= \sum_j \sum_{k,k'=0}^{\infty} |U_{\alpha j}|^2 |W_j^{(k)}|^2 |W_j^{(k')}|^2. \end{aligned} \quad (\text{G.37})$$

where we used the fact that $U_{\text{PMNS}} U_{\text{PMNS}}^{\dagger} = U_{\text{PMNS}}^{\dagger} U_{\text{PMNS}} = \mathbb{1}$. Using the expression reported in Eq. (G.35) we obtain

$$\sum_{\beta} \mathcal{P}(\nu_{\alpha} \rightarrow \nu_{\beta}) \simeq \sum_j \left[\left(1 - \frac{\pi^2}{6} \xi_j^2 \right) + \xi_j^2 \sum_{k=1}^{\infty} \frac{1}{k^2} \right] \left[\left(1 - \frac{\pi^2}{6} \xi_j^2 \right) + \xi_j^2 \sum_{k'=1}^{\infty} \frac{1}{k'^2} \right] |U_{\alpha j}|^2. \quad (\text{G.38})$$

Now we recognize that the Riemann zeta function is defined for $\text{Re}(s) > 1$ as

$$\zeta(s) \equiv \sum_{k=1}^{\infty} \frac{1}{k^s} \quad \zeta(2) = \frac{\pi^2}{6} \quad (\text{G.39})$$

thus we get at order ξ^2 the validity of Eq. (G.36). Similar relations hold for the sum over initial states. It is easy to understand that the relation is verified also at the next order in the same way because $\zeta(4) = \pi^4/90$.

H

NSI oscillation probabilities

In this Appendix we report the main formulae for the oscillation probability in the context of NSI scenario. For the experiments of interest for this Thesis we can neglect the matter effect in the propagation of the neutrino states. Hence we can write the Hamiltonian of (4.19) approximatively as

$$H_{\alpha\beta} = \frac{1}{2E_\nu} \left[U_{\alpha j} \begin{pmatrix} 0 & 0 & 0 \\ 0 & \Delta m_{21}^2 & 0 \\ 0 & 0 & \Delta m_{21}^2 \end{pmatrix}_{jk} (U^\dagger)_{k\beta} \right] \quad (\text{H.1})$$

where the U is the PMNS matrix in the Standard parametrization. From the (4.19) and (H.1) expanding for small ε (the absolute value of the NSI coupling) and neglecting terms of order $\mathcal{O}(\varepsilon^2)$, the oscillation probability for the disappearance channel at T2K is simplified as

$$\begin{aligned} \mathcal{P}(\nu_\mu \rightarrow \nu_\mu) &= \mathcal{P}_{\text{SM}}(\nu_\mu \rightarrow \nu_\mu) + 2|\varepsilon_{\mu\mu}^s| \cos \phi_{\mu\mu}^s + 2|\varepsilon_{\mu\mu}^d| \cos \phi_{\mu\mu}^d + \\ &- \left[2|\varepsilon_{\mu\mu}^s| \cos \phi_{\mu\mu}^s + 2|\varepsilon_{\mu\mu}^d| \cos \phi_{\mu\mu}^d \right] \sin^2 2\theta_{23} \sin^2 \left[\frac{\Delta m_{31}^2 L}{4E_\nu} \right] + \\ &- 2 \left(|\varepsilon_{\mu\tau}^s| \cos \phi_{\mu\tau}^s + |\varepsilon_{\tau\mu}^d| \cos \phi_{\tau\mu}^d \right) \cos 2\theta_{23} \sin 2\theta_{23} \sin^2 \left[\frac{\Delta m_{31}^2 L}{4E_\nu} \right] + \\ &+ \left(|\varepsilon_{\mu\tau}^s| \sin \phi_{\mu\tau}^s + |\varepsilon_{\tau\mu}^d| \sin \phi_{\tau\mu}^d \right) \sin 2\theta_{23} \sin \left[\frac{\Delta m_{31}^2 L}{4E_\nu} \right] + \mathcal{O} \left(\frac{\Delta m_{21}^2}{\Delta m_{31}^2} \right) + \mathcal{O}(\sin \theta_{13}\varepsilon) + \mathcal{O}(\varepsilon^2) \end{aligned} \quad (\text{H.2})$$

where the SM part is discussed in (A.1).

Notice that in this formula exhibits zero distance effects that modify the probability with respect to the SM also for $L = 0$.

Using the same procedure it is possible to obtain the appearance probability

$$\begin{aligned} \mathcal{P}(\nu_\mu \rightarrow \nu_e) &= \sin^2 \theta_{23} \sin^2 2\theta_{13} \sin^2 \left(\frac{\Delta m_{31}^2 L}{4E_\nu} \right) + \\ &- 2 \sin 2\theta_{12} \sin 2\theta_{23} \sin \left(\frac{\Delta m_{21}^2 L}{4E_\nu} \right) \sin \theta_{13} \cos^2 \theta_{13} \sin^2 \left(\frac{\Delta m_{31}^2 L}{4E_\nu} \right) \sin \delta + \mathcal{P}_0 + \mathcal{P}_1 \end{aligned} \quad (\text{H.3})$$

where $\mathcal{P}_{0,1}$ are the leading and next to leading effect of NSI parameters evaluated with perturbative procedure

$$\begin{aligned}
\mathcal{P}_0 = & -4|\varepsilon_{\mu e}^s| \sin \theta_{13} \sin \theta_{23} \cos(\delta + \phi_{\mu e}^s) \sin^2 \left(\frac{\Delta m_{31}^2 L}{4E_\nu} \right) + \\
& -4|\varepsilon_{\mu e}^s| \sin \theta_{13} \sin \theta_{23} \sin(\delta + \phi_{\mu e}^s) \sin \left(\frac{\Delta m_{31}^2 L}{4E_\nu} \right) \cos \left(\frac{\Delta m_{31}^2 L}{4E_\nu} \right) + \\
& -4\varepsilon_{e\mu} \sin \theta_{13} \sin \theta_{23} \cos(\delta - \phi_{e\mu}) \cos 2\theta_{23} \sin^2 \left(\frac{\Delta m_{31}^2 L}{4E_\nu} \right) + \\
& -4\varepsilon_{e\mu} \sin \theta_{13} \sin \theta_{23} \sin(\delta - \phi_{e\mu}) \sin \left(\frac{\Delta m_{31}^2 L}{4E_\nu} \right) \cos \left(\frac{\Delta m_{31}^2 L}{4E_\nu} \right) + \\
& + 8\varepsilon_{e\tau} \sin \theta_{13} \sin^2 \theta_{23} \cos \theta_{23} \cos(\delta - \phi_{e\tau}) \sin^2 \left(\frac{\Delta m_{31}^2 L}{4E_\nu} \right) + \mathcal{O}(\varepsilon_{ee}^d \sin^2 \theta_{13}) + \\
& + \mathcal{O}(\varepsilon_{\mu\tau}^s \sin^2 \theta_{13}) + \mathcal{O}(\varepsilon_{\mu\mu}^s \sin^2 \theta_{13}) + \mathcal{O}(\varepsilon_{\mu e}^s \sin^3 \theta_{13}) + \mathcal{O}(\varepsilon_{e\mu(e\tau)} \sin^3 \theta_{13}) + \mathcal{O}(\varepsilon^2) \quad (\text{H.4a})
\end{aligned}$$

$$\begin{aligned}
\mathcal{P}_1 = & -|\varepsilon_{\mu e}^s| \sin 2\theta_{12} \cos \theta_{23} \sin \phi_{\mu e}^s \frac{\Delta m_{21}^2 L}{2E_\nu} + \\
& + 2\varepsilon_{e\mu} \sin 2\theta_{12} \sin^2 \theta_{23} \cos \theta_{23} \cos \phi_{e\mu} \frac{\Delta m_{21}^2 L}{4E_\nu} \sin \left(\frac{\Delta m_{31}^2 L}{2E_\nu} \right) + \\
& + \varepsilon_{e\mu} \sin 2\theta_{12} \cos \theta_{23} \sin \phi_{e\mu} \frac{\Delta m_{21}^2 L}{2E_\nu} \left[1 - 2 \sin^2 \theta_{23} \sin^2 \left(\frac{\Delta m_{31}^2 L}{4E_\nu} \right) \right] + \\
& + 2\varepsilon_{e\tau} \sin 2\theta_{12} \sin \theta_{23} \cos^2 \theta_{23} \cos \phi_{e\tau} \frac{\Delta m_{21}^2 L}{4E_\nu} \sin \left(\frac{\Delta m_{31}^2 L}{2E_\nu} \right) + \\
& - 2\varepsilon_{e\tau} \sin 2\theta_{12} \sin \theta_{23} \cos^2 \theta_{23} \sin \phi_{e\tau} \frac{\Delta m_{21}^2 L}{2E_\nu} \sin^2 \left(\frac{\Delta m_{31}^2 L}{4E_\nu} \right) + \mathcal{O} \left(\varepsilon \sin \theta_{13} \frac{\Delta m_{21}^2 L}{4E_\nu} \right) + \mathcal{O}(\varepsilon^2) \quad (\text{H.4b})
\end{aligned}$$

For DB the relevant formula is

$$\begin{aligned}
\mathcal{P}(\bar{\nu}_e \rightarrow \bar{\nu}_e) = & 1 - \sin^2 2\theta_{13} \sin^2 \left(\frac{\Delta m_{31}^2 L}{4E_\nu} \right) + 4\varepsilon_{ee} \sin \phi_{ee} + \\
& - 4[\varepsilon_{e\mu} \sin 2\theta_{13} \sin \theta_{23} \cos 2\theta_{13} \cos(\delta - \phi_{e\mu})] \sin^2 \left(\frac{\Delta m_{31}^2 L}{4E_\nu} \right) + \\
& - 4[\varepsilon_{e\tau} \sin 2\theta_{13} \sin \theta_{23} \cos 2\theta_{13} \cos(\delta - \phi_{e\tau})] \sin^2 \left(\frac{\Delta m_{31}^2 L}{4E_\nu} \right) + \mathcal{O}(\varepsilon^2) \quad (\text{H.5})
\end{aligned}$$

where in the first line the zero-distance term is proportional to ε_{ee} .

Bibliography

- [1] W. PAULI. *Dear radioactive ladies and gentlemen*. Phys. Today **31N9**, 27, (1978).
- [2] C. L. COWAN, F. REINES, F. B. HARRISON, H. W. KRUSE and A. D. MCGUIRE. *Detection of the free neutrino: A Confirmation*. Science **124**, 103-104, (1956).
- [3] E. MAJORANA. *Theory of the Symmetry of Electrons and Positrons*. Nuovo Cim. **14**, 171-184, (1937).
- [4] B. PONTECORVO. *Mesonium and anti-mesonium*. Sov. Phys. JETP **6**, 429, (1957). [Zh. Eksp. Teor. Fiz.33,549(1957)].
- [5] B. PONTECORVO. *Inverse beta processes and nonconservation of lepton charge*. Sov. Phys. JETP **7**, 172-173, (1958). [Zh. Eksp. Teor. Fiz.34,247(1957)].
- [6] Z. MAKI, M. NAKAGAWA and S. SAKATA. *Remarks on the unified model of elementary particles*. Prog. Theor. Phys. **28**, 870-880, (1962).
- [7] B. PONTECORVO. *Neutrino Experiments and the Problem of Conservation of Leptonic Charge*. Sov. Phys. JETP **26**, 984-988, (1968). [Zh. Eksp. Teor. Fiz.53,1717(1967)].
- [8] C. GIUNTI and C. W. KIM. *Fundamentals of Neutrino Physics and Astrophysics*. Oxford, UK: Univ. Pr., 710 p (2007).
- [9] S. P. MIKHEEV and A. YU. SMIRNOV. *Resonance Amplification of Oscillations in Matter and Spectroscopy of Solar Neutrinos*. Sov. J. Nucl. Phys. **42**, 913-917, (1985). [Yad. Fiz.42,1441(1985)].
- [10] L. WOLFENSTEIN. *Neutrino Oscillations in Matter*. Phys. Rev. **D17**, 2369-2374, (1978).
- [11] R. DAVIS, JR., D. S. HARMER and K. C. HOFFMAN. *Search for neutrinos from the sun*. Phys. Rev. Lett. **20**, 1205-1209, (1968).
- [12] Y. FUKUDA *et al.* [KAMIOKANDE COLLABORATION]. *Solar neutrino data covering solar cycle 22*. Phys. Rev. Lett. **77**, 1683-1686, (1996).
- [13] Y. FUKUDA *et al.* [SUPER-KAMIOKANDE COLLABORATION]. *Evidence for oscillation of atmospheric neutrinos*. Phys. Rev. Lett. **81**, 1562-1567, (1998). hep-ex/9807003.
- [14] Y. FUKUDA *et al.* [SUPER-KAMIOKANDE COLLABORATION]. *Study of the atmospheric neutrino flux in the multi-GeV energy range*. Phys. Lett. **B436**, 33-41, (1998). hep-ex/9805006.
- [15] B. T. CLEVELAND, T. DAILY, R. DAVIS, JR., J. R. DISTEL, K. LANDE, C. K. LEE, P. S. WILDENHAIN and J. ULLMAN. *Measurement of the solar electron neutrino flux with the Homestake chlorine detector*. Astrophys. J. **496**, 505-526, (1998).
- [16] J. N. ABDURASHITOV *et al.* [SAGE COLLABORATION]. *Solar neutrino flux measurements by the Soviet-American Gallium Experiment (SAGE) for half the 22 year solar cycle*. J. Exp. Theor. Phys. **95**, 181-193, (2002). [Zh. Eksp. Teor. Fiz.122,211(2002)], astro-ph/0204245.
- [17] W. HAMPSEL *et al.* [GALLEX COLLABORATION]. *GALLEX solar neutrino observations: Results for GALLEX IV*. Phys. Lett. **B447**, 127-133, (1999).
- [18] S. FUKUDA *et al.* [SUPER-KAMIOKANDE COLLABORATION]. *Determination of solar neutrino oscillation parameters using 1496 days of Super-Kamiokande I data*. Phys. Lett. **B539**, 179-187, (2002). hep-ex/0205075.
- [19] Q. R. AHMAD *et al.* [SNO COLLABORATION]. *Measurement of the rate of $\nu_e + d \rightarrow p + p + e^-$ interactions produced by ^8B solar neutrinos at the Sudbury Neutrino Observatory*. Phys. Rev. Lett. **87**, 071301, (2001). nucl-ex/0106015.
- [20] Q. R. AHMAD *et al.* [SNO COLLABORATION]. *Direct evidence for neutrino flavor transformation from neutral current interactions in the Sudbury Neutrino Observatory*. Phys. Rev. Lett. **89**, 011301, (2002). nucl-ex/0204008.
- [21] Q. R. AHMAD *et al.* [SNO COLLABORATION]. *Measurement of day and night neutrino energy spectra at SNO and constraints on neutrino mixing parameters*. Phys. Rev. Lett. **89**, 011302, (2002). nucl-ex/0204009.
- [22] C. ARPESELLA *et al.* [BOREXINO COLLABORATION]. *First real time detection of Be-7 solar neutrinos by Borexino*. Phys. Lett. **B658**, 101-108, (2008). arXiv:0708.2251.
- [23] G. BELLINI *et al.* [BOREXINO COLLABORATION]. *Measurement of the solar ^8B neutrino rate with a liquid scintillator target and 3 MeV energy threshold in the Borexino detector*. Phys. Rev. **D82**, 033006, (2010). arXiv:0808.2868.

- [24] G. BELLINI *et al.* [BOREXINO COLLABORATION]. *Precision measurement of the ^7Be solar neutrino interaction rate in Borexino.* Phys. Rev. Lett. **107**, 141302, (2011). [arXiv:1104.1816](#).
- [25] K. EGUCHI *et al.* [KAMLAND COLLABORATION]. *First results from KamLAND: Evidence for reactor anti-neutrino disappearance.* Phys. Rev. Lett. **90**, 021802, (2003). [hep-ex/0212021](#).
- [26] T. ARAKI *et al.* [KAMLAND COLLABORATION]. *Measurement of neutrino oscillation with KamLAND: Evidence of spectral distortion.* Phys. Rev. Lett. **94**, 081801, (2005). [hep-ex/0406035](#).
- [27] S. ABE *et al.* [KAMLAND COLLABORATION]. *Precision Measurement of Neutrino Oscillation Parameters with KamLAND.* Phys. Rev. Lett. **100**, 221803, (2008). [arXiv:0801.4589](#).
- [28] G. L. FOGLI, E. LISI, A. MARRONE and A. PALAZZO. *Global analysis of three-flavor neutrino masses and mixings.* Prog. Part. Nucl. Phys. **57**, 742-795, (2006). [hep-ph/0506083](#).
- [29] Y. FUKUDA *et al.* [KAMIOKANDE COLLABORATION]. *Atmospheric muon-neutrino / electron-neutrino ratio in the multiGeV energy range.* Phys. Lett. **B335**, 237-245, (1994).
- [30] Y. ASHIE *et al.* [SUPER-KAMIOKANDE COLLABORATION]. *A Measurement of atmospheric neutrino oscillation parameters by SUPER-KAMIOKANDE I.* Phys. Rev. **D71**, 112005, (2005). [hep-ex/0501064](#).
- [31] M. H. AHN *et al.* [K2K COLLABORATION]. *Indications of neutrino oscillation in a 250 km long baseline experiment.* Phys. Rev. Lett. **90**, 041801, (2003). [hep-ex/0212007](#).
- [32] E. ALIU *et al.* [K2K COLLABORATION]. *Evidence for muon neutrino oscillation in an accelerator-based experiment.* Phys. Rev. Lett. **94**, 081802, (2005). [hep-ex/0411038](#).
- [33] D. G. MICHAEL *et al.* [MINOS COLLABORATION]. *Observation of muon neutrino disappearance with the MINOS detectors and the NuMI neutrino beam.* Phys. Rev. Lett. **97**, 191801, (2006). [hep-ex/0607088](#).
- [34] K. ABE *et al.* [T2K COLLABORATION]. *Precise Measurement of the Neutrino Mixing Parameter θ_{23} from Muon Neutrino Disappearance in an Off-Axis Beam.* Phys. Rev. Lett. **112**(18), 181801, (2014). [arXiv:1403.1532](#).
- [35] K. ABE *et al.* [T2K COLLABORATION]. *Observation of Electron Neutrino Appearance in a Muon Neutrino Beam.* Phys. Rev. Lett. **112**, 061802, (2014). [arXiv:1311.4750](#).
- [36] P. ADAMSON *et al.* [NOvA COLLABORATION]. *First measurement of muon-neutrino disappearance in NOvA.* Phys. Rev. **D93**(5), 051104, (2016). [arXiv:1601.05037](#).
- [37] P. ADAMSON *et al.* [NOvA COLLABORATION]. *First measurement of electron neutrino appearance in NOvA.* Phys. Rev. Lett. **116**(15), 151806, (2016). [arXiv:1601.05022](#).
- [38] N. AGAFONOVA *et al.* [OPERA COLLABORATION]. *Observation of a first ν_τ candidate in the OPERA experiment in the CNGS beam.* Phys. Lett. **B691**, 138-145, (2010). [arXiv:1006.1623](#).
- [39] Y. ABE *et al.* [DOUBLE CHOOZ COLLABORATION]. *Reactor electron antineutrino disappearance in the Double Chooz experiment.* Phys. Rev. **D86**, 052008, (2012). [arXiv:1207.6632](#).
- [40] F. P. AN *et al.* [DAYA BAY COLLABORATION]. *Improved Measurement of Electron Antineutrino Disappearance at Daya Bay.* Chin. Phys. **C37**, 011001, (2013). [arXiv:1210.6327](#).
- [41] J. K. AHN *et al.* [RENO COLLABORATION]. *Observation of Reactor Electron Antineutrino Disappearance in the RENO Experiment.* Phys. Rev. Lett. **108**, 191802, (2012). [arXiv:1204.0626](#).
- [42] K. ABE *et al.* [T2HK COLLABORATION]. *Letter of Intent: The Hyper-Kamiokande Experiment – Detector Design and Physics Potential –* (2011). [arXiv:1109.3262](#).
- [43] T. AKIRI *et al.* [LBNE COLLABORATION]. *The 2010 Interim Report of the Long-Baseline Neutrino Experiment Collaboration Physics Working Groups* (2011). [arXiv:1110.6249](#).
- [44] Z. DJURCIC *et al.* [JUNO COLLABORATION]. *JUNO Conceptual Design Report* (2015). [arXiv:1508.07166](#).
- [45] M. C. GONZALEZ-GARCIA, M. MALTONI and T. SCHWETZ. *Updated fit to three neutrino mixing: status of leptonic CP violation.* JHEP **1411**, 052, (2014). [arXiv:1409.5439](#).
- [46] F. CAPOZZI, E. LISI, A. MARRONE, D. MONTANINO and A. PALAZZO. *Neutrino masses and mixings: Status of known and unknown 3ν parameters.* Nucl. Phys. **B908**, 218-234, (2016). [arXiv:1601.07777](#).
- [47] D. V. FORERO, M. TORTOLA and J. W. F. VALLE. *Neutrino oscillations refitted.* Phys. Rev. **D90**(9), 093006, (2014). [arXiv:1405.7540](#).
- [48] J. BERGSTROM, M. C. GONZALEZ-GARCIA, M. MALTONI and T. SCHWETZ. *Bayesian global analysis of neutrino oscillation data.* JHEP **1509**, 200, (2015). [arXiv:1507.04366](#).
- [49] V. M. LOBASHEV. *The search for the neutrino mass by direct method in the tritium beta-decay and perspectives of study it in the project KATRIN.* Nucl. Phys. **A719**, 153-160, (2003).
- [50] A. OSIPOWICZ *et al.* [KATRIN COLLABORATION]. *KATRIN: A Next generation tritium beta decay experiment with sub-eV sensitivity for the electron neutrino mass. Letter of intent* (2001). [hep-ex/0109033](#).
- [51] S. MERTENS [KATRIN COLLABORATION]. *Status of the KATRIN Experiment and Prospects to Search for keV-mass Sterile Neutrinos in Tritium β -decay.* Phys. Procedia **61**, 267-273, (2015).

- [52] J. LESGOURGUES and S. PASTOR. *Neutrino mass from Cosmology*. Adv. High Energy Phys. **2012**, 608515, (2012). [arXiv:1212.6154](#).
- [53] P. A. R. ADE *et al.* [PLANCK COLLABORATION]. *Planck 2015 results. XIII. Cosmological parameters*. Astron. Astrophys. **594**, A13, (2016). [arXiv:1502.01589](#).
- [54] R. LAURELIS *et al.* [EUCLID COLLABORATION]. *Euclid Definition Study Report* (2011). [arXiv:1110.3193](#).
- [55] L. AMENDOLA *et al.* [EUCLID THEORY WORKING GROUP COLLABORATION]. *Cosmology and fundamental physics with the Euclid satellite*. Living Rev. Rel. **16**, 6, (2013). [arXiv:1206.1225](#).
- [56] W. RODEJOHANN. *Neutrino-less Double Beta Decay and Particle Physics*. Int. J. Mod. Phys. **E20**, 1833-1930, (2011). [arXiv:1106.1334](#).
- [57] W. RODEJOHANN. *Neutrinoless double beta decay and neutrino physics*. J. Phys. **G39**, 124008, (2012). [arXiv:1206.2560](#).
- [58] A. GIULIANI and A. POVES. *Neutrinoless Double-Beta Decay*. Adv. High Energy Phys. **2012**, 857016, (2012).
- [59] S. DELL'ORO, S. MARCOCCI, M. VIEL and F. VISSANI. *Neutrinoless double beta decay: 2015 review*. Adv. High Energy Phys. **2016**, 2162659, (2016). [arXiv:1601.07512](#).
- [60] A. S. BARABASH. *Double Beta Decay: Historical Review of 75 Years of Research*. Phys. Atom. Nucl. **74**, 603-613, (2011). [arXiv:1104.2714](#).
- [61] M. AGOSTINI *et al.* [GERDA COLLABORATION]. *Results on Neutrinoless Double- β Decay of ^{76}Ge from Phase I of the GERDA Experiment*. Phys. Rev. Lett. **111**(12), 122503, (2013). [arXiv:1307.4720](#).
- [62] H. V. KLAPDOR-KLEINGROTHAUS. *Neutrino mass from laboratory: Contribution of double beta decay to the neutrino mass matrix*. Nucl. Phys. Proc. Suppl. **100**, 309-313, (2001). [,309(2000)], [hep-ph/0102276](#).
- [63] C. E. AALSETH *et al.* *Recent results of the IGEX Ge-76 double-beta decay experiment*. Phys. Atom. Nucl. **63**, 1225-1228, (2000). [Yad. Fiz.63,1299(2000)].
- [64] A. S. BARABASH [NEMO COLLABORATION]. *NEMO 3 double beta decay experiment: Latest results*. J. Phys. Conf. Ser. **173**, 012008, (2009). [arXiv:0807.2336](#).
- [65] M. AUGER *et al.* [EXO-200 COLLABORATION]. *Search for Neutrinoless Double-Beta Decay in ^{136}Xe with EXO-200*. Phys. Rev. Lett. **109**, 032505, (2012). [arXiv:1205.5608](#).
- [66] A. GANDO *et al.* [KAMLAND-ZEN COLLABORATION]. *Search for Majorana Neutrinos near the Inverted Mass Hierarchy Region with KamLAND-Zen*. Phys. Rev. Lett. **117**(8), 082503, (2016). [arXiv:1605.02889](#).
- [67] H. ISHIMORI, T. KOBAYASHI, H. OHKI, Y. SHIMIZU, H. OKADA and M. TANIMOTO. *Non-Abelian Discrete Symmetries in Particle Physics*. Prog. Theor. Phys. Suppl. **183**, 1-163, (2010). [arXiv:1003.3552](#).
- [68] G. ALTARELLI and F. FERUGLIO. *Discrete Flavor Symmetries and Models of Neutrino Mixing*. Rev. Mod. Phys. **82**, 2701-2729, (2010). [arXiv:1002.0211](#).
- [69] S. F. KING and C. LUHN. *Neutrino Mass and Mixing with Discrete Symmetry*. Rept.Prog.Phys. **76**, 056201, (2013). [arXiv:1301.1340](#).
- [70] W. GRIMUS and P. O. LUDL. *Finite flavour groups of fermions*. J. Phys. **A45**, 233001, (2012). [arXiv:1110.6376](#).
- [71] F. FERUGLIO, C. HAGEDORN and R. ZIEGLER. *Lepton Mixing Parameters from Discrete and CP Symmetries*. JHEP **1307**, 027, (2013). [arXiv:1211.5560](#).
- [72] M. HOLTHAUSEN, M. LINDNER and M. A. SCHMIDT. *CP and Discrete Flavour Symmetries*. JHEP **1304**, 122, (2013). [arXiv:1211.6953](#).
- [73] G.-J. DING, S. F. KING and A. J. STUART. *Generalised CP and A_4 Family Symmetry*. JHEP **1312**, 006, (2013). [arXiv:1307.4212](#).
- [74] F. FERUGLIO, C. HAGEDORN and R. ZIEGLER. *A realistic pattern of lepton mixing and masses from S_4 and CP*. Eur. Phys. J. **C74**, 2753, (2014). [arXiv:1303.7178](#).
- [75] G.-J. DING, S. F. KING, C. LUHN and A. J. STUART. *Spontaneous CP violation from vacuum alignment in S_4 models of leptons*. JHEP **1305**, 084, (2013). [arXiv:1303.6180](#).
- [76] I. GIRARDI, A. MERONI, S. T. PETCOV and M. SPINRATH. *Generalised geometrical CP violation in a T' lepton flavour model*. JHEP **1402**, 050, (2014). [arXiv:1312.1966](#).
- [77] S.-J. RONG. *Lepton mixing patterns from the group $\Sigma(36 \times 3)$ with the generalized CP* (2016). [arXiv:1604.08482](#).
- [78] G.-J. DING and Y.-L. ZHOU. *Lepton mixing parameters from $\Delta(48)$ family symmetry and generalised CP*. JHEP **1406**, 023, (2014). [arXiv:1404.0592](#).
- [79] G.-J. DING and S. F. KING. *Generalized CP and $\Delta(96)$ family symmetry*. Phys. Rev. **D89**(9), 093020, (2014). [arXiv:1403.5846](#).
- [80] C. HAGEDORN, A. MERONI and E. MOLINARO. *Lepton mixing from $\Delta(3n^2)$ and $\Delta(6n^2)$ and CP*. Nucl. Phys. **B891**, 499-557, (2015). [arXiv:1408.7118](#).

- [81] G.-J. DING, S. F. KING and T. NEDER. *Generalised CP and $\Delta(6n^2)$ family symmetry in semi-direct models of leptons*. JHEP **1412**, 007, (2014). [arXiv:1409.8005](#).
- [82] S. F. KING and T. NEDER. *Lepton mixing predictions including Majorana phases from $\Delta(6n^2)$ flavour symmetry and generalised CP*. Phys. Lett. **B736**, 308-316, (2014). [arXiv:1403.1758](#).
- [83] C.-C. LI, C.-Y. YAO and G.-J. DING. *Lepton Mixing Predictions from Infinite Group Series $D_{9n,3n}^{(1)}$ with Generalized CP*. JHEP **1605**, 007, (2016). [arXiv:1601.06393](#).
- [84] S. F. KING. *Models of Neutrino Mass, Mixing and CP Violation*. J. Phys. **G42**, 123001, (2015). [arXiv:1510.02091](#).
- [85] A. DI IURA, C. HAGEDORN and D. MELONI. *Lepton mixing from the interplay of the alternating group A_5 and CP*. JHEP **1508**, 037, (2015). [arXiv:1503.04140](#).
- [86] C.-C. LI and G.-J. DING. *Lepton Mixing in A_5 Family Symmetry and Generalized CP*. JHEP **1505**, 100, (2015). [arXiv:1503.03711](#).
- [87] P. BALLETT, S. PASCOLI and J. TURNER. *Mixing angle and phase correlations from A_5 with generalized CP and their prospects for discovery*. Phys. Rev. **D92**(9), 093008, (2015). [arXiv:1503.07543](#).
- [88] R. M. FONSECA and W. GRIMUS. *Classification of lepton mixing matrices from finite residual symmetries*. JHEP **09**, 033, (2014). [arXiv:1405.3678](#).
- [89] P. F. HARRISON and W. G. SCOTT. *Symmetries and generalizations of tri - bimaximal neutrino mixing*. Phys. Lett. **B535**, 163-169, (2002). [hep-ph/0203209](#).
- [90] P. F. HARRISON and W. G. SCOTT. *μ - τ reflection symmetry in lepton mixing and neutrino oscillations*. Phys. Lett. **B547**, 219-228, (2002). [hep-ph/0210197](#).
- [91] X. G. HE and A. ZEE. *Some simple mixing and mass matrices for neutrinos*. Phys. Lett. **B560**, 87-90, (2003). [hep-ph/0301092](#).
- [92] F. VISSANI. *A Study of the scenario with nearly degenerate Majorana neutrinos* (1997). [hep-ph/9708483](#).
- [93] V. D. BARGER, S. PAKVASA, T. J. WEILER and K. WHISNANT. *Bimaximal mixing of three neutrinos*. Phys. Lett. **B437**, 107-116, (1998). [hep-ph/9806387](#).
- [94] A. J. BALTZ, A. S. GOLDBABER and M. GOLDBABER. *The Solar neutrino puzzle: An Oscillation solution with maximal neutrino mixing*. Phys. Rev. Lett. **81**, 5730-5733, (1998). [hep-ph/9806540](#).
- [95] A. DATTA, F.-S. LING and P. RAMOND. *Correlated hierarchy, Dirac masses and large mixing angles*. Nucl. Phys. **B671**, 383-400, (2003). [hep-ph/0306002](#).
- [96] Y. KAJIYAMA, M. RAIDAL and A. STRUMIA. *The Golden ratio prediction for the solar neutrino mixing*. Phys. Rev. **D76**, 117301, (2007). [arXiv:0705.4559](#).
- [97] L. L. EVERETT and A. J. STUART. *Icosahedral A_5 Family Symmetry and the Golden Ratio Prediction for Solar Neutrino Mixing*. Phys. Rev. **D79**, 085005, (2009). [arXiv:0812.1057](#).
- [98] F. FERUGLIO and A. PARIS. *The Golden Ratio Prediction for the Solar Angle from a Natural Model with A_5 Flavour Symmetry*. JHEP **03**, 101, (2011). [arXiv:1101.0393](#).
- [99] W. RODEJOHANN. *Unified Parametrization for Quark and Lepton Mixing Angles*. Phys. Lett. **B671**, 267-271, (2009). [arXiv:0810.5239](#).
- [100] A. ADULPRAVITCHAI, A. BLUM and W. RODEJOHANN. *Golden Ratio Prediction for Solar Neutrino Mixing*. New J. Phys. **11**, 063026, (2009). [arXiv:0903.0531](#).
- [101] C. H. ALBRIGHT, A. DUECK and W. RODEJOHANN. *Possible Alternatives to Tri-bimaximal Mixing*. Eur. Phys. J. **C70**, 1099-1110, (2010). [arXiv:1004.2798](#).
- [102] J. E. KIM and M.-S. SEO. *Quark and lepton mixing angles with a dodeca-symmetry*. JHEP **02**, 097, (2011). [arXiv:1005.4684](#).
- [103] T. OHLSSON and G. SEIDL. *A Flavor symmetry model for bilarge leptonic mixing and the lepton masses*. Nucl. Phys. **B643**, 247-279, (2002). [hep-ph/0206087](#).
- [104] C. S. LAM. *Symmetry of Lepton Mixing*. Phys. Lett. **B656**, 193-198, (2007). [arXiv:0708.3665](#).
- [105] C. S. LAM. *Determining Horizontal Symmetry from Neutrino Mixing*. Phys. Rev. Lett. **101**, 121602, (2008). [arXiv:0804.2622](#).
- [106] C. S. LAM. *The Unique Horizontal Symmetry of Leptons*. Phys. Rev. **D78**, 073015, (2008). [arXiv:0809.1185](#).
- [107] E. MA. *Neutrino mass matrix from S_4 symmetry*. Phys. Lett. **B632**, 352-356, (2006). [hep-ph/0508231](#).
- [108] R. DE ADELHART TOOROP, F. FERUGLIO and C. HAGEDORN. *Finite Modular Groups and Lepton Mixing*. Nucl. Phys. **B858**, 437-467, (2012). [arXiv:1112.1340](#).
- [109] C. JARLSKOG. *Commutator of the Quark Mass Matrices in the Standard Electroweak Model and a Measure of Maximal CP Violation*. Phys. Rev. Lett. **55**, 1039, (1985).

- [110] F. CAPOZZI, G. L. FOGLI, E. LISI, A. MARRONE, D. MONTANINO and A. PALAZZO. *Status of three-neutrino oscillation parameters, circa 2013*. Phys. Rev. **D89**, 093018, (2014). [arXiv:1312.2878](#).
- [111] G. ALTARELLI, F. FERUGLIO and L. MERLO. *Revisiting Bimaximal Neutrino Mixing in a Model with S_4 Discrete Symmetry*. JHEP **0905**, 020, (2009). [arXiv:0903.1940](#).
- [112] C. S. LAM. *Group Theory and Dynamics of Neutrino Mixing*. Phys. Rev. **D83**, 113002, (2011). [arXiv:1104.0055](#).
- [113] G.-J. DING, L. L. EVERETT and A. J. STUART. *Golden Ratio Neutrino Mixing and A_5 Flavor Symmetry*. Nucl. Phys. **B857**, 219-253, (2012). [arXiv:1110.1688](#).
- [114] C.-S. CHEN, T. W. KEPHART and T.-C. YUAN. *An A_5 Model of Four Lepton Generations*. JHEP **1104**, 015, (2011). [arXiv:1011.3199](#).
- [115] I. DE MEDEIROS VARZIELAS and L. LAVOURA. *Golden ratio lepton mixing and nonzero reactor angle with A_5* . J. Phys. **G41**, 055005, (2014). [arXiv:1312.0215](#).
- [116] M.-C. CHEN, M. FALLBACHER, K. T. MAHANTHAPPA, M. RATZ and A. TRAUTNER. *CP Violation from Finite Groups*. Nucl. Phys. **B883**, 267-305, (2014). [arXiv:1402.0507](#).
- [117] W. GRIMUS and M. N. REBELO. *Automorphisms in gauge theories and the definition of CP and P*. Phys. Rept. **281**, 239-308, (1997). [hep-ph/9506272](#).
- [118] G. ECKER, W. GRIMUS and H. NEUFELD. *Spontaneous CP Violation in Left-right Symmetric Gauge Theories*. Nucl. Phys. **B247**, 70-82, (1984).
- [119] G. ECKER, W. GRIMUS and H. NEUFELD. *A Standard Form for Generalized CP Transformations*. J. Phys. **A20**, L807, (1987).
- [120] H. NEUFELD, W. GRIMUS and G. ECKER. *Generalized CP Invariance, Neutral Flavor Conservation and the Structure of the Mixing Matrix*. Int. J. Mod. Phys. **A3**, 603-616, (1988).
- [121] D. MELONI. *Checking Flavour Models at Neutrino Facilities*. Phys. Lett. **B728**, 118-124, (2014). [arXiv:1308.4578](#).
- [122] P. BALLETT, S. F. KING, C. LUHN, S. PASCOLI and M. A. SCHMIDT. *Testing atmospheric mixing sum rules at precision neutrino facilities*. Phys. Rev. **D89**(1), 016016, (2014). [arXiv:1308.4314](#).
- [123] P. BALLETT, S. F. KING, C. LUHN, S. PASCOLI and M. A. SCHMIDT. *Testing solar lepton mixing sum rules in neutrino oscillation experiments*. JHEP **1412**, 122, (2014). [arXiv:1410.7573](#).
- [124] I. GIRARDI, S. T. PETCOV and A. V. TITOV. *Determining the Dirac CP Violation Phase in the Neutrino Mixing Matrix from Sum Rules*. Nucl. Phys. **B894**, 733-768, (2015). [arXiv:1410.8056](#).
- [125] P. F. HARRISON and W. G. SCOTT. *The Simplest neutrino mass matrix*. Phys. Lett. **B594**, 324-332, (2004). [hep-ph/0403278](#).
- [126] W. GRIMUS and L. LAVOURA. *A Nonstandard CP transformation leading to maximal atmospheric neutrino mixing*. Phys. Lett. **B579**, 113-122, (2004). [hep-ph/0305309](#).
- [127] N. KAWANAKA and H. MATSUYAMA. *A twisted version of the Frobenius-Schur indicator and multiplicity-free permutation representations*. Hokkaido Math. J. **19**(3), 495-508, (1990).
- [128] D. BUMP and D. GINZBURG. *Generalized Frobenius-Schur numbers*. Journal of Algebra **278**(1), 294-313, (2004).
- [129] C. R. VINROOT. *Twisted Frobenius-Schur indicators of finite symplectic groups*. Journal of Algebra **293**(1), 279-311, (2005).
- [130] X.-G. HE and A. ZEE. *Minimal modification to the tri-bimaximal neutrino mixing*. Phys. Lett. **B645**, 427-431, (2007). [hep-ph/0607163](#).
- [131] W. GRIMUS and L. LAVOURA. *A Model for trimaximal lepton mixing*. JHEP **0809**, 106, (2008). [arXiv:0809.0226](#).
- [132] Y. LIN. *Tri-bimaximal Neutrino Mixing from A_4 and $\theta_{13} \sim \theta_C$* . Nucl. Phys. **B824**, 95-110, (2010). [arXiv:0905.3534](#).
- [133] W. GRIMUS, L. LAVOURA and A. SINGRABER. *Trimaximal lepton mixing with a trivial Dirac phase*. Phys. Lett. **B686**, 141-145, (2010). [arXiv:0911.5120](#).
- [134] J. BIAN [NOVA COLLABORATION]. *First Results of ν_e Appearance Analysis and Electron Neutrino Identification at NO ν A* (2015). [arXiv:1510.05708](#), URL <https://inspirehep.net/record/1399048/files/arXiv:1510.05708.pdf>.
- [135] C. BACKHOUSE and R. B. PATTERSON. *Library Event Matching event classification algorithm for electron neutrino interactions in the NO ν A detectors*. Nucl. Instrum. Meth. **A778**, 31-39, (2015). [arXiv:1501.00968](#).
- [136] P. CHEN, C.-C. LI and G.-J. DING. *Lepton Flavor Mixing and CP Symmetry*. Phys. Rev. **D91**, 033003, (2015). [arXiv:1412.8352](#).

- [137] S.-B. KIM. *New results from RENO and prospects with RENO-50*. Nucl. Part. Phys. Proc. **265-266**, 93-98, (2015). [arXiv:1412.2199](#).
- [138] D. S. AYRES *et al.* [NOvA COLLABORATION]. *NOvA: Proposal to build a 30 kiloton off-axis detector to study $\nu_\mu \rightarrow \nu_e$ oscillations in the NuMI beamline* (2004). [hep-ex/0503053](#).
- [139] C. LUHN. *Trimaximal TM_1 neutrino mixing in S_4 with spontaneous CP violation*. Nucl. Phys. **B875**, 80-100, (2013). [arXiv:1306.2358](#).
- [140] C.-C. LI and G.-J. DING. *Generalised CP and trimaximal TM_1 lepton mixing in S_4 family symmetry*. Nucl. Phys. **B881**, 206-232, (2014). [arXiv:1312.4401](#).
- [141] C.-C. LI and G.-J. DING. *Deviation from bimaximal mixing and leptonic CP phases in S_4 family symmetry and generalized CP*. JHEP **1508**, 017, (2015). [arXiv:1408.0785](#).
- [142] G. C. BRANCO, I. DE MEDEIROS VARZIELAS and S. F. KING. *Invariant approach to CP in family symmetry models*. Phys. Rev. **D92**(3), 036007, (2015). [arXiv:1502.03105](#).
- [143] C.-C. LI, J.-N. LU and G.-J. DING. *A_4 and CP symmetry and a model with maximal CP violation* (2016). [arXiv:1608.01860](#).
- [144] G. C. BRANCO, I. DE MEDEIROS VARZIELAS and S. F. KING. *Invariant approach to CP in unbroken $\Delta(27)$* . Nucl. Phys. **B899**, 14-36, (2015). [arXiv:1505.06165](#).
- [145] G.-J. DING and Y.-L. ZHOU. *Predicting lepton flavor mixing from $\Delta(48)$ and generalized CP symmetries*. Chin. Phys. **C39**(2), 021001, (2015). [arXiv:1312.5222](#).
- [146] C. HAGEDORN and E. MOLINARO. *Flavor and CP symmetries for leptogenesis and $0\nu\beta\beta$ decay* (2016). [arXiv:1602.04206](#).
- [147] C. D. FROGGATT and H. B. NIELSEN. *Hierarchy of Quark Masses, Cabibbo Angles and CP Violation*. Nucl. Phys. **B147**, 277-298, (1979).
- [148] J. BARRY and W. RODEJOHANN. *Neutrino Mass Sum-rules in Flavor Symmetry Models*. Nucl. Phys. **B842**, 33-50, (2011). [arXiv:1007.5217](#).
- [149] L. DORAME, D. MELONI, S. MORISI, E. PEINADO and J. W. F. VALLE. *Constraining Neutrinoless Double Beta Decay*. Nucl. Phys. **B861**, 259-270, (2012). [arXiv:1111.5614](#).
- [150] S. F. KING, A. MERLE and A. J. STUART. *The Power of Neutrino Mass Sum Rules for Neutrinoless Double Beta Decay Experiments*. JHEP **1312**, 005, (2013). [arXiv:1307.2901](#).
- [151] S. F. KING, A. MERLE, S. MORISI, Y. SHIMIZU and M. TANIMOTO. *Neutrino Mass and Mixing: from Theory to Experiment*. New J. Phys. **16**, 045018, (2014). [arXiv:1402.4271](#).
- [152] S. WEINBERG. *Baryon and Lepton Nonconserving Processes*. Phys. Rev. Lett. **43**, 1566-1570, (1979).
- [153] M. MAGG and C. WETTERICH. *Neutrino Mass Problem and Gauge Hierarchy*. Phys. Lett. **B94**, 61-64, (1980).
- [154] G. LAZARIDES, Q. SHAFI and C. WETTERICH. *Proton Lifetime and Fermion Masses in an $SO(10)$ Model*. Nucl. Phys. **B181**, 287-300, (1981).
- [155] R. N. MOHAPATRA and G. SENJANOVIC. *Neutrino Masses and Mixings in Gauge Models with Spontaneous Parity Violation*. Phys. Rev. **D23**, 165, (1981).
- [156] P. MINKOWSKI. *$\mu \rightarrow e\gamma$ at a Rate of One Out of 10^9 Muon Decays?* Phys. Lett. **B67**, 421-428, (1977).
- [157] R. N. MOHAPATRA and G. SENJANOVIC. *Neutrino Mass and Spontaneous Parity Violation*. Phys. Rev. Lett. **44**, 912, (1980).
- [158] T. YANAGIDA. *Horizontal Symmetry and Masses of Neutrinos*. Prog. Theor. Phys. **64**, 1103, (1980).
- [159] M. GELL-MANN, P. RAMOND and R. SLANSKY. *Complex Spinors and Unified Theories*. Conf. Proc. **C790927**, 315-321, (1979). [arXiv:1306.4669](#).
- [160] R. FOOT, H. LEW, X. G. HE and G. C. JOSHI. *Seesaw Neutrino Masses Induced by a Triplet of Leptons*. Z. Phys. **C44**, 441, (1989).
- [161] E. MA. *Pathways to naturally small neutrino masses*. Phys. Rev. Lett. **81**, 1171-1174, (1998). [hep-ph/9805219](#).
- [162] G. SENJANOVIC. *Neutrino mass: From LHC to grand unification*. Riv. Nuovo Cim. **34**, 1-68, (2011).
- [163] G. ALTARELLI and F. FERUGLIO. *Tri-bimaximal neutrino mixing, A_4 and the modular symmetry*. Nucl. Phys. **B741**, 215-235, (2006). [hep-ph/0512103](#).
- [164] S. P. MARTIN. *A Supersymmetry primer*. Adv. Ser. Direct. High Energy Phys. **18,1** (1997). [hep-ph/9709356](#).
- [165] G. ALTARELLI, F. FERUGLIO and C. HAGEDORN. *A SUSY $SU(5)$ Grand Unified Model of Tri-Bimaximal Mixing from A_4* . JHEP **0803**, 052-052, (2008). [arXiv:0802.0090](#).
- [166] D. MELONI. *Bimaximal mixing and large θ_{13} in a SUSY $SU(5)$ model based on S_4* . JHEP **1110**, 010, (2011). [arXiv:1107.0221](#).
- [167] K. A. OLIVE *et al.* [PARTICLE DATA GROUP COLLABORATION]. *Review of Particle Physics*. Chin. Phys. **C38**, 090001, (2014).

- [168] L. L. EVERETT and A. J. STUART. *The Double Cover of the Icosahedral Symmetry Group and Quark Mass Textures*. Phys. Lett. **B698**, 131-139, (2011). [arXiv:1011.4928](#).
- [169] R. ACCIARRI *et al.* [DUNE COLLABORATION]. *Long-Baseline Neutrino Facility (LBNF) and Deep Underground Neutrino Experiment (DUNE)* (2015). [arXiv:1512.06148](#).
- [170] E. BAUSSAN *et al.* [ESS ν SB COLLABORATION]. *A very intense neutrino super beam experiment for leptonic CP violation discovery based on the European spallation source linac*. Nucl. Phys. **B885**, 127-149, (2014). [arXiv:1309.7022](#).
- [171] K. ABE *et al.* [T2K COLLABORATION]. *Measurements of neutrino oscillation in appearance and disappearance channels by the T2K experiment with 6.6×10^{20} protons on target*. Phys. Rev. **D91**(7), 072010, (2015). [arXiv:1502.01550](#).
- [172] A. DI IURA, I. GIRARDI and D. MELONI. *Probing new physics scenarios in accelerator and reactor neutrino experiments*. J. Phys. **G42**, 065003, (2015). [arXiv:1411.5330](#).
- [173] I. GIRARDI and D. MELONI. *Constraining new physics scenarios in neutrino oscillations from Daya Bay data*. Phys. Rev. **D90**(7), 073011, (2014). [arXiv:1403.5507](#).
- [174] I. GIRARDI, D. MELONI and S. T. PETCOV. *The Daya Bay and T2K results on $\sin^2 2\theta_{13}$ and Non-Standard Neutrino Interactions*. Nucl. Phys. **B886**, 31-42, (2014). [arXiv:1405.0416](#).
- [175] N. ARKANI-HAMED, S. DIMOPOULOS and G. R. DVALI. *The Hierarchy problem and new dimensions at a millimeter*. Phys. Lett. **B429**, 263-272, (1998). [hep-ph/9803315](#).
- [176] I. ANTONIADIS, N. ARKANI-HAMED, S. DIMOPOULOS and G. R. DVALI. *New dimensions at a millimeter to a Fermi and superstrings at a TeV*. Phys. Lett. **B436**, 257-263, (1998). [hep-ph/9804398](#).
- [177] N. ARKANI-HAMED, S. DIMOPOULOS and G. R. DVALI. *Phenomenology, astrophysics and cosmology of theories with submillimeter dimensions and TeV scale quantum gravity*. Phys. Rev. **D59**, 086004, (1999). [hep-ph/9807344](#).
- [178] R. N. MOHAPATRA, S. NANDI and A. PEREZ-LORENZANA. *Neutrino masses and oscillations in models with large extra dimensions*. Phys. Lett. **B466**, 115-121, (1999). [hep-ph/9907520](#).
- [179] R. N. MOHAPATRA and A. PEREZ-LORENZANA. *Sterile neutrino as a bulk neutrino*. Nucl. Phys. **B576**, 466-478, (2000). [hep-ph/9910474](#).
- [180] R. N. MOHAPATRA and A. PEREZ-LORENZANA. *Three flavor neutrino oscillations in models with large extra dimensions*. Nucl. Phys. **B593**, 451-470, (2001). [hep-ph/0006278](#).
- [181] R. BARBIERI, P. CREMINELLI and A. STRUMIA. *Neutrino oscillations from large extra dimensions*. Nucl. Phys. **B585**, 28-44, (2000). [hep-ph/0002199](#).
- [182] H. DAVOUDIASHI, P. LANGACKER and M. PERELSTEIN. *Constraints on large extra dimensions from neutrino oscillation experiments*. Phys. Rev. **D65**, 105015, (2002). [hep-ph/0201128](#).
- [183] E. G. ADELBERGER, J. H. GUNDLACH, B. R. HECKEL, S. HOEDL and S. SCHLAMMINGER. *Torsion balance experiments: A low-energy frontier of particle physics*. Prog. Part. Nucl. Phys. **62**, 102-134, (2009).
- [184] P. A. N. MACHADO, H. NUNOKAWA and R. ZUKANOVICH FUNCHAL. *Testing for Large Extra Dimensions with Neutrino Oscillations*. Phys. Rev. **D84**, 013003, (2011). [arXiv:1101.0003](#).
- [185] Y. GROSSMAN. *Nonstandard neutrino interactions and neutrino oscillation experiments*. Phys. Lett. **B359**, 141-147, (1995). [hep-ph/9507344](#).
- [186] T. OHLSSON. *Status of non-standard neutrino interactions*. Rept. Prog. Phys. **76**, 044201, (2013). [arXiv:1209.2710](#).
- [187] J. KOPP, M. LINDNER, T. OTA and J. SATO. *Non-standard neutrino interactions in reactor and superbeam experiments*. Phys. Rev. **D77**, 013007, (2008). [arXiv:0708.0152](#).
- [188] T. OTA and J. SATO. *Can ICARUS and OPERA give information on a new physics?* Phys. Lett. **B545**, 367-372, (2002). [hep-ph/0202145](#).
- [189] N. SEVERIJNS, M. BECK and O. NAVILIAT-CUNCIC. *Tests of the standard electroweak model in beta decay*. Rev. Mod. Phys. **78**, 991-1040, (2006). [nucl-ex/0605029](#).
- [190] M. M. GUZZO, A. MASIERO and S. T. PETCOV. *On the MSW effect with massless neutrinos and no mixing in the vacuum*. Phys. Lett. **B260**, 154-160, (1991).
- [191] E. ROULET. *MSW effect with flavor changing neutrino interactions*. Phys. Rev. **D44**, 935-938, (1991).
- [192] D. MELONI, T. OHLSSON, W. WINTER and H. ZHANG. *Non-standard interactions versus non-unitary lepton flavor mixing at a neutrino factory*. JHEP **1004**, 041, (2010). [arXiv:0912.2735](#).
- [193] T. OHLSSON, H. ZHANG and S. ZHOU. *Nonstandard interaction effects on neutrino parameters at medium-baseline reactor antineutrino experiments*. Phys. Lett. **B728**, 148-155, (2014). [arXiv:1310.5917](#).
- [194] C. BIGGIO, M. BLENNOW and E. FERNANDEZ-MARTINEZ. *Loop bounds on non-standard neutrino interactions*. JHEP **0903**, 139, (2009). [arXiv:0902.0607](#).

- [195] O. G. MIRANDA and H. NUNOKAWA. *Non standard neutrino interactions: current status and future prospects*. New J. Phys. **17**(9), 095002, (2015). [arXiv:1505.06254](#).
- [196] P. HUBER, M. LINDNER and W. WINTER. *Simulation of long-baseline neutrino oscillation experiments with GLOBES (General Long Baseline Experiment Simulator)*. Comput. Phys. Commun. **167**, 195, (2005). [hep-ph/0407333](#).
- [197] P. HUBER, J. KOPP, M. LINDNER, M. ROLINEC and W. WINTER. *New features in the simulation of neutrino oscillation experiments with GLOBES 3.0: General Long Baseline Experiment Simulator*. Comput. Phys. Commun. **177**, 432-438, (2007). [hep-ph/0701187](#).
- [198] K. ABE *et al.* [T2K COLLABORATION]. *Measurement of the inclusive ν_μ charged current cross section on carbon in the near detector of the T2K experiment*. Phys. Rev. **D87**(9), 092003, (2013). [arXiv:1302.4908](#).
- [199] D. MELONI and M. MARTINI. *Revisiting the T2K data using different models for the neutrino–nucleus cross sections*. Phys. Lett. **B716**, 186-192, (2012). [arXiv:1203.3335](#).
- [200] P. HUBER, M. LINDNER and W. WINTER. *Superbeams versus neutrino factories*. Nucl. Phys. **B645**, 3-48, (2002). [hep-ph/0204352](#).
- [201] Y. ITOW *et al.* [T2K COLLABORATION]. *The JHF-Kamioka neutrino project*. In *Neutrino oscillations and their origin. Proceedings, 3rd International Workshop, NOON 2001, Kashiwa, Tokyo, Japan, December 508, 2001*, pp. 239–248 (2001). [hep-ex/0106019](#).
- [202] P. HUBER, M. LINDNER, T. SCHWETZ and W. WINTER. *Reactor neutrino experiments compared to superbeams*. Nucl. Phys. **B665**, 487-519, (2003). [hep-ph/0303232](#).
- [203] P. COLOMA, P. HUBER, J. KOPP and W. WINTER. *Systematic uncertainties in long-baseline neutrino oscillations for large θ_{13}* . Phys. Rev. **D87**(3), 033004, (2013). [arXiv:1209.5973](#).
- [204] F. P. AN *et al.* [DAYA BAY COLLABORATION]. *A side-by-side comparison of Daya Bay antineutrino detectors*. Nucl. Instrum. Meth. **A685**, 78-97, (2012). [arXiv:1202.6181](#).
- [205] T. A. MUELLER *et al.* *Improved Predictions of Reactor Antineutrino Spectra*. Phys. Rev. **C83**, 054615, (2011). [arXiv:1101.2663](#).
- [206] P. HUBER. *On the determination of anti-neutrino spectra from nuclear reactors*. Phys. Rev. **C84**, 024617, (2011). [Erratum: Phys. Rev.C85,029901(2012)], [arXiv:1106.0687](#).
- [207] F. P. AN *et al.* [DAYA BAY COLLABORATION]. *Spectral measurement of electron antineutrino oscillation amplitude and frequency at Daya Bay*. Phys. Rev. Lett. **112**, 061801, (2014). [arXiv:1310.6732](#).
- [208] P. VOGEL and J. F. BEACOM. *Angular distribution of neutron inverse beta decay, $\bar{\nu}_e + p \rightarrow e^+ + n$* . Phys. Rev. **D60**, 053003, (1999). [hep-ph/9903554](#).
- [209] G. L. FOGLI, E. LISI, A. MARRONE, D. MONTANINO and A. PALAZZO. *Getting the most from the statistical analysis of solar neutrino oscillations*. Phys. Rev. **D66**, 053010, (2002). [hep-ph/0206162](#).
- [210] X. QIAN and P. VOGEL. *Neutrino Mass Hierarchy*. Prog. Part. Nucl. Phys. **83**, 1-30, (2015). [arXiv:1505.01891](#).
- [211] M. BLENNOW, P. COLOMA, P. HUBER and T. SCHWETZ. *Quantifying the sensitivity of oscillation experiments to the neutrino mass ordering*. JHEP **1403**, 028, (2014). [arXiv:1311.1822](#).
- [212] M. BLENNOW, P. COLOMA and E. FERNANDEZ-MARTINEZ. *Reassessing the sensitivity to leptonic CP violation*. JHEP **1503**, 005, (2015). [arXiv:1407.3274](#).
- [213] J. ELEVANT and T. SCHWETZ. *On the determination of the leptonic CP phase*. JHEP **1509**, 016, (2015). [arXiv:1506.07685](#).
- [214] A. ESMAILI, O. L. G. PERES and Z. TABRIZI. *Probing Large Extra Dimensions With IceCube*. JCAP **1412**(12), 002, (2014). [arXiv:1409.3502](#).
- [215] E. K. AKHMEDOV, R. JOHANSSON, M. LINDNER, T. OHLSSON and T. SCHWETZ. *Series expansions for three flavor neutrino oscillation probabilities in matter*. JHEP **04**, 078, (2004). [hep-ph/0402175](#).
- [216] A. DONINI, E. FERNANDEZ-MARTINEZ, D. MELONI and S. RIGOLIN. *ν_μ disappearance at the SPL, T2K-I, NO ν A and the neutrino factory*. Nucl. Phys. **B743**, 41-73, (2006). [hep-ph/0512038](#).
- [217] H. MINAKATA, H. NUNOKAWA, S. J. PARKE and R. ZUKANOVICH FUNCHAL. *Determining neutrino mass hierarchy by precision measurements in electron and muon neutrino disappearance experiments*. Phys. Rev. **D74**, 053008, (2006). [hep-ph/0607284](#).
- [218] H. GEORGI. *Lie Algebras in Particle Physics. From Isospin to Unified Theories*. Front. Phys. **54**, 1-255, (1982).
- [219] W. K. TUNG. *Group Theory in Physics*. Singapore, Singapore: World Scientific, 344p (1985).
- [220] P. RAMOND. *Group theory: A physicist's survey*. Cambridge, UK: Univ. Pr., 310p (2010).
- [221] S. ANTUSCH, J. KERSTEN, M. LINDNER, M. RATZ and M. A. SCHMIDT. *Running neutrino mass parameters in see-saw scenarios*. JHEP **0503**, 024, (2005). [hep-ph/0501272](#).

Acknowledgements

I would like to express my thanks and appreciation to my advisor Dr. Davide Meloni. I would like to thank you for encouraging my research and for allowing me to grow as a scientist. Your advice on both research as well as on my career have been priceless.

I would especially like to thank all the Collaborators I had the good fortune to work with for three years: Dr. Ivan Girardi, Dr. Claudia Hagedorn and Dr. Juan Herrero-Garcia.

A special thanks to my family. Words cannot express how grateful I am to my parents for all of the sacrifices that you have made on my behalf. I would also like to thank all of my friends who supported me in writing and stimulate me to strive towards my goal. A special thanks to the "I05's" guys: Alessandro, Danilo, Pietro and Matteo (via ssh) for their support during these years. In particular Erica for her precious support and the friendship of many years.